COMPARISON OF A_4 NEUTRINO MASS MODELS

A thesis submitted in fulfilment of the

requirements for the degree of

MASTER OF SCIENCE

of

RHODES UNIVERSITY

by

JAMES MUNNIK HAMILTON BARRY

November 2009

Abstract

The present neutrino oscillation data are compatible with tri-bimaximal mixing, to leading order. The addition of an A_4 family symmetry and extended Higgs sector to the Standard Model can generate this mixing pattern, assuming the correct vacuum expectation value alignment of Higgs scalars. The effect of deviating this alignment is studied, for different types of A_4 models, with a phenomenological emphasis: the effect of perturbations on the model predictions for the neutrino oscillation and neutrino mass observables.

The standard theoretical description of neutrino oscillations is presented, along with a summary of the past, present and future experimental efforts aimed at measuring the neutrino mixing parameters. Additionally, the current constraints on the sum of absolute neutrino masses and the amplitude for neutrinoless double beta decay, which is yet to be observed, are discussed. These constraints provide a model-independent test of family symmetery models.

The Standard Model is reviewed, and extensions to the Standard Model such as the seesaw mechanism(s) are discussed: these are designed to endow neutrinos with mass, and can be incorporated into A_4 symmetry models.

Models with different A_4 particle assignments are analysed for deviations from tri-bimaximal mixing. There are nine models presented in Chapter 5, with lepton doublets transforming as $\underline{3}$ and right-handed charged leptons transforming as $\underline{1}$, $\underline{1}'$, $\underline{1}''$; five of these include right-handed neutrinos transforming as $\underline{3}$, and make use of the seesaw mechanism. Chapter 6 contains the analysis of six models that assign all leptons to the $\underline{3}$ representation, with four of these utilising the seesaw mechanism.

The models are tested for any degree of fine tuning of the parameters that define the mass matrices. The effect of perturbations on the mixing angle observables, in particular $\sin^2\theta_{13}$ and $\sin^2\theta_{23}$, is studied, as well as the effect on the Jarlskog invariant, J_{CP}. Investigations of the $\langle m_{ee}\rangle - \sum m_\nu$ parameter space allow for comparison with current data, and can lead to the possible exclusion of a particular model by constraints from future data.

Acknowledgements

I would like to thank Prof. Steven Karataglidis for his steadfast support, motivation and counsel, and for providing me with the facilities needed to complete this project. My grateful thanks go to Dr. Jennifer Williams for her continual encouragement and guidance, and for sparking my interest in neutrino physics. I acknowledge the late Dr. Paul Nathanson, for always spurring me on towards excellence during my time at Rhodes University, and for encouraging me to pursue a career in physics.

This work would not have been possible without the assistance of Dr. Werner Rodejohann, to whom I am indebted for his patience, guidance and kind hospitality at the Max-Planck-Institut für Kernphysik (MPIK) in Heidelberg. I would like to thank my colleagues at the MPIK, Dr. Thomas Schwetz, Dr. Alexander Blum, Alexander Merle and Adisorn Adulpravitchai, for useful discussions on neutrino physics, group theory and on research in general.

The financial support of the Deutscher Akademischer Austauschdienst (DAAD), the National Research Foundation (NRF) and a Henderson Postgraduate Scholarship is gratefully acknowledged. In particular, I would like to thank the DAAD for giving me the opportunity to travel to Heidelberg for three months. I am also indebted to John Gillam, for helping me secure the funding for my masters work.

I thank my labmates Laura Richter, Kim McAlpine and Steven Liddell, for their friendship over the last several years, and Fred Otten, for useful discussions on Linux and other computing issues.

Finally, and most importantly, I would like to thank my family, for their continual guidance and support; and my fiancée, Joanne Rodgerson, for her empathy, love and patience during the course of this project, and her unwavering loyalty towards me.

Above all, I thank the Lord for His presence in my life; He is the source of my strength.

The scientific theorist is not to be envied. For Nature, or more precisely experiment, is an inexorable and not very friendly judge of his work. It never says "Yes" to a theory. In the most favourable cases it says "Maybe," and in the great majority of cases simply "No." If an experiment agrees with a theory it means for the latter "Maybe," and if it does not agree it means "No." Probably every theory will someday experience its "No" – most theories, soon after conception.

Albert Einstein
in "Albert Einstein: The Human Side"

Contents

List of Tables

List of Figures

List of Acronyms

ACBAR	Arcminute Cosmology Bolometer Array Receiver
BAO	Baryonic Acoustic Oscillation
BBN	Big Bang Nucleosynthesis
BOOMERANG	Balloon Observations Of Millimetric Extragalactic Radiation ANd Geophysics
BooNE	Booster Neutrino Experiment
CBI	Cosmic Background Imager
CKM	Cabibbo-Kobayashi-Maskawa
CMB	Cosmic Microwave Background
CNGS	CERN to Gran Sasso
CUORE	Cryogenic Underground Observatory for Rare Events
CUORICINO	"small" CUORE
GALLEX	Gallium Experiment
GERDA	GERmanium Detector Array
GNO	Gallium Neutrino Observatory
GUT	Grand Unified Theory
HM	Heidelberg-Moscow
HST	Hubble Space Telescope
ICARUS	Imaging Cosmic And Rare Underground Signals

IGEX	International Germanium Experiment
IMB	Irvine-Michigan-Brookhaven
K2K	KEK to Super-Kamiokande
Kamiokande	Kamioka Nucleon Decay Experiment
KamLAND	Kamioka Liquid scintillator AntiNeutrino Detector
KARMEN	KArlsruhe Rutherford Medium Energy Neutrino experiment
KATRIN	KArlsruhe TRItium Neutrino experiment
KEK	High Energy Accelerator Research Organization, Tsukuba
LBL	long-baseline
LMA	Large Mixing Angle
LSND	Liquid Scintillator Neutrino Detector
MiniBooNE	first phase of BooNE
MINOS	Main Injector Neutrino Oscillation Search
MPT	Mixing Parameter Tools
MSW	Mikheyev-Smirnov-Wolfenstein
NEMO	Neutrino Ettore Majorana Observatory
NOνA	NuMI Off-Axis Neutrino Appearance
OPERA	Oscillation Project with Emulsion-tRacking Apparatus
PMNS	Pontecorvo-Maki-Nakagawa-Sakata
SAGE	Soviet-American Gallium Experiment
SBL	short-baseline
SDSS	Sloan Digital Sky Survey
SM	Standard Model (of particle physics)
SNO	Sudbury Neutrino Observatory

SUSY	SUperSYmmetry
T2K	Tokai to Kamioka
TBM	tri-bimaximal mixing
VEV	vacuum expectation value
VLBL	very long-baseline
VSA	Very Small Array
WMAP	Wilkinson Microwave Anisotropy Probe

Chapter 1

Introduction

The idea of neutrino mixing dates back to Pontecorvo in the 1950's [1, 2]: the oscillation of active neutrinos into sterile ones was thought to be an explanation for the solar neutrino problem [3]. However, his ideas came before the discovery of the second and third families of charged leptons and their associated neutrinos. In 1998, the Super-Kamiokande experiment [4–6] presented the first model-independent signature of atmospheric neutrino oscillations. The Sudbury Neutrino Observatory (SNO) [7–9] gave the corresponding evidence for solar neutrino oscillations in 2002. These results encouraged further investigations into the origins and descriptions of neutrino oscillations (see, for example, the reviews in Refs. [10–17]).

The evidence of neutrino oscillations implies massive neutrinos, which contradicts the predictions of the Standard Model (SM). While the seesaw mechanism, be it of type I, II or III, is believed to explain the smallness of neutrino mass, more physics input is required to explain the peculiar features of the mixing. Although two of the three neutrino mixing angles have been measured, the third mixing angle and the CP violating Dirac phase have not been measured and the absolute masses and mass hierarchy of neutrinos are not known. There are currently many experiments (see the reviews in Refs. [15, 17–22]) focussed on precise measurements of the neutrino mass and mixing parameters: neutrino physics can be said to have entered the "precision era".

Global fits to the latest neutrino oscillation data [23–26] show that the lepton mixing matrix is very close to the tri-bimaximal mixing (TBM) matrix, first proposed in Ref. [27]. Since the allowed deviations from TBM can only be small (10-15%), this mixing pattern represents at least a zeroth order approximation to lepton mixing. This is completely different to the mixing in the quark sector, and has motivated extensive research into models of family symmetries [28].

There are two approaches [29] in the literature: (i) the "bottom-up" approach, which starts from the observations of neutrino masses and mixings and attempts to look for a symmetry basis in which flavour (family) symmetry is realised; and (ii) the "top-down" approach, which starts with a general symmetry, perhaps even a Grand Unified Theory (GUT), with motivations outside of neutrino physics, and attempts to go from this bigger picture down to the observed properties of neutrinos. It is evident that both approaches are complementary and helpful in characterising the physics of flavour.

The website *Neutrino Unbound* [30] is an archive of thousands of papers in the field of neutrino physics. The "Models" page lists all papers that propose models for neutrino masses and mixings, from 1972 to the present day, and contains some 900 papers. Among this plethora of models there are many that employ discrete family symmetries in an attempt to explain the TBM scheme. In essence, the addition of a family symmetry to the SM constrains the form of the lepton mass matrices, reducing the number of parameters and thus providing more predictive power. Unfortunately, this is not without the addition of extra Higgs scalars (more parameters), with non-zero vacuum expectation values (VEVs) that break the family symmetry and lead to TBM.

Some of the discrete family symmetries used in the literature are: A_4 [31–35], S_3 [36–39], S_4 [40–46], T' [47–51], $\Delta(27)$ [52–55], and $\Sigma(81)$ [56–58]; there are also models that employ continuous symmetries such as $SU(3)$ [59–61], $SO(3)$ [62,63], and $SO(5)$ [64]. Very often the TBM scheme is obtained only approximately, or with the cost of fine tuning and/or various assumptions, such as unexplained VEV alignment or radiative corrections. This is a crucial point: the vacuum expectation values of the various scalar fields must be aligned in order to make the models work.

An attractive theory is one that is economical in terms of parameters, and one that makes predictions that can be verified. Although some authors [65] disagree, the A_4 models have a very economical structure in terms of group representations and field content [66,67]. This characteristic, combined with the relative abundance of A_4 models in the literature has motivated the study of A_4 models in this work. One could indeed analyse other flavour symmetry models using the same criteria, but that is beyond the scope of this thesis.

Ma & Rajasekaran [34] were the first to use the A_4 symmetry to construct models of neutrino mass. Ma later refers [68,69] to A_4 as "Plato's fire", with reference to a Greek theory matching the four basic elements to the perfect geometric solids. In the original model [34] the seesaw-induced neutrino masses are degenerate, so that the model does not fit with the neutrino oscillation data. Babu et al. [70] proposed a supersymmetric

solution to this problem, where radiative corrections lift the degeneracy. At this stage TBM had not yet been suggested, and it was only after the work of Harrison et al. [27] that TBM was considered seriously as an alternative.

Ma proposed [31] the first A_4 model that could reproduce the TBM pattern. The seesaw mechanism is absent in this model – the key difference is the introduction of new Higgs scalars, which transform as triplets and singlets under A_4, for which symmetry breaking gives the required mass matrix. In order for this model to work, the Higgs triplets must have a certain VEV alignment, which is somewhat ad-hoc; it is not justified in the original paper.

Altarelli and Feruglio [32] then expanded upon Ma's original model, in an attempt to solve the vacuum alignment problem. In their model, the Higgs scalars are gauge singlets (not doublets, as in Ma's model [31]), and the alignment problem is solved using extra dimensions. Yet the mass matrix leading to TBM takes the same form. Another way to solve the vacuum alignment problem is presented in Ma's supersymmetric seesaw model [71], where there are three Higgs doublets transforming as $\underline{3}$, three heavy neutrino singlets transforming as $\underline{3}$ and one Higgs doublet transforming as $\underline{1}$. This "naturally" produces the alignment proportional to $(1,0,0)$ in the neutrino sector, so that the heavy neutrino mass matrix has the right form to give TBM using the seesaw mechanism.

Other authors [72–74] propose models with the VEV alignment of Higgs triplet scalars proportional to $(0,1,0)$. In those models the combination of charged lepton and neutrino mixing still gives TBM, but the neutrino sector looks slightly different. The vacuum alignment problem is still present, with the authors often introducing additional symmetries or invoking supersymmetry (SUSY) [73] in order to solve it.

Chen, Frigerio and Ma [75, 76] were the first to propose a model where the right-handed lepton singlets transform as $\underline{3}$, since all of the previous models had them transforming as A_4 singlets. The introduction of more Higgs doublets transforming as $\underline{1}$, $\underline{1}'$, $\underline{1}''$ results in a diagonal charged-lepton mass matrix, but exact TBM is not achieved.

As was shown in Refs. [77, 78], even with both left-handed doublets and lepton singlets transforming as $\underline{3}$, it is still possible to achieve TBM. Thus models combining A_4 with the GUT groups SU(5) [79] and SO(10) [80–82] could be constructed, since all leptons could now transform as $\underline{3}$ under A_4.

All of the above models employ the same basis for A_4; this is often termed the "Ma-Rajasekaran basis". In an attempt to connect A_4 models with the modular symmetry and thus the larger framework of string theory, Altarelli and Feruglio [33] employed a different basis for A_4, where the generator T is diagonal, the so-called "Altarelli-Feruglio

basis". The two bases[1] are related by a phase change, and the main difference is that the alignment of the Higgs fields that generate the charged lepton and neutrino mass matrices are effectively "swapped", so that the charged leptons immediately come out as diagonal in the A-F basis. There is still the problem of different vacuum alignments in the charged lepton and neutrino sectors, and the authors present [33] a supersymmetric solution, as well as studying the effects of higher order terms on the mass matrices.

Other types of models have been presented with, for example, lepton doublets transforming as A_4 singlets [83], right-handed neutrinos transforming as A_4 singlets [76, 84], or both right-handed leptons and neutrinos transforming as A_4 singlets [85]. Herein the analysis will focus on the models that give TBM, but a complete list [66,67] of all published A_4 models is included.

More recent models include: (i) the use of $A_4 \propto (Z_2)^3$ [86], which provides a different way to solve the VEV alignment problem, and (ii) models in which the right-handed charged lepton singlets all transform as $\underline{1}$ under A_4 [87,88], instead of as $\underline{1}$, $\underline{1}'$, $\underline{1}''$. In the latter case, the VEV alignment of the Higgs field in the charged lepton sector is proportional to $(0,1,0)$, providing a different way to explain the charged lepton mass hierarchy.

In summary, this thesis presents a phenomenological analysis of those A_4 flavour symmetry models that reproduce the TBM pattern. The effect of deviating the VEV alignments in these models is studied, with an emphasis on the neutrino oscillation and mass dependent observables measured by current and future experiments. In Chapter 2 the neutrino oscillation formalism is outlined, and there is a summary of experimental work in the field. Chapter 3 reviews the SM and the extensions to the SM required to accommodate massive neutrinos; Chapter 4 is an introduction to discrete family symmetries. Chapters 5 and 6 contain the analytical and numerical results that compare fifteen different A_4 models from the literature, and Chapter 7 presents the conclusions.

[1] A discussion of the two bases is given in Appendix A.

Chapter 2

Neutrino Oscillations

The standard theory of neutrino oscillations is well-developed and explains the experimental data adequately [17, 89]. However, the nature of the propagation of neutrinos is still to be understood, and various approaches exist to describe it. The standard approach [17] is to treat neutrinos as plane waves and then use a relativistic approximation to obtain the neutrino oscillation probability. Other approaches employ a more rigorous quantum mechanical treatment, using: (i) wave packets to describe the neutrinos as they propagate through space [20, 90], or (ii) a quantum field theoretical description, with neutrinos as "virtual particles" on the internal line of a Feynman diagram [91,92]. Ref. [93] presents an in depth model of neutrino oscillations, treating the neutrinos as wave-packets and following a field theoretical approach.

2.1 Standard approach: the plane wave approximation

Using the notation of Refs. [17, 20], the leptonic charged current is given by

$$\begin{aligned} j^{\rho}_{W,L} &= 2 \sum_{\alpha=e,\mu,\tau} \overline{\nu_{\alpha L}} \gamma^{\rho} \ell_{\alpha L} \\ &= 2 \sum_{\alpha=e,\mu,\tau} \sum_{k} U^{*}_{\alpha k} \overline{\nu_{kL}} \gamma^{\rho} \ell_{\alpha L} \ , \end{aligned} \tag{2.1}$$

where $\nu_{\alpha L}$ and $\ell_{\alpha L}$ are neutrino and charged lepton flavour states, respectively, ν_{kL} is a neutrino mass eigenstate, and $U^{*}_{\alpha k}$ is an element of the mixing matrix. Eq. (2.1) is valid for both Dirac and Majorana neutrinos. This generates a superposition of massive neutrinos, as long as the energy and momenta of the particles involved in the

production and detection processes have sufficient uncertainty to prevent an energy-momentum conservation determination of the neutrino mass, which is indeed the case in neutrino oscillation experiments [20, 90].

Consider the decay $W^+ \to \ell_\alpha^+ + \nu$, and assume that a neutrino with flavour α and momentum $\vec{p}$ can be described by the flavour state

$$|\nu_\alpha\rangle = \sum_k U_{\alpha k}^* |\nu_k\rangle \qquad (\alpha = e, \mu, \tau) \ , \tag{2.2}$$

which is a superposition of mass eigenstates ν_k. The dependence of Eq. (2.2) on the production and detection processes can be shown to be negligible [20]. The inverse of Eq. (2.2) is

$$|\nu_k\rangle = \sum_\beta U_{\beta k} |\nu_\beta\rangle \qquad (\beta = e, \mu, \tau) \ . \tag{2.3}$$

In Eqs. (2.2) and (2.3) there are three active flavour neutrinos, but the number of massive neutrinos may in fact be more. If there are more than three massive neutrinos then their counterparts in the flavour basis do not have a charged lepton partner and are termed "sterile", as these neutrinos do not participate in SM interactions (see Section 3.2.3).

Neutrino oscillations are a quantum mechanical process, and the amplitude for oscillation depends on the coherence of different states. The method outlined in Ref. [20] involves neutrino flavour states propagating in time, whereas the approach in Ref. [17] takes into consideration the work of Ref. [94], describing neutrinos propagating in space.

2.1.1 Propagation in time

The Schrödinger equation for massive neutrino states is

$$i\frac{d}{dt}|\nu_k(t)\rangle = \mathscr{H}|\nu_k\rangle \ , \tag{2.4}$$

and if one assumes a definite momentum $\mathbf{p}$, referred to as the "equal momentum assumption", the energy eigenvalues are

$$E_k = \sqrt{\mathbf{p}^2 + m_k^2} \ , \tag{2.5}$$

where m_k is the mass of $|\nu_k\rangle$. The neutrino states are assumed to be plane waves, which evolve in time as

$$|\nu_k(t)\rangle = e^{-iE_k t}|\nu_k\rangle. \tag{2.6}$$

From Eqs. (2.2) and (2.6), the time evolution of a flavour neutrino state $|\nu_\alpha(t)\rangle$ may be written as

$$|\nu_\alpha(t)\rangle = \sum_k U^*_{\alpha k} e^{-iE_k t}|\nu_k\rangle \ , \tag{2.7}$$

with $|\nu_\alpha(t=0)\rangle = |\nu_\alpha\rangle$. Substituting Eq. (2.3) into Eq. (2.7) gives

$$|\nu_\alpha(t)\rangle = \sum_{\beta=e,\mu,\tau} \left(\sum_k U^*_{\alpha k} e^{-iE_k t} U_{\beta k} \right) |\nu_\beta\rangle \ , \tag{2.8}$$

so that a neutrino of definite flavour at $t = 0$ becomes a superposition of different flavour states as time progresses, unless U is diagonal. The amplitude for the oscillation $\nu_\alpha \to \nu_\beta$ is

$$\begin{aligned} \mathcal{A}_{\nu_\alpha \to \nu_\beta}(t) &\equiv \langle \nu_\beta | \nu_\alpha(t) \rangle \\ &= \sum_k U^*_{\alpha k} U_{\beta k} e^{-iE_k t} \ , \end{aligned} \tag{2.9}$$

so that the oscillation probability becomes

$$\begin{aligned} P_{\nu_\alpha \to \nu_\beta} &= |\mathcal{A}_{\nu_\alpha \to \nu_\beta}(t)|^2 \\ &= \sum_{k,j} U^*_{\alpha k} U_{\beta k} U_{\alpha j} U^*_{\beta j} e^{-i(E_k - E_j)t}. \end{aligned} \tag{2.10}$$

Since observed neutrinos are ultrarelativistic particles, with $|\mathbf{p}| \gg m$, Eq. (2.5) can be approximated by

$$E_k \simeq E + \frac{m_k^2}{2E} \ , \tag{2.11}$$

where $E = |\mathbf{p}|$ is the neutrino energy. Hence the probability in Eq. (2.10) becomes

$$P_{\nu_\alpha \to \nu_\beta}(t) = \sum_{k,j} U^*_{\alpha k} U_{\beta k} U_{\alpha j} U^*_{\beta j} \exp\left(-i \frac{\Delta m^2_{kj} t}{2E} \right) \ , \tag{2.12}$$

where $\Delta m^2_{kj} \equiv m^2_k - m^2_j$ and $E = |\mathbf{p}|$. m_k and m_j represent the masses of the k^{th} and j^{th} neutrino, respectively.

One more assumption is used: the "light-ray approximation". Ultrarelativistic

neutrinos travel at almost the speed of light, so that $t \approx L$, where L is the oscillation length, from which one can make the approximation:

$$P_{\nu_\alpha \to \nu_\beta}(L, E) = \sum_{k,j} U^*_{\alpha k} U_{\beta k} U_{\alpha j} U^*_{\beta j} \exp\left(-i \frac{\Delta m^2_{kj} L}{2E}\right). \tag{2.13}$$

2.1.2 Propagation in space

Complementary to the description of propagation of neutrinos in time is the description of propagation of neutrinos in space. Refs. [94–96] assume that neutrinos with the same energy and different momenta lead to oscillations. In this method, the relative phases of the propagation amplitudes are taken into account, and a neutrino detector must be able to detect the relative phases of different components. The amplitude for the oscillation $\nu_\alpha \to \nu_\beta$ is the coherent sum

$$\mathcal{A}_{\nu_\alpha \to \nu_\beta} = \sum_k U^*_{\alpha k} \, \mathrm{Prop}(\nu_k) \, U_{\beta k}. \tag{2.14}$$

The propagation amplitude, $\mathrm{Prop}(\nu_k)$, is $e^{-im_k\tau_k}$, where τ_k is the proper time that elapses during propagation in the ν_k rest frame. By Lorentz invariance,

$$m_k \tau_k = E_k t - p_k L \ , \tag{2.15}$$

with L the source-detector distance and E_k and p_k the energy and momentum of the k^{th} neutrino, in the lab-frame.

Since the probability is given by the amplitude squared, only the relative phases have physical consequences. The relative phase is

$$\delta\phi_{kj} = (p_k - p_j)L - (E_k - E_j)t \ . \tag{2.16}$$

To a good approximation [94], $t \simeq L/\overline{v}$ in Eq. (2.16), where

$$\overline{v} = \frac{p_k + p_j}{E_k + E_j} \tag{2.17}$$

is an approximation to the average of the velocities of the ν_k and ν_j components of the neutrino beam. Hence,

$$\delta\phi_{kj} \simeq \frac{p_k^2 - p_j^2}{p_k + p_j} L - \frac{E_k^2 - E_j^2}{p_k + p_j} L \simeq \left(m_j^2 - m_k^2\right) \frac{L}{2E} \ , \tag{2.18}$$

where $E \approx p_k \approx p_j$ for ultrarelativistic neutrinos. The amplitude in Eq. (2.14) becomes

$$\mathcal{A}_{\nu_\alpha \to \nu_\beta} = \sum_k U^*_{\alpha k} e^{-i(m_k^2/2E)L} U_{\beta k} \ , \tag{2.19}$$

so that the probability for the oscillation $\nu_\alpha \to \nu_\beta$ is

$$P_{\nu_\alpha \to \nu_\beta}(L,E) = \sum_{k,j} U^*_{\alpha k} U_{\beta k} U_{\alpha j} U^*_{\beta j} \exp\left(-i \frac{\Delta m^2_{kj} L}{2E}\right) , \tag{2.20}$$

which is the same as Eq. (2.13).

In neutrino oscillation experiments the distance L and the neutrino energy E are measured, and determine the oscillation phase [Eq. (2.18)]. That can also be written as

$$\delta\phi_{kj} = -\frac{\Delta m^2_{kj} L}{2E} \ . \tag{2.21}$$

The phase shows a dependence on the mass-squared differences, whereas the amplitude of oscillations is given by the elements of the mixing matrix U. Hence, oscillation experiments are used to find the values of the constants Δm^2_{kj} and $U_{\alpha k}$.

From the unitarity of U, Eq. (2.20) can be split accordingly, as

$$\begin{aligned} P_{\nu_\alpha \to \nu_\beta}(L,E) = \delta_{\alpha\beta} &- 4 \sum_{k>j} \Re\mathrm{e}\left[U^*_{\alpha k} U_{\beta k} U_{\alpha j} U^*_{\beta j}\right] \sin^2\left(\frac{\Delta m^2_{kj} L}{4E}\right) \\ &+ 2 \sum_{k>j} \Im\mathrm{m}\left[U^*_{\alpha k} U_{\beta k} U_{\alpha j} U^*_{\beta j}\right] \sin\left(\frac{\Delta m^2_{kj} L}{2E}\right) . \end{aligned} \tag{2.22}$$

In the case of antineutrinos the kinematics are unaltered and the standard derivation of the oscillation probability holds [20]. Following the same procedure outlined above, the probability for the oscillation $\overline{\nu}_\alpha \to \overline{\nu}_\beta$ is

$$\begin{aligned} P_{\overline{\nu}_\alpha \to \overline{\nu}_\beta}(L,E) = \delta_{\alpha\beta} &- 4 \sum_{k>j} \Re\mathrm{e}\left[U^*_{\alpha k} U_{\beta k} U_{\alpha j} U^*_{\beta j}\right] \sin^2\left(\frac{\Delta m^2_{kj} L}{4E}\right) \\ &- 2 \sum_{k>j} \Im\mathrm{m}\left[U^*_{\alpha k} U_{\beta k} U_{\alpha j} U^*_{\beta j}\right] \sin\left(\frac{\Delta m^2_{kj} L}{2E}\right) . \end{aligned} \tag{2.23}$$

Since CPT invariance is a property of all local quantum field theories [20], the relation

$$P_{\nu_\alpha \to \nu_\beta} = P_{\overline{\nu}_\beta \to \overline{\nu}_\alpha} \tag{2.24}$$

holds. Comparing Eqs. (2.22) and (2.23), the only difference is the sign of the term depending on the imaginary parts of the quartic products of elements of U. If there is no CP violation then the mixing matrix is real, the second line of each equation vanishes, and the equations are identical.

2.2 Oscillations with wave packets

In the standard derivation of the neutrino oscillation probability in Section 2.1, the neutrinos are considered to be plane waves with definite energy and momentum. However, a wave-packet description of oscillations is necessary as: (i) plane waves are periodic and cannot describe the localised events of neutrino production and detection; and (ii) in order to produce different massive neutrinos, an amount of uncertainty in the production and detection process is required. By the uncertainty principle, this implies a spread of momentum in the propagating neutrinos.

Ref. [97] describes an experiment in which pions decay via $\pi^+ \rightarrow \mu^+\nu_\mu$, and the detector looks for electron neutrinos. By adding an apparatus which measures the momenta of the pion and the muon, the mass squared of the neutrino, m^2_ν, may be found, identifying the ν flavour produced. This effectively destroys the oscillation pattern at the detector: the more accurately the pion momentum is measured the more uncertain its position will be, and the production process is not localized. Thus the neutrino oscillations cannot be observed unless the neutrino source is localised within a region much smaller than the oscillation length [97].

There are a number of quantum mechanical models of neutrino oscillations [20, 90, 97, 98]. In most practical cases the plane-wave approximation may be used to derive the neutrino oscillation probability, and one might wonder why a wave-packet treatment is necessary at all. However, it is important to take into account the localisation of the production and detection processes and the associated momentum uncertainties. The only way to verify the existence of massive neutrino wave packets experimentally is to measure the transition probability as a function of both the distance and the time interval between production and detection. For a discussion of coherence effects in neutrino oscillations see Ref. [99].

2.3 Standard three-neutrino mixing scenario

The mixing matrix U [Eq. (2.22)] is often referred to as the Pontecorvo-Maki-Nakagawa-Sakata (PMNS) matrix [2, 3, 100]. In the standard parameterisation [17], U_{PMNS} is

divided into a unitary mixing matrix $U^{\rm D}$ and a diagonal unitary phase matrix $D^{\rm M}$ [19,20], *viz.*

$$\begin{aligned} U_{\rm PMNS} &= U^{\rm D} D^{\rm M} \\ &= (R_{23} W_{13} R_{12}) D(\lambda_2, \lambda_3) \\ &= \begin{pmatrix} 1 & 0 & 0 \\ 0 & c_{23} & s_{23} \\ 0 & -s_{23} & c_{23} \end{pmatrix} \begin{pmatrix} c_{13} & 0 & s_{13} e^{-i\delta} \\ 0 & 1 & 0 \\ -s_{13} e^{-i\delta} & 0 & c_{13} \end{pmatrix} \begin{pmatrix} c_{12} & s_{12} & 0 \\ -s_{12} & c_{12} & 0 \\ 0 & 0 & 1 \end{pmatrix} \begin{pmatrix} 1 & 0 & 0 \\ 0 & e^{i\lambda_2} & 0 \\ 0 & 0 & e^{i\lambda_3} \end{pmatrix} \\ &= \begin{pmatrix} c_{12}c_{13} & s_{12}c_{13} & s_{13}e^{-i\delta} \\ -s_{12}c_{23} - c_{12}s_{23}s_{13}e^{i\delta} & c_{12}c_{23} - s_{12}s_{23}s_{13}e^{i\delta} & s_{23}c_{13} \\ s_{12}s_{23} - c_{12}c_{23}s_{13}e^{i\delta} & -c_{12}s_{23} - s_{12}c_{23}s_{13}e^{i\delta} & c_{23}c_{13} \end{pmatrix} \begin{pmatrix} 1 & 0 & 0 \\ 0 & e^{i\lambda_2} & 0 \\ 0 & 0 & e^{i\lambda_3} \end{pmatrix} \end{aligned} \tag{2.25}$$

where $c_{ij} \equiv \cos\theta_{ij}$, $s_{ij} \equiv \sin\theta_{ij}$ and $\theta_{12}, \theta_{13}, \theta_{23}$ $(0 \leq \theta_{ij} \leq \pi/2)$ are the three mixing angles. There are three phases in Eq. (2.25): δ is the CP violating Dirac phase, and λ_2 and λ_3 are the Majorana phases, with $0 \leq \delta, \lambda_2, \lambda_3 \leq 2\pi$. R_{23} and R_{12} are real rotations in the $2-3$ and $1-2$ planes, respectively, and W_{13} is a complex rotation in the $1-3$ plane.

The factorised form in the third line of Eq. (2.25) is useful for interpreting the data: the first matrix contains the parameter θ_{23}, relevant for atmospheric and accelerator neutrino oscillations, the second matrix the parameter θ_{13}, accessible to short baseline reactor experiments, and the third matrix contains the parameter θ_{12}, which is measured in solar neutrino experiments. The CP violating phase, δ, is associated with the parameter θ_{13}. Note that the Majorana phases, λ_2 and λ_3, do not affect the neutrino oscillation probability. Indeed, these phases have physical consequences only if neutrinos are Majorana particles,[1] influencing the amplitude for neutrinoless double beta ($0\nu\beta\beta$) decay, discussed in Section 2.5.2 below.

In order to quantify the magnitude of CP violation in a rephasing-invariant [20] way, one can define the Jarlskog invariant [101, 102]

$$J_{CP} = \Im\mathrm{m}[U_{\mu 3} U_{e2} U^*_{\mu 2} U^*_{e3}] = \Im\mathrm{m}[U^D_{\mu 3} U^D_{e2} U^{D*}_{\mu 2} U^{D*}_{e3}]\,, \tag{2.26}$$

[1] See Section 3.2.2.

which in the parameterisation of Eq. (2.25) becomes

$$\begin{aligned} J_{CP} &= c_{12}s_{12}c_{23}s_{23}c_{13}^2 s_{13}\sin\delta \\ &= \frac{1}{8}\sin 2\theta_{12}\sin 2\theta_{23}\cos\theta_{13}\sin 2\theta_{13}\sin\delta\,. \end{aligned} \tag{2.27}$$

Note that since the Dirac phase always appears as the combination $\sin\theta_{13}e^{-i\delta}$ in Eq. (2.25), a sufficiently small value of θ_{13} can always mask any CP violating effects.

In the case of three-neutrino mixing, there are three independent mass-squared differences [Eq. (2.22)], with

$$\Delta m_{21}^2 \ll \Delta m_{31}^2 \simeq \Delta m_{32}^2\,, \tag{2.28}$$

and the massive neutrinos can be labelled such that

$$\Delta m_{\rm SOL}^2 = \Delta m_{21}^2\,, \quad \Delta m_{\rm ATM}^2 = |\Delta m_{31}^2|\,. \tag{2.29}$$

Since the sign of $\Delta m_{\rm ATM}^2$ is not known, there are two possible arrangements for the neutrino mass hierarchy, as shown in Fig. 2.1. In the "normal" hierarchy, the smallest mass-squared difference is between the two lightest neutrinos, and a natural neutrino mass hierarchy can be realised, whereas in the "inverted" hierarchy, the smallest mass-squared difference is between the two heaviest neutrinos, which become almost degenerate. Note that oscillations only yield information on the mass-squared differences, not the absolute masses themselves. Instead, information on the masses may be obtained from beta decay and $0\nu\beta\beta$ decay, as well as from cosmological considerations.

2.4 Experimental evidence for oscillations

The different oscillation experiments can be classified according to the ratio L/E [Eq. (2.21)], which defines the range of Δm^2 to which an experiment is sensitive. There are three types: (i) short-baseline (SBL) experiments, (ii) long-baseline (LBL) and atmospheric experiments, and (iii) very long-baseline (VLBL) and solar experiments.

It is more convenient to classify the experiments in terms of the mixing angles measured [Eq. (2.25)] with solar and VLBL experiments measuring θ_{12}, atmospheric and LBL experiments measuring θ_{23}, and reactor and LBL experiments measuring θ_{13}. There are several recent analyses of the global neutrino oscillation data [20,24-26,104],

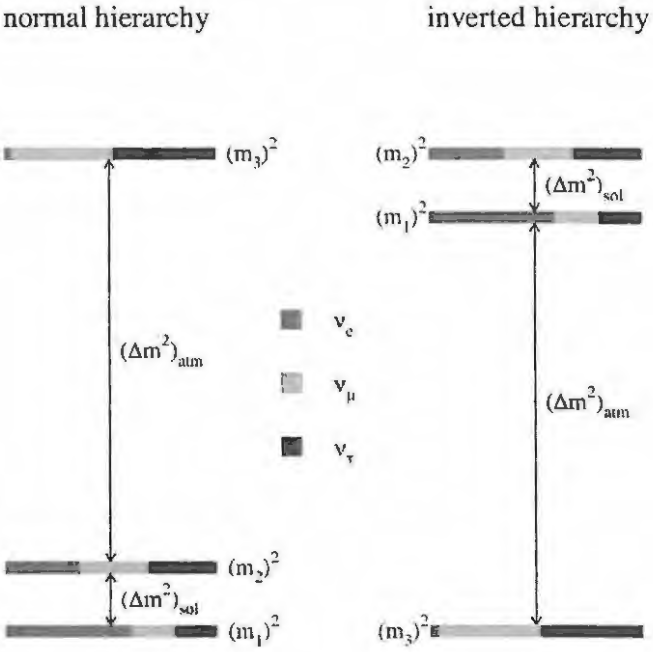

Figure 2.1: (From Ref. [103].) The two distinct neutrino mass hierarchies that fit all of the current neutrino data. The colour coding indicates the fraction $|U_{\alpha i}|$ of each distinct flavour ν_α, $\alpha = e, \mu, \tau$ contained in each mass eigenstate ν_k, $k = 1, 2, 3$.

constraining the values of the three mixing angles and two mass-squared differences. The data from Ref. [25], shown in Table. 2.1, were used in this work.

Table 2.1: Best-fit values and allowed $n\sigma$ ranges for the global three flavour neutrino oscillation parameters, from Ref. [25].

Parameter	Δm^2_{21} $(10^{-5}\,\mathrm{eV}^2)$	$\sin^2\theta_{12}$	$\sin^2\theta_{13}$	$\sin^2\theta_{23}$	Δm^2_{31} $(10^{-3}\,\mathrm{eV}^2)$
Best fit	7.67	0.312	0.016	0.466	2.39
1σ range	7.48–7.83	0.294–0.331	0.006–0.026	0.408–0.539	2.31–2.50
2σ range	7.31–8.01	0.278–0.352	<0.036	0.366–0.602	2.19–2.66
3σ range	7.14–8.19	0.263–0.375	<0.046	0.331–0.644	2.06–2.81

2.4.1 Solar neutrinos and KamLAND

In the late 1960's, the Homestake experiment [105, 106] began to detect solar neutrinos from the decay of ^{7}Be and ^{8}B, and continued taking data for about 30 years. The radiochemical detector recorded a deficit in the flux of electron neutrinos, compared to that predicted by the standard solar model [107]; this was called "the solar neutrino problem". The Homestake result was confirmed by the water Cherenkov Kamiokande

experiment [108–111], which detected ^{8}B neutrinos, as well as its upgrade, the Super-Kamiokande experiment [112–118], on the same site.

Since the Kamiokande experiments were only sensitive to the higher euergy ^{8}B solar neutrinos, the GALLEX [119–123] and SAGE [124–126] collaborations conducted complementary radiochemical tests, targeting the lowest energy solar neutrinos, and thus confirming the Homestake results.[2] The GALLEX experiment was upgraded to GNO [128, 129], with similar results.

The first definitive, model-independent proof of solar neutrino oscillations came from the SNO detector [7–9], which employed charged-current (CC) and neutral-current (NC) reactions to measure the electron neutrino and total neutrino flux, respectively. The first "D_2O phase" [130] of the experiment was improved upon by the "salt phase" [131, 132], and the recent "third phase" [133] gave a more accurate measurement of the NC process. The ratio [133]

$$\frac{\phi_{\mathrm{CC}}^{\mathrm{SNO}}}{\phi_{\mathrm{NC}}^{\mathrm{SNO}}} = 0.301 \pm 0.033\,, \tag{2.30}$$

where $\phi_{\mathrm{CC}}^{\mathrm{SNO}}$ is the flux of electron neutrinos, and $\phi_{\mathrm{NC}}^{\mathrm{SNO}}$ is the total flux of active neutrinos, confirms that solar electron neutrinos oscillate into muon and/or tau neutrinos on their way to earth.

The KamLAND VLBL reactor experiment [134–136] confirmed the Large Mixing Angle (LMA) MSW solution to the solar neutrino problem, and placed further constraints on the parameter Δm_{21}^2, as shown in Fig. 2.2. The Borexino [137, 138] low energy solar neutrino experiment gave further confirmation of this solution.

2.4.2 Atmospheric neutrinos, K2K and MINOS

An independent confirmation of the theory neutrino oscillations came from the observation of atmospheric muon neutrino disappearance in the Super-Kamiokande experiment in 1998 [4–6]. This confirmed the earlier results from the IMB collaboration [139–141] and Kamiokande [142, 143], both of which found a deficit in the atmospheric muon neutrino flux. Super-Kamiokande discovered the up-down asymmetry of high-energy events generated by atmospheric muon neutrinos, which provided a model-independent proof of the oscillation of atmospheric neutrinos.

The LBL accelerator experiment KEK to Super-Kamiokande (K2K) [144] confirmed

[2] These results also confirmed the Mikheyev-Smirnov-Wolfenstein (MSW) effect [127], which describes matter enhanced neutrino oscillations.

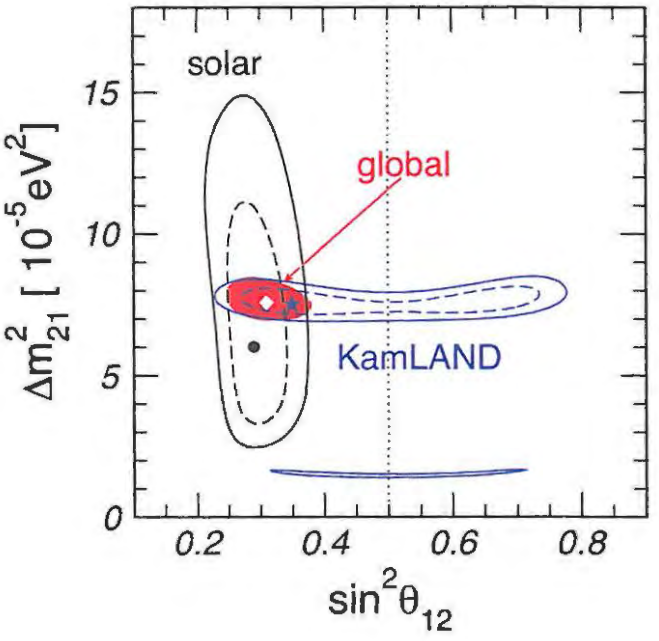

Figure 2.2: (From Ref. [26].) Determination of the leading "solar" parameters, with data from artificial and natural neutrino sources. The best fit points of the solar, KamLAND and global data are denoted by the dot, star and diamond, respectively.

the neutrino oscillation interpretation of the atmospheric neutrino data, observing the disappearance of accelerator muon neutrinos over 250 km. Fig. 2.3 presents the current constraints on the "atmospheric parameters" θ_{23} and Δm^2_{31}, with the combination of Super-Kamiokande and K2K data, along with the recent results from the Main Injector Neutrino Oscillation Search (MINOS) experiment [145–147].

In another effort to complete the global neutrino oscillation picture, future experiments such as the OPERA [148] and ICARUS [149] experiments of the CERN to Gran Sasso (CNGS) program will attempt a direct measurement of $\nu_\mu \rightarrow \nu_\tau$ oscillation, over a baseline of about 730 km. The Tokai to Kamioka (T2K) experiment [150] also aims to improve the precision of the atmospheric parameters.

2.4.3 Reactor neutrinos, CHOOZ and θ_{13}

The CHOOZ reactor experiment looked for the disappearance of electron antineutrinos at a distance of about 1 km, and the negative result [151–153] showed that the oscillations of electron neutrinos at the atmospheric scale of Δm^2 are small or zero (solar and atmospheric neutrino oscillations are practically decoupled). This implies that θ_{13} must be quite small, which means that observation of the CP violating phase

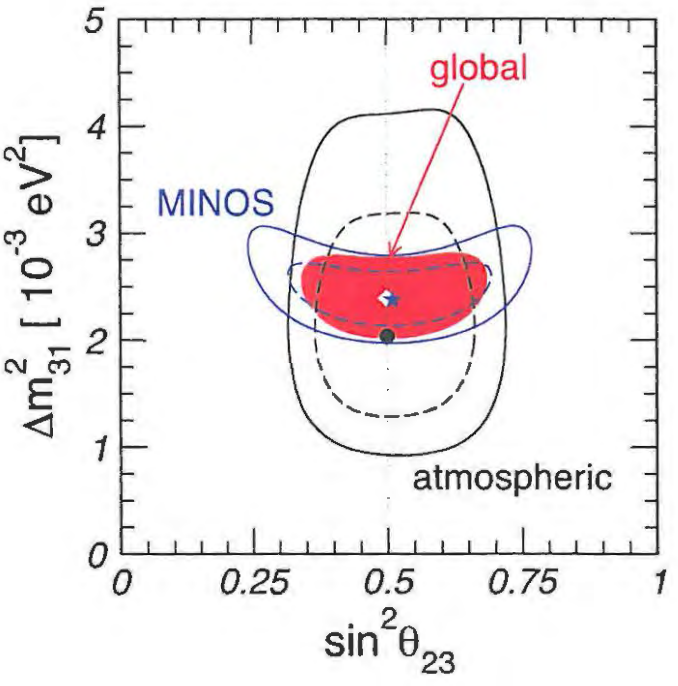

Figure 2.3: (From Ref. [26].) As for Fig. 2.2, but for "atmospheric" parameters. The best fit points of the atmospheric, MINOS and global data are denoted by the dot, star and diamond, respectively.

δ is rather difficult [Eq. (2.25)].

A recent analysis of neutrino oscillation data [25, 104], including the MINOS results [145–147], reveals two independent hints of $\theta_{13} > 0$ at the 1σ limit.[3] Ref. [155] demonstrates that a non-zero value of θ_{13} could account for the observed difference between the best fit values of the solar neutrino and KamLAND data. Future experiments, such as Double-CHOOZ [156, 157], T2K [150], NOνA [158, 159] and Daya Bay [160] will aim to measure θ_{13} with greater precision, as well as try to probe the value of the CP phase, δ.

2.4.4 LSND and MiniBooNE

The experimental results discussed so far are compatible with the standard three-neutrino mixing scheme presented in Section 2.3. However, the Liquid Scintillator Neutrino Detector (LSND) experiment claimed to observe SBL $\overline{\nu}_\mu \to \overline{\nu}_e$ oscillations at the $\Delta m^2 \sim 1\text{eV}^2$ scale [161, 162]. The related KArlsruhe Rutherford Medium Energy Neutrino experiment (KARMEN) experiment [163] did not see any indication for this

[3]Note that Ref. [154] regards the indication for $\theta_{13} > 0$ found in Ref. [104] as the result of statistical variations, which may or may not be confirmed by future experiments.

oscillation, but did not exclude the entire portion of the neutrino parameter space favoured by LSND.

The LSND result is not compatible with the two mass-squared differences in Table 2.1 and Fig. 2.1, and there have been various attempts to explain the LSND result with sterile neutrinos [164–166]. However, the recent MiniBooNE experiment [167–169] excludes the two-neutrino oscillation interpretation of LSND at 98% C.L. In spite of this, MiniBooNE also has an unexplained excess of low-energy events, and some proposed explanations include heavy neutrino decay [170], or sterile neutrinos [171]. Other ideas include models of energy dependent masses and mixings [172]. Ref. [171] finds that models with 3 + 2 sterile neutrinos may be favoured by both MiniBooNE and LSND, but there is significant tension between appearance and disappearance data, and Ref. [173] states that: "allowing for mixing with multiple sterile neutrino states or CP violation does not seem sufficient to allow incorporating all SBL experiments within a CPT-conserving, sterile neutrino oscillation framework."

2.5 Absolute neutrino mass

As stated in Section 2.3, the absolute neutrino mass scale is still an open question. The most sensitive ways to probe these masses are: (i) the observation of the end-point part of the electron spectrum in β-decay, (ii) the search for neutrinoless double beta decay and (iii) the observation of large-scale structures in the early universe. The past, present and future experimental efforts in this regard are reviewed below, with emphasis on the constraints these parameters place on neutrino mass models.

2.5.1 Beta decay

Studies of the electron energy spectrum in β-decay allow one to probe the quantity

$$m_\beta = \sqrt{\sum_{k=1}^{3} |U_{ek}|^2 m_k^2} \,, \tag{2.31}$$

where U_{ek} are the elements of the first row of the PMNS matrix in Eq. 2.25, and m_k are the light neutrino masses. m_β is referred to as the "effective electron neutrino mass in β-decay". The results of the Mainz [174] and Troitsk [175] Tritium β-decay experiments, with the combined analysis in Ref. [23, 176], give the upper limit (at the

2σ limit) of

$$m_\beta < 1.8 \text{ eV} . \tag{2.32}$$

The upcoming KATRIN experiment [177], with a sensitivity of $m_\beta \sim 0.3$ eV, will aim to constrain the absolute neutrino mass spectrum even further. Note that the "direct" search for neutrino mass in β-decay experiments is not sensitive to their Dirac or Majorana nature (see Section 3.2).

2.5.2 Neutrinoless double beta decay

Observation of the lepton number violating $0\nu\beta\beta$ decay ($\mathcal{N}(A,Z) \to \mathcal{N}(A,Z+2)+2e^-$) would imply that neutrinos are Majorana particles.[4] The amplitude for this process is proportional to the effective Majorana mass

$$\langle m_{ee} \rangle = \left| \sum_{k=1}^{3} U_{ek}^2 \, m_k \right| , \tag{2.33}$$

with U_{ek} and m_k as defined in Eq. (2.31). However, this definition depends on the nature of the physics beyond the SM, so that in principle other contributions to the term in Eq. (2.33) are possible. The Heidelberg-Moscow (HM) [178–180] and IGEX [181,182] groups conducted experiments with ^{76}Ge, and the resulting upper limit for $\langle m_{ee} \rangle$ was between about 0.3 eV and 1.3 eV. The CUORICINO [183] experiment (with ^{130}Te) gives the improved upper bound at 2σ of [25][5]

$$\langle m_{ee} \rangle < 0.23 - 0.85 \text{ eV} . \tag{2.34}$$

Although part of the HM collaboration claims a positive signal for $0\nu\beta\beta$ [179], this is still considered somewhat controversial [184,185], and requires independent confirmation. Future experiments such as CUORE [186,187], GERDA [188], NEMO [189–191] and Majorana [192,193] will attempt to improve the sensitivity of these measurements, down to about $\langle m_{ee} \rangle \sim 0.05$ eV.

[4] Refer to Section 3.2.2 for a discussion of Majorana neutrinos.

[5] The large uncertainty range comes from uncertainties in the nuclear matrix elements.

2.5.3 Neutrino masses from cosmology

The standard theory of large scale structure formation in the early universe places a strong bound on the sum of absolute neutrino masses

$$\sum m_\nu = |m_1| + |m_2| + |m_3| \,, \tag{2.35}$$

since neutrinos suppress the growth of fluctuations on scales below the horizon when they become non-relativistic [20,24]. The contribution of relic neutrinos to the density of the universe also places a limit on $\sum m_\nu$, though not as stringent as the bound from structure formation.

The latest data from the Wilkinson Microwave Anisotropy Probe (WMAP) [194, 195] constrains the sum of neutrino masses to $\sum m_\nu < 0.67$ eV, which, when combined with the observed mass-squared differences, gives an upper bound of about

$$|m_k| \lesssim 0.2 \text{ eV} \quad (k = 1, 2, 3) \tag{2.36}$$

for each individual neutrino mass. The Sloan Digital Sky Survey (SDSS) [196] reports a bound of $\sum m_\nu < 0.94$ eV, at 95% C.L.

2.5.4 Limits on mass parameters

The parameters $\langle m_{ee} \rangle$ and $\sum m_\nu$, discussed above, provide a model-independent test of neutrino mass models. Since these quantities both depend on the neutrino oscillation data, it is possible to find bounds in $\langle m_{ee} \rangle - \sum m_\nu$ parameter space (see Fig. 2.4). Combining this with limits from cosmological data and $0\nu\beta\beta$ decay experiments gives a well-defined region that is allowed. The variation between the solid (best fit) lines in Fig. 2.4 comes from the Majorana phases, with the additional variation (dashed and dotted lines) from the 3σ variation in oscillation data.

The analysis in Ref. [25] considers five different combinations of cosmological data in constraining $\sum m_\nu$; three of these are included as vertical lines in Fig. 2.4. The blue line represents cosmic microwave background (CMB) anisotropy data from the WMAP 5y [194, 195], ACBAR [197], VSA [198], CBI [199] and BOOMERANG [200] experiments; the green line includes the above CMB data plus data from the Hubble space telescope (HST) [201] as well as the luminosity distance SN-Ia data [202]; the violet line is a combination of CMB, HST, SN-Ia and BAO [203] data, as well as the primordial spectrum from Lyman-alpha (Lyα) forest clouds [204, 205].

The horizontal lines in Fig. 2.4 correspond to the HM $0\nu\beta\beta$ decay claim, which is

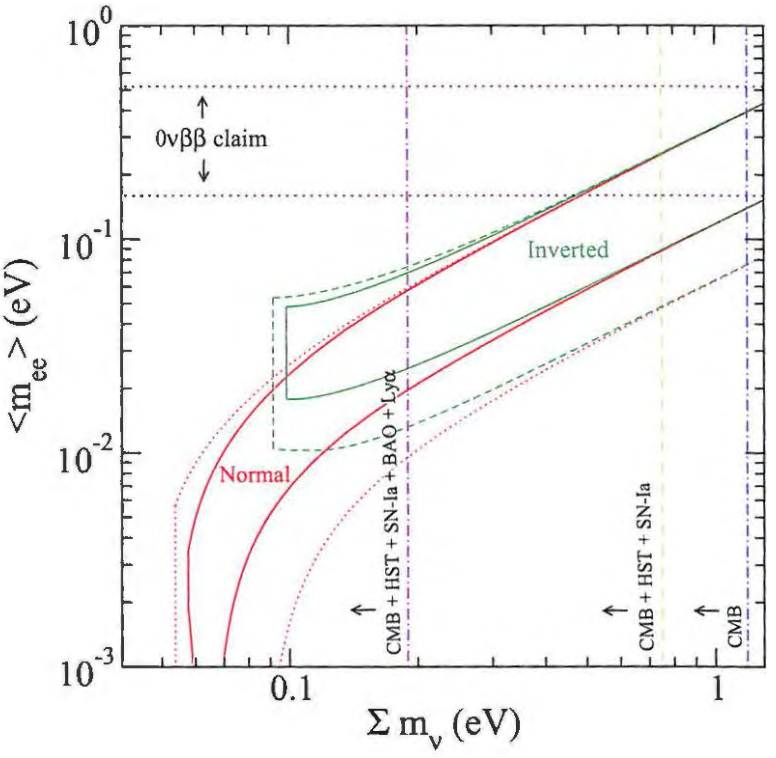

Figure 2.4: Allowed bands in the $\langle m_{ee} \rangle - \sum m_\nu$ parameter space, using the best fit (solid lines) and 3σ (dashed/dotted lines) values of the oscillation data, for normal (red) and inverted (green) neutrino mass hierarchies. Vertical lines show the cosmological constraints on the sum of neutrino masses, $\sum m_\nu$, taken from different data sets; horizontal lines give the range allowed by the Heidelberg-Moscow $0\nu\beta\beta$ claim [25].

subject to uncertainties in nuclear matrix elements [25]. A combination of the weakest limit on $\sum m_\nu$ (i.e. just the CMB data), the HM $0\nu\beta\beta$ claim and the global oscillation data reveals a small allowed region in $\langle m_{ee} \rangle - \sum m_\nu$ parameter space. The addition of further cosmological data (the green line in Fig. 2.4) constrains this allowed region even further, and with the Lyα data (the violet line in Fig. 2.4), this overlap disappears.

Chapter 3

Neutrino Mass and the Standard Model

3.1 Electroweak interactions in the Standard Model

Using the notation of Ref. [20], the Standard Model (SM) of particle physics is based on the symmetry group $SU(3)_C \times SU(2)_L \times U(1)_Y$, where C, L and Y denote colour, left-handed chirality and weak hypercharge, respectively. The number of vector gauge bosons is determined by the generators of the group, with eight massless gluons, three massive bosons ($W^{\pm}$ and Z) and a massless photon (γ) coming from the generators of $SU(3)_C$, $SU(2)_L$ and $U(1)_Y$ respectively. However, the Z boson and the photon are in fact linear combinations of the gauge bosons of $SU(2)_L$ and $U(1)_Y$, mixed by the Weinberg angle, θ_W. For this reason the electromagnetic and weak interactions are unified into the electroweak theory, based on the symmetry group $SU(2)_L \times U(1)_Y$. Since there is no mixing between the $SU(3)_C$ and $SU(2)_L \times U(1)_Y$ sectors, the electroweak interactions can be studied separately from the strong interactions. Neutrinos are leptons, so that they do not participate in strong interactions, and can be described by the SM electroweak theory.

The elementary fermions in the standard model are divided into two categories: quarks and leptons, and these in turn form three generations, shown in Table 3.1. Quarks participate in all the interactions of the SM (strong, weak, electromagnetic and gravitational), whereas leptons participate in all but strong interactions. Each fermion has a corresponding antifermion, with the same mass but opposite electric charge, and all are spin 1/2 particles.

The three generations of fermions can be defined as left-handed weak isospin dou-

Table 3.1: Classification of fermions in the Standard Model [20].

Generation	Quarks		Leptons	
1^{st}	u (up)	d (down)	ν_e (electron neutrino)	e (electron)
2^{nd}	c (charm)	s (strange)	ν_μ (muon neutrino)	μ (muon)
3^{rd}	t (top)	b (bottom)	ν_τ (tau neutrino)	e (tau)

blets

$$L'_{eL} \equiv \begin{pmatrix} \nu'_{eL} \\ e'_L \end{pmatrix}, \quad L'_{\mu L} \equiv \begin{pmatrix} \nu'_{\mu L} \\ \mu'_L \end{pmatrix}, \quad L'_{\tau L} \equiv \begin{pmatrix} \nu'_{\tau L} \\ \tau'_L \end{pmatrix}, \tag{3.1}$$

$$Q'_{1L} \equiv \begin{pmatrix} u'_L \\ d'_L \end{pmatrix}, \quad Q'_{2L} \equiv \begin{pmatrix} c'_L \\ s'_L \end{pmatrix}, \quad Q'_{3L} \equiv \begin{pmatrix} t'_L \\ b'_L \end{pmatrix}, \tag{3.2}$$

and right-handed singlets

$$\ell'_{eR} \equiv e'_R, \quad \ell'_{\mu R} \equiv \mu'_R, \quad \ell'_{\tau R} \equiv \tau'_R, \tag{3.3}$$

$$q'^U_{uR} \equiv u'_R, \quad q'^U_{cR} \equiv c'_R, \quad q'^U_{tR} \equiv t'_R, \tag{3.4}$$

$$q'^D_{dR} \equiv d'_R, \quad q'^D_{sR} \equiv s'_R, \quad q'^D_{bR} \equiv b'_R. \tag{3.5}$$

The electroweak SM Lagrangian is

$$\begin{aligned} \mathscr{L} = {} & \text{fermion kinetic terms} + \text{gauge boson kinetic terms} \\ & + \text{gauge boson self-couplings} + \text{Higgs Lagrangian} \\ & + \text{Higgs-fermion Yukawa coupling terms.} \end{aligned} \tag{3.6}$$

The last line in Eq. (3.6) comprises mass terms for the quarks and leptons: the lepton mass terms are given by

$$\mathscr{L}_{H,L} = -\sum_{\alpha,\beta=e,\mu\tau} \left(Y'^{\ell}_{\alpha\beta} \overline{L'_{\alpha L}} \Phi \ell'_{\beta R} + Y'^{\ell *}_{\alpha\beta} \overline{\ell'_{\beta R}} \Phi^\dagger L'_{\alpha L} \right), \tag{3.7}$$

where the SM Higgs field is represented by the doublet

$$\Phi(x) = \begin{pmatrix} \phi^+(x) \\ \phi^0(x) \end{pmatrix}, \tag{3.8}$$

and $Y'^{\ell}_{\alpha\beta}$ is a matrix of Yukawa coupling constants. The Higgs doublet in Eq. (3.8) contains two complex scalar fields: the charged field $\phi^+(x)$ and the neutral field $\phi^0(x)$.

The Higgs part of the electroweak Lagrangian in Eq. (3.6) is

$$\mathscr{L}_H = (D_\mu\Phi)^\dagger(D^\mu\Phi) - \mu^2\Phi^\dagger\Phi - \lambda(\Phi^\dagger\Phi)^2 \ , \tag{3.9}$$

where μ is a mass-like coefficient and λ is the coefficient of the quartic self-couplings of the Higgs fields. Although the Higgs Lagrangian in Eq. (3.9) is invariant under the symmetry $\mathrm{SU}(2)_L \times \mathrm{U}(1)_Y$, the mechanism of spontaneous symmetry breaking can generate mass terms for the Higgs field as well as for the gauge bosons and fermions. The vacuum expectation value (VEV) of the Higgs field is electrically neutral and is given by[1]

$$\langle\Phi\rangle = \frac{1}{\sqrt{2}}\begin{pmatrix}0\\ v\end{pmatrix}, \tag{3.10}$$

where $v \equiv \sqrt{-\frac{\mu^2}{\lambda}}$. The squared mass-like coefficient μ^2 is assumed to be negative, $\mu^2 < 0$, in order to generate a nonzero VEV. This causes the symmetry breaking

$$\mathrm{SU}(2)_L \times \mathrm{U}(1)_Y \rightarrow \mathrm{U}(1)_Q \ , \tag{3.11}$$

where $\mathrm{U}(1)_Q$ is the unbroken symmetry group of the electromagnetic interactions. Thus the symmetry is broken by the vacuum. The Higgs doublet in the unitary gauge is written as

$$\Phi(x) = \frac{1}{\sqrt{2}}\begin{pmatrix}0\\ v + H(x)\end{pmatrix}, \tag{3.12}$$

with the physical Higgs field desribed by $H(x)$. Upon spontaneous symmetry breaking, the coupling of the field in Eq. (3.12) with the fermion fields results in the masses of the charged fermions and the W and Z gauge bosons.

The fermion mass terms in Eq. (3.7) contain left- and right-handed fields,[2] and since there are no right-handed neutrino fields in the SM [Eqs. (3.3)–(3.5)], it follows that neutrinos remain massless in this model. However, this contradicts the evidence of neutrino oscillations presented in Chapter 2, and the SM must be extended to include massive neutrino fields. Although these have never been observed, they are introduced into most unified models [206].

[1]The VEV $\langle\Phi\rangle$ of the Higgs field corresponds to the lowest energy state of the Higgs potential, $V(\Phi) = \mu^2\Phi^\dagger\Phi + \lambda(\Phi^\dagger\Phi)^2$.

[2]Indeed, all fermion mass terms must involve a coupling of left- and right-handed fields.

3.2 Massive neutrinos

In the SM, the flavour neutrino fields ν_e, ν_μ, ν_τ are defined in order to couple with the corresponding charged lepton fields in the charged weak current in Eq. (2.1). Since the neutrinos are assumed to be massless, these flavour neutrino fields are also mass eigenstates (any linear combination of massless fields is also massless). However, due to the observed phenomenon of neutrino oscillations, the flavour neutrino fields become a mixture of mass eigenstates (Sections 2.1 and 3.2.6). These massive neutrinos can be either Dirac or Majorana particles, but the exact origin of this mass is not known.

3.2.1 Dirac neutrinos

Chirality, or handedness, is an important property of fermions. A spinor field ψ can be decomposed into its chiral components such that

$$\psi = \psi_R + \psi_L \ . \tag{3.13}$$

ψ_R and ψ_L denote right-handed and left-handed fields, respectively, which are obtained from the field ψ using the projection operators

$$P_R \equiv \frac{1+\gamma^5}{2} \tag{3.14}$$

$$P_L \equiv \frac{1-\gamma^5}{2} \ . \tag{3.15}$$

The chiral fields are also called Weyl spinors. Using the properties of the chirality matrix, γ^5, the Dirac Lagrangian may be written as [20]

$$\mathscr{L} = \overline{\psi_R}\, i\partial\!\!\!/\, \psi_R + \overline{\psi_L}\, i\partial\!\!\!/\, \psi_L - m\,(\overline{\psi_R}\,\psi_L + \overline{\psi_L}\psi_R) \ , \tag{3.16}$$

showing that the chiral fields are coupled only in the mass term, and the field equations become

$$i\partial\!\!\!/\psi_R = m\psi_L \tag{3.17}$$

$$i\partial\!\!\!/\psi_L = m\psi_R \ . \tag{3.18}$$

The Weyl spinors have only two independent components: assuming the chiral representation of the Dirac γ matrices, the four-component spinor may be expressed

as

$$\psi = \begin{pmatrix} \chi_R \\ \chi_L \end{pmatrix}, \tag{3.19}$$

so that

$$\psi_R = \begin{pmatrix} \chi_R \\ 0 \end{pmatrix}, \quad \psi_L = \begin{pmatrix} 0 \\ \chi_L \end{pmatrix}, \tag{3.20}$$

where χ_R and χ_L are two-component spinors.

In terms of χ_R and χ_L, the Dirac equation is

$$\begin{pmatrix} m & i(\partial_0 + \vec{\sigma} \cdot \vec{\nabla}) \\ i(\partial_0 - \vec{\sigma} \cdot \vec{\nabla}) & m \end{pmatrix} \begin{pmatrix} \chi_L \\ \chi_R \end{pmatrix} = 0 \tag{3.21}$$

For $m = 0$, the field equations become

$$i \partial\!\!\!/ \, \psi_R = 0 \,, \tag{3.22}$$

$$i \partial\!\!\!/ \, \psi_L = 0 \,, \tag{3.23}$$

and only one chiral field is needed to describe the massless fermion. In this case it is evident that chirality is equal to helicity, and it can be shown that a massless right-handed (left-handed) chiral field with definite four-momentum has positive (negative) helicity. Since the neutrino was originally considered to be massless, and as neutrinos are neutral particles, the helicity is the only property that enables one to distinguish between neutrinos (negative helicity) and antineutrinos (positive helicity).

Studies of inverse beta decay [207] have shown that neutrinos occur with spin antiparallel to momentum (negative helicity), whereas antineutrinos have spin parallel to momentum (positive helicity). This empirical evidence, combined with the theory of massless chiral fields, leads to the conclusion that neutrinos are massless. Note that the statement, "neutrinos are always left-handed" is strictly correct only if the rest-mass is exactly zero [207]. A non-zero neutrino mass allows one to find a Lorentz transformation that transforms a left-handed neutrino into a right-handed one.

3.2.2 Majorana neutrinos

The operation of charge conjugation transforms the spinor field ψ as

$$\psi(x) \xrightarrow{\mathrm{C}} \psi^{\mathrm{C}}(x) = \xi_{\mathrm{C}} \mathcal{C} \overline{\psi}^T(x) \,, \tag{3.24}$$

where C is the charge conjugation operator, with the defining property

$$C\gamma_\mu^T C^{-1} = -\gamma_\mu \quad \Longrightarrow \quad C^\dagger = C^{-1} \quad \text{and} \quad C^T = -C \; . \tag{3.25}$$

The coefficient ξ_C is a phase which represents the intrinsic charge parity of the field.

It was shown in Section 3.2.1 that it is possible to describe a massless field in terms of one chiral spinor with two components [Eqs. (3.22) and (3.23)]. Using the properties of the field under charge conjugation, Majorana showed [208] that a four-componenet spinor is not necessary to describe a massless field. In this case, Eqs. (3.17) and (3.18) become

$$i\,\gamma^\mu \partial_\mu \psi_L = m\, C\, \overline{\psi_L}^T \; , \tag{3.26}$$

known as the Majorana equation.

Since $\psi_R = C\,\overline{\psi_L}^T$, the Majorana condition is

$$\psi = C\,\overline{\psi}^T = \psi^C \; , \tag{3.27}$$

where ψ^C is just the charge conjugated field defined in Eq. (3.24). This implies that the particle and antiparticle are now indistinguishable. Neutrinos are the only neutral fundamental fermions, and may be candidates for Majorana particles. The Majorana theory has half the degrees of freedom of the Dirac theory, and thus most theories beyond the SM incorporate massive neutrinos as Majorana particles. Note that neutrino oscillations cannot determine the Dirac or Majorana nature of neutrinos; the only experimental signature of Majorana neutrinos is $0\nu\beta\beta$ decay, the search of which is continuing, and has yet to be observed (Section 2.5.2).

3.2.3 Dirac mass terms

A fermion mass term must contain left-handed and right-handed fields (Section 3.1). This means that Dirac masses can in theory be generated by the SM Higgs mechanism, with the addition of right-handed neutrino fields, $\nu_{\alpha R}$ ($\alpha = e, \mu, \tau$). These right-handed fields are singlets of $\mathrm{SU}(3)_C \times \mathrm{SU}(2)_L$, with hypercharge $Y = 0$. Therefore, they do not participate in weak interactions and are termed "sterile" (their only interaction is gravitational), whereas the SM left-handed neutrino fields do participate in weak interactions and are termed "active". Ref. [209] distinguishes between "fully sterile" and "weakly sterile" neutrinos: the former feel no gauge interactions, including forces postulated in theories beyond the SM, while the latter do not feel SM interactions. Since these particles have no real interactions one can also speculate whether they

are heavy or light. The seesaw mechanism favours heavy sterile neutrinos, whereas light sterile neutrinos could have implications for cosmology: a significant light sterile neutrino component would increase the standard expansion rate of the universe during Big Bang Nucleosynthesis (BBN) [209].

It is interesting to note that, in principle, an arbitrary number of sterile right-handed neutrino fields could be added to the SM. Since these fields are singlets they are not constrained by the symmetries of the SM. The "minimally extended Standard Model" contains three right-handed neutrino fields, but in fact only one such neutrino need be added. There are also models with two [210], four [211,212] or five [213] heavy neutrinos.

To generate Dirac masses in the minimally extended SM, another term is added to the Higgs-lepton Yukawa Lagrangian in Eq. (3.7), so that

$$\mathscr{L}_{H,L} = -\sum_{\alpha,\beta=e,\mu,\tau} Y^{\prime\ell}_{\alpha\beta}\overline{L_{\alpha L}}\Phi\ell'_{\beta R} - \sum_{\alpha,\beta=e,\mu,\tau} Y^{\prime\nu}_{\alpha\beta}\overline{L_{\alpha L}}\tilde{\Phi}\nu'_{\beta R} + \text{h.c}\ , \tag{3.28}$$

where Y'^{ν} is a matrix of Yukawa couplings for the neutrino. The term $\tilde{\Phi} = i\sigma_2\Phi^*$ appears in Eq. (3.28) to ensure invariance under the electroweak symmetry. To find the massive fields, the matrices Y'^{ℓ} and Y'^{ν} must be diagonalised, *viz.*

$$\begin{aligned} V_L^{\ell\dagger}Y'^{\ell}V_R^{\ell} &= Y^{\ell}, \quad \text{with} \quad Y^{\ell}_{\alpha\beta} = y^{\ell}_{\alpha}\delta_{\alpha\beta} \quad (\alpha,\beta = e,\mu,\tau) \\ \text{and} \quad V_L^{\nu\dagger}Y'^{\nu}V_R^{\nu} &= Y^{\nu}, \quad \text{with} \quad Y^{\nu}_{\alpha\beta} = y^{\nu}_{\alpha}\delta_{\alpha\beta} \quad (\alpha,\beta = e,\mu,\tau)\ , \end{aligned} \tag{3.29}$$

with the 3×3 unitary matrices V_L^{ℓ}, V_R^{ℓ}, V_L^{ν} and V_R^{ν}.

By defining the arrays of left- and right-handed leptons

$$\ell'_L \equiv \begin{pmatrix} e'_L \\ \mu'_L \\ \tau'_L \end{pmatrix}, \qquad \ell'_R \equiv \begin{pmatrix} e'_R \\ \mu'_R \\ \tau'_R \end{pmatrix}, \tag{3.30}$$

$$\nu'_L \equiv \begin{pmatrix} \nu'_{eL} \\ \nu'_{\mu L} \\ \nu'_{\tau L} \end{pmatrix}, \qquad \nu'_R \equiv \begin{pmatrix} \nu'_{eR} \\ \nu'_{\mu R} \\ \nu'_{\tau R} \end{pmatrix}, \tag{3.31}$$

and arrays of massive leptons

$$\boldsymbol{\ell}_L = V_L^{\ell\dagger}\boldsymbol{\ell}'_L \equiv \begin{pmatrix} e_L \\ \mu_L \\ \tau_L \end{pmatrix}, \qquad \boldsymbol{\ell}_R = V_R^{\ell\dagger}\boldsymbol{\ell}'_R \equiv \begin{pmatrix} e_R \\ \mu_R \\ \tau_R \end{pmatrix}, \tag{3.32}$$

$$\boldsymbol{n}_L = V_L^{\nu\dagger}\boldsymbol{\nu}'_L \equiv \begin{pmatrix} \nu_{1L} \\ \nu_{2L} \\ \nu_{3L} \end{pmatrix}, \qquad \boldsymbol{n}_R = V_R^{\nu\dagger}\boldsymbol{\nu}'_R \equiv \begin{pmatrix} \nu_{1R} \\ \nu_{2R} \\ \nu_{3R} \end{pmatrix}, \tag{3.33}$$

the Lagrangian in Eq. (3.28) can be written (in the unitary gauge) as

$$\begin{aligned} \mathscr{L}_{H,L} \;=\; & -\left(\frac{v+H}{\sqrt{2}}\right)\left[\overline{\boldsymbol{\ell}_L} Y^{\ell} \boldsymbol{\ell}_R + \overline{\boldsymbol{n}_L} Y^{\nu} \boldsymbol{n}_R\right] + \text{h.c.} \\ & -\left(\frac{v+H}{\sqrt{2}}\right)\left[\sum_{\alpha=e,\mu,\tau} y_\alpha^{\ell}\overline{\ell_{\alpha L}}\ell_R + \sum_{k=1}^{3} y_k^{\nu}\overline{\nu_{kL}}\nu_{kR}\right] + \text{h.c.} \end{aligned} \tag{3.34}$$

The charged lepton masses are

$$m_\alpha = \frac{y_\alpha^{\ell} v}{\sqrt{2}} \quad (\alpha = e, \mu, \tau)\,, \tag{3.35}$$

and with the Dirac neutrino fields defined as

$$\nu_k = \nu_{kL} + \nu_{kR} \qquad (k = 1, 2, 3), \tag{3.36}$$

the neutrino masses are given by

$$m_k = \frac{y_k^{\nu} v}{\sqrt{2}} \qquad (k = 1, 2, 3). \tag{3.37}$$

This shows that, with the addition of right-handed neutrinos, both charged leptons and neutrinos can have Dirac mass terms. Since the SM Higgs mechanism does not set any value for the Yukawa couplings with the Higgs particle for all particles, there is no explanation as to the values of the quark and lepton masses. The smallness of neutrino masses points to new physics beyond the SM, and the see-saw mechanism (Section 3.2.7) is one way to explain this.

3.2.4 Majorana mass terms

Defining the right-handed charge conjugated neutrino field

$$\nu_L^C \equiv C\,\overline{\nu_L}^T, \tag{3.38}$$

the Lagrangian becomes [20]

$$\mathscr{L}^{\mathrm{M}} = \frac{1}{2}\left[\overline{\nu_L} i\partial\!\!\!/ \nu_L + \overline{\nu_L^C} i\partial\!\!\!/ \nu_L^C - m\left(\overline{\nu_L^C}\nu_L + \overline{\nu_L}\nu_L^C\right)\right], \tag{3.39}$$

which is Lorentz invariant and desribes the Majorana field with the equation

$$i\partial\!\!\!/\,\nu_L = m C\,\overline{\nu_L}^T. \tag{3.40}$$

The mass term

$$\mathscr{L}^{\mathrm{M}}_{\mathrm{mass}} = -\frac{1}{2} m\,\overline{\nu_L^C}\nu_L + \mathrm{h.c.} \tag{3.41}$$

can also be written as

$$\mathscr{L}^{\mathrm{M}}_{\mathrm{mass}} = -\frac{m}{2}(-\nu_L^T C^\dagger \nu_L + \overline{\nu_L} C \overline{\nu_L}^T)\,. \tag{3.42}$$

It is important to note that ν_L^C is right-handed, so that the coupling $\overline{\nu_L^C}\nu_L$ does not vanish and forms part of the mass term (remember that fermion mass terms require a coupling of left- and right-handed fields).

If three generations of massive Majorana neutrinos are assumed, it is possible to write the three-generation Majorana Lagrangian as

$$\mathscr{L}^{\mathrm{M}} = \frac{1}{2}\sum_{k=1}^{3} \overline{\nu_k}\left(i\partial\!\!\!/ - m_k\right)\nu_k = \frac{1}{2}\overline{\boldsymbol{n}}\left(i\partial\!\!\!/ - M\right)\boldsymbol{n}, \tag{3.43}$$

with the column of massive neutrino fields

$$\boldsymbol{n} = \begin{pmatrix} \nu_1 \\ \nu_2 \\ \nu_3 \end{pmatrix}, \tag{3.44}$$

and M the diagonal mass matrix, obtained by diagonalising the original symmetric mass matrix in the flavour basis. This process is similar to the one outlined in Section 3.2.3, where a unitary matrix can be chosen to diagonalise the symmetric mass

matrix. It is this unitary matrix which changes the basis and leads to neutrino mixing between the flavour and mass eigenstates.

Note that in the case of both Dirac and Majorana neutrinos, the leptonic charged-current of Eq. (2.1) can be written as

$$j^{\rho}_{W,L} = 2\overline{n_L} U^{\dagger} \gamma^{\rho} \ell_L \ , \tag{3.45}$$

with the mixing matrix U given by

$$U = V_L^{\ell\dagger} V_L^{\nu} \ . \tag{3.46}$$

This shows that the mixing originates from both the charged lepton and neutrino sectors.

3.2.5 Effective Majorana mass

Since the Majorana mass term in Eq. (3.41) only involves the left-handed chiral field ν_L, one may ask whether it is possible for Majorana masses to be accommodated in the SM. A closer look at the term $\overline{\nu_L^C}\nu_L$ reveals that it has the third component of weak isospin $I_3 = 1$ and hypercharge $Y = -2$, which is not acceptable in the framework of the SM (there is no weak isospin triplet with $Y = 2$ in the Standard Model).

It is possible, however, to construct a non-renormalisable Lagrangian term that is invariant under $\mathrm{SU}(2)_L \times \mathrm{U}(1)_Y$ and generates Majorana neutrino mass [19, 20]. The lowest dimensional term is the lepton number violating term

$$\mathscr{L}_5 = \frac{g}{\mathcal{M}} (L_L^T \sigma_2 \Phi) C^{\dagger} (\Phi^T \sigma_2 L_L) + \mathrm{h.c.}, \tag{3.47}$$

where g is a dimensionless constant and $\mathcal{M}$ is a constant with dimension of mass. The doublet L_L is the SM lepton doublet in Eq. (3.1), and Φ is the Higgs doublet in Eq. (3.8).

Electroweak symmetry breaking (Section 3.1) generates the Majorana mass term

$$\mathscr{L}^{\mathrm{M}}_{\mathrm{mass}} = \frac{1}{2} \frac{gv^2}{\mathcal{M}} \nu_L^T C^{\dagger} \nu_L + \mathrm{h.c.} \ , \tag{3.48}$$

which gives the field ν_L the Majorana mass

$$m = \frac{gv^2}{\mathcal{M}} \ . \tag{3.49}$$

The Lagrangian in Eq. (3.47) is not renormalisable, so that it cannot exist in the SM. It can, however, be accommodated in theories that regard the SM as an effective low-energy theory: the product of the symmetry breaking of a high-energy unified theory. The Lagrangian is then referred to as an "effective dimension-five operator" [19]. This shows that the physics of neutrino masses provides an accessible "low energy window" on new physics beyond the SM [20]. We note that the Majorana mass in Eq. (3.49) is similar in structure to the mass obtained via the seesaw mechanism, to be discussed in Section 3.2.7 – the heavier the mass $\mathcal{M}$, the lighter the neutrino mass m.

3.2.6 Dirac-Majorana masses and mixing

It is possible to construct Dirac and Majorana mass terms for the neutrino, respectively, as was shown in Sections 3.2.3 and 3.2.4. Right-handed neutrino singlets were added in the Dirac model [Eq. (3.31)], while in the Majorana case the right-handed charge conjugated field was assumed [Eq. (3.38)]. In the general case the Dirac-Majorana mass term can be formed, *viz.*

$$\mathscr{L}^{\mathrm{D+M}}_{\mathrm{mass}} = \mathscr{L}^{L}_{\mathrm{mass}} + \mathscr{L}^{R}_{\mathrm{mass}} + \mathscr{L}^{\mathrm{D}}_{\mathrm{mass}} \,, \tag{3.50}$$

with the two Majorana mass terms

$$\mathscr{L}^{L}_{\mathrm{mass}} = \frac{1}{2} \sum_{\alpha,\beta=e,\mu,\tau} \nu'^{T}_{\alpha L} C^{\dagger} M^{L}_{\alpha\beta} \nu'_{\beta L} + \mathrm{h.c.} \,, \tag{3.51}$$

$$\mathscr{L}^{R}_{\mathrm{mass}} = \frac{1}{2} \sum_{s,s'=s_1,\ldots,s_{N_s}} \nu'^{T}_{sR} C^{\dagger} M^{R}_{ss'} \nu'_{s'R} + \mathrm{h.c.} \,, \tag{3.52}$$

and the Dirac mass term

$$\mathscr{L}^{\mathrm{D}}_{\mathrm{mass}} = - \sum_{s,s'=s_1,\ldots,s_{N_s}} \sum_{\alpha=e,\mu,\tau} \overline{\nu_{sR}} M^{\mathrm{D}}_{s\alpha} \nu'_{\alpha L} + \mathrm{h.c.} \tag{3.53}$$

Since the right-handed fields are sterile singlets, it is possible to add an arbitrary number N_s of right-handed neutrinos ν_{sR} ($s = s_1, \ldots, s_{N_s}$) to the SM without creating anomalies (see Section 3.2.3). The three matrices M^L, M^R and M^{D} are complex, and the Majorana mass matrices M^L and M^R are symmetric [20]. M^L is a 3×3 matrix, M^R is an $N_s \times N_s$ matrix and M^{D} is an $N_s \times 3$ matrix.

In order to find the neutrino fields with definite masses, the Dirac-Majorana mass term $\mathscr{L}^{\mathrm{D+M}}_{\mathrm{mass}}$ must be diagonalised. The column matrix of $N = 3 + N_s$ left-handed fields

is defined as

$$\boldsymbol{N}'_L \equiv \begin{pmatrix} \boldsymbol{\nu}'_L \\ \boldsymbol{\nu}^C_R \end{pmatrix}, \tag{3.54}$$

with $\boldsymbol{\nu}'_L$ defined in Eq. (3.31) and the column matrix of right-handed sterile neutrinos

$$\boldsymbol{\nu}^C_R \equiv \begin{pmatrix} \nu^C_{s_1 R} \\ \vdots \\ \nu^C_{s_{N_s} R} \end{pmatrix}. \tag{3.55}$$

After some matrix algebra, the Dirac-Majorana mass term can be written in the form

$$\mathscr{L}^{\mathrm{D+M}}_{\mathrm{mass}} = \frac{1}{2} \boldsymbol{N}'^T_L \mathcal{C}^\dagger M^{\mathrm{D+M}} \boldsymbol{N}'_L + \mathrm{h.c.}, \tag{3.56}$$

with the $N \times N$ symmetric mass matrix

$$M^{\mathrm{D+M}} \equiv \begin{pmatrix} M^L & M^{\mathrm{D}^T} \\ M^{\mathrm{D}} & M^R \end{pmatrix}. \tag{3.57}$$

In order to diagonalise the Dirac-Majorana mass term, a unitary matrix V^ν_L is chosen, so that the left-handed fields in Eq. (3.54) can be written in terms of the components of fields with definite mass,

$$\boldsymbol{N}'_L = V^\nu_L \boldsymbol{n}_L \ , \quad \text{with} \quad \boldsymbol{n}_L = \begin{pmatrix} \nu_{1L} \\ \vdots \\ \nu_{NL} \end{pmatrix}, \tag{3.58}$$

and V^ν_L diagonalises the matrix $M^{\mathrm{D+M}}$, *viz.*

$$(V^\nu_L)^T M^{\mathrm{D+M}} V^\nu_L = M, \tag{3.59}$$

where $M_{kj} = m_k \delta_{kj}$ $(k, j = 1, \ldots, N)$, and m_k are real and positive neutrino masses. Using this procedure the Dirac-Majorana mass term in Eq. (3.56) can be rewritten as

$$\begin{aligned} \mathscr{L}^{\mathrm{D+M}}_{\mathrm{mass}} &= -\frac{1}{2} \overline{\boldsymbol{n}^C_L} M \boldsymbol{n}_L + \mathrm{h.c.} \\ &= -\frac{1}{2} \sum_{k=1}^{N} m_k \overline{\nu^C_{kL}} \nu_{kL} + \mathrm{h.c.} \ , \end{aligned} \tag{3.60}$$

which is a sum of Majorana mass terms for the massive Majorana fields

$$\nu_k = \nu_{kL} + \nu_{kL}^C \qquad (k = 1, \ldots, N)\,, \tag{3.61}$$

satisfying the constraint

$$\nu_k^C = \nu_k\ . \tag{3.62}$$

This shows that by diagonalising a general Dirac-Majorana mass term one arrives at the Majorana condition: in this case the massive neutrinos are Majorana particles.

The SM does not accommodate neutrino mixing (since neutrinos are massless), and so the mass and flavour eigenstates are equivalent. In the case of massive neutrinos, however, the leptonic charged-current of Eq. (2.1) becomes

$$j^\rho_{W,L} = 2\overline{\boldsymbol{n}_L} U^\dagger \gamma^\rho \boldsymbol{\ell}_L\ , \tag{3.63}$$

with the mixing matrix U given by

$$U_{\alpha k} = \sum_{\beta=e,\mu,\tau} (V_L^{\ell\dagger})_{\alpha\beta} (V_L^\nu)_{\beta k}\ . \tag{3.64}$$

The matrix V_L^ℓ is the unitary 3×3 matrix defined in Eq. (3.29), whereas the matrix V_L^ν is a unitary $N \times N$ matrix. This makes the mixing matrix U in Eq. (3.64) a rectangular $3 \times N$ matrix, which is not unitary.

From Eqs. (3.54), (3.55) and (3.58), it is evident that active-sterile mixing is possible: this is given by

$$\nu_{\alpha L} = \sum_{k=1}^{N} U_{\alpha k} \nu_{kL} \qquad (\alpha = e, \mu, \tau), \tag{3.65}$$

$$\nu_{sR}^C = \sum_{k=1}^{N} (V_L^\nu)_{sk} \nu_{kL} \quad (s = s_1, \ldots, s_{N_s}). \tag{3.66}$$

In some models of neutrino mass the charged lepton mass matrix is considered to be diagonal [214], so the matrix $V_L^{\ell\dagger}$ falls away in Eq. (3.64), and the mixing comes solely from the neutrino sector. The addition of an arbitrary number of sterile neutrinos is a purely theoretical idea [215], but a symmetric extension to the SM should contain only three such right-handed neutrino singlets. In this case and with the possibility of active-sterile mixing, $N_s = 3$ and $N = 6$, so that the mixing matrix U in Eq. (3.64) is a 3×6 matrix and the mass matrix in Eq. (3.57) is a 6×6 matrix.

3.2.7 The seesaw mechanism

The Dirac-Majorana mass matrix in Eq. (3.57) with $M^L = 0$ is

$$M^{\mathrm{D+M}} = \begin{pmatrix} 0 & M^{\mathrm{D}^T} \\ M^{\mathrm{D}} & M^R \end{pmatrix} , \tag{3.67}$$

and with the assumption

$$M^{\mathrm{D}}_{ij} \ll M^R_{ij} , \tag{3.68}$$

the elements of the Dirac mass matrix are much smaller than the elements of the right-handed Majorana mass matrix. This is the type I seesaw mechanism [216–220].

A Majorana mass term for left-handed neutrinos is forbidden by the SM, hence $M^L = 0$ may be assumed. Since Dirac masses are generated by the Higgs mechanism, the elements of M^{D} are expected to be of the order of the electroweak symmetry breaking scale (10^2 GeV), so that Dirac masses are protected by the SM symmetries. The right-handed fields are singlets of the SM, implying that the elements of M^R are not protected by the SM symmetries, and the masses of the right-handed neutrinos may be generated by new physics beyond the SM.

Ref. [20] shows that the mass matrix in Eq. (3.67) can be diagonalized by blocks, up to corrections of the order $(M^R)^{-1}M^{\mathrm{D}}$:

$$W^T M^{\mathrm{D+M}} W \simeq \begin{pmatrix} M_{\mathrm{light}} & 0 \\ 0 & M_{\mathrm{heavy}} \end{pmatrix} , \tag{3.69}$$

with

$$W \simeq \begin{pmatrix} 1 - \frac{1}{2} M^{\mathrm{D}\dagger} (M^R M^{R\dagger})^{-1} M^{\mathrm{D}} & [(M^R)^{-1} M^{\mathrm{D}}]^\dagger \\ -(M^R)^{-1} M^{\mathrm{D}} & 1 - \frac{1}{2} (M^R)^{-1} M^{\mathrm{D}} M^{\mathrm{D}\dagger} (M^{R\dagger})^{-1} \end{pmatrix} . \tag{3.70}$$

After diagonalization, a light 3×3 mass matrix, M_{light}, and a heavy $N_s \times N_s$ mass matrix, M_{heavy}, are obtained, *viz.*

$$M_{\mathrm{light}} \simeq -M^{\mathrm{D}^T} (M^R)^{-1} M^{\mathrm{D}}, \quad M_{\mathrm{heavy}} \simeq M^R. \tag{3.71}$$

The eigenvalues of M^R give the masses of the heavy neutrinos, whereas the eigenvalues of M_{light} are the light neutrino masses. The light masses are suppressed with respect to the elements of M^{D} by the factor M^{D^T}. The expression for M_{light} in Eq. (3.71) is similar to that obtained in Eq. (3.49) with the dimension-five operator. In an al-

ternative derivation of the see-saw mechanism [20, 214], the right-handed chiral field can be integrated away from a standard Dirac-Majorana mass term with $M^L = 0$, leading to a dimension-five operator and ultimately the same see-saw formula as in Eqs. (3.49) and (3.71).

It is also possible to generate the dimension-five operator in Eq. (3.47) by the exchange of heavy Higgs triplets, $\Delta \sim (1,3,1)$ of $SU(2)_L$, without introducing new right-handed neutrino states. These can be written in the matrix representation as [221, 222]

$$\Delta = \begin{pmatrix} \Delta^0 & -\Delta^+/\sqrt{2} \\ -\Delta^+/\sqrt{2} & -\Delta^{++} \end{pmatrix} . \tag{3.72}$$

This case is referred to as the type II see-saw mechanism [29]. The neutrino mass term comes from the Lagrangian

$$\mathscr{L}_{\text{type II}} = -f_\Delta L_L^T \Delta L_L - V(\Phi, \Delta) , \tag{3.73}$$

where the scalar potential contains additional interaction terms. The non-zero VEV of Δ gives a neutrino mass term of the form

$$M^L = f_\Delta \langle \Delta \rangle . \tag{3.74}$$

In this case, the elements of M^L are non-zero, but much smaller than the other elements of $M^{\text{D+M}}$, resulting in the light neutrino mass matrix

$$M_{\text{light}} = M^L - M^{\text{D}^T} (M^R)^{-1} M^{\text{D}} . \tag{3.75}$$

Another alternative is the type III seesaw mechanism [223], in which heavy triplet fermions couple with the SM lepton doublets, generating light seesaw neutrino masses. In this model the SM Higgs sector is unchanged, and a set of self-conjugate $SU(2)_L$ triplets of exotic leptons is introduced.

The seesaw mechanisms described above can be incorporated into flavour symmetry models of neutrino mass.

3.3 Neutrino mixing

As discussed in Section 3.2.6, the addition of massive neutrinos to the SM creates the phenomenon of neutrino mixing: the charged-current in Eq. (3.63) contains the mixing matrix U defined in Eq. (3.64). This mixing is analogous to the mixing observed in

the quark sector, and the matrix U can be likened to the CKM matrix. Henceforth, the active-sterile mixing in Eqs. (3.65) and (3.66) will not be considered, so that the matrix U is assumed to be a 3×3 unitary matrix mixing active neutrino states, as in Eq. (3.46).

The mixing matrix U can be parameterised in terms of three mixing angles and one Dirac phase [Eq. (2.25)], and the oscillation experiments described in Section 2.4 measure these mixing angles. There are certain special cases of neutrino mixing, which will be relevant for the subsequent discussion of flavour symmetry models of neutrino mass.

If the absolute values of all the elements of the mixing matrix U are equal, the mixing is termed "trimaximal". Since U is unitary,

$$\sum_k |U_{\alpha k}|^2 = 1, \quad \text{and} \quad \sum_\alpha |U_{\alpha k}|^2 = 1, \tag{3.76}$$

which means that the absolute value of every element is

$$|U_{\alpha k}| = \frac{1}{\sqrt{3}} \,. \tag{3.77}$$

Wolfenstein [224] shows that a real mixing matrix cannot satisfy the requirement in Eq. (3.77) – CP violation is necessary for trimaximal mixing. This can be obtained for $\theta_{12} = \theta_{23} = \pi/4$, $s_{13} = 1/\sqrt{3}$ and $\sin\delta_{13} = \pm 1$, which in the parameterisation of Eq. (2.25) is [20]

$$U^D = \begin{pmatrix} \frac{1}{\sqrt{3}} & \frac{1}{\sqrt{3}} & \mp\frac{i}{\sqrt{3}} \\ -\frac{1}{2} \mp \frac{i}{2\sqrt{3}} & \frac{1}{2} \mp \frac{i}{2\sqrt{3}} & \frac{1}{\sqrt{3}} \\ \frac{1}{2} \mp \frac{i}{2\sqrt{3}} & -\frac{1}{2} \mp \frac{i}{2\sqrt{3}} & \frac{1}{\sqrt{3}} \end{pmatrix} = \frac{1}{\sqrt{3}} \begin{pmatrix} 1 & 1 & \mp i \\ e^{\mp i5\pi/6} & e^{\mp i\pi/6} & 1 \\ e^{\mp i\pi/6} & e^{\mp i5\pi/6} & 1 \end{pmatrix}, \tag{3.78}$$

where U^D is the Dirac part of the mixing matrix.

In this case, there is maximal CP violation, and the Jarlskog invariant in Eq. (2.26) is given by

$$J_{CP} = \pm\frac{1}{6\sqrt{3}} \,, \tag{3.79}$$

so that $|J_{CP}|$ takes its maximal value. Ref. [20] describes the permutation symmetry of a trimaximal Dirac mixing matrix: it is physically invariant under cyclic permutations of the columns and of the rows, but the exchange of two columns or two rows transforms one matrix into another, with the opposite Jarlskog invariant.

If there is maximal mixing in both the 2-3 and 1-2 sectors, then the mixing matrix

is termed "bimaximal", defined by

$$U_{BM} = U_{23}^{M} U_{12}^{M}, \tag{3.80}$$

where U_{23}^{M} and U_{12}^{M} are the matrices of the maximal ($\pi/4$) rotations in the 2-3 and 1-2 subspaces respectively. This gives the mixing matrix [29]

$$U_{BM} \equiv \begin{pmatrix} \frac{1}{\sqrt{2}} & \frac{1}{\sqrt{2}} & 0 \\ -\frac{1}{2} & \frac{1}{2} & \frac{1}{\sqrt{2}} \\ \frac{1}{2} & -\frac{1}{2} & \frac{1}{\sqrt{2}} \end{pmatrix}. \tag{3.81}$$

The original trimaximal model is inconsistent with the atmospheric neutrino data (Section 2.4), which points to "twofold" maximal $\nu_\mu - \nu_\tau$ mixing. Combining the results of solar, atmospheric and reactor experiments, the following assumptions give an adequate description of the data [27]:

$$|U_{e3}| \equiv 0, \quad |U_{\mu 3}|^2 \equiv 1/2, \quad |U_{e2}|^2 \equiv 1/3. \tag{3.82}$$

These three values, combined with the unitarity and orthogonality of U, constrain the matrix to the tri-bimaximal mixing (TBM) form,

$$U_{TBM} \equiv \begin{pmatrix} \frac{2}{\sqrt{6}} & \frac{1}{\sqrt{3}} & 0 \\ -\frac{1}{\sqrt{6}} & \frac{1}{\sqrt{3}} & \frac{1}{\sqrt{2}} \\ -\frac{1}{\sqrt{6}} & \frac{1}{\sqrt{3}} & -\frac{1}{\sqrt{2}} \end{pmatrix}. \tag{3.83}$$

In this mixing scheme the ν_3 is bimaximally mixed and the ν_2 trimaximally mixed, hence "tri-bimaximal" mixing. Ref. [27] presents a simple model of mass matrices to generate TBM.

The form of the TBM matrix in Eq. (3.83) implies that the mixing angles are independent of the mass eigenvalues, which means that the neutrino mass matrix must be "form-diagonalisable": the diagonalisation matrix depends only on the *form* of the mass matrix [225–227]. Indeed, mass matrices of the form

$$M_\nu = \begin{pmatrix} x & y & y \\ y & x+v & y-v \\ y & y-v & x+v \end{pmatrix} \tag{3.84}$$

generate TBM [228], a unique structure that could imply an underlying symmetry.

This is the subject of the remainder of this thesis.

Chapter 4

Symmetries and Neutrino Mass Models

4.1 Introduction to flavour symmetry models

The experimental efforts of the last decade (Section 2.4) have shown that neutrinos do mix, and the mixing angles have been determined to a great degree of accuracy. The question is whether the elements of the mixing matrix U_{PMNS}, and ultimately the elements of the lepton mass matrices, are simply random numbers or whether they point to some deeper structure or symmetry. It is natural to imagine that there is a family (flavour) symmetry that links the three lepton families [74]. An early discussion of family symmetry can be found in Ref. [229].

Following Ref. [225], it is evident from Eq. (3.64) that the lepton mixing matrix U_{PMNS} depends on mixing in both the charged lepton and neutrino sectors. That is expressed as the product,

$$U_{PMNS} = V_L^{\ell\dagger} V_L^{\nu} \ . \tag{4.1}$$

The unitary matrices V_L^{ℓ} and V_L^{ν} diagonalise the charged lepton and neutrino mass matrices respectively, *viz.*

$$V_L^{\ell\dagger} M_\ell V_R^{\ell} = m_\alpha \delta_{kj} \ , \tag{4.2}$$

$$V_L^{\nu\dagger} M_\nu V_R^{\nu *} = m_k \delta_{kj} \ , \tag{4.3}$$

where m_α ($\alpha = e, \mu, \tau$) and m_k ($k = 1, 2, 3$) are the charged lepton and neutrino masses, respectively.

The SM symmetries discussed in Section 3.1 do not constrain the form of the mass

matrices; the matrix M_ℓ can be any 3×3 matrix, and for Majorana neutrinos M_ν must be symmetric (Section 3.2.6). The addition of a family symmetry, G_{family}, extends the SM symmetries to

$$G = SU(3)_C \times SU(2)_L \times U(1)_Y \times G_{\text{family}} \ , \tag{4.4}$$

which constrains the mass matrices further, requiring that the Lagrangian remain invariant under the following transformations of the three generations of left-handed lepton doublets, right-handed charged lepton singlets and (if appropriate), right-handed Majorana neutrinos:

$$L_L \to X_L L_L \ , \quad \ell_R \to X_R \ell_R \ , \quad \nu_R \to X_\nu \nu_R \ . \tag{4.5}$$

The unitary matrices X_ν, X_L and X_R will belong to a representation of some symmetry group (G_{family}), thus constraining the form of the mass matrices by

$$M_\nu^{\text{R}} = X_\nu^\dagger M_\nu^{\text{R}} X_\nu^* \, , \tag{4.6}$$

$$M_\nu^{\text{D}} = X_L^\dagger M_\nu^{\text{D}} X_\nu \, , \tag{4.7}$$

$$M_\ell = X_L^\dagger M_\ell X_R \ . \tag{4.8}$$

The models in the literature look to find an underlying symmetry that can explain the pattern of neutrino mixing, with many employing a bottom-up approach [29,230]. The idea is to start with the TBM hypothesis of Ref. [27], and look for a symmetry basis which will reproduce this mixing pattern.

It is clear from the "road map" for present day neutrino mass model builders [28] in Fig. 4.1 that there are many possible routes to take in finding a model, which explains why so many models exist in the literature. This work will not contain an exhaustive list of models; instead the focus will be on mass models with family symmetries, which lead to TBM. From Fig. 4.1: in order to get TBM one must assume that LSND is false (Section 2.4.4), and that neutrinos are Majorana particles.

For reference, the TBM pattern of Eq. (3.83) is

$$U_{TBM} \equiv \begin{pmatrix} \frac{2}{\sqrt{6}} & \frac{1}{\sqrt{3}} & 0 \\ -\frac{1}{\sqrt{6}} & \frac{1}{\sqrt{3}} & \frac{1}{\sqrt{2}} \\ -\frac{1}{\sqrt{6}} & \frac{1}{\sqrt{3}} & -\frac{1}{\sqrt{2}} \end{pmatrix} . \tag{4.9}$$

The model surveys in [231,232] provide a good reference list of neutrino mass models,

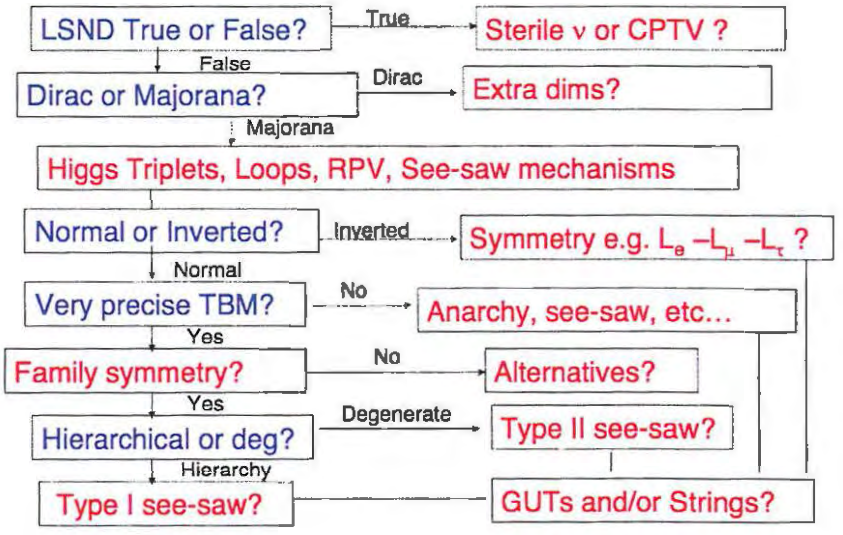

Figure 4.1: (From Ref. [28].) Neutrino mass models roadmap.

with the emphasis on the model predictions for the oscillation parameters and not on the details of the models themselves. A few simple flavour symmetry models are introduced below, before the in-depth analysis of A_4 models in Chapters 5 and 6.

4.2 A $\mu - \tau$ symmetric mass matrix

Refs. [215,233–235] propose a class of models where the mass matrix is invariant under exchange of the μ and τ elements. In the basis where the charged lepton mass matrix is diagonal, the light neutrino Majorana mass matrix, M_ν, is diagonalised by the unitary mixing matrix U, *viz.*

$$U^T M_\nu U = m_k \delta_{kj} \ . \tag{4.10}$$

The neutrino masses are given by m_k, for $k = 1, 2, 3$. Now, if M_ν is $\mu - \tau$ symmetric then

$$M_\nu = M^{(\mu\tau)} \equiv \begin{pmatrix} x & y & y \\ y & z & w \\ y & w & z \end{pmatrix} \ , \tag{4.11}$$

and atmospheric mixing is maximal ($|U_{\mu 3}| = |U_{\tau 3}|$). This symmetry can be represented by the matrix

$$T = \begin{pmatrix} 1 & 0 & 0 \\ 0 & 0 & 1 \\ 0 & 1 & 0 \end{pmatrix} \ , \tag{4.12}$$

so that $TM_\nu T = M_\nu$, which is a $\mathbb{Z}_2$ symmetry. Diagonalising the mass matrix in Eq. (4.11) gives the mixing matrix [215]

$$U = \begin{pmatrix} \cos\theta_{12} & \sin\theta_{12} & 0 \\ -\frac{\sin\theta_{12}}{\sqrt{2}} & \frac{\cos\theta_{12}}{\sqrt{2}} & \frac{1}{\sqrt{2}} \\ -\frac{\sin\theta_{12}}{\sqrt{2}} & \frac{\cos\theta_{12}}{\sqrt{2}} & -\frac{1}{\sqrt{2}} \end{pmatrix} , \tag{4.13}$$

up to Majorana phases. If the solar mixing angle is set to $\sin^2\theta_{12} = \frac{1}{3}$, a somewhat ad-hoc estimate, the matrix in Eq. (4.13) becomes the TBM matrix of Eq. (4.9).

4.3 C_3 and $S_2 \times S_2$ symmetry

TBM was first introduced by Harrison et al. [27], who propose a simple model based on two discrete symmetries. Their initial idea is elaborated upon in [36, 236], where the mass matrices are shown to be related to the symmetry groups C_3 and S_3 and their class operators.

In order to reproduce TBM, one can start with mass matrices of the form [27, 225]

$$M_\ell = \begin{pmatrix} a & b & c \\ c & a & b \\ b & c & a \end{pmatrix} , \qquad M_\nu = \begin{pmatrix} x & 0 & y \\ 0 & z & 0 \\ y & 0 & x \end{pmatrix} , \tag{4.14}$$

where a, b, c are related to the charged lepton masses, and x, y, z are related to three independent neutrino masses. The matrix M_ℓ is of circulant form, and can be generated by a C_3 symmetry (a cyclic permutation of three objects), whereas the matrix M_ν is generated by an $S_2 \times S_2$ symmetry.

For an Abelian symmetry, a mass matrix that is invariant under the regular representation of the group is a linear combination of the representation matrices themselves [225]. In the case of C_3, the regular representation is given by

$$\left\{ \begin{pmatrix} 1 & 0 & 0 \\ 0 & 1 & 0 \\ 0 & 0 & 1 \end{pmatrix} , \begin{pmatrix} 0 & 1 & 0 \\ 0 & 0 & 1 \\ 1 & 0 & 0 \end{pmatrix} , \begin{pmatrix} 0 & 0 & 1 \\ 1 & 0 & 0 \\ 0 & 1 & 0 \end{pmatrix} \right\} , \tag{4.15}$$

and it is obvious that the matrix M_ℓ in Eq. (4.14) is a linear combination of the matrices in Eq. (4.15).

The mass matrices M_ℓ and M_ν in Eq. (4.14) are diagonalised by

$$V_L^\ell = V_R^\ell = \frac{1}{\sqrt{3}} \begin{pmatrix} 1 & 1 & 1 \\ 1 & \omega & \omega^2 \\ 1 & \omega^2 & \omega \end{pmatrix}, \quad \text{and} \quad V_L^\nu = V_R^\nu = \begin{pmatrix} \frac{1}{\sqrt{2}} & 0 & -\frac{1}{\sqrt{2}} \\ 0 & 1 & 0 \\ \frac{1}{\sqrt{2}} & 0 & \frac{1}{\sqrt{2}} \end{pmatrix}, \tag{4.16}$$

respectively, where $\omega \equiv e^{2\pi i/3}$ and $\omega^2 \equiv e^{-2\pi i/3}$. Combining these two matrices using Eq. (4.1) gives TBM.[1]

In the case of the C_3 Abelian symmetry, the columns of the diagonalisation matrix $V_L^\ell = V_R^\ell$ correspond to the one-dimensional representations of the group:

$$\{1,1,1\}, \{1,\omega,\omega^2\}, \{1,\omega^2,\omega\}. \tag{4.17}$$

and the matrix is normalised. Since all the irreducible representations of Abelian groups are one-dimensional, these representations can be obtained from the character table for the group, shown in Table 4.1, providing a quick way to obtain the diagonalisation matrix.

Table 4.1: Character table of C_3 [36,237,238].

Class	$\chi^{(1)}$	$\chi^{(2)}$	$\chi^{(3)}$
C_1	1	1	1
C_2	1	ω	ω^2
C_3	1	ω^2	ω

In the case of the $S_2 \times S_2$ symmetry, the representation used in [225] to generate the neutrino mass matrix M_ν is not the regular representation, but rather

$$\left\{ \begin{pmatrix} 1 & 0 & 0 \\ 0 & 1 & 0 \\ 0 & 0 & 1 \end{pmatrix}, \begin{pmatrix} 0 & 0 & 1 \\ 0 & 1 & 0 \\ 1 & 0 & 0 \end{pmatrix}, \begin{pmatrix} 1 & 0 & 0 \\ 0 & -1 & 0 \\ 0 & 0 & 1 \end{pmatrix} \right\}. \tag{4.18}$$

The mixing matrix V^ν is in this case not clearly related to the representation of the symmetry $S_2 \times S_2$, but the mass matrix M_ν in Eq. (4.14) is a linear combination of the matrices in Eq. (4.18).

[1] The matrices in Eq. (4.16) are often used in the A_4 models in Chapters 5 and 6, since A_4 is broken down to the subgroups $Z_3 \cong C_3$ and Z_2. The matrix diagonalising the charged leptons is often referred to as the "magic matrix", and from now on will be denoted as U_ω.

The current data favour TBM, and the symmetries proposed above provide a simple way to implement this hypothesis. This model can also be extended [225] to accommodate mixing in the quark sector, using similar mass matrices and the same C_3 symmetry.

However, the problem with this model is that it is not compatible with the $SU(2)_L$ symmetry of the standard model, with its left-handed lepton doublets [Eq. (3.1)]. According to Eqs. (4.15) and (4.18), the left-handed neutrinos transform in a different way to the left-handed charged leptons, breaking the $SU(2)_L$ symmetry. In the general case, "discrete unbroken generation symmetries (Abelian and non-Abelian) with the $SU(2)_L$ constraint... cannot generate tri-bimaximal mixing" [225], so that Higgs scalars with non-zero VEVs must be introduced into the framework of neutrino mass models. It has also been shown [239] that an Abelian symmetry with an extended Higgs sector can only predict $\theta_{13} = 0$, leaving the other mixing angles as free parameters, which is clearly not compatible with TBM.

4.4 A_4 tetrahedral symmetry

4.4.1 Why use A_4?

Assuming TBM, the neutrino mass matrix can be written as

$$M_\nu = U_{\text{TBM}}\, m_k \delta_{kj}\, U_{\text{TBM}}^T \,, \tag{4.19}$$

which, combined with Eq. (4.9) gives [32]

$$M_\nu = \left[\frac{m_3}{2} \begin{pmatrix} 0 & 0 & 0 \\ 0 & 1 & -1 \\ 0 & -1 & 1 \end{pmatrix} + \frac{m_2}{3} \begin{pmatrix} 1 & 1 & 1 \\ 1 & 1 & 1 \\ 1 & 1 & 1 \end{pmatrix} + \frac{m_1}{6} \begin{pmatrix} 4 & -2 & -2 \\ -2 & 1 & 1 \\ -2 & 1 & 1 \end{pmatrix} \right]. \tag{4.20}$$

The eigenvalues of M_ν are m_1, m_2, m_3, with eigenvectors $(-2,1,1)/\sqrt{6}$, $(1,1,1)/\sqrt{3}$ and $(0,1,-1)/\sqrt{2}$, respectively, and the simplicity of these column vectors motivates an underlying non-Abelian family symmetry [28].

There have been many attempts in the literature (see Table 5.1 on page 53 for a list of references) to construct models of neutrino mass and mixing based on the non-Abelian group A_4, the tetrahedral group. The natural 3-dimensional representation (denoted by $\underline{3}$) makes A_4 a good candidate for describing the symmetry of the three

Table 4.2: Particle assignments of the Altarelli-Feruglio A_4 model

Lepton	$SU(2)_L$	A_4
L	2	3
e^c	1	1
μ^c	1	$1'$
τ^c	1	$1''$
Scalar		
h_u	2	1
h_d	2	1
φ	1	3
φ'	1	3
ξ	1	1

families observed in nature [74].[2]

In constructing a model, different types of particles are assigned to the irreducible representations of A_4, which are $\underline{1}$, $\underline{1}'$, $\underline{1}''$ and $\underline{3}$. The group multiplication rules [Eqs. (A.5) – (A.10)] and product composition rules [Eqs. (A.11) – (A.15)] dictate the form of the resulting Lagrangian, which in turn gives the structure of the neutrino and charged lepton mass matrices. This procedure can be illustrated with a simple example from the literature, which will be developed further in Chapter 5.

4.4.2 Case study: the Altarelli-Feruglio A_4 model

In the original Altarelli-Feruglio model [32, 228], lepton doublets are assigned to the $\underline{3}$ representation, and right-handed lepton singlets to the $\underline{1}$, $\underline{1}'$ and $\underline{1}''$ representations. There are two SM Higgs doublets, which are invariant under A_4, along with two real triplets φ and φ', and a real singlet ξ, all three of which are gauge singlets (see Table 4.2).

Using the A_4 multiplication rules (see Appendices A and B),[3] the Lagrangian of the Yukawa interactions in the lepton sector can be written as

$$\mathscr{L}_Y = y_e e^c(\varphi\ell) + y_\mu \mu^c(\varphi\ell)'' + y_\tau \tau^c(\varphi\ell)' + x_a\xi(\ell\ell) + x_d(\varphi'\ell\ell) + \text{h.c.} + \dots \,, \qquad (4.21)$$

where $(\underline{3}\underline{3})$ transforms as $\underline{1}$, $(\underline{3}\underline{3})'$ transforms as $\underline{1}'$, and $(\underline{3}\underline{3})''$ transforms as $\underline{1}''$, and y_α, x_a

[2] See Appendix A for a discussion of the A_4 group.

[3] Note that this model is in the original, or "Ma-Rajasekaran" basis, where the S matrix is diagonal (Section A.2.1).

and x_d are coupling constants. The notation in Eq. (4.21) is somewhat simplified (the Higgs doublet fields h_u and h_d, and the cut-off scale Λ are set to 1). The dots stand for higher dimensional operators – in this model these are suppressed by additional powers of the cut-off Λ, as long as the VEVs are sufficiently smaller than Λ. For the model to work, the scalar fields must develop VEVs along the directions:

$$\begin{aligned} \langle \varphi \rangle &= (v, v, v) \,, \\ \langle \varphi' \rangle &= (v', 0, 0) \,, \\ \langle \xi \rangle &= u \,. \end{aligned} \tag{4.22}$$

This vacuum alignment is a crucial part of all A_4 models: the realisation of these specific alignments breaks the A_4 symmetry in the correct way, so that TBM is achieved. In general, corrections to the VEV alignment can come from higher order operators or the tree-level exchange of heavy fermions [32].[4]

Assuming the VEV alignment in Eq. (4.22), the mass matrices M_ℓ and M_ν for charged leptons and neutrinos are

$$M_\ell = v_d \frac{v}{\Lambda} \begin{pmatrix} y_e & y_e & y_e \\ y_\mu & y_\mu \omega^2 & y_\mu \omega \\ y_\tau & y_\tau \omega & y_\tau \omega^2 \end{pmatrix} \,, \tag{4.23}$$

$$M_\nu = \frac{v_u^2}{\Lambda} \begin{pmatrix} a & 0 & 0 \\ 0 & a & d \\ 0 & d & a \end{pmatrix} \,, \tag{4.24}$$

where

$$a \equiv x_a \frac{u}{\Lambda} \,, \quad d \equiv x_d \frac{v'}{\Lambda} \,. \tag{4.25}$$

The matrix diagonalising the charged lepton mass matrix is

$$V^\ell = \frac{1}{\sqrt{3}} \begin{pmatrix} 1 & 1 & 1 \\ 1 & \omega^2 & \omega \\ 1 & \omega & \omega^2 \end{pmatrix} \,, \tag{4.26}$$

which is the same as the matrix in Eq. (4.16) (with a phase change). This similarity comes from the fact that C_3 is a subgroup of A_4.

[4] The effects of deviating the VEV alignment in A_4 models will be analysed in Chapters 5 and 6.

The charged fermion masses are

$$m_e = \sqrt{3} y_e v_d \frac{v}{\Lambda} , \quad m_\mu = \sqrt{3} y_\mu v_d \frac{v}{\Lambda} , \quad m_\tau = \sqrt{3} y_\tau v_d \frac{v}{\Lambda} . \tag{4.27}$$

To obtain the observed mass hierarchy among the masses in Eq. (4.27), the authors of Ref. [32] introduce an additional $\mathrm{U}(1)_F$ symmetry, which only affects the right-handed lepton sector. In the flavour basis,[5] the neutrino mass matrix is

$$M_\nu^f = \frac{v_u^2}{\Lambda} \begin{pmatrix} a + 2d/3 & -d/3 & -d/3 \\ -d/3 & 2d/3 & a - d/3 \\ -d/3 & a - d/3 & 2d/3 \end{pmatrix} , \tag{4.28}$$

which is diagonalised by the transformation

$$U^T M_\nu U = \frac{v_u^2}{\Lambda} \mathrm{diag}(a + d, a, -a + d) , \tag{4.29}$$

with $U = U_{TBM}$, as in Eq. (4.9). Thus TBM is achieved. Note that, in general, the parameters a and d are complex, i.e., with the Majorana phases still attached.

Since the first paper by Ma [34],[6] many authors have constructed models based on A_4. The model presented above is a simple case of the application of A_4 to neutrino mixing, and this can be extended to more elaborate models (Chapters 5 and 6). Although some attempts have been made to categorise and/or compare these models [35], there are no comprehensive studies of this type.

The next two chapters contain a model-independent study of all A_4 models in the literature, with a study of the observables related to neutrino oscillations, double beta decay and cosmology. The quark sector is not studied in this work, nevertheless, it is worth mentioning the application of the group T' to quark mixing.

4.5 T' and the quark sector

Although the models described above achieve some success in explaining the neutrino mixing pattern, a truly unified theory should also include the quark sector. Various

[5] The flavour (e, μ, τ) basis is by definition the basis in which the charged leptons are diagonal.

[6] It is interesting to study the history and development of A_4 models (Chapter 1). The fact that the parameters in M_ν (Eq. (4.24)) were chosen to be a and d (rather than a and b) reveals that this model is in fact identical to Ma's original TBM model [31], with $b = c = 0$. However, the authors of Ref. [32] study the vacuum alignment problem in much more detail, providing an extra-dimensional solution.

authors [47–49,51,240,241] have considered the binary tetrahedral group T' as a natural extension of the A_4 symmetry, since T' can accommodate quarks in the $\underline{2}$ representation. The model in Ref. [47] is identical to the Altarelli-Feruglio A_4 model (Section 4.4.2) in all respects (M_ℓ and M_ν are the same), but the additional $\underline{2}$, $\underline{2}'$ and $\underline{2}''$ representations allow the construction of mass matrices of the form

$$M_{u,d} = \begin{pmatrix} 0 & 0 & 0 \\ 0 & \times & \times \\ 0 & \times & \times \end{pmatrix} \tag{4.30}$$

for the quarks, which can reproduce the correct mixing pattern in the quark sector. Note that the inclusion of higher order operators is essential in this model, in order to acheive a realistic mass spectrum for the quarks. Ref. [47] shows that the corrections induced by these operators do not spoil the prediction of TBM in the lepton sector.

Ref. [51] uses T' in a slightly different way, imposing the condition of renormalisability [50]. This method reduces the number of parameters in the Higgs sector, as well as those associated with higher-order operators. The "Minimal Renormalisable T' Model" in Ref. [51] is extended to a "Next-to Minimal Renormalisable T' Model" in Ref. [49], with further predictions for the mixing angles of quarks and leptons.

Chapter 5

A_4 Model Analysis: Type A & Type B

5.1 Deviations from tri-bimaximal mixing

As shown in Section 4.4.2, the A_4 family symmetry can reproduce the TBM pattern, with suitable VEV alignments in the Higgs sectors. The development of different models has also led to various numerical analyses [242–246], which show the effect of higher order corrections and deviations from exact TBM.

In general, deviations from TBM will lead to non-vanishing U_{e3} and non-maximal θ_{23} [247, 248]. Recent developments in the global analysis of neutrino oscillation data [25,104,249] have shown that $\sin^2\theta_{13} > 0$ at the 1σ level, prompting various studies into deviation from TBM in neutrino mass models (e.g. [248, 250]). These deviations are phenomenologically interesting, as they provide a way to analyse and compare different neutrino mass models.

5.1.1 Explicit breaking

Albright and Rodejohann [247] perform a model-independent analysis of TBM models, using an explicit breaking of the TBM texture. This is done by adding small complex perturbations to the neutrino mass matrix.

Using the definition of TBM in Eq. (4.9), the neutrino mass matrix that gives rise

to TBM can be written as

$$(M_\nu)_{\rm TBM} = U^*_{\rm TBM}\, m_k \delta_{kj}\, U^\dagger_{\rm TBM}$$
$$= \begin{pmatrix} A & B & B \\ \cdot & \frac{1}{2}(A+B+D) & \frac{1}{2}(A+B-D) \\ \cdot & \cdot & \frac{1}{2}(A+B+D) \end{pmatrix}, \qquad (5.1)$$

where the complex parameters A, B and D are

$$A = \frac{1}{3}(2m_1 + m_2 e^{-2i\alpha}) ,$$
$$B = \frac{1}{3}(m_2 e^{-2i\alpha} - m_1) ,$$
$$D = m_3 e^{-2i\beta} , \qquad (5.2)$$

m_k $(k = 1, 2, 3)$ are the neutrino masses, and α and β are Majorana phases.

In general, deviations from TBM can be parameterised by small complex parameters $\epsilon_i = |\epsilon_i| e^{i\phi_i}$, for $i = 1 \ldots 6$, so that the mass matrix becomes

$$M'_\nu = \begin{pmatrix} A(1+\epsilon_1) & B(1+\epsilon_2) & B(1+\epsilon_3) \\ \cdot & \frac{1}{2}(A+B+D)(1+\epsilon_4) & \frac{1}{2}(A+B-D)(1+\epsilon_5) \\ \cdot & \cdot & \frac{1}{2}(A+B+D)(1+\epsilon_6) \end{pmatrix}. \qquad (5.3)$$

$|\epsilon_i| \leq 0.2$ has been used previously [247], with $0 \leq \phi_i \leq 2\pi$. Varying the complex parameters A, B, D and ϵ_i affects the neutrino mixing angles, which are found by diagonalising the matrix in Eq. (5.3), and these can be compared with the predictions of $SO(10)$ GUTs [247].

5.1.2 Radiative corrections

In a "modified Altarelli-Feruglio model" [242], three singlet charged scalars, which mediate a one-loop radiative neutrino mass, are introduced. The neutrino mass matrix of Eq. (4.28) becomes

$$M^f_\nu = \frac{v_u^2}{\Lambda} \begin{pmatrix} a + 2d/3 & -d/3 & -d/3 - \epsilon \\ -d/3 & 2d/3 & a - d/3 + c \\ -d/3 - \epsilon & a - d/3 + \epsilon & 2d/3 \end{pmatrix}, \qquad (5.4)$$

where the ϵ terms come from the one-loop radiative corrections. One can then perform a phenomenological analysis of this mass matrix, to show the effect on the neutrino oscillation observables, in particular the value of U_{e3}.

5.1.3 The effects of VEV misalignment

As has been discussed earlier, the VEV alignment of the Higgs scalars play a crucial role in the construction and application of A_4 models to lepton mixing. In the Altarelli-Feruglio (A-F) model in Section 4.4.2, the vacuum alignment required to make the model work was introduced [Eq. (4.22)], without an explanation of its origin. The Higgs triplets responsible for symmetry breaking in the charged lepton and neutrino sectors must take on different VEV alignments, which correspond to the minima of the scalar potential.

This problem pervades all A_4 models, and different solutions have been proposed in the literature. Some approaches include the use of supersymmetry [33, 71, 72, 78, 251], extra dimensions [32] as well as orbifolding [252].

The neutrino mass matrices and observables in the original A-F model [32] can be analysed [243] by adding different numbers of Higgs singlets, as well as altering the alignment of the Higgs triplet in the neutrino sector. In addition to varying the number of Higgs singlets, one can also [246] include the effect of deviations in the charged lepton sector, where the VEV alignments of both Higgs triplets are modified. This technique can be applied to all A_4 models.

5.2 A_4 model comparison

Table 5.1 lists [66,67] the previous work on A_4 models, indicating the chosen A_4 particle assignments in each case. Type A and type B models are analysed in this chapter, and type C and type D models in Chapter 6. The former are largely motivated by a simple bottom-up [29] approach, whereas the latter are often formulated in the context of a GUT group like $SO(10)$. Note from Table 5.1 that type B and type D models contain right-handed neutrinos, and employ the seesaw mechanism; this is absent in type A and type C models. A summary of the main different types of models is provided in Table 5.2 on page 55, Table 5.4 on page 79, Table 6.1 on page 101 and Table 6.3 on page 111. Those models that predict TBM are analysed in detail in the text.

In contrast to existing numerical studies of A_4 models [84, 243, 246, 259], the same numerical tests are performed on each different model, in order to provide a 'model-

Table 5.1: Particle assignments of A_4 models in the literature.

Type	L_i	ℓ_i^c	ν_i^c	References
A	3	1, 1′, 1″	-	[31–33, 74, 86, 242, 243, 246, 252–255]
B	3	1, 1′, 1″	3	[33, 34, 70–73, 227, 251, 256–260]
C	3	3	-	[74, 77, 78, 244, 261]
D	3	3	3	[75, 79–82, 262, 263]
E	3	3	1, 1′, 1″	[76, 84]
F	1, 1′, 1″	3	3	[83]
G	3	1, 1′, 1″	1, 1′, 1″	[85]
H	3	1, 1, 1	(3)	[87, 88, 264]

independent" comparison. In each model, the chosen VEV alignment is modified by random deviations, perturbing the structure of both the neutrino (M_ν) and charged lepton (M_ℓ) mass matrices. Diagonalisation of M_ν and M_ℓ gives the mixing matrices (U_ν and U_ℓ), which combine to form the PMNS matrix [Eq. (3.64)]. Using the mixing matrix and eigenvalues, the neutrino mixing angles and mass-squared differences are obtained, along with the CP violation invariant J_{CP} and the mass-dependent observables $\langle m_{ee} \rangle$ and $\sum m_\nu$ (see Appendix B for details).

Note that although all parameters defining the mass matrices should in general be complex, it is possible[1] to absorb some of the complex phases by rephasing the neutrino and charged lepton fields. Therefore, w.l.o.g., one can take some of the parameters to be real, thus reducing the number of parameters. Unless otherwise indicated, all parameters are taken to be complex, and a full list of parameters for each model is given in Appendix C.

5.3 Type A models

In Type A models, lepton doublets transform as $\underline{3}$, charged lepton singlets as $\underline{1}, \underline{1}', \underline{1}''$, and right handed neutrinos are absent. In this case the neutrino mass usually comes from dimension-5 operators (Section 3.2.5), which is a minimalist framework [74].

Although Table 5.1 contains a long list of references for type A models, many of these works are phenomenological analyses of the same few models. Table 5.2 is a summary

[1] An explicit example is given in Appendix B.

of type A models: the "Ma TBM" model [31] and the "A-F TBM" model [32] are essentially the same (in the three singlet case), with the only difference being the use of extra dimensions (in the A-F TBM model) to explain the VEV alignment problem. The "Altarelli-Feruglio" model [33], is also the same model, with the difference here being the basis used for A_4 (the A-F basis).

5.3.1 The original Ma TBM model

In the original Ma TBM model [31], heavy Higgs triplets are introduced to give the neutrinos mass, but the necessary VEV alignments are not discussed. The particle assignments are almost identical to those described in Chapter 4 (Table 4.2), except that there are three Higgs singlets introduced. The particle assignments are given in Table 5.3. The analysis herein follows Ref. [246], where the effect of VEV misalignment is studied.

Using the A_4 product rules, the Yukawa couplings of leptons are given by the Lagrangian

$$\begin{aligned}\mathcal{L}_Y = &\frac{y_e}{\Lambda}e^c(\varphi\ell_L)h_d + \frac{y_\mu}{\Lambda}\mu^c(\varphi\ell_L)''h_d + \frac{y_\tau}{\Lambda}\tau^c(\varphi\ell_L)'h_d + \frac{x_a}{\Lambda^2}\xi(\ell_L h_u \ell_L h_u) \\ &+ \frac{x_b}{\Lambda^2}\xi''(\ell_L h_u \ell_L h_u)' + \frac{x_c}{\Lambda^2}\xi'(\ell_L h_u \ell_L h_u)'' + \frac{x}{\Lambda^2}(\varphi'\ell_L h_u \ell_L h_u) + \text{h.c.}\,, \end{aligned} \tag{5.5}$$

where y_α, x_i and x are dimensionless coefficients, h_u and h_d are the SM Higgs doublets (as in Table 5.3), and Λ is the cut-off scale. This effective Lagrangian is similar to the one in Eq. (4.21), with the addition of the terms containing ξ' and ξ''. However, the notation in Eq. (5.5) is somewhat clumsier, since the SM Higgs doublets h_u and h_d, as well as the cut-off scale Λ are included. The "flavon" fields acquire VEVs, *viz.*

$$\langle\xi\rangle = u_a\,,\quad \langle\xi'\rangle = u_c\,,\quad \langle\xi''\rangle = u_b\,,\quad \langle\varphi\rangle = (v_1, v_2, v_3)\,,\quad \langle\varphi'\rangle = (v_1', v_2', v_3')\,. \tag{5.6}$$

The charged lepton mass matrix is

$$M_\ell = \begin{pmatrix} h_1 v_1 & h_2 v_1 & h_3 v_1 \\ h_1 v_2 & h_2\omega v_2 & h_3\omega^2 v_2 \\ h_1 v_3 & h_2\omega^2 v_3 & h_3\omega v_3 \end{pmatrix}, \tag{5.7}$$

Table 5.2: Summary of type A A_4 models.

Model	M_ℓ	M_ν	TBM?	Comments
Ma TBM Model [31, 246, 253]	$\propto U_\omega \begin{pmatrix} y_e & 0 & 0 \\ 0 & y_\mu & 0 \\ 0 & 0 & y_\tau \end{pmatrix}$	$\propto \begin{pmatrix} a+b+c & 0 & 0 \\ 0 & a+\omega b+\omega^2 c & d \\ 0 & d & a+\omega^2 b+\omega c \end{pmatrix}$	Yes	Need $b=c$ for exact TBM Analysis in [246]
A-F TBM Model [32]	As above	As above	Yes	Original (M-R) basis Similar model in [252, 254] Analysis in [242]
Zee [74]	As above	$\propto \begin{pmatrix} a^2+b^2 & 0 & ab \\ 0 & a^2+3b^2 & 0 \\ ab & 0 & a^2+b^2 \end{pmatrix}$	Yes	Dimension-5 operators
Altarelli-Feruglio [33]	$\propto \begin{pmatrix} y_e & 0 & 0 \\ 0 & y_\mu & 0 \\ 0 & 0 & y_\tau \end{pmatrix}$	$\propto \begin{pmatrix} a+\frac{2d}{3} & b-\frac{d}{3} & c-\frac{d}{3} \\ b-\frac{d}{3} & c+\frac{2d}{3} & a-\frac{d}{3} \\ c-\frac{d}{3} & a-\frac{d}{3} & b+\frac{2d}{3} \end{pmatrix}$	Yes	Need $b=c$ for exact TBM Analysis in [243]
Morisi [86]	As above	$\propto \begin{pmatrix} a+2b & -b & -b \\ -b & 2b & a-b \\ -b & a-b & 2b \end{pmatrix}$	Yes	Extra $(Z_2)^3$ symmetry

Table 5.3: Particle assignments of the original Ma TBM model [31,246].

Lepton	$SU(2)_L$	A_4
L	2	$\underline{3}$
e^c	1	$\underline{1}$
μ^c	1	$\underline{1}'$
τ^c	1	$\underline{1}''$
Scalar		
h_u	2	$\underline{1}$
h_d	2	$\underline{1}$
φ	1	$\underline{3}$
φ'	1	$\underline{3}$
ξ	1	$\underline{1}$
ξ'	1	$\underline{1}'$
ξ''	1	$\underline{1}''$

where $h_i = \frac{y_\alpha}{\Lambda} v_d$, and the neutrino mass matrix is

$$M_\nu = \frac{v_u^2}{\Lambda} \begin{pmatrix} a+b+c & f & e \\ f & a+\omega b+\omega^2 c & d \\ e & d & a+\omega^2 b+\omega c \end{pmatrix}, \tag{5.8}$$

where

$$\begin{aligned} a &= x_a \frac{u_a}{\Lambda}\,, \quad b = x_b \frac{u_b}{\Lambda}\,, \quad c = x_c \frac{u_c}{\Lambda}\,, \\ d &= x \frac{v_1'}{\Lambda}\,, \quad e = x \frac{v_2'}{\Lambda}\,, \quad f = x \frac{v_3'}{\Lambda}\,, \end{aligned} \tag{5.9}$$

with v_d and v_u the VEVs of h_d and h_u, respectively.

Assuming that $v_1 = v_2 = v_3 = v$ (i.e. the Higgs triplet φ has the VEV $\langle\varphi\rangle \propto (1,1,1)$), M_ℓ can be diagonalised by

$$U_L^\dagger M_\ell U_R = \sqrt{3} v_d \frac{v}{\Lambda} \begin{pmatrix} y_e & 0 & 0 \\ 0 & y_\mu & 0 \\ 0 & 0 & y_\tau \end{pmatrix} = \mathrm{diag}\,(m_e, m_\mu, m_\tau), \tag{5.10}$$

where $U_L = U_\omega$ (the magic matrix) and U_R is the unit matrix. With the additional assumption that $e = f = 0$ (i.e. the Higgs triplet φ' has the VEV $\langle\varphi'\rangle \propto (1,0,0)$), the

neutrino mass matrix becomes

$$M_\nu = m_0 \begin{pmatrix} a+b+c & 0 & 0 \\ 0 & a+\omega b+\omega^2 c & d \\ 0 & d & a+\omega^2 b+\omega c \end{pmatrix} , \tag{5.11}$$

or, in the flavour (e, μ, τ) basis,

$$M_\nu^{(e,\mu,\tau)} = m_0 \begin{pmatrix} a+\frac{2d}{3} & b-\frac{d}{3} & c-\frac{d}{3} \\ b-\frac{d}{3} & c+\frac{2d}{3} & a-\frac{d}{3} \\ c-\frac{d}{3} & a-\frac{d}{3} & b+\frac{2d}{3} \end{pmatrix} , \tag{5.12}$$

where $m_0 = \frac{v_u^2}{\Lambda}$.

In order to give exact TBM, the condition $b = c$ is also necessary, which means that the product of the VEVs of ξ' and ξ'' (u_c and u_b) with their corresponding dimensionless constants (x_c and x_b) must be equal [Eq. (5.9)]. Different cases of this model have been studied, both analytically [253] and numerically [246].

The two different vacuum alignments (proportional to $(1,1,1)$ and $(1,0,0)$) in the charged lepton and neutrino sectors are a vital part of this and in fact all other A_4 models. Deviations from TBM may occur if this alignment is modified, which could be caused by higher dimensional operators [32], or the effect of renormalisation group evolution of the coupling constants [265].

In order to study this model numerically, the following definitions are used:

$$c = b\,(1+\epsilon_1) \ , \ e = \epsilon_2\, d \ , \ f = \epsilon_3\, d \ , \tag{5.13}$$

so that the small (in general complex) parameters ϵ_i $(i = 1,2,3)$ lead to deviations from TBM. Substituting Eq. (5.13) into the original neutrino mass matrix in Eq. (5.8) gives

$$M'_\nu = m_0 \begin{pmatrix} a+2b+b\epsilon_1 & d\,\epsilon_3 & d\,\epsilon_2 \\ \cdot & a+\omega b(\omega+\omega\epsilon_1+1) & d \\ \cdot & \cdot & a+\omega b(\omega+\epsilon_1+1) \end{pmatrix} , \tag{5.14}$$

which can be diagonalised numerically (see Ref. [246] for an approximate analytical expression for the resulting mixing matrix). The parameters a, b and d are set to be of

order one,[2] with a real, and the parameter m_0 is fixed, which defines the mass scale. One could in principle vary m_0, or choose different values for m_0 in order to study different regions of the neutrino mass spectrum. However, in this analysis, $m_0 = 0.025$ eV is defined for the normal hierarchy, and $m_0 = 0.05$ eV for the inverted hierarchy, giving neutrinos in the hierarchical region. The parameters ϵ_1 and ϵ_2 are also real, but ϵ_3 is complex. $|\epsilon_i| \leq 0.3$ was taken, and this value will be used throughout this work.

The scatter plots in Fig. 5.1 show the allowed region in $a - b - d$ parameter space, obtained by diagonalising Eq. (5.14), with no perturbations applied ($\epsilon_1 = \epsilon_2 = \epsilon_3 = 0$), and using the 3σ ranges of the oscillation parameters as inputs. These plots are rather general, and show no evidence of fine tuning of the parameters.

In the charged lepton sector, the new Higgs VEV is defined as

$$\langle \varphi \rangle = (v, (1 + \epsilon_1^{ch})v, (1 + \epsilon_2^{ch})v) \ , \tag{5.15}$$

so that the charged lepton mass matrix [Eq. (5.7)] becomes

$$M'_\ell = v_d \frac{v}{\Lambda} \begin{pmatrix} y_e & y_\mu & y_\tau \\ y_e(\epsilon_1^{ch} + 1) & y_\mu(\epsilon_1^{ch} + 1)\omega & y_\tau(\epsilon_1^{ch} + 1)\omega^2 \\ y_e(\epsilon_2^{ch} + 1) & y_\mu(\epsilon_2^{ch} + 1)\omega^2 & y_\tau(\epsilon_2^{ch} + 1)\omega \end{pmatrix} \ , \tag{5.16}$$

which can also be numerically diagonalised. The mass scale for the charged leptons is also fixed ($v_d v/\Lambda = 10^6/\sqrt{3}$ eV), and each coefficient y_α ($\alpha = e, \mu, \tau$) is varied randomly, such that the charged lepton masses are within 10% of their experimental values.

Combining the mixing matrices obtained from diagonalising Eqs. (5.14) and (5.16) gives the U_{PMNS} matrix, from which the neutrino oscillation observables can be calculated. In Ref. [246], the different cases of this model (with differing numbers of Higgs singlets and/or different triplet VEV alignments) are studied separately. However, in this work the general case is presented, where all the deviation parameters (ϵ_1, ϵ_2, ϵ_3 and ϵ_1^{ch}, ϵ_2^{ch}) are non-zero, and all Higgs scalars are present.

In this case, with all perturbations applied, the mixing angle observables fill the whole 3σ range, as shown in Fig. 5.2, and no new insights are possible. The plot of the Jarlskog invariant, J_{CP}, against $|U_{e3}|$ [Fig. 5.3(a)], also shows a spread across the entire 3σ range, which means that for all values of $|U_{e3}|$ within the 3σ limit, CP violation can take any value from zero up to its maximum, depending on the Dirac and Majorana

[2]These parameters come from the product of the VEVs of Higgs scalars with coupling constants, as in Eq. (5.9).

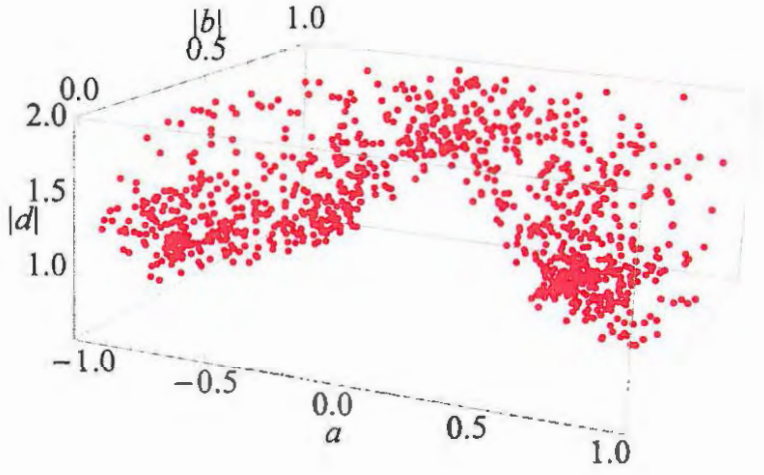

(a)

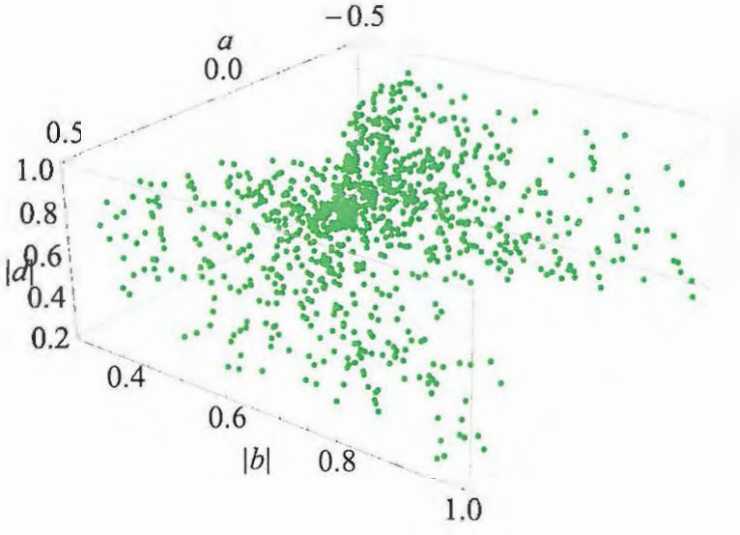

(b)

Figure 5.1: Scatter plots of the $a-b-d$ parameter space for Ma's original TBM model, for normal (a) and inverted (b) hierarchies. The parameter m_0 was set to 0.025 eV in the normal hierarchy and 0.05 eV in the inverted hierarchy.

phases.

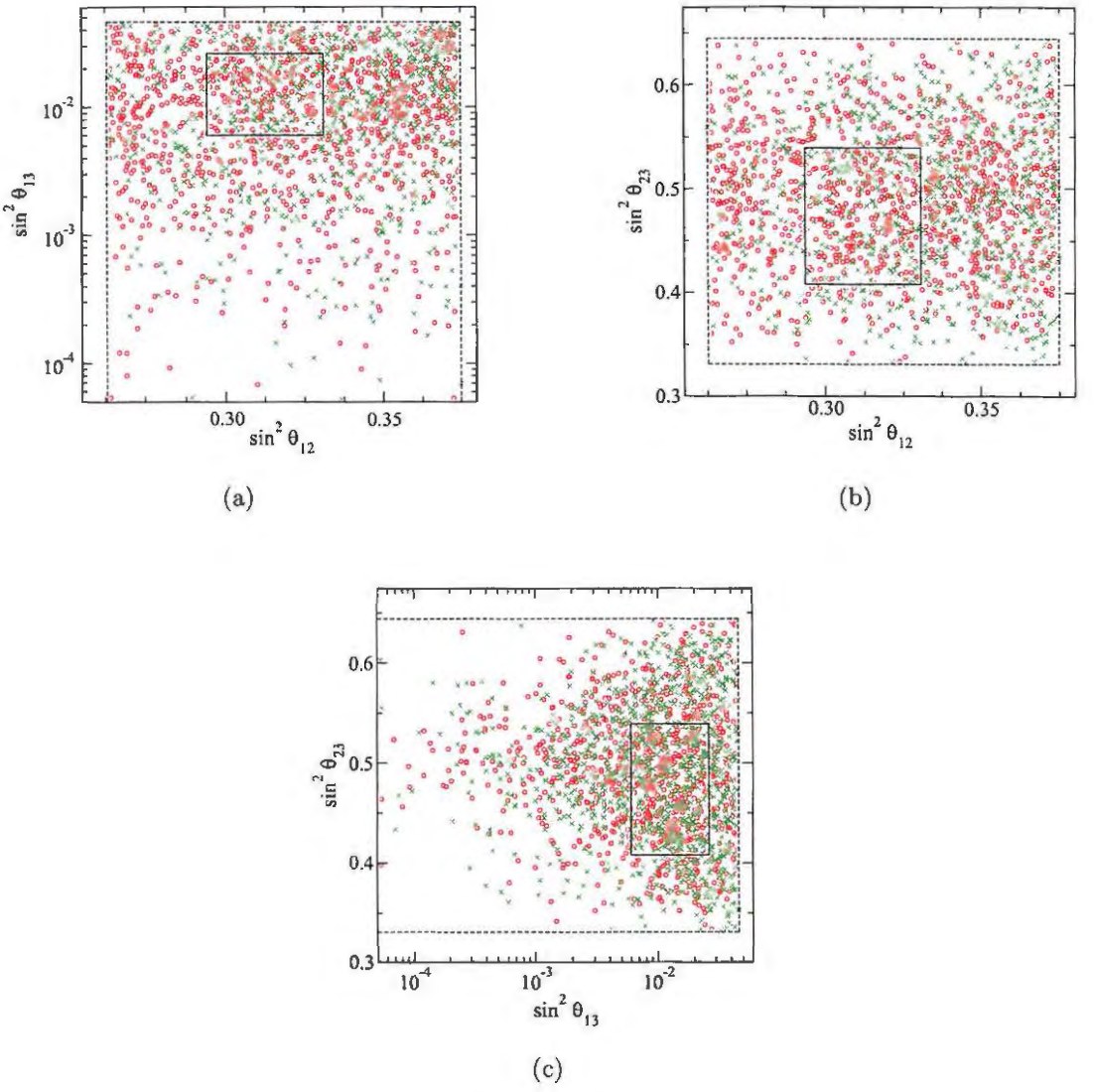

Figure 5.2: Scatter plots of mixing angle observables for Ma's original TBM model, for normal (red circles) and inverted (green crosses) hierarchies, with the 1σ (solid lines) and 3σ (dashed lines) allowed regions from Ref. [25].

For exact TBM, the mass eigenvalues are independent of the mixing angles (Section 3.3), and a plot of Δm^2_{21} against Δm^2_{31} [Fig. 5.3(b)] shows this to be the case. However, it is interesting to study the amplitude for $0\nu\beta\beta$ decay ($\langle m_{ee} \rangle$) and the sum of the absolute neutrino masses ($\sum m_\nu$) predicted by different models. The former quantity depends on the entries in the first row of the mixing matrix, which incorporates the Majorana phases, whereas the latter depends on the absolute values of the

mass eigenvalues.

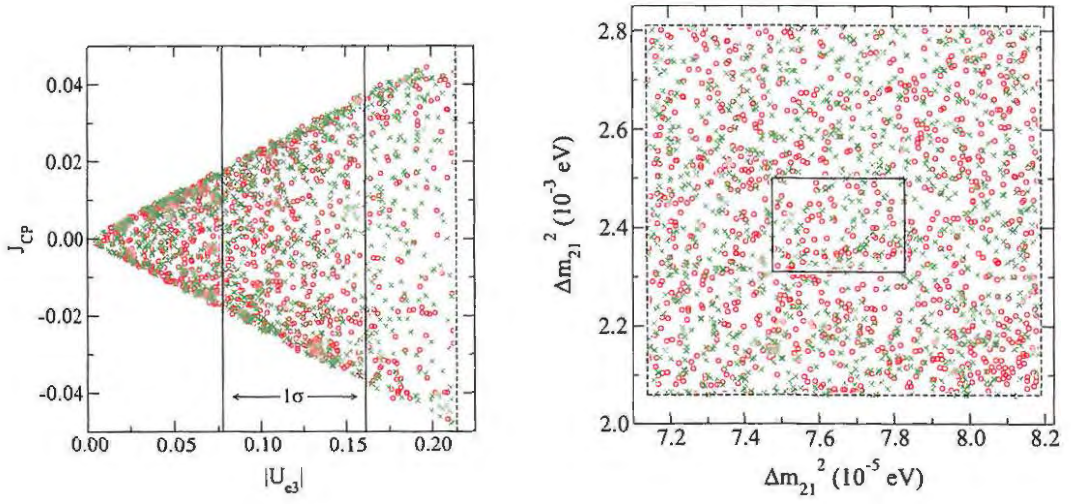

(a) (b)

Figure 5.3: Scatter plots of (a) J_{CP} against $|U_{e3}|$ and (b) mass squared differences in eV, for Ma's original TBM model, with normal (red circles) and inverted (green crosses) hierarchy. The 1σ limits are given by solid lines, and the 3σ limits by dashed lines [25].

The relationship between $\langle m_{ee} \rangle$ and $\sum m_\nu$ is shown in Fig. 5.4, for both normal and inverted mass hierarchies. In both cases it is evident that the effect of perturbing the mass matrix [Eqs. (5.14) and (5.16)] is to allow for a lower value of $\langle m_{ee} \rangle$ (with a minimum of 0.0012 eV) than in the unperturbed case. Since the mass scale m_0 was fixed [Eq. (5.14)], the sum of absolute neutrino masses lies in the hierarchical region, and is greater for inverted hierarchy, as expected. There are some points in the inverted hierarchy that are excluded by the most stringent cosmological limit; this limit includes the Lyα data.

As can be seen from the results in Figs. 5.2 and 5.3, if the maximum number of VEV alignment deviations are applied in this model, the scatter plots of mixing angle observables are randomly distributed, so that no conclusions can be drawn. Figs. 5.2 and 5.3 are typical of the results obtained in the present analysis, and will be referred to throughout this work.

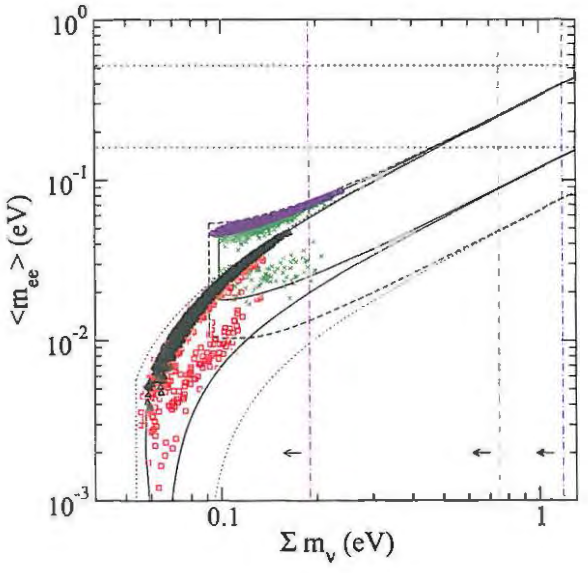

Figure 5.4: Scatter plot of $\langle m_{ee} \rangle$ against $\sum m_\nu$ for Ma's original TBM model, with normal (unperturbed given by black triangles, perturbed by red squares) and inverted (unperturbed given by indigo circles, perturbed by green crosses) hierarchies.

5.3.2 The Altarelli-Feruglio model

The Altarelli-Feruglio model [33] is equivalent to the Ma model [31] (except for a basis change), and the numerical results in fact confirm this similarity, but it is instructive to give a detailed analysis, as in Refs. [243, 246].

The original Ma [31] and A-F [32,228] models employed the so-called 'Ma-Rajasekaran' basis for A_4, in which the charged lepton mass matrix is given by Eq. (5.7) and the neutrino mass matrix by Eq. (5.8). In the 'Altarelli-Feruglio' basis, the charged lepton mass matrix becomes diagonal, which means that the neutrino mass matrix is given by Eq. (5.12). The two bases are simply related by a phase change, and the multiplication rules differ (see Appendix A).

With the new multiplication rules, and assigning the right-handed charged leptons

e^c, μ^c, τ^c to $\underline{1}$, $\underline{1}''$ and $\underline{1}'$,[3] the Lagrangian is[4]

$$\begin{aligned}\mathscr{L}_Y = \; & y_e e^c(\varphi\ell) + y_\mu \mu^c(\varphi\ell)' + y_\tau \tau^c(\varphi\ell)'' + x_a\xi(\ell\ell) + x(\varphi'\ell\ell) \\ & + x_c\xi'(\ell\ell)'' + x_b\xi''(\ell\ell)' + \text{h.c.} + \dots \;,\end{aligned} \tag{5.17}$$

where the SM Higgs doublets and cut-off scale have been omitted [as in Eq. (4.21)], and the dots stand for higher dimensional operators. The two terms on the second line of Eq. (5.17) come from additional Higgs singlets.

Upon symmetry breaking, the VEVs of the Higgs triplets are

$$\langle\varphi\rangle = (v, 0, 0) \;, \quad \text{and} \quad \langle\varphi'\rangle = (v', v', v') \;, \tag{5.18}$$

so that the VEV alignments are effectively swapped in this new basis. The charged lepton mass matrix is

$$M_\ell = v_d \frac{v}{\Lambda} \begin{pmatrix} y_e & 0 & 0 \\ 0 & y_\mu & 0 \\ 0 & 0 & y_\tau \end{pmatrix} \;, \tag{5.19}$$

and when only one Higgs singlet (ξ) is present, the neutrino mass matrix is

$$M_\nu = m_0 \begin{pmatrix} a + \frac{2d}{3} & -\frac{d}{3} & -\frac{d}{3} \\ -\frac{d}{3} & \frac{2d}{3} & a - \frac{d}{3} \\ -\frac{d}{3} & a - \frac{d}{3} & \frac{2d}{3} \end{pmatrix} \;, \tag{5.20}$$

with $m_0 = \frac{v_u^2}{\Lambda}$, $a = 2x_a\frac{u_a}{\Lambda}$ and $d = 2x\frac{v'}{\Lambda}$. The mass matrix in Eq. (5.20) is identical to the one in Eq. (4.28), as the models are equivalent. Note that with only one Higgs singlet it is impossible to get the inverted mass hierarchy in this model, as shown in Appendix B.

It is interesting to note that in the case of one Higgs singlet, with the mass matrix in Eq. (5.20), some fine tuning is required between the parameters a and d for the model to give the correct neutrino mass squared differences [243]. This seems rather contrived, since a and d come from the products of different Yukawa couplings with the VEVs of the Higgs singlet ξ and triplet φ', respectively. As can be seen in Fig. 5.5, if both a and d are real (as in Ref. [243]), there is a linear relationship between the two parameters, but if d is complex (as in this analysis) there is only a slightly greater

[3]Note that the assignments of μ^c and τ^c are swapped.

[4]The notation in Eq. (5.17) is consistent with that in Eq. (5.5); this differs from the notation in Refs [33, 243].

allowed region in the $a-d$ parameter space.[5] There are no perturbations applied in this case, and the parameter m_0 is set to 0.025 eV. This "fine tuning test" can be applied to all flavour symmetry models, by examining the allowed values of the parameters that make up the mass matrix, before perturbations are applied.

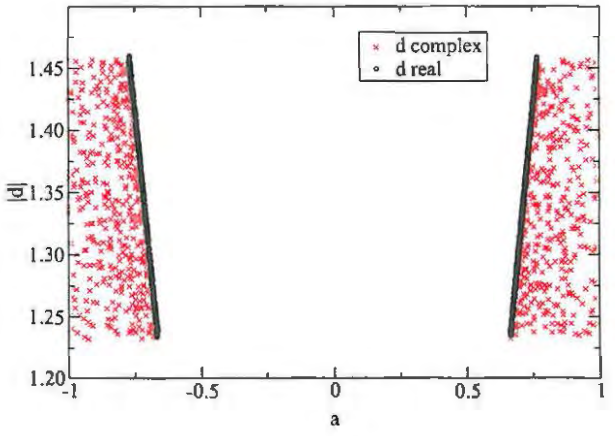

Figure 5.5: Scatter plot showing allowed regions (for 3σ ranges of the oscillation parameters) in the $a-d$ parameter space for the original Altarelli-Feruglio model, with one Higgs singlet and normal hierarchy [243].

In the framework of this model, it is also possible to achieve TBM with both two or three Higgs singlets [243]. In the first case (two singlets), the resulting mass matrix is

$$M_\nu = m_0 \begin{pmatrix} \frac{2d}{3} & b-\frac{d}{3} & c-\frac{d}{3} \\ b-\frac{d}{3} & c+\frac{2d}{3} & -\frac{d}{3} \\ c-\frac{d}{3} & -\frac{d}{3} & b+\frac{2d}{3} \end{pmatrix} , \tag{5.21}$$

with b and c defined in Eq. (5.9), and exact TBM is achieved when $b=c$, as before. Note that only the singlets ξ' and ξ'' give the correct result; the other possible combinations of two singlets (i.e. ξ and ξ'' or ξ and ξ') give the wrong mixing matrix [243]. In the second case (three singlets), the resulting matrix is

$$M_\nu = m_0 \begin{pmatrix} a+\frac{2d}{3} & b-\frac{d}{3} & c-\frac{d}{3} \\ b-\frac{d}{3} & c+\frac{2d}{3} & a-\frac{d}{3} \\ c-\frac{d}{3} & a-\frac{d}{3} & b+\frac{2d}{3} \end{pmatrix} , \tag{5.22}$$

[5]Note that w.l.o.g., a can be chosen to be real.

and the requirement for exact TBM is that $a \neq b = c$.

The three mass matrices in Eqs. (5.20), (5.21) and (5.22) are phenomenologically interesting, and will be numerically analysed below. Note that with additional Higgs singlets, the inverted mass hierarchy is possible. In Ref. [243], each case was analysed in turn,[6] under the assumption that the Higgs triplet had the alignment in Eq. (5.18), but the effect of changing this alignment was studied separately. The present analysis combines the effects of different numbers of Higgs singlets and deviated triplet alignment, as well as the effect of deviations in the charged lepton sector.

The requirement $b = c$ can be seen in the scatter plots of $b - c - d$ parameter space in Fig. 5.6, in addition to the fact that the $b - d$ parameter space is quite tightly constrained. In the three singlet case with $b = c$, there is more freedom in choosing parameters, as can be seen from the scatter plots of $a - c - d$ parameter space in Fig. 5.7. A comparison with Fig. 5.1 shows that the A-F model with three singlets is equivalent to the Ma TBM model.

In order to study deviations from TBM, the VEV alignment of the Higgs triplets is perturbed, so that

$$\langle \varphi \rangle = (v, v\,\epsilon_1^{ch}, v\,\epsilon_2^{ch}) \quad \text{and} \quad \langle \varphi' \rangle = (v', v'(1+\epsilon_1), v'(1+\epsilon_2)) \;, \tag{5.23}$$

and $b = c(1+\epsilon_3)$ is defined in order to study the effect of changing the relative alignment of the Higgs singlets. The resulting charged lepton mass matrix is

$$M_\ell' = v_d \frac{v}{\Lambda} \begin{pmatrix} y_e & y_e\,\epsilon_2^{ch} & y_e\,\epsilon_1^{ch} \\ y_\mu\,\epsilon_1^{ch} & y_\mu & y_\mu\,\epsilon_2^{ch} \\ y_\tau\,\epsilon_2^{ch} & y_\tau\,\epsilon_1^{ch} & y_\tau \end{pmatrix} . \tag{5.24}$$

The neutrino mass matrix with one Higgs singlet is

$$M_\nu' = m_0 \begin{pmatrix} a + \frac{2d}{3} & -\frac{d}{3}(1+\epsilon_2) & -\frac{d}{3}(1+\epsilon_1) \\ \cdot & \frac{2d}{3}(1+\epsilon_1) & a - \frac{d}{3} \\ \cdot & \cdot & \frac{2d}{3}(1+\epsilon_2) \end{pmatrix} , \tag{5.25}$$

[6] Note again that the notation in Ref. [243] is different, so that the parameters b, c and d do not correlate with those used here.

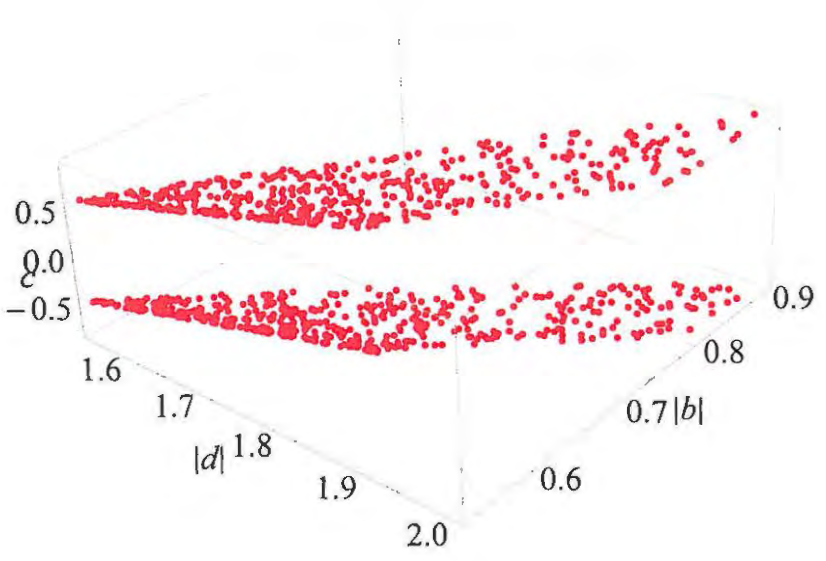

(a)

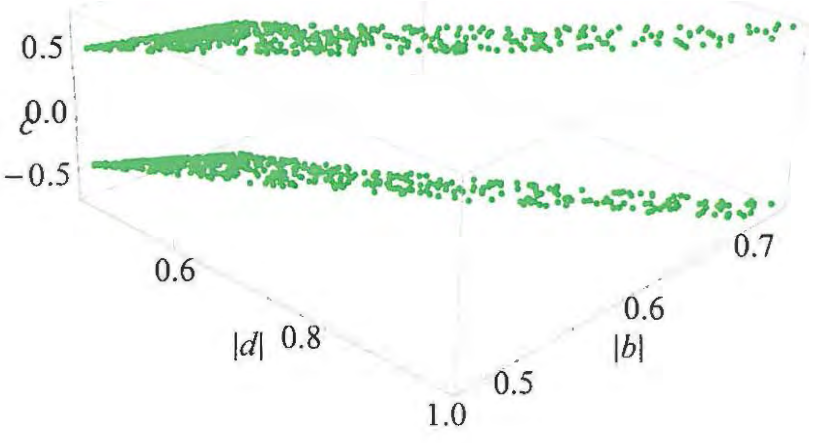

(b)

Figure 5.6: Scatter plots of the $b - c - d$ parameter space for the A-F model with two Higgs singlets, for normal (a) and inverted (b) hierarchies. The parameter m_0 was set to 0.025 eV in the normal hierarchy and 0.05 eV in the inverted hierarchy.

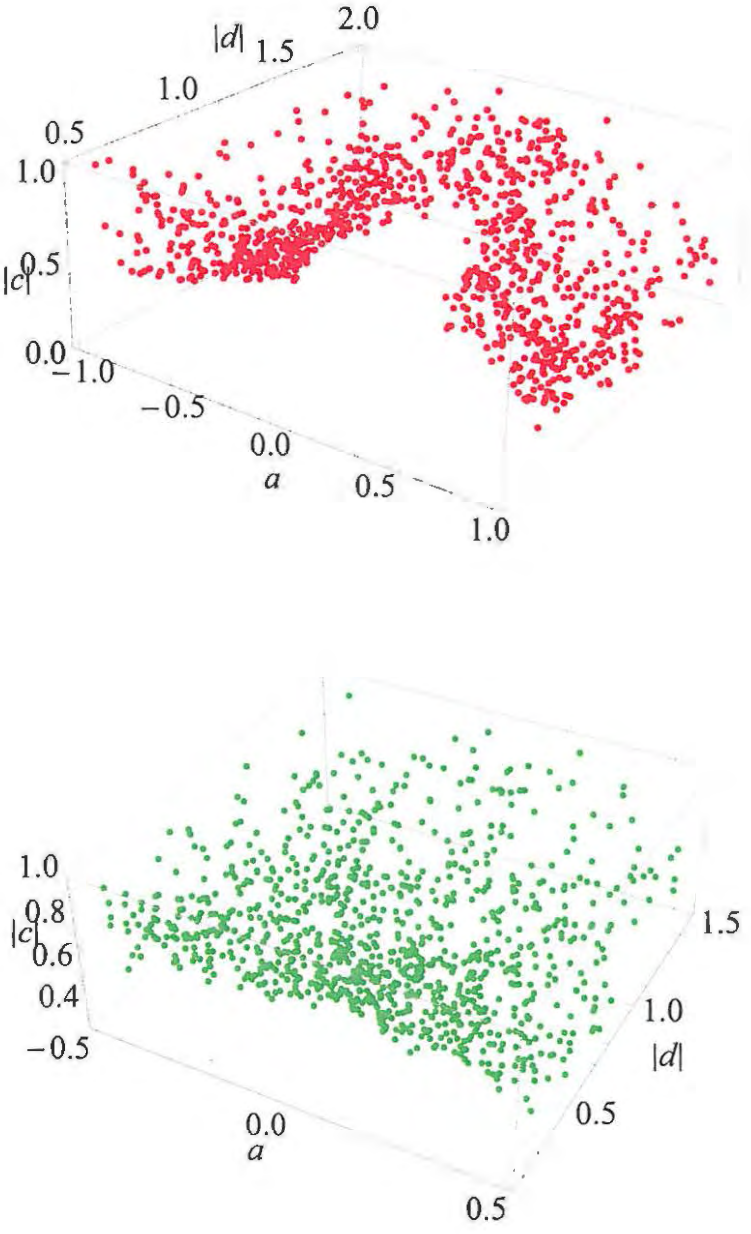

Figure 5.7: Scatter plots of the $a - c - d$ parameter spaces for the A-F model with three Higgs singlets, for normal (red) and inverted (green) hierarchies.

and with two Higgs singlets is

$$M'_\nu = m_0 \begin{pmatrix} \frac{2d}{3} & c(1+\epsilon_3) - \frac{d}{3}(1+\epsilon_2) & c - \frac{d}{3}(1+\epsilon_1) \\ \cdot & c + \frac{2d}{3}(1+\epsilon_1) & -\frac{d}{3} \\ \cdot & \cdot & c(1+\epsilon_3) + \frac{2d}{3}(1+\epsilon_2) \end{pmatrix} . \tag{5.26}$$

The most general case (three Higgs singlets) is

$$M'_\nu = m_0 \begin{pmatrix} a + \frac{2d}{3} & c(1+\epsilon_3) - \frac{d}{3}(1+\epsilon_2) & c - \frac{d}{3}(1+\epsilon_1) \\ \cdot & c + \frac{2d}{3}(1+\epsilon_1) & a - \frac{d}{3} \\ \cdot & \cdot & c(1+\epsilon_3) + \frac{2d}{3}(1+\epsilon_2) \end{pmatrix} . \tag{5.27}$$

where the condition $a \neq c$ still holds.

It is interesting to compare the deviations from TBM for different numbers of Higgs singlets, with the same perturbations applied to M_ℓ in each case [Eq. (5.24)]. Fig. 5.8 shows the results for the normal mass hierarchy (it is impossible to get the inverted hierarchy with one Higgs singlet). In the case of one Higgs singlet, $\sin^2\theta_{13}$ is small, lying below the 1σ range, whereas in the case of two and three Higgs singlets it is larger, but with more deviation from maximal θ_{23}. Note also from Fig. 5.8(b) that for $U_{e3} > 0.1$, the three singlet case allows for a larger value of J_{CP} than the case with two singlets.

The deviations from TBM for the normal and inverted mass hierarchy in the case of two Higgs singlets are presented in Fig. 5.9. In the inverted hierarchy case, the value of $\sin^2\theta_{12}$ tends to be greater than the TBM value of $1/3$, whereas for normal hierarchy it is spread across the 3σ range [Fig. 5.9(a)]. In the inverted hierarchy there is less deviation from maximal θ_{23} than for the normal hierarchy [Fig. 5.9(b)]. One can see from Fig. 5.9(c) that for larger values of $|U_{e3}|$, the value of J_{CP} is greater in the inverted hierarchy than in the normal one. Note also that in the case of three Higgs singlets (not shown here), there is not much difference between the normal and inverted hierarchies.

The mass-dependent observables allow for comparison between the three cases presented above. In Fig. 5.10, one can distinguish the different cases of one, two and three Higgs singlets by the scatter plots in $\langle m_{ee} \rangle - \sum m_\nu$ parameter space. The three singlet case [Fig. 5.10(c)] is equivalent to the Ma model, and comparison with Fig. 5.4 shows this to be the case. Once again, $\langle m_{ee} \rangle$ takes its maximum value in the unperturbed case, and the VEV alignment deviations allow for smaller values of $\langle m_{ee} \rangle$. The devi-

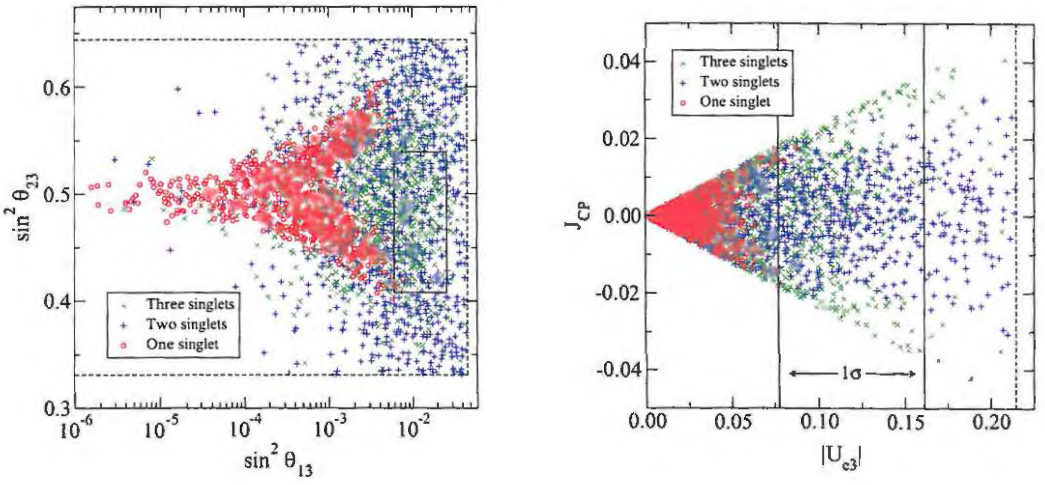

(a) (b)

Figure 5.8: Scatter plots of (a) $\sin^2\theta_{23}$ against $\sin^2\theta_{13}$ and (b) J_{CP} against $|U_{e3}|$ for the Altarelli-Feruglio model, normal hierarchy, with one (red circles), two (blue plus signs) and three (green crosses) Higgs singlets.

ations from TBM allow for some overlap between normal and inverted hierarchies in Figs. 5.10(b) and 5.10(c). Increasing the number of Higgs singlets effectively increases the sum of neutrino masses, $\sum m_\nu$ - the one singlet case lies in the hierarchical region, whereas the cases with additional singlets move into the quasi-degenerate region.

5.3.3 Zee model

In Ref. [74], Zee discusses the use of A_4 in great detail, explaining the construction of dimension-5 operators and how this leads to a certain form for the neutrino mass matrix. This process clearly illustrates the bottom-up approach: with the usual type A particle assignments (Table 5.1) and one Higgs scalar (φ) transforming as $\underline{3}$, the charged lepton mixing matrix will always be U_ω, which means that to achieve TBM the neutrino mixing matrix must be the matrix in Eq. (4.16):

$$V_\nu = \frac{1}{\sqrt{2}} \begin{pmatrix} 1 & 0 & -1 \\ 0 & \sqrt{2} & 0 \\ 1 & 0 & 1 \end{pmatrix} . \tag{5.28}$$

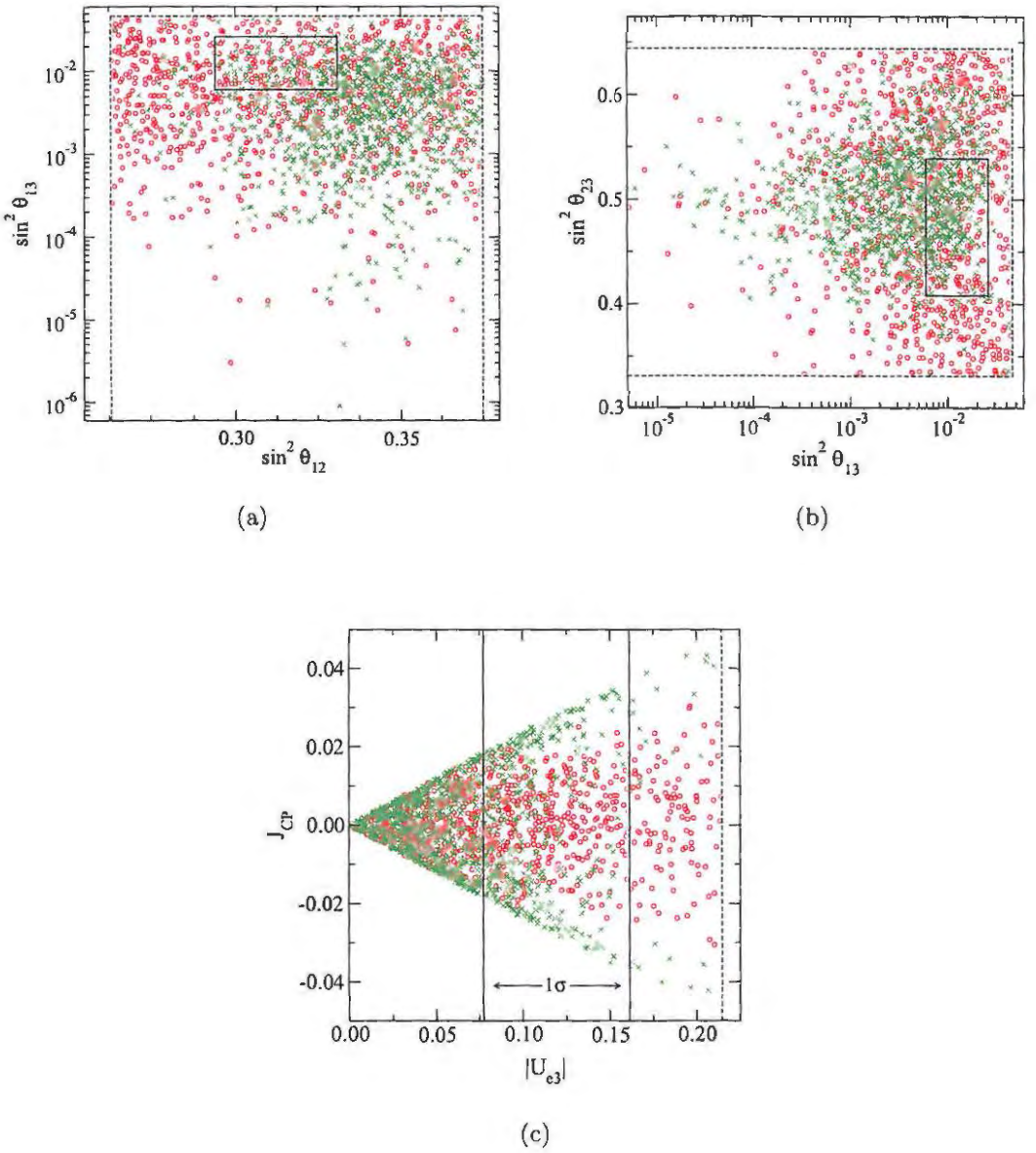

Figure 5.9: Scatter plots of mixing angles ((a) and (b)) and J_{CP} against $|U_{e3}|$ (c) for the A-F model, with two Higgs singlets, for normal (red circles) and inverted (green crosses) hierarchies.

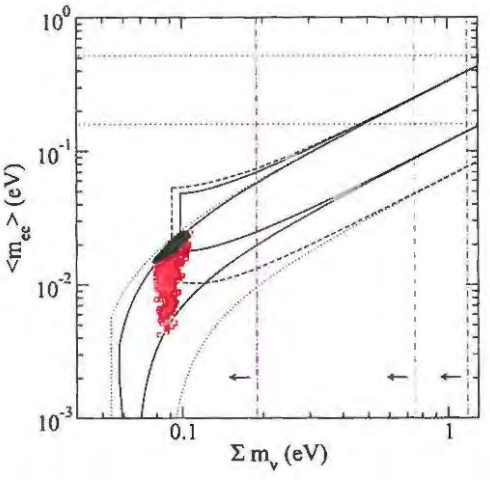

(a)

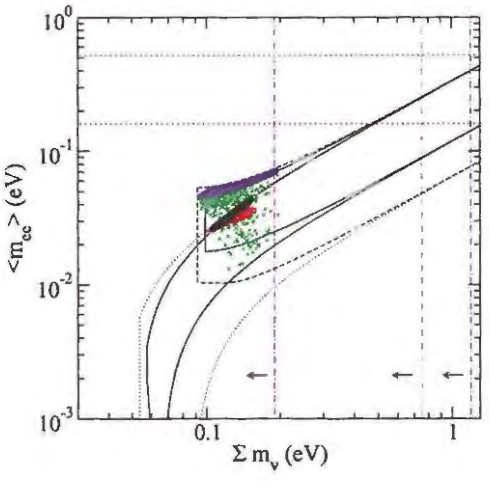

(b)

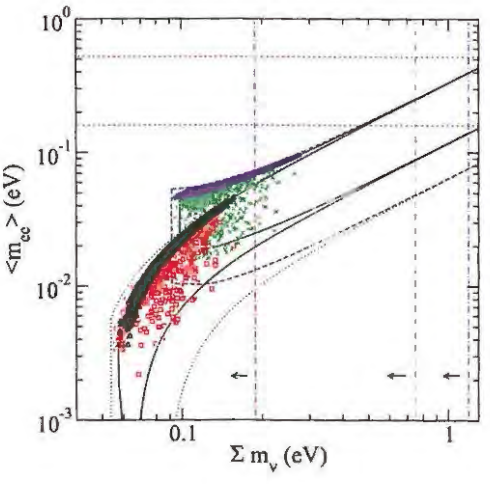

(c)

Figure 5.10: Scatter plots of $\langle m_{ee} \rangle$ against $\sum m_\nu$ for the original A-F model, with: (a) one Higgs singlet (normal mass hierarchy only); (b) two Higgs singlets and (c) three Higgs singlets [243]. See the caption of Fig. 5.4 for an explanation of the symbols used.

In order to obtain this mixing matrix, the mass matrix must be of the form

$$M_\nu = \begin{pmatrix} \alpha & 0 & \beta \\ 0 & \gamma & 0 \\ \beta & 0 & \alpha \end{pmatrix} , \tag{5.29}$$

as in Eq. (4.14), which is difficult to achieve without additional Higgs scalars.

The Higgs doublets ξ and φ', transforming as $\underline{1}$ and $\underline{3}$, respectively, are introduced. Hence, there are three types of dimension-5 (O_5) operators allowed by the A_4 symmetry: $(\xi\ell)^2$, $(\xi\ell)(\varphi'\ell)$ and $(\varphi'\ell)^2$. There is an additional discrete symmetry to prevent the other Higgs scalar (φ) from entering into the O_5 operators (this is a feature of most A_4 models, as the charged lepton and neutrino sectors are effectively "decoupled" from each other).

Examining each of the O_5 operators in turn allows the construction of the neutrino mixing matrix, as detailed in Ref. [74]. Here the VEV alignment of the triplet φ' is assumed to be proportional to $(0, 1, 0)$, which is justified by an analysis of the Higgs potential (see the Appendix of Ref. [74]). By modifying this VEV alignment, so that

$$\langle\varphi'\rangle = (v'\epsilon_1, v', v'\epsilon_2) , \tag{5.30}$$

and analysing each term in the three O_5 operators, the deviated neutrino mass matrix

$$M'_\nu = m_0 \begin{pmatrix} a^2 + b^2\left(1 + 3\epsilon_1^2 + \epsilon_2^2\right) & ab\epsilon_2 + b^2\epsilon_1 & ab + b^2\epsilon_1\epsilon_2 \\ \cdot & a^2 + b^2\left(3 + \epsilon_1^2 + \epsilon_2^2\right) & ab\epsilon_1 + b^2\epsilon_2 \\ \cdot & \cdot & a^2 + b^2\left(1 + \epsilon_1^2 + 3\epsilon_2^2\right) \end{pmatrix} \tag{5.31}$$

can be constructed,[7] where a and b come from the VEVs $\langle\xi\rangle$ and $\langle\varphi'\rangle$ respectively. The details of this analysis are in Appendix B. For $\epsilon_1 = \epsilon_2 = 0$, this matrix reduces to the form in Eq. (5.29), and is diagonalised by Eq. (5.28), with eigenvalues a^2+ab+b^2, a^2+3b^2 and a^2-ab+b^2. Thus exact TBM is achieved, and, by setting ϵ_1 and ϵ_2 to be non-zero the effect of VEV misalignment can be studied. Note that with $m_0 = 0.025$ eV and $m_0 = 0.05$ eV for the normal and inverted hierarchies, respectively, the $a-b$ parameter space is constrained as shown in Fig. 5.11.

Only one plot of mixing angle observables is displayed in Fig. 5.12, since in this case most of the plots cover the full 3σ range. Here the effect of deviations in Eqs. (5.31)

[7] Note that here the effective coupling constants in front of the two symmetric triplet combinations are assumed to be equal (see Eqs. (B.14) and (B.16) in Section B.1).

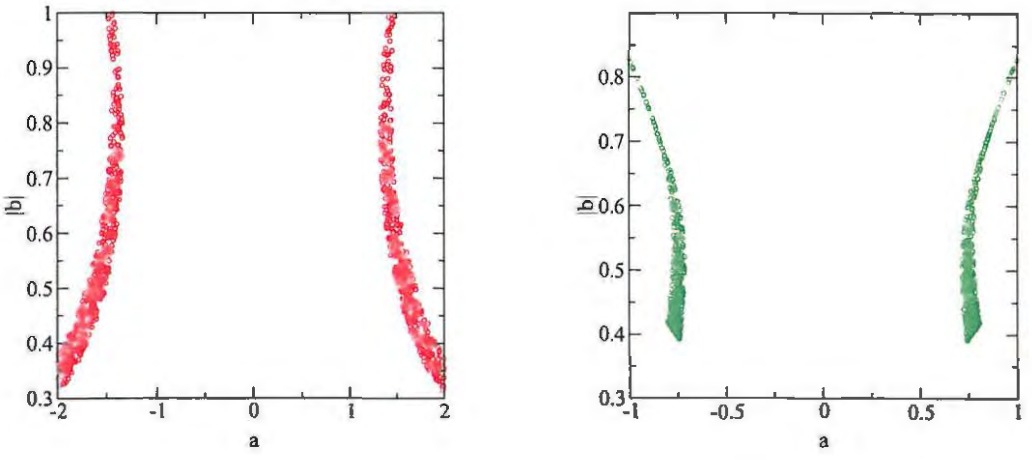

(a) (b)

Figure 5.11: Scatter plots of the $a - b$ parameter space for the Zee model, for normal (a) and inverted (b) hierarchies.

and (5.16) can be seen: $\sin^2\theta_{23}$ is spread evenly around its TBM value, whereas $\sin^2\theta_{13}$ becomes greater than zero, and can take larger values in the normal hierarchy case.

Since the value of m_0 was fixed to 0.025 eV and 0.05 eV in the normal and inverted hierarchy case,[8] respectively, the scatter plot in Fig. 5.13 allows only certain values for $\sum m_\nu$. There is not much separation in the value of $\langle m_{ee}\rangle$ between the normal and inverted hierarchies, as most of the points lie close to the quasi-degenerate region ($\sum m_\nu \gtrsim 0.117$ eV). This is the effect of a large value of $\sin^2\theta_{13}$ [266]. Note that for the chosen values of m_0, the value of $\sum m_\nu$ can be greater for the normal hierarchy than for the inverted hierarchy.

5.3.4 Morisi $(Z_2)^3$ model

This model [86] has the same structure as the Altarelli-Feruglio model [33] in Section 5.3.2 above, except that the vacuum alignment problem is tackled in a somewhat different fashion. The flavour group is enlarged from A_4 to $G_f = A_4 \ltimes (Z_e \times Z_\mu \times Z_\tau)$, which is the semidirect product of A_4 with the group $(Z_2)^3 \equiv (Z_e \times Z_\mu \times Z_\tau)$. The approach is similar to that in Ref. [74], where charged lepton masses come from dimension-four operators and neutrino masses from dimension-five operators. Other authors [37, 267] have made use of additional Z_2 symmetries in S_3 models; this model

[8] These values of m_0 were used throughout this work.

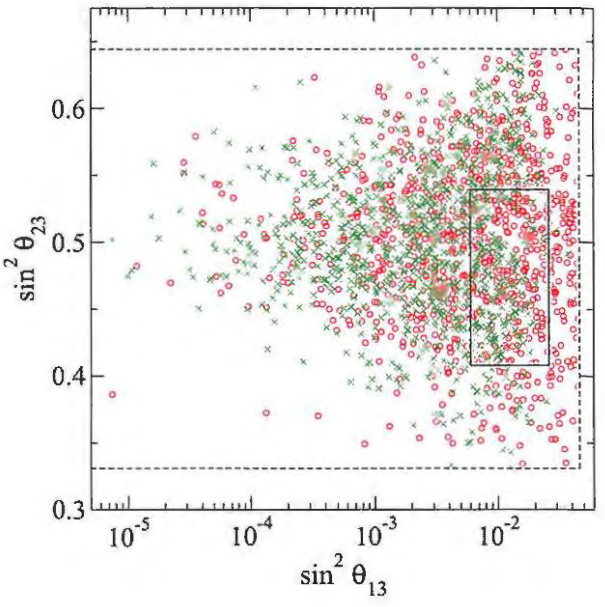

Figure 5.12: Scatter plot of $\sin^2\theta_{23}$ against $\sin^2\theta_{13}$ for the Zee model [74], for normal (red circles) and inverted (green crosses) hierarchy.

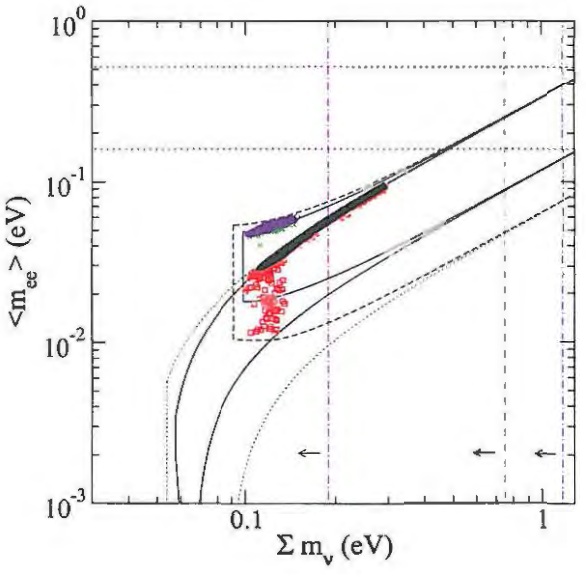

Figure 5.13: Scatter plot of $\langle m_{ee}\rangle$ vs $\sum m_\nu$ for the Zee model [74], with symbols as defined in Fig. 5.4.

uses the same idea, but applied to a model with A_4 family symmetry.

The essential feature of this model is that each right handed field ℓ^c_α is charged under the corresponding $Z_{2\alpha}$ with $\alpha = e, \mu, \tau$. In addition, each scalar field φ_i $(i = 1, 2, 3)$ of the Higgs triplet φ transforms with respect to $Z_{2\alpha}$. The $(Z_2)^3$ symmetries "glue" each ℓ^c_α with the corresponding φ_i, so that there are no off-diagonal terms in the charged lepton sector. Hence, exact TBM can be acheived with both Higgs triplets taking the VEV alignment proportional to $(1, 1, 1)$, *viz.*

$$\langle \varphi \rangle = (v, v, v) \quad \text{and} \quad \langle \varphi' \rangle = (v', v', v') \ . \tag{5.32}$$

With this alignment the charged lepton mass matrix is diagonal and the neutrino mass matrix is given by

$$M_\nu = m_0 \begin{pmatrix} a+2b & -b & -b \\ -b & 2b & a-b \\ -b & a-b & 2b \end{pmatrix} \tag{5.33}$$

which is in effect equivalent to the Altarelli-Feruglio model, with one Higgs singlet (the factor of $\frac{1}{3}$ is omitted from the A_4 product rules in Ref. [86], and the parameter d in Eq. (5.20) is called b in Eq. (5.33)). This matrix has eigenvalues $a+3b$, a and $-a+3b$, and is diagonalised by the TBM matrix, with only the normal hierarchy of neutrino masses possible. Note that a plot of a against b yields the same information as Fig. 5.5, i.e., a very small allowed region in $a - b$ parameter space.

If the alignment in Eq. (5.32) is deviated to

$$\langle \varphi \rangle = (v, v(1+\epsilon_1^{ch}), v(1+\epsilon_2^{ch})) \quad \text{and} \quad \langle \varphi' \rangle = (v', v'(1+\epsilon_1), v'(1+\epsilon_2)) \ , \tag{5.34}$$

the mass matrices are

$$M'_\ell = v_d \frac{v}{\Lambda} \begin{pmatrix} y_e & 0 & 0 \\ 0 & y_\mu(1+\epsilon_1^{ch}) & 0 \\ 0 & 0 & y_\tau(1+\epsilon_2^{ch}) \end{pmatrix} \tag{5.35}$$

and

$$M'_\nu = m_0 \begin{pmatrix} a+2b & -b(\epsilon_1+1) & -b(\epsilon_2+1) \\ \cdot & 2b(\epsilon_2+1) & a-b \\ \cdot & \cdot & 2b(\epsilon_1+1) \end{pmatrix} \ , \tag{5.36}$$

which can be analysed for deviations from TBM.

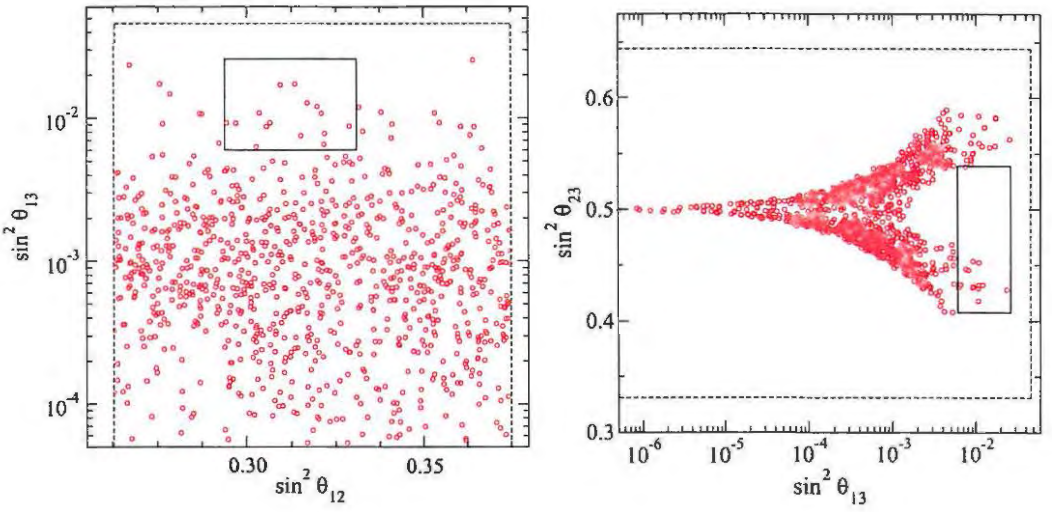

(a) (b)

Figure 5.14: Scatter plots of mixing angle observables for the Morisi $(Z_2)^3$ model, normal hierarchy.

The only difference between this model and the Altarelli-Feruglio model (with one Higgs singlet) is the structure of the charged lepton sector: the deviated M_ℓ in Eq. (5.35) differs from that in Eq. (5.24). However, a comparison of Fig. 5.14 with Fig. 5.8(a) shows that the perturbations have almost the same effect, and the value of $\sin^2\theta_{13}$ remains low (below 0.005). The value of $\sin^2\theta_{23}$ deviates from maximal (both above and below 0.5) for increasing θ_{13}, with slightly less deviation than in the Altarelli-Feruglio model [Fig. 5.8(a)], since the deviated M_ℓ in Eq. (5.35) is diagonal. The plot of J_{CP} against $|U_{e3}|$ in Fig. 5.15 is similar to that in Fig. 5.8(b). The points in $\langle m_{ee}\rangle - \sum m_\nu$ parameter space (Fig. 5.16) confirm the similarity with the A-F model [see Fig. 5.10(a)], with the only reason for the increase in $\sum m_\nu$ being the omission of the factor 1/3 in the A_4 product rules, so that $\sum m_\nu = |a+3b| + |a| + |-a+3b|$.

5.4 Type B models

Type B models have lepton doublets transforming as $\underline{3}$, charged lepton singlets as $\underline{1}, \underline{1}', \underline{1}''$, and right handed neutrinos transforming as $\underline{3}$, with neutrino mass generated by the seesaw mechanism. The Ma TBM model [31] with no right handed neutrinos, discussed in Section 5.3, was the first to predict TBM. However, the original Ma model [34] was a type B model, which predicted degenerate neutrinos. This is not compatible

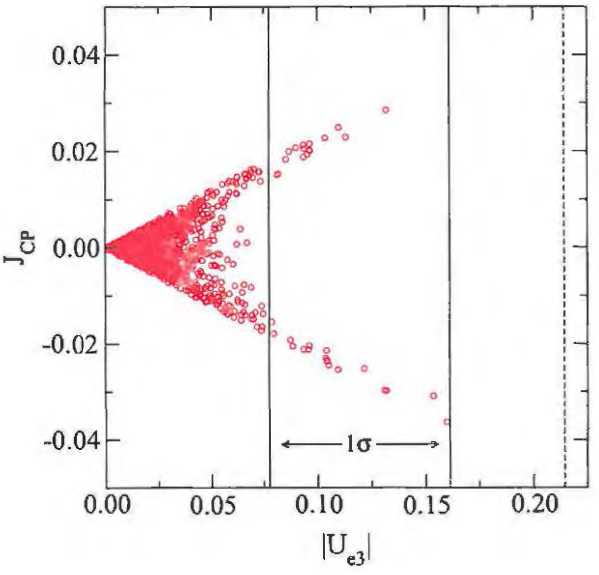

Figure 5.15: Scatter plot of J_{CP} against $|U_{e3}|$ for the Morisi $(Z_2)^3$ model, normal hierarchy.

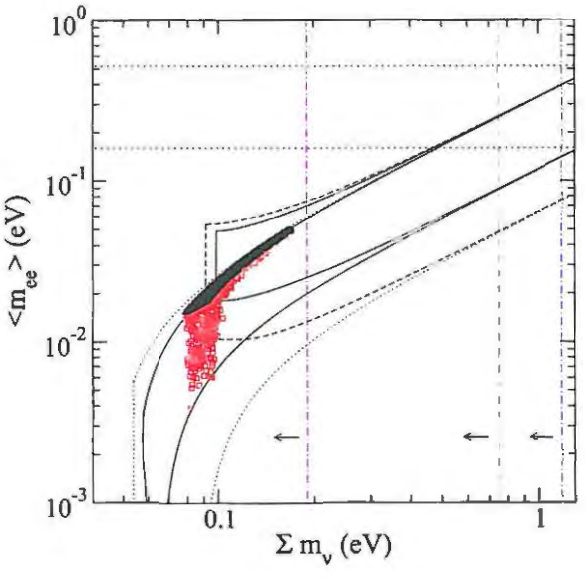

Figure 5.16: Scatter plot of $\langle m_{ee} \rangle$ against $\sum m_\nu$ for the Morisi $(Z_2)^3$ model, normal mass hierarchy, with symbols as defined in Fig. 5.4 above.

with TBM and the current neutrino data (for a phenomenological analysis of this model see Ref. [257]), and radiative corrections can be used to lift this degeneracy [70]. Table 5.4 contains a summary of published type B models, and the analysis that follows will focus on those that predict TBM.

5.4.1 Babu & He model

This model [72] is formulated "in the context of low energy supersymmetry", with the normal SM gauge group and A_4. In addition to this, there is a $Z_4 \times Z_3$ discrete symmetry, which is broken softly in the superpotential. The introduction of supersymmetry and additional discrete symmetries is essentially a way to explain the VEV alignment – the superpotential of the model is formulated in such a way that the alignments

$$\langle\varphi\rangle = (v, v, v) \quad \text{and} \quad \langle\varphi'\rangle = (0, v', 0) \tag{5.37}$$

are obtained from minimizing the potential. In the analysis herein, details of the supersymmetrical realization of the model are omitted, with the focus being the symmetry breaking structure (this is similar to the approach in Ref. [73], where the basic tree-level structure of the model is discussed and details of its "dynamical completion" are in the appendix).

Since the A_4 particle assignments for charged leptons are the same as those in Type A models, the charged lepton mass matrix is also given by Eq. (5.7), and the VEV alignment in Eq. (5.37) means that M_ℓ is diagonalised by U_ω. It follows that the deviated charged lepton mass matrix is the same as Eq. (5.16), with the parameters ϵ_1^{ch} and ϵ_2^{ch} defined in Eq. (5.15).

The superpotential relevant for neutrino masses is

$$W_{Y_\nu} = f_\nu(\ell_L h_u N_R) + \frac{1}{2} f_\xi \xi (N_R N_R) + \frac{1}{2} f_{\varphi'}(\varphi' N_R N_R) \ , \tag{5.38}$$

with right-handed neutrinos N_R, coupling constants f_ξ, $f_{\varphi'}$ and f_ν, and the Higgs doublet h_u. The first term in Eq. (5.38) is made up of two A_4 triplets, so that the Dirac mass matrix is diagonal:

$$M_{\rm D} = \begin{pmatrix} f_\nu v_u & 0 & 0 \\ 0 & f_\nu v_u & 0 \\ 0 & 0 & f_\nu v_u \end{pmatrix} \ , \tag{5.39}$$

with v_u the VEV of the Higgs doublet h_u. The second and third terms in the super-

Table 5.4: Summary of type B A_4 models.

Model	M_ℓ	M_ν	TBM?	Comments
Ma 1 [34, 256, 257]	$\propto \begin{pmatrix} h_1v_1 & h_2v_1 & h_3v_1 \\ h_1v_2 & h_2\omega v_2 & h_3\omega^2 v_2 \\ h_1v_3 & h_2\omega^2 v_3 & h_3\omega v_3 \end{pmatrix}$	$\propto \begin{pmatrix} 1 & 0 & 0 \\ 0 & 0 & 1 \\ 0 & 1 & 0 \end{pmatrix}$	No	Degenerate neutrino masses
Babu, Ma, Valle [70]	As above	$\propto \begin{pmatrix} 1+\delta_0+2\delta+2\delta' & \delta'' & \delta'' \\ \delta'' & \delta & 1+\delta_0+\delta \\ \delta'' & 1+\delta_0+\delta & \delta \end{pmatrix}$	No	Radiative corrections
Babu & He [72, 73]	As above	$\propto \begin{pmatrix} 1 & 0 & x \\ 0 & 1-x^2 & 0 \\ x & 0 & 1 \end{pmatrix}$	Yes	SUSY
Ma SUSY Seesaw [71]	As above	$\propto \frac{a}{(b^2-c^2)} \begin{pmatrix} b^2-c^2 & 0 & 0 \\ 0 & ab & -ac \\ 0 & -ac & ab \end{pmatrix}$	Yes	SUSY
A-F Seesaw [33][a]	$\propto \begin{pmatrix} y_e & 0 & 0 \\ 0 & y_\mu & 0 \\ 0 & 0 & y_\tau \end{pmatrix}$	$\propto \frac{1}{3a(a+b)} \begin{pmatrix} 3a+b & b & b \\ b & \frac{2ab+b^2}{b-a} & \frac{b^2-ab-3a^2}{b-a} \\ b & \frac{b^2-ab-3a^2}{b-a} & \frac{2ab+b^2}{b-a} \end{pmatrix}$	Yes	SUSY
Yin [258]	As in Ma 1 model	$\propto \begin{pmatrix} \gamma & 0 & 0 \\ 0 & \alpha & \beta \\ 0 & \beta & \alpha \end{pmatrix}$	Yes	$3-3-1$ model
Chen & King [227]	As in AFSS model	$M_{\rm D} = \begin{pmatrix} 2\alpha_s+\alpha_0 & -\alpha_s & -\alpha_s \\ -\alpha_s & 2\alpha_s & -\alpha_s+\alpha_0 \\ -\alpha_s & -\alpha_s+\alpha_0 & 2\alpha_s \end{pmatrix}$	Yes	With seesaw
AFSU5 [251]	$\propto \begin{pmatrix} st^3+st''^3 & st^2t'' & stt''^2 \\ \cdots & st & st'' \\ \cdots & \cdots & 1 \end{pmatrix}$	$\propto \frac{1}{3a(a+b)} \begin{pmatrix} 3a+b & b & b \\ b & \frac{2ab+b^2}{b-a} & \frac{b^2-ab-3a^2}{b-a} \\ b & \frac{b^2-ab-3a^2}{b-a} & \frac{2ab+b^2}{b-a} \end{pmatrix}$	Yes	SUSY SU(5)

[a] This model uses the A-F-basis for A_4.

potential define the couplings of right-handed neutrinos with the Higgs scalars, giving the Majorana mass matrix

$$M_{\rm R} = \begin{pmatrix} f_\xi u & 0 & f_{\varphi'} v' \\ 0 & f_\xi u & 0 \\ f_{\varphi'} v' & 0 & f_\xi u \end{pmatrix} , \tag{5.40}$$

where u is the VEV of the singlet ξ, and the triplet φ' takes the VEV in Eq. (5.37). Using the seesaw mechanism [Eq. (3.71)], the light neutrino mass matrix is

$$M_\nu = M_0 \begin{pmatrix} 1 & 0 & x \\ 0 & 1-x^2 & 0 \\ x & 0 & 1 \end{pmatrix} , \tag{5.41}$$

where $M_0 = f_\nu^2 v_u^2 f_\xi u / (f_\xi^2 u^2 - f_{\varphi'}^2 v'^2)$, and $x = -f_{\varphi'} v' / f_\xi u$. Once again, this matrix can be diagonalised by the mixing matrix in Eq. (5.28), which combines with U_ω to give TBM.

The effect of deviating the VEV alignments of the Higgs triplet φ is the same as that discussed in Section 5.3.1, so that the new charged lepton matrix is given by Eq. (5.16). Changing the VEV alignment of the Higgs triplet φ' to

$$\langle \varphi' \rangle = (v'\epsilon_1, v', v'\epsilon_2) , \tag{5.42}$$

results in the new Majorana mass matrix

$$M'_{\rm R} = \begin{pmatrix} b & c\,\epsilon_1 & c \\ c\,\epsilon_1 & b & c\,\epsilon_2 \\ c & c\,\epsilon_2 & b \end{pmatrix} , \tag{5.43}$$

with $b = f_\xi u$ and $c = f_{\varphi'} v'$. The seesaw mechanism gives the light neutrino mass matrix

$$M'_\nu = \frac{m_0}{m} \begin{pmatrix} a^2(b - c\,\epsilon_2)(b + c\,\epsilon_2) & a^2 c\,(c\,\epsilon_2 - b\,\epsilon_1) & a^2 c\,(c\,\epsilon_1\epsilon_2 - b) \\ \cdot & a^2(b-c)(b+c) & a^2 c\,(c\,\epsilon_1 - b\,\epsilon_2) \\ \cdot & \cdot & a^2(b - c\,\epsilon_1)(b + c\,\epsilon_1) \end{pmatrix} , \tag{5.44}$$

where $m = b^3 - c^2(\epsilon_1^2 + \epsilon_2^2 + 1)b + 2c^3\epsilon_1\epsilon_2$, $a = f_\nu v_u$ and the constant m_0 is used to fix the mass scale, as before. The scatter plots in Fig. 5.17 show the allowed region in $a - b - c$ parameter space, before perturbations are applied. One can see that

the parameters a, b and c must take specific values in order to reproduce the correct neutrino mass-squared differences.

An analysis of the deviations from TBM in this model gives rather general results, with the mixing angles spread across their 3σ allowed regions, J_{CP} taking all possible values, and not much variation between the normal and inverted hierarchy. The results are similar to those shown in Figs. 5.2 and 5.3. A feature of this model is the distinct separation in the value of $\langle m_{ee} \rangle$, as seen in Fig. 5.18, where $\langle m_{ee} \rangle_{NH} < \langle m_{ee} \rangle_{IH}$. In addition, the allowed region for $\langle m_{ee} \rangle$ and $\sum m_\nu$ in the normal hierarchy, unperturbed case is very small. The neutrino mass in the case of normal hierarchy lies in the hierarchical mass region, and the perturbations have the effect of increasing the allowed values of $\langle m_{ee} \rangle$, whereas those for the inverted hierarchy lie in the quasidegenerate region, with perturbations having very little effect on the allowed region in $\langle m_{ee} \rangle - \sum m_\nu$ parameter space. As discussed in Ref. [72], it is possible to get degenerate neutrino masses with the inverted hierarchy for large m_3, and here the value of $\sum m_\nu$ increases above the second cosmological limit in Fig. 5.18. The inverted hierarchy in this model is compatible with the Heidelberg-Moscow $0\nu\beta\beta$ claim [179,180].

5.4.2 Ma supersymmetric seesaw model

In this model [71] there are heavy right-handed neutrino singlet superfields, N_i, transforming as $\underline{3}$ under A_4. There are 3 Higgs doublets $(\varphi_i'^0, \varphi_i'^-)$ transforming as $\underline{3}$, and when the VEV $\langle \varphi_i'^0 \rangle = v$ (for $i = 1,2,3$), M_ℓ takes the same form as in the previous model. The neutrino sector contains the Higgs doublet (ξ^+, ξ^0), which is an A_4 singlet.

The most general invariant superpotential of N_i (up to quartic terms) is

$$\begin{aligned} W = & \frac{1}{2} m_N (N_1^2 + N_2^2 + N_3^2) + f N_1 N_2 N_3 \\ & + \frac{\lambda_1}{4 M_{\rm Pl}} (N_1^4 + N_2^4 + N_3^4) \\ & + \frac{\lambda_2}{2 M_{\rm Pl}} (N_2^2 N_3^2 + N_3^2 N_1^2 + N_1^2 N_2^2) \ , \end{aligned} \tag{5.45}$$

where $M_{\rm Pl} = 1.2 \times 10^{19}$ GeV is the Planck mass. By minimising the resulting scalar potential, Ma shows [71] that

$$\langle N_{2,3} \rangle = 0 \ , \quad \langle N_1 \rangle^2 = \frac{-m_N M_{\rm Pl}}{\lambda_1} \tag{5.46}$$

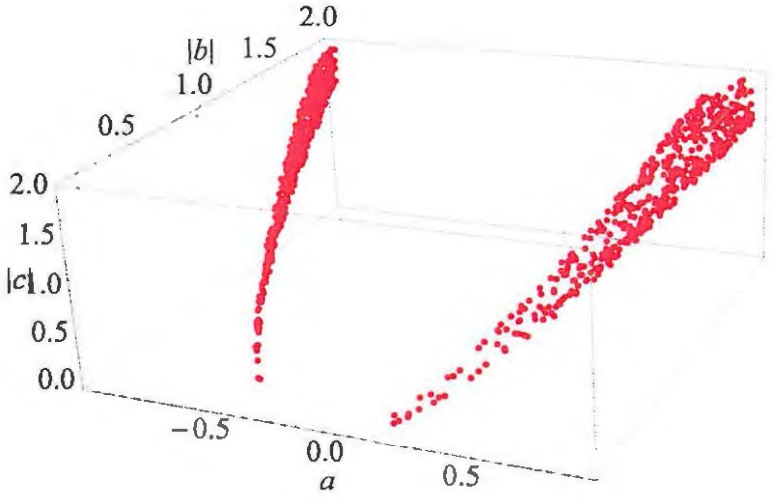

(a)

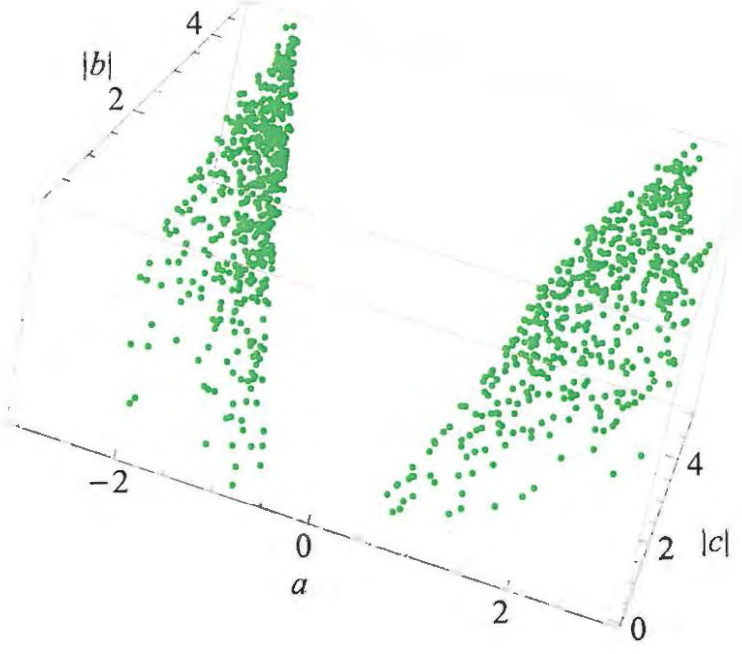

(b)

Figure 5.17: Scatter plots of the $a - b - c$ parameter space for the Babu & He model, for normal (a) and inverted (b) hierarchies.

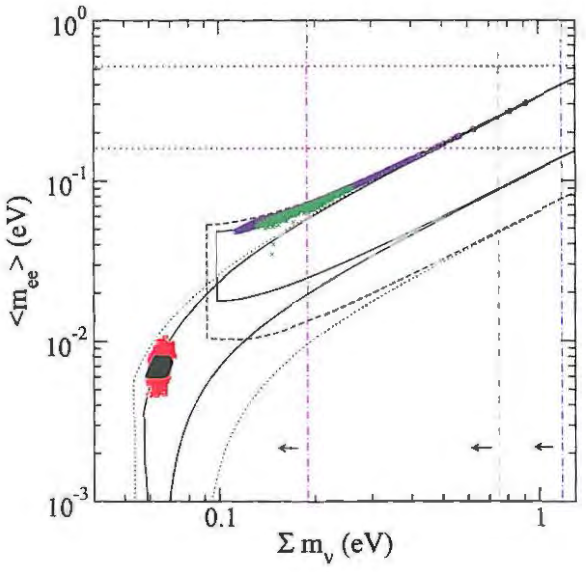

Figure 5.18: Scatter plot of $\langle m_{ee} \rangle$ against $\sum m_\nu$ for the Babu & He supersymmetric model, for normal and inverted mass hierarchy, with symbols as defined in Fig. 5.4.

is a "natural" solution, which means that the Majorana mass matrix becomes

$$M_{\rm N} = \begin{pmatrix} a & 0 & 0 \\ 0 & b & c \\ 0 & c & b \end{pmatrix} , \tag{5.47}$$

with $a = -2m_N$, $b = (1 - \lambda_2/\lambda_1)m_N$, and $c = f\langle N_1 \rangle$. The Dirac mass matrix is diagonal, so that the resulting light neutrino mass matrix is

$$M_\nu = \frac{m_0}{a(b^2 - c^2)} \begin{pmatrix} b^2 - c^2 & 0 & 0 \\ 0 & ab & -ac \\ 0 & -ac & ab \end{pmatrix} , \tag{5.48}$$

which is diagonalised by Eq. (5.28), giving exact TBM. The allowed region in $a - b - c$ parameter space is shown in Fig. 5.19, and it is evident that the parameters must take very specific values in order for the model to give the correct mass neutrino mass-squared differences.

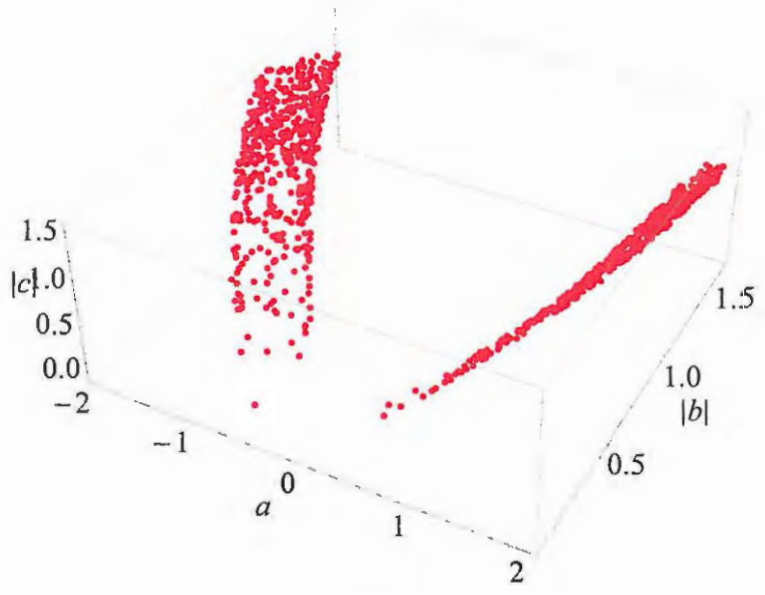

(a)

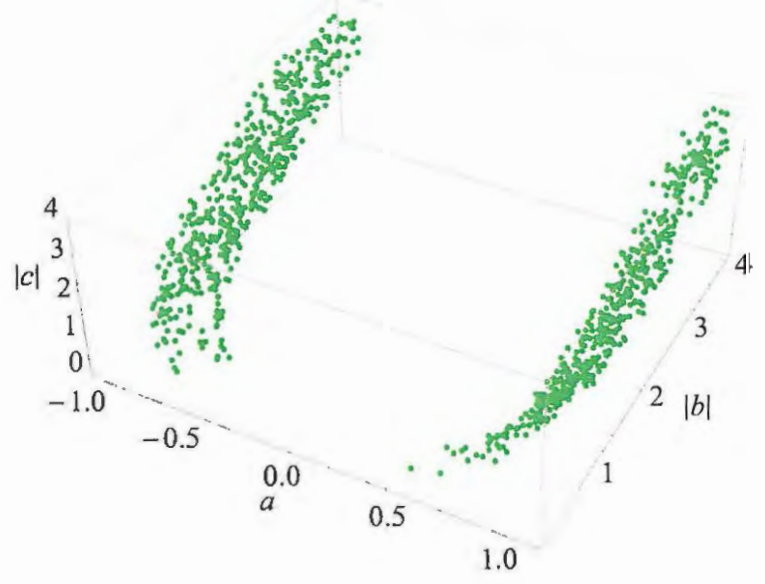

(b)

Figure 5.19: Scatter plots of the $a-b-c$ parameter space for the Ma supersymmetric seesaw model, for normal (a) and inverted (b) hierarchies.

In order to deviate this VEV alignment, the fields

$$\langle N_2\rangle^2 = \epsilon_1\langle N_1\rangle^2 \quad \text{and} \quad \langle N_3\rangle^2 = \epsilon_2\langle N_1\rangle^2 \,, \tag{5.49}$$

can be defined, with $\langle N_1\rangle^2$ from Eq. (5.46). To find the new mass terms, the shifted fields $N_i' \equiv N_i - \langle N_i\rangle$ $(i = 1, 2, 3)$ are substituted into the superpotential in Eq. (5.45), and terms quadratic in N_i' are picked out as mass terms. After some algebra, the Majorana mass matrix is

$$M_{\rm N}' = \begin{pmatrix} a + \frac{1}{2}(a+2b)(\epsilon_1+\epsilon_2) & 2\sqrt{\epsilon_1}(a+2b) + c\sqrt{\epsilon_2} & 2\sqrt{\epsilon_2}(a+2b) + c\sqrt{\epsilon_1} \\ \cdot & b(\epsilon_2+1) + \frac{1}{2}a(3\epsilon_1+\epsilon_2) & 2\sqrt{\epsilon_1\epsilon_2}(a+2b) + c \\ \cdot & \cdot & b(\epsilon_1+1) + \frac{1}{2}a(\epsilon_1+3\epsilon_2) \end{pmatrix} , \tag{5.50}$$

with a, b and c as defined above. Using the matrix in Eq. (5.50) and the diagonal Dirac mass matrix, $M_{\rm D}$, a new light neutrino mass matrix is obtained.[9] The charged lepton alignment is deviated in the same way as before.

In this model both normal and inverted hierarchies are possible, but once perturbations are applied, the Fortran program takes very long to find solutions that lie within the 3σ range of the data. This could be attributed to the small allowed region in $a - b - c$ parameter space in Fig. 5.19(b). As can be seen in Fig. 5.20, the value of $\sin^2\theta_{13}$ deviates considerably from its TBM value of zero, with the majority of points lying close to the upper bound (at 3σ) of 0.046. The deviation from maximal θ_{23} is uniform across the whole 3σ range.

In Fig. 5.21 the results for normal and inverted hierarchies are plotted in $\langle m_{ee}\rangle - \sum m_\nu$ parameter space, but the effects of perturbations are shown only in the normal hierarchy case.[10] With perturbations applied [Eq. (5.50)], specific values of the parameters a, b and c were chosen to allow the program to find solutions, so that these points (red squares) lie in a certain region of parameter space. In the normal hierarchy, the effect of perturbations is to allow for a lower value of $\langle m_{ee}\rangle$ than in the unperturbed case, and the neutrino masses lie in the hierarchical region. For the inverted hierarchy and in the unperturbed case, $\langle m_{ee}\rangle$ takes its maximum value.

[9] An explicit definition of the deviated light neutrino mass matrix M_ν' is omitted, for brevity.
[10] The program did not converge to solutions for the perturbed inverted hierarchy.

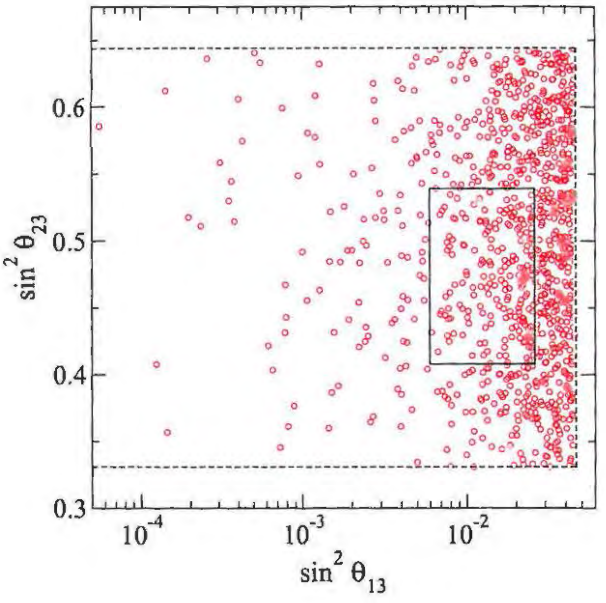

Figure 5.20: Scatter plot of $\sin^2\theta_{23}$ against $\sin^2\theta_{13}$ for the Ma supersymmetric seesaw model, normal hierarchy.

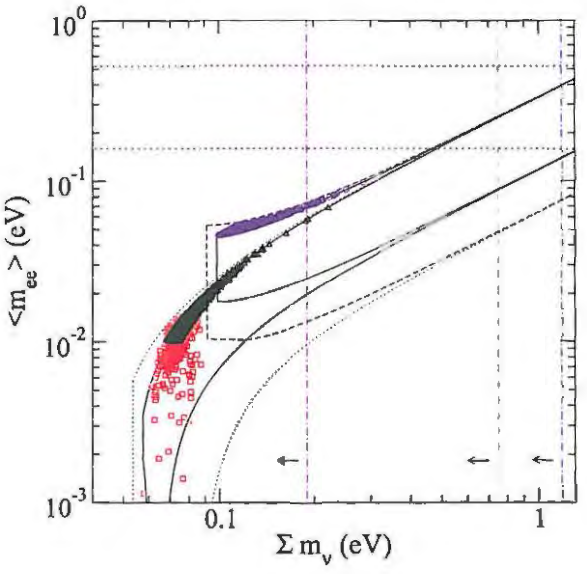

Figure 5.21: Scatter plot of $\langle m_{ee}\rangle$ against $\sum m_\nu$ for the Ma supersymmetric seesaw model, with normal and inverted mass hierarchy. See the caption of Fig. 5.4 for an explanation of the symbols used.

5.4.3 Altarelli-Feruglio seesaw model

The Altarelli-Feruglio model in Section 5.3.2 can be extended by introducing right-handed neutrino fields ν^c, transforming as $\underline{3}$ under A_4 [33]. The new Lagrangian contains all the terms in Eq. (5.17), along with the additional terms

$$\begin{aligned}\mathscr{L}_{Y(\text{seesaw})} = \; & y(\nu^c \ell) h_u + x_A \xi (\nu^c \nu^c) + x_D (\varphi' \nu^c \nu^c) \\ & [+x_C \xi' (\nu^c \nu^c)'' + x_B \xi'' (\nu^c \nu^c)'] + \text{h.c.} + \ldots \,, \end{aligned} \tag{5.51}$$

where y is a coupling constant.[11] Most details of the model remain the same, with the charged lepton mass matrix given by Eq. (5.19). The Dirac mass matrix is diagonal, and the Majorana mass matrix has the same form as Eq. (5.20). With the seesaw mechanism, the light neutrino mass matrix is[12]

$$M_\nu = \frac{m_0}{3a(a+d)} \begin{pmatrix} 3a+d & d & d \\ d & \frac{2ad+d^2}{d-a} & \frac{d^2-ad-3a^2}{d-a} \\ d & \frac{d^2-ad-3a^2}{d-a} & \frac{2ad+d^2}{d-a} \end{pmatrix} , \tag{5.52}$$

where $a = 2x_A \frac{u_a}{\Lambda}$, $d = 2x_D \frac{v'}{\Lambda}$ and $m_0 = y^2 \frac{v_u^2}{\Lambda}$. In order for the correct values of the neutrino oscillation observables to be reproduced, the parameters a and d must take specific values, as shown in Fig. 5.22. This is similar to the A-F model without seesaw (see Fig. 5.5). Note that the inverted hierarchy is possible in the seesaw version of this model.

With the deviated VEV alignment of Eq. (5.23), the charged lepton mass matrix is defined by Eq. (5.24), and the light neutrino mass matrix is

$$\begin{aligned} M'_\nu &= \frac{3m_0}{m} \begin{pmatrix} ((d_1-3a)^2 - 4d_2 d_3) & -2d_3^2 + 3ad_2 - d_1 d_2 & -2d_2^2 + 3ad_3 - d_1 d_3 \\ \cdot & (d_2^2 - 6ad_3 - 4d_1 d_3) & 9a^2 + 3d_1 a - 2d_1^2 - d_2 d_3 \\ \cdot & \cdot & (d_3^2 - 6ad_2 - 4d_1 d_2) \end{pmatrix} , \\ m &= 27a^3 - 9a\left(d_1^2 + 2d_2 d_3\right) + 2\left(d_1^3 - 3d_1 d_2 d_3 + d_2^3 + d_3^3\right) , \end{aligned} \tag{5.53}$$

with $d_1 = d$, $d_2 = d(1+\epsilon_1)$ and $d_3 = d(1+\epsilon_2)$.

Although the model in Ref. [33] has one Higgs singlet, it was shown in Section 5.3 that it is possible to achieve TBM with both two and three singlets. This idea [243]

[11] In Eq. (5.51) the compact notation of Eq. (5.17) does not apply.

[12] For consistency with the analysis in Section 5.3.2, the parameter d was used, intead of b, which is used in Ref. [33].

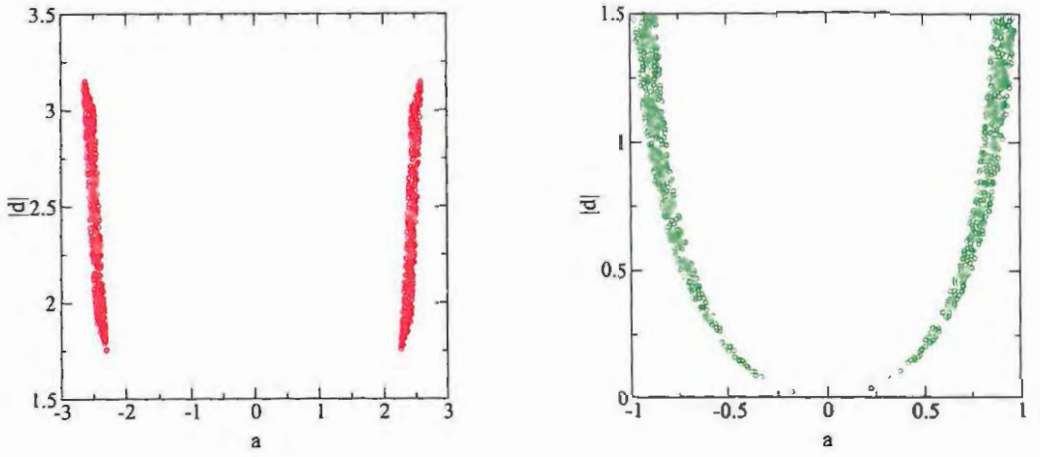

(a) (b)

Figure 5.22: Scatter plots of the $a-d$ parameter space for the A-F seesaw model, with one Higgs singlet, for normal (a) and inverted (b) hierarchies.

can be applied to the A-F seesaw model: herein the case of three Higgs singlets with seesaw is analysed, where the deviated Majorana mass matrix takes the same form as Eq. (5.27). The resulting neutrino mass matrix is

$$M'_\nu = \frac{3m_0}{m}\begin{pmatrix} M'_{11} & M'_{12} & M'_{13} \\ \cdot & M'_{22} & M'_{23} \\ \cdot & \cdot & M'_{33} \end{pmatrix} , \tag{5.54}$$

where

$$M'_{11} = \left((d_1 - 3a)^2 - (3c + 2d_2)(3b + 2d_3)\right) \tag{5.55}$$
$$M'_{12} = \left(9b^2 + 3d_3 b - 2d_3^2 + (d_1 - 3a)(3c - d_2)\right) \tag{5.56}$$
$$M'_{13} = \left(9c^2 + 3d_2 c - 2d_2^2 + 3bd_1 - d_1 d_3 + 3a(d_3 - 3b)\right) \tag{5.57}$$
$$M'_{22} = -\left((3a + 2d_1)(3b + 2d_3) - (d_2 - 3c)^2\right) \tag{5.58}$$
$$M'_{23} = \left(9a^2 + 3d_1 a - 2d_1^2 + 3b(d_2 - 3c) + 3cd_3 - d_2 d_3\right) \tag{5.59}$$
$$M'_{33} = -\left((3a + 2d_1)(3c + 2d_2) - (d_3 - 3b)^2\right) , \tag{5.60}$$

and

$$m = 27a^3 - 9a\left(9bc + d_1^2 + 2d_2d_3\right) + 27b^3 - 9b\left(2d_1d_2 + d_3^2\right) - 6d_1d_3(3c + d_2) + (d_2 - 3c)^2(3c + 2d_2) + 2d_1^3 + 2d_3^3 \,, \tag{5.61}$$

with d_1, d_2 and d_3 as defined above. The parameters b and c are defined by $b = 2x_B\frac{u_b}{\Lambda}$ and $c = 2x_C\frac{u_c}{\Lambda}$. The scatter plots in Fig. 5.23 show the allowed regions in $a - b - d$ parameter space. Since the condition $c = b$ is required for TBM, the effect of deviations can be studied by setting $c = b(1 + \epsilon_3)$.

Fig. 5.24 shows scatter plots for the mixing angles, from diagonalisation of Eqs. (5.53) and (5.54). For the normal hierarchy, there is not much difference between the plots for one singlet and those for three singlets. Figs. 5.24(a) and 5.24(b) show that, in the case of one singlet, the deviations of $\sin^2\theta_{13}$ from zero are greater for the normal hierarchy than for the inverted hierarchy. The solar and atmospheric mixing angles (θ_{12} and θ_{23}) take on a spread of values in the 3σ range. The scatter plots in Fig. 5.25 show that for one Higgs singlet, the value of J_{CP} is closer to maximal for the inverted hierarchy than for the normal hierarchy, but for three Higgs singlets there is little difference in the J_{CP} values between mass hierarchies.

It is interesting to compare the deviation of mixing angle observables in the A-F model with and without seesaw, as shown in Fig. 5.26. This comparison is only performed for the normal hierarchy, since the inverted hierarchy cannot be realised in the usual A-F model with one singlet. Fig. 5.26(a) shows that in the case of one singlet, $\sin^2\theta_{13}$ is closer to zero without seesaw than with seesaw, but in the case of three singlets [Fig. 5.26(b)] there is little difference in the deviation of $\sin^2\theta_{13}$.

The mass dependent observables are plotted in Fig. 5.27: in the one singlet case there is a distinct separation of normal and inverted hierarchy in the $\langle m_{ee}\rangle - \sum m_\nu$ parameter space, and deviations simply allow for a smaller value of $\langle m_{ee}\rangle$. For the inverted hierarchy, the masses are in the quasi-degenerate region, and for $\sum m_\nu \gtrsim 0.17$ eV, the deviations from TBM have little effect on $\langle m_{ee}\rangle$. The scatter plot in the three singlet case in Fig. 5.27(b) is in fact similar to the plot without seesaw, [Fig. 5.10(c)], as the normal and inverted hierarchy regions are closer together. However, the deviations from TBM have little effect on the normal hierarchy, in contrast to the large deviations in Fig. 5.10(c). The value of $\sum m_\nu$ is greater in the inverted hierarchy, and deviations have the effect of allowing a smaller value of $\langle m_{ee}\rangle$.

Note that the "AFSU5" model [251] listed in Table 5.4 is in fact very similar to the seesaw model presented here, except that it is formulated in $4+1$ dimensions, and

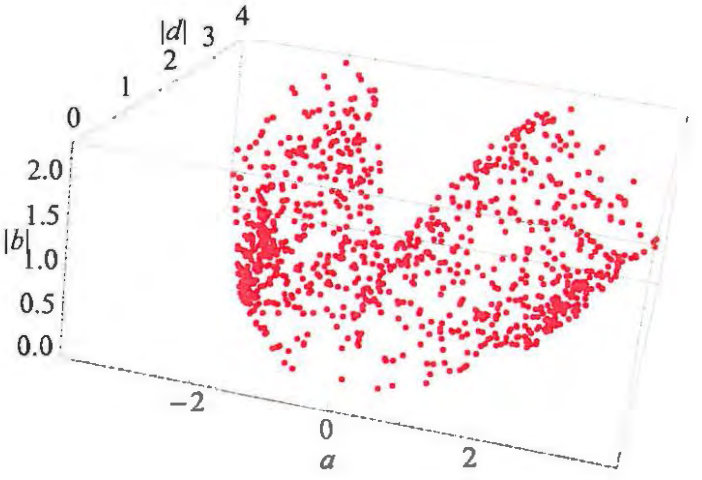

(a)

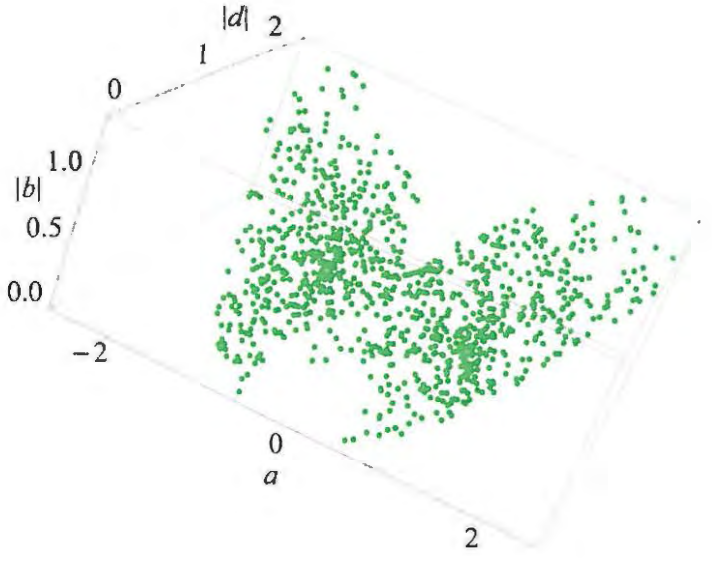

(b)

Figure 5.23: Scatter plots of the $a - b - d$ parameter space for the A-F seesaw model, with three Higgs singlet, for normal (a) and inverted (b) hierarchies.

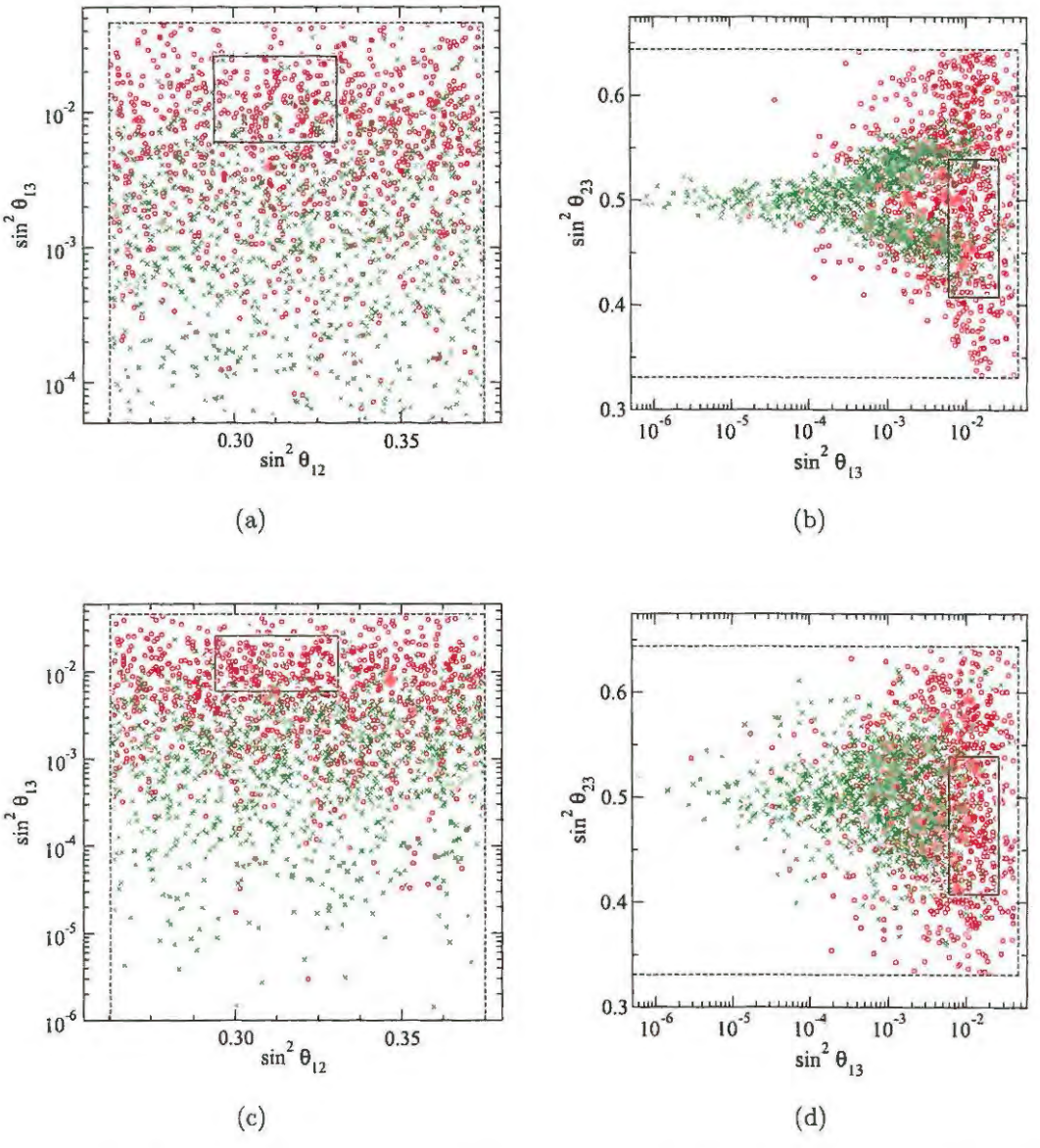

Figure 5.24: Scatter plots of mixing angle observables for the A-F seesaw model [33], with both one Higgs singlet ((a) and (b)) and three Higgs singlets ((c) and (d)). Both normal (red circles) and inverted (green crosses) hierarchies are included.

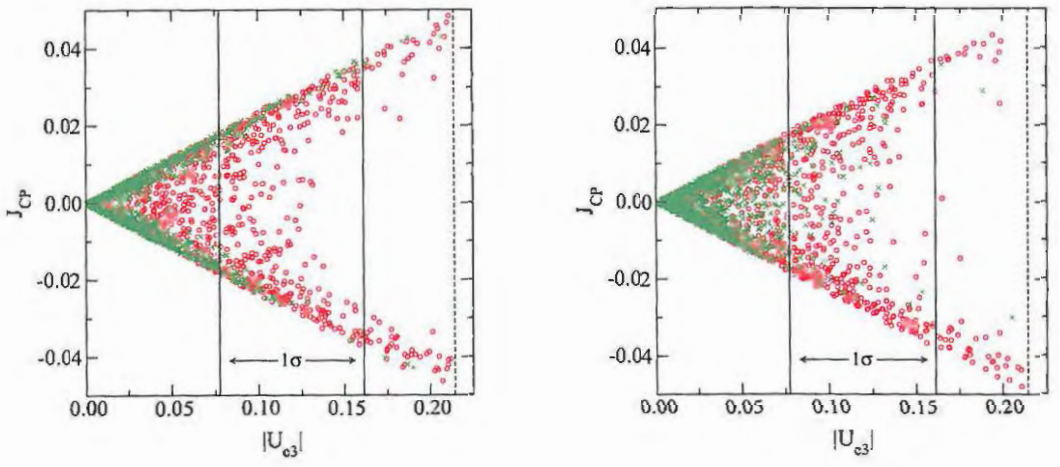

(a) (b)

Figure 5.25: Scatter plot of J_{CP} against $|U_{e3}|$ for the A-F seesaw model, with one (a) and three (b) Higgs singlets, for normal (red circles) and inverted (green crosses) hierarchies.

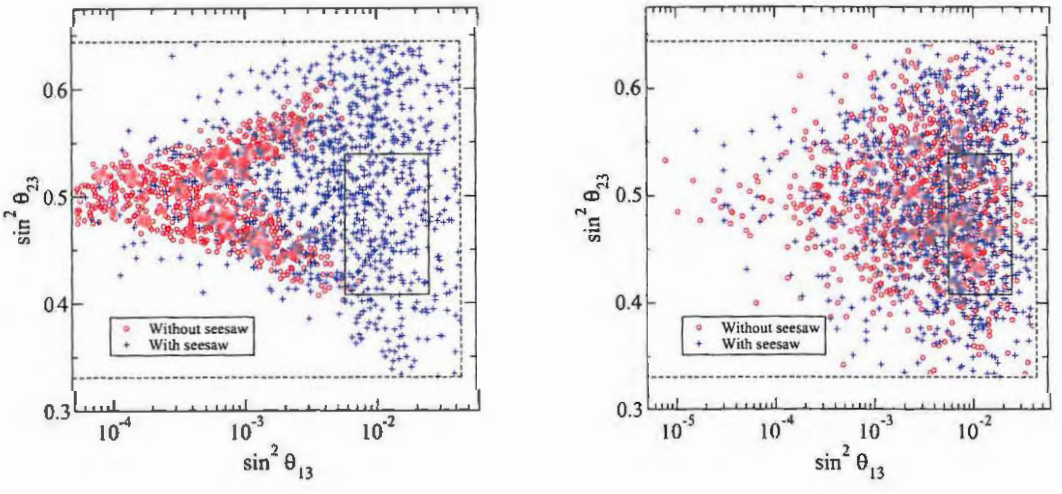

(a) (b)

Figure 5.26: Scatter plots of $\sin^2\theta_{23}$ against $\sin^2\theta_{13}$ for the A-F model with one (a) and three (b) Higgs singlets, with and without seesaw.

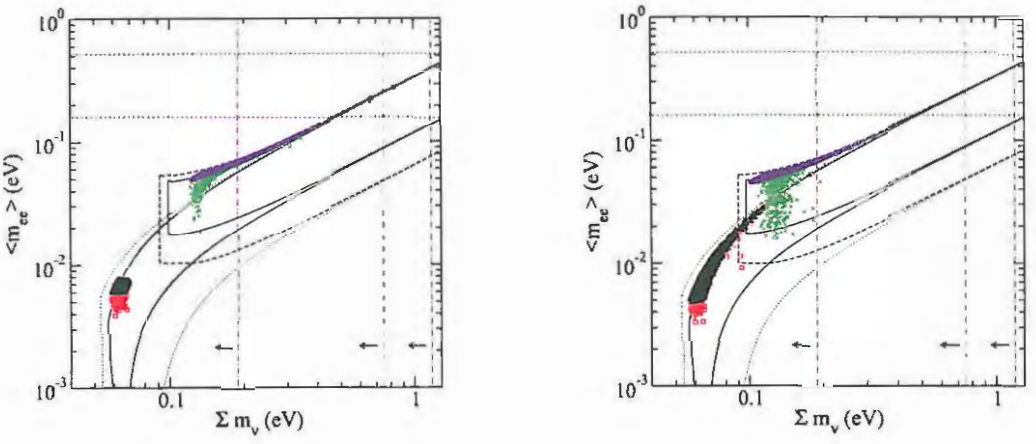

(a) (b)

Figure 5.27: Scatter plot of $\langle m_{ee} \rangle$ vs $\sum m_\nu$ for the A-F seesaw model, with one (a) and three (b) Higgs singlets. See the caption of Fig. 5.4 for an explanation of the symbols used.

the matter fields are grouped into supermultiplets, transforming as 10, $\bar{5}$ and 1 under $SU(5)$. The charged lepton mass matrix takes a different form, but the neutrino mass matrix is the same as Eq. (5.53). This model will not be studied here.

5.4.4 The Yin 3-3-1 model

The application of A_4 to neutrino mixing is usually in the framework of the SM gauge group, however, this can be extended [258] to the local gauge group $SU(3)_c \times SU(3)_L \times U(1)_X$, which is called the "3-3-1 model". In this model there are additional negatively charged heavy leptons, which make up $SU(3)$ triplets with the usual SM lepton doublets, as well as heavy right-handed neutrino singlets, N_R. It is the A_4 symmetry breaking structure of the model that leads to TBM, and this can be studied without entering into the details of the 3-3-1 structure of the model.

With the lepton triplets transforming as $\underline{3}$ and right-handed charged leptons as $\underline{1}$, $\underline{1}'$, $\underline{1}''$ under A_4, the charged lepton sector takes the same form as before [Eqs. (5.7), (5.15) and (5.16)]. The invariant Yukawa Lagrangian for the neutrino sector is

$$\mathcal{L}_y = M_N (N_R)^c N_R + f_\xi \xi (\ell_L N_R) + f_{\varphi'} (\varphi' \ell_L N_R) \,, \tag{5.62}$$

where a 3-3-1 singlet scalar generates the tree-level Majorana mass term containing

M_N, and f_ξ and $f_{\varphi'}$ are coupling constants. The bare Majorana mass term is trivial, so that the matrix M_R is simply M_N times the identity. The second term in Eq. (5.62) gives the term $f_\xi u$ on the diagonal of the Dirac mass matrix (u is the VEV of the singlet ξ). Assuming the VEV alignment

$$\langle \varphi' \rangle = (v', 0, 0) \ , \tag{5.63}$$

for the Higgs triplet φ', the Dirac mass matrix becomes

$$M_{\rm D} = \begin{pmatrix} f_\xi u & 0 & 0 \\ 0 & f_\xi u & f_{\varphi'} v' \\ 0 & f_{\varphi'} v' & f_\xi u \end{pmatrix} \ , \tag{5.64}$$

and with the seesaw mechanism, the light neutrino mass matrix is

$$M_\nu = \frac{1}{M_N} \begin{pmatrix} (f_\xi u)^2 & 0 & 0 \\ 0 & (f_\xi u)^2 + (f_{\varphi'} v')^2 & 2 f_\xi f_{\varphi'} u v' \\ 0 & 2 f_\xi f_{\varphi'} u v' & (f_\xi u)^2 + (f_{\varphi'} v')^2 \end{pmatrix} \ . \tag{5.65}$$

Note that the matrix in Eq. (5.65) has the same form as the matrix in Eq. (4.24) (the Ma-AF model with one Higgs singlet). However, in this case the seesaw mechanism is present, whereas in the Ma-AF model the neutrino mass is generated by dimension-5 operators. It is impossible to get the inverted mass hierarchy in this model.

In analogy with Eq. (5.13), if the VEV alignment of φ' is deviated to

$$\langle \varphi' \rangle = (v', v'\epsilon_1, v'\epsilon_2) \ , \tag{5.66}$$

then the Dirac mass matrix gets additional off-diagonal terms, and the light neutrino mass matrix takes the form

$$M'_\nu = \frac{m_0}{c} \begin{pmatrix} a^2 + b^2(\epsilon_1^2 + \epsilon_2^2) & b(b\epsilon_1 + 2a\epsilon_2) & b(2a\epsilon_1 + b\epsilon_2) \\ \cdot & a^2 + b^2(\epsilon_2^2 + 1) & b(2a + b\epsilon_1\epsilon_2) \\ \cdot & \cdot & a^2 + b^2(\epsilon_1^2 + 1) \end{pmatrix} \ , \tag{5.67}$$

where the substitutions $a = f_\xi u$, $b = f_{\varphi'} v'$, and $c = M_N$ have been made, and m_0 fixes the mass scale. Fig. 5.28 shows the allowed region in $a - b - c$ parameter space, with $\epsilon_1 = \epsilon_2 = 0$, and $m_0 = 0.025$ eV.

Once deviations are applied, the solar mixing angle $\sin^2\theta_{12}$ takes on a range of values (not shown here), and the value of $\sin^2\theta_{13}$ is greater than zero, with most of

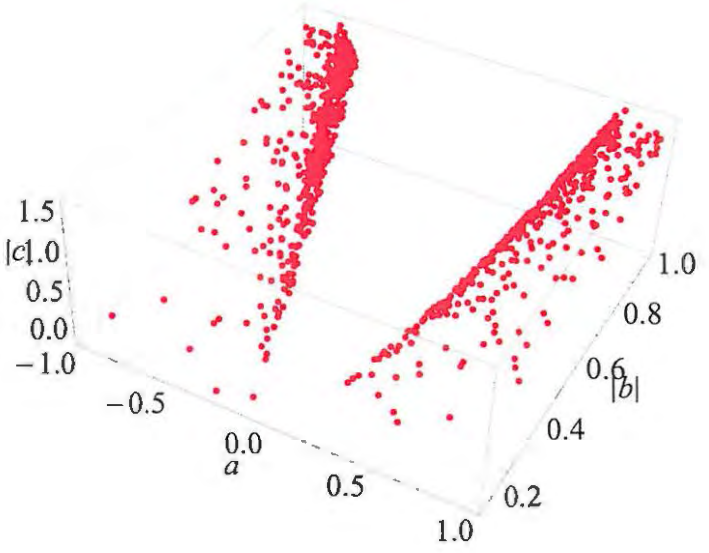

Figure 5.28: Scatter plot of the $a - b - c$ parameter space for the Yin 3-3-1 model, for normal hierarchy.

the points lying within the 1σ range, as shown in Fig. 5.29. One can also see that the deviation of θ_{23} from maximal depends on the value of $\sin^2\theta_{13}$: there is more deviation for larger values of $\sin^2\theta_{13}$.

Note from Fig. 5.30 that the neutrino masses lie in the hierarchical region (since the value of m_0 was fixed at 0.025 eV). The effect of TBM deviations is only seen for $\sum m_\nu \lesssim 0.066$ eV, where $\langle m_{ee}\rangle$ becomes smaller than in the undeviated case.

5.4.5 Chen & King "alternative seesaw" model

All of the models discussed so far have employed a diagonal Dirac mass matrix; here a seesaw model [227] in the diagonal right-handed neutrino mass basis is considered. The model is constructed in the A-F basis for A_4, so that the charged lepton mass matrix is diagonal, as in Eq. (5.19).

The Dirac mass matrix is generated by two terms: the coupling of lepton doublets and right-handed neutrino singlets to (i) an A_4 singlet (ξ); and (ii) an A_4 triplet (φ'). When the triplet acquires the VEV in Eq. (5.18), the Dirac mass matrix is

$$M_{\rm D} = \begin{pmatrix} a+2b & -b & -b \\ -b & 2b & a-b \\ -b & a-b & 2b \end{pmatrix} v_u \ , \tag{5.68}$$

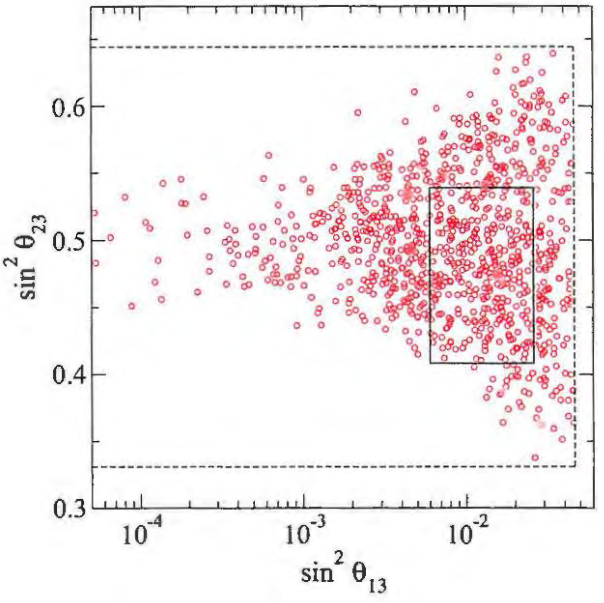

Figure 5.29: Scatter plot of $\sin^2\theta_{23}$ vs $\sin^2\theta_{13}$ for Yin's 3-3-1 model, normal hierarchy.

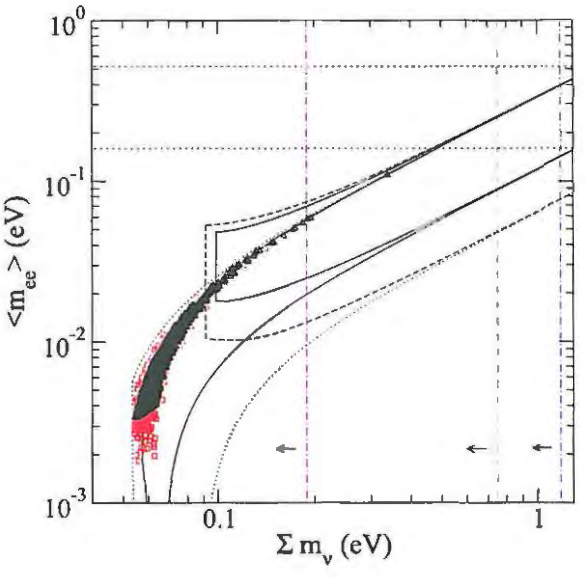

Figure 5.30: Scatter plot of $\langle m_{ee}\rangle$ against $\sum m_\nu$ for the Yin 3-3-1 model, for normal mass hierarchy, with symbols as defined in Fig. 5.4.

with

$$a = \frac{u}{\Lambda} \quad \text{and} \quad b = \frac{v'}{\Lambda} \,, \tag{5.69}$$

where u, v' and v_u denote the VEVs of ξ, φ' and the Higgs doublet h_u respectively.

With right-handed neutrinos N_R^c transforming as $\underline{3}$ under A_4, the Majorana mass matrix is

$$M_{\rm R} = \begin{pmatrix} 1 & 0 & 0 \\ 0 & 0 & 1 \\ 0 & 1 & 0 \end{pmatrix} M \,, \tag{5.70}$$

so that the neutrino mass matrix becomes

$$M_\nu = \frac{v_u^2}{M} \begin{pmatrix} a^2+4ab+6b^2 & -b(2a+3b) & -b(2a+3b) \\ \cdot & b(4a-3b) & a^2-2ab+6b^2 \\ \cdot & \cdot & b(4a-3b) \end{pmatrix} \,, \tag{5.71}$$

where M is the mass scale of the heavy right-handed neutrinos. This matrix has the correct form for TBM, and can be analysed for deviations induced by changing the VEV alignment of φ', as before [Eq. (5.23)]. In this case the deviations come from the Dirac mass matrix, and the new neutrino mass matrix is

$$M'_\nu = m_0 \begin{pmatrix} M'_{11} & M'_{12} & M'_{13} \\ \cdot & M'_{22} & M'_{23} \\ \cdot & \cdot & M'_{33} \end{pmatrix} \,, \tag{5.72}$$

where

$$M'_{11} = 2(\epsilon_1+1)(\epsilon_2+1)b^2 + (a+2b)^2 \tag{5.73}$$

$$M'_{12} = -b\left(2a(\epsilon_2+1) + b\left(2\epsilon_1^2+4\epsilon_1+\epsilon_2+3\right)\right) \tag{5.74}$$

$$M'_{13} = -b\left(2a(\epsilon_1+1) + b\left(2\epsilon_2^2+4\epsilon_2+\epsilon_1+3\right)\right) \tag{5.75}$$

$$M'_{22} = b\left(b(\epsilon_2+1)^2 + 4(a-b)(\epsilon_1+1)\right) \tag{5.76}$$

$$M'_{23} = (a-b)^2 + 5b^2(\epsilon_1+1)(\epsilon_2+1) \tag{5.77}$$

$$M'_{33} = b\left(b(\epsilon_1+1)^2 + 4(a-b)(\epsilon_2+1)\right) \,, \tag{5.78}$$

and $m_0 = v_u^2/M$. Note that the inverted hierarchy is not possible in this model, and there is a narrow allowed range in $a-b$ parameter space, as shown in Fig. 5.31.

The scatter plots of mixing angle observables show a uniform spread of points, as in Figs. 5.2, but in this model the behaviour of J_{CP} is different. In Fig. 5.32, it can

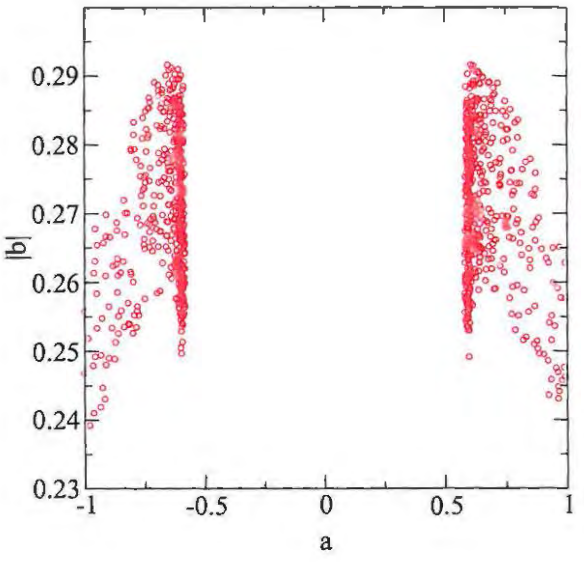

Figure 5.31: Scatter plot of the $a - b$ parameter space for the Chen & King seesaw model, for normal hierarchy.

be noted that for $|U_{e3}| \gtrsim 0.1$, CP violation is close to maximal. In contrast to the claim made in Ref. [227], with $m_0 = 0.025$ eV in Eq. (5.72), neutrino masses in the hierarchical region can be obtained (Fig. 5.33), and the effect of TBM deviations is to simply "extend" the allowed region in $\langle m_{ee} \rangle - \sum m_\nu$ parameter space, without changing its shape. The value of $\langle m_{ee} \rangle$ was found to be as low as 0.0014 eV in the perturbed case.

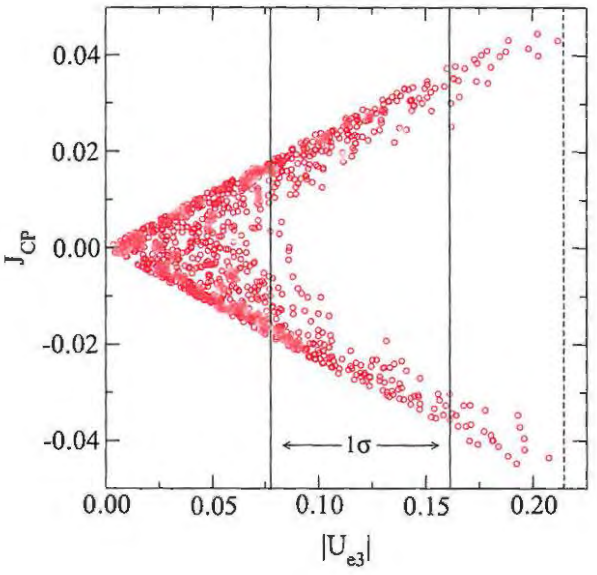

Figure 5.32: Scatter plot of J_{CP} against $|U_{e3}|$ for the Chen & King "alternative seesaw" model, normal hierarchy.

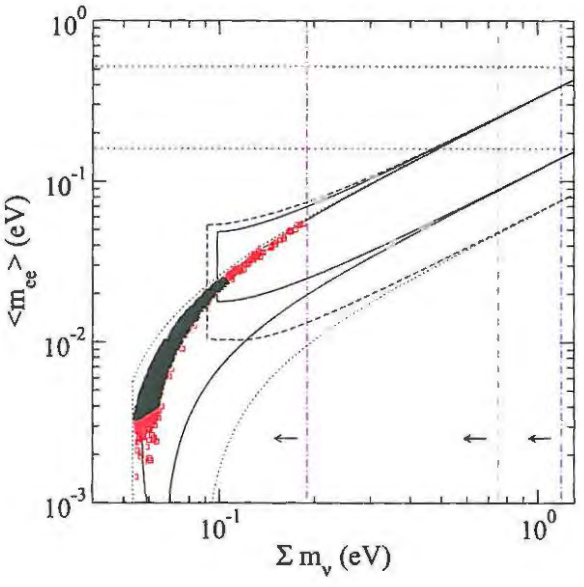

Figure 5.33: Scatter plot of $\langle m_{ee} \rangle$ against $\sum m_\nu$ for the Chen & King "alternative seesaw" model, for normal mass hierarchy, with symbols as defined in Fig. 5.4.

Chapter 6

A_4 Model Analysis: Type C & Type D

Type C and type D models are different to the models discussed in Chapter 5; in this case all the matter fields transform as $\underline{3}$ under A_4. This allows for the construction of grand unified models in $SU(5)$ [79] and $SO(10)$ [80–82], since all leptons can be accommodated in one multiplet of the gauge group.

6.1 Type C models

The Type C models are similar to the Type A models discussed in Section 5.3 above, in that there are no right-handed neutrinos, but here the new particle assignments change the structure of the charged lepton mass matrix. There are a number of models of this type in the literature (see Table 6.1), yet only two of them [78,261] predict exact TBM.

6.1.1 Ma supersymmetric $A_4 \times Z_3$ model

Ma [77,78] was the first to present an A_4 model that could achieve TBM using a different particle assignment for the charged leptons. The particle content of that model is given in Table 6.2, and it exhibits the characteristic feature of all A_4 models: there are a number of Higgs scalars transforming as singlets and triplets of A_4. The Z_3 symmetry ensures that the neutrino and charged lepton sectors do not mix, effectively disallowing terms containing the product of φ and φ' from appearing in the superpotential of the theory.[1]

[1] Ref. [78] also discusses a model without the Z_3 symmetry, and in this case there are deviations from TBM due to corrections to the charged lepton mass matrix.

Table 6.1: Summary of type C A_4 models.

Model	M_ℓ	M_ν	TBM?	Comments
Hirsch et al. [244]	$\propto \begin{pmatrix} h_1v_1 & h_2v_2 & h_3v_3 \\ h_3v_3 & h_1v_1 & h_2v_2 \\ h_2v_2 & h_3v_3 & h_1v_1 \end{pmatrix}$	$\propto \begin{pmatrix} a+b+c & f & e \\ f & a+\omega b+\omega^2 c & d \\ e & d & a+\omega^2 b+\omega c \end{pmatrix}$	No	Six Higgs triplets TBM only with assumptions Focus on $0\nu\beta\beta$
Zee 2 [74]	As above	Not explicitly stated	No	Zee's "Model B"
Ma 2 [77, 78]	$\propto \begin{pmatrix} h_0v_0 & h_1v_3 & h_2v_2 \\ h_2v_3 & h_0v_0 & h_1v_1 \\ h_1v_2 & h_2v_1 & h_2v_0 \end{pmatrix}$	$\propto \begin{pmatrix} a & 0 & 0 \\ 0 & a & d \\ 0 & d & a \end{pmatrix}$	Yes	SUSY $A_4 \times Z_3$
Bazzocchi et al. (BM) [261]	As above	$\propto \begin{pmatrix} a & b & 0 \\ b & a\omega & 0 \\ 0 & 0 & a\omega^2 \end{pmatrix}$	Yes	SUSY A_4 embedded into $SO(3)_L \times SO(3)_R$ Discussion of GUT group $SO(10)$

Table 6.2: Particle assignments of Ma's Type C TBM model [78].

Superfield	$SU(2) \times U(1)$	A_4	Z_3
$L = (\nu, \ell)$	$(2, -1/2)$	$\underline{3}$	1
ℓ^c	$(1, 1)$	$\underline{3}$	1
$\Phi_1 = (\phi_1^0, \phi_1^-)$	$(2, -1/2)$	$\underline{1}$	1
$\Phi_2 = (\phi_2^+, \phi_2^0)$	$(2, 1/2)$	$\underline{1}$	1
φ	$(1, 0)$	$\underline{3}$	1
φ'	$(1, 0)$	$\underline{3}$	ω
ξ	$(1, 0)$	$\underline{1}$	ω
$\chi_1 = (\chi_1^{++}, \chi_1^+, \chi_1^0)$	$(3, 1)$	$\underline{1}$	ω^2
$\chi_2 = (\chi_2^0, \chi_2^-, \chi_2^{--})$	$(3, -1)$	$\underline{1}$	ω^2

In the charged lepton sector, the terms $L\ell^c\Phi_1$ and $L\ell^c\varphi\Phi_1$ result in the mass matrix

$$M_\ell = \begin{pmatrix} h_0 v_0 & h_1 v_3 & h_2 v_2 \\ h_2 v_3 & h_0 v_0 & h_1 v_1 \\ h_1 v_2 & h_2 v_1 & h_0 v_0 \end{pmatrix} , \tag{6.1}$$

where $v_0 = \langle \phi_1^0 \rangle$ and $v_i = \langle \varphi_i \rangle \langle \phi_1^0 \rangle / \Lambda$ $(i = 1, 2, 3)$, and h_0, h_1 and h_2 are coupling constants. If the Higgs triplet φ takes the alignment proportional to $(1, 1, 1)$, so that $v_1 = v_2 = v_3 = v$, then the mass matrix in Eq. 6.2 can be diagonalised by U_ω, *viz.*

$$M_\ell = U_\omega \begin{pmatrix} h_0 v_0 + (h_1 + h_2)v & 0 & 0 \\ 0 & h_0 v_0 + (\omega h_1 + \omega^2 h_2)v & 0 \\ 0 & 0 & h_0 v_0 + (\omega^2 h_1 + \omega h_2)v \end{pmatrix} U_\omega^\dagger . \tag{6.2}$$

The elements of the diagonal matrix in Eq. (6.2) should correspond to the charged lepton masses, leading to the relations

$$h_0 = \frac{1}{v_0} \frac{m_e + m_\mu + m_\tau}{3} , \tag{6.3}$$

$$h_1 = \frac{1}{v} \frac{m_e + m_\mu \omega^2 + m_\tau \omega}{3} , \tag{6.4}$$

$$h_2 = \frac{1}{v} \frac{m_e + m_\mu \omega + m_\tau \omega^2}{3} . \tag{6.5}$$

This means that h_0, h_1 and h_2 are fixed, up to phases, by the charged lepton masses.

If $v_0 = v = 1$ and each mass m_α is replaced by its experimental value, one solution is

$$h_0 = 627.327\ , \quad h_1 = -313.918 - 482.431i\ , \quad h_2 = -313.918 + 482.431i\ , \tag{6.6}$$

which was used in this analysis.[2]

The terms $LL\xi\chi_1$ and $LL\varphi'\chi_1$ define the neutrino sector, so that the neutrino mass matrix is

$$M_\nu = \begin{pmatrix} f_0 u_0 & f_1 u_3 & f_1 u_2 \\ f_1 u_3 & f_0 u_0 & f_1 u_1 \\ f_1 u_2 & f_1 u_1 & f_0 u_0 \end{pmatrix}\ , \tag{6.7}$$

where $u_0 = \langle\xi\rangle\langle\chi_1^0\rangle/\Lambda$ and $u_i = \langle\varphi_i'\rangle\langle\chi_1^0\rangle/\Lambda$. With the usual Higgs triplet alignment proportional to $(1,0,0)$, i.e. $u_2 = u_3 = 0$, the neutrino mass matrix takes the form of Eq. (4.24), and exact TBM is obtained. The supersymmetry of the theory must still be preserved, which can be achieved [78] with the vacuum alignments used to get TBM. This is done by finding a solution (corresponding to the chosen VEV alignments) that will make the minimum of the resulting scalar potential equal to zero.

Using the VEV alignments

$$\langle\varphi\rangle = (v, v(1+\epsilon_1^{ch}), v(1+\epsilon_2^{ch})) \quad \text{and} \quad \langle\varphi'\rangle = (u, u\epsilon_1, u\epsilon_2)\ , \tag{6.8}$$

the deviations from TBM can be studied, so that the charged lepton mass matrix becomes

$$M_\ell' = \begin{pmatrix} h_0 v_0 & h_1 v(1+\epsilon_2^{ch}) & h_2 v(1+\epsilon_1^{ch}) \\ h_2 v(1+\epsilon_2^{ch}) & h_0 v_0 & h_1 v \\ h_1 v(1+\epsilon_1^{ch}) & h_2 v & h_0 v_0 \end{pmatrix}\ , \tag{6.9}$$

and the neutrino mass matrix is

$$M_\nu' = \begin{pmatrix} a & b\epsilon_2 & b\epsilon_1 \\ b\epsilon_2 & a & b \\ b\epsilon_1 & b & a \end{pmatrix}\ , \tag{6.10}$$

where $a = f_0 u_0$ and $b = f_1 u$. Note that in the case of no perturbations, the parameters a and b are related as in Fig. 5.5 in the A-F model, and that only the normal hierarchy is possible in this model.

The matrices in Eqs. (6.9) and (6.10) can be numerically analysed, but it turns out

[2] One could in principle vary the charged lepton masses around their experimental values, as discussed in Section 5.3.1.

that the charged lepton mass matrix in Eq. (6.9) is extremely sensitive to deviations. The Fortran diagonalisation program[3] could not find solutions for deviations of order 0.3, so that separate analyses were performed: (i) the neutrino mass matrix was perturbed with $\epsilon \sim 0.3$ (keeping M_ℓ unperturbed), and (ii) both M_ℓ and M_ν [Eqs. (6.9) and (6.10)] were perturbed with $\epsilon \sim 0.03$. This technique was used for all subsequent type C and type D model analyses, since all of these models have the same charged lepton mass matrix structure.

The scatter plots in Fig. 6.1 show the effect of perturbations on the mixing angle observables, and illustrate the point that the value of $\sin^2\theta_{13}$ is lower with perturbations to both M_ν and M_ℓ of order 0.03 than it is for perturbations of order 0.3 to M_ν only, which is to be expected. However, in Fig. 6.1(b) it is evident that the atmospheric mixing angle θ_{23} remains close to its maximal TBM value, even with deviations $\epsilon \sim 0.3$ applied to M_ν. Fig. 6.1(c) shows that if small perturbations are applied to both mass matrices, J_{CP} takes on specific values for each value of $|U_{e3}|$, but with larger perturbations to M_ν only, it can take on values throughout the allowed range.

The neutrino mass matrix in Eq. (6.10) is equivalent to the matrix in Eq.(5.25),[4] and Fig. 6.2 is similar to the plot of mass parameters in Figs. 5.10(a) and 5.16. The neutrino masses lie in the hierarchical region, and the effect of perturbations to M_ν [Eq. (6.10)] is to allow for lower values of $\langle m_{ee}\rangle$. Note that for small perturbations ($\epsilon \sim 0.03$) in both charged lepton and neutrino mass matrices, there is very little deviation from the unperturbed case, and these points are not included in the plot in Fig. 6.2.

6.1.2 Bazzocchi et al. left-right model

The aim of this model is explicitly stated in Ref. [261] – to describe "the mass hierarchy and the large lepton mixing angles". Left-right flavour symmetry explains the mass hierarchies, whereas A_4 symmetry explains the mixing patterns, and there is a discussion on the origin of the Cabibbo angle in the quark sector.

The model is formulated in the context of supersymmetry, with matter fields transforming as either $(\underline{3},\underline{1})$ (left-handed) or $(\underline{1},\underline{3})$ (right-handed) under the group $SO(3)_L \times SO(3)_R$, and as $\underline{3}$ under A_4. There are the usual Higgs fields which transform as singlets (ξ) and triplets (φ and φ') of A_4, and an additional Z_5 symmetry which separates the charged lepton and neutrino sectors.

[3] See Appendix C.

[4] Note that there is a different basis used for A_4 in the two models.

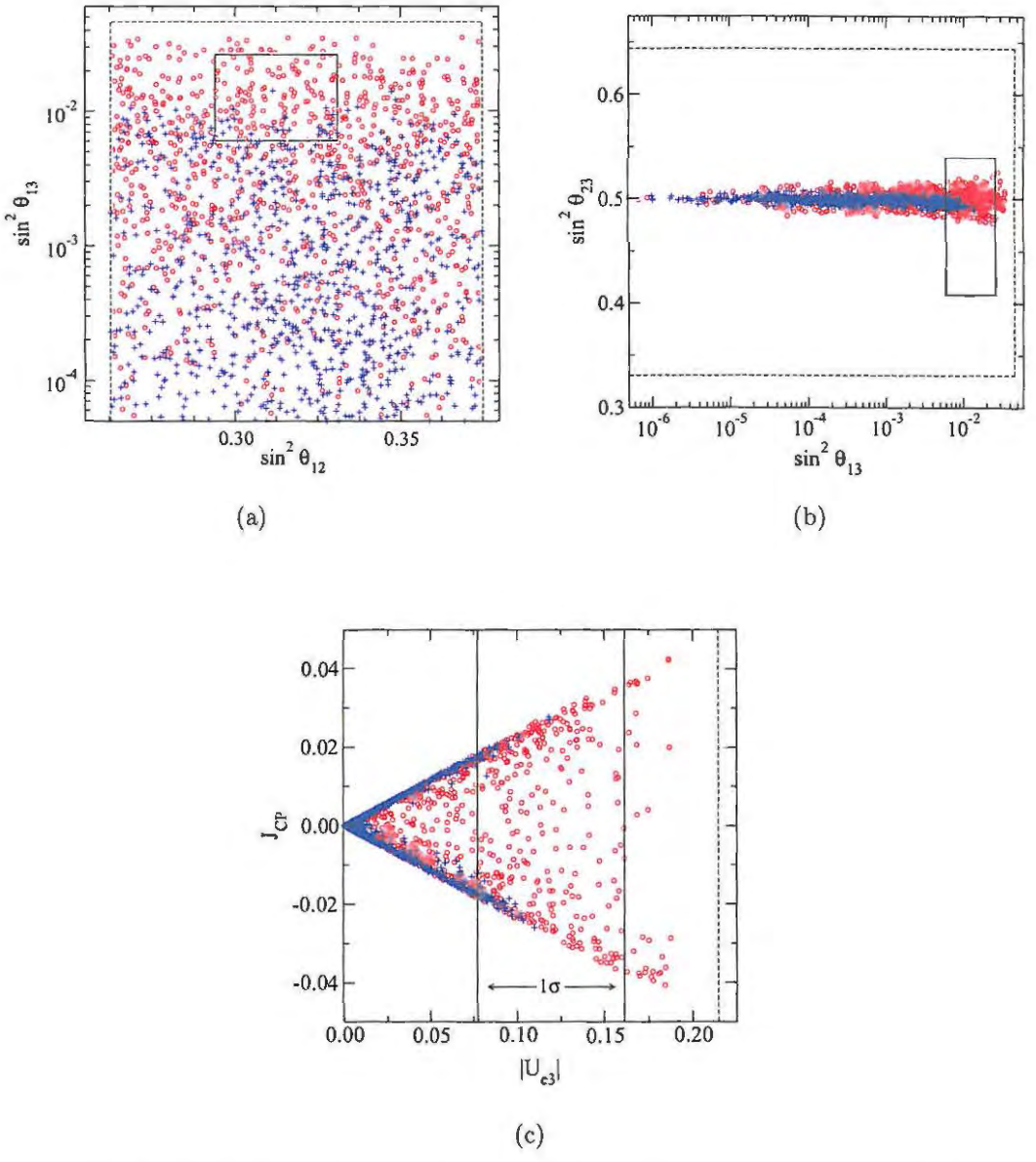

Figure 6.1: Scatter plots of mixing angle observables ((a) and (b)) and J_{CP} against $|U_{e3}|$ (c) for Ma's supersymmetric Type C model, normal hierarchy. Perturbations of order 0.03 were applied to both M_ν and M_ℓ (blue plus signs), and perturbations of order 0.3 were applied to M_ν only (red circles).

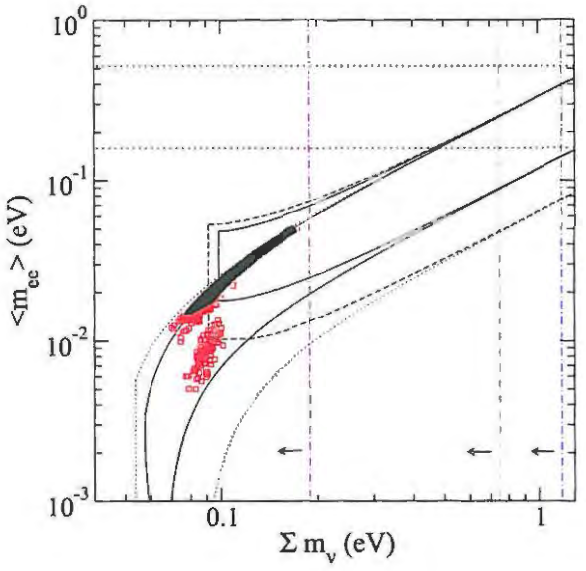

Figure 6.2: Scatter plot of $\langle m_{ee} \rangle$ against $\sum m_\nu$ for Ma's supersymmetric Type C model, for normal mass hierarchy, both unperturbed (black triangles), and with perturbations in M_ν (red squares).

Details of the Yukawa terms and the left-right symmetry are omitted in this analysis; rather, the structure of the resulting mass matrices is studied. In most left-right symmetric models, the charged fermion mass matrix is the democratic mass matrix,[5] and when φ takes the VEV proportional to $(1, 1, 1)$, it is perturbed to take the form

$$M_\ell = \frac{m_\tau}{3} \begin{pmatrix} 1 & 1 & 1 \\ 1 & 1 & 1 \\ 1 & 1 & 1 \end{pmatrix} \to v_d \begin{pmatrix} h_0 & h_1 & h_2 \\ h_2 & h_0 & h_1 \\ h_1 & h_2 & h_0 \end{pmatrix} , \tag{6.11}$$

which is similar to Eq. (6.2). This matrix can be diagonalised by U_ω, as before, with the parameters h_i [Eq. (6.6)] chosen in order to replicate the charged lepton mass hierarchy. Note that in Ref. [261], a slightly different "magic matrix" is used, which is effectively just a phase change, *viz.*

$$U'_\omega = \frac{1}{\sqrt{3}} \begin{pmatrix} \omega & \omega^2 & 1 \\ \omega^2 & \omega & 1 \\ 1 & 1 & 1 \end{pmatrix} . \tag{6.12}$$

[5] This is the matrix $\left(\begin{smallmatrix} 1 & 1 & 1 \\ 1 & 1 & 1 \\ 1 & 1 & 1 \end{smallmatrix}\right)$.

In the neutrino sector there are Yukawa terms formed with both the singlet ξ and the triplet φ', and when the triplet takes the VEV alignment proportional to $(0,0,1)$, the neutrino mass matrix is

$$M_\nu = m_0 \begin{pmatrix} a & b & 0 \\ b & \omega a & 0 \\ 0 & 0 & \omega^2 a \end{pmatrix} , \tag{6.13}$$

where m_0 fixes the mass scale. This matrix is diagonalised by

$$V_\nu = \frac{1}{\sqrt{2}} \begin{pmatrix} \omega & 0 & -i\omega \\ \omega^2 & 0 & i\omega^2 \\ 0 & 1 & 0 \end{pmatrix} , \tag{6.14}$$

a rephased version of Eq. (5.28), which combines with Eq. (6.12) to give TBM. The two parameter mass matrix in Eq. (6.13) is similar to the matrix in Eq. (6.7), so that in terms of A_4 symmetry breaking structure this model is equivalent to Ma's model in Section 6.1.1; only normal hierarchy is possible, and the $a-b$ parameter space is again the same as that shown in Fig. 5.5. However, the rephasing of the fields does affect the response of observables to perturbations in the mass matrices, as noted below.

VEV alignment deviations in the charged lepton sector give the mass matrix in Eq. (6.9), and if the triplet φ' takes the alignment

$$\langle \varphi' \rangle = (v'\epsilon_1, v'\epsilon_2, v') , \tag{6.15}$$

then the neutrino mass matrix becomes

$$M'_\nu = m_0 \begin{pmatrix} a & b & b\epsilon_1 \\ b & a\omega & b\epsilon_2 \\ b\epsilon_1 & b\epsilon_2 & a\omega^2 \end{pmatrix} . \tag{6.16}$$

In contrast to the scatter plot in Fig. 6.1(b), here the atmospheric mixing angle θ_{23} deviates considerably from its maximal value, as shown in Fig. 6.3. There is a correlation between large $\sin^2\theta_{13}$ and non-maximal $\sin^2\theta_{23}$, so that if $\sin^2\theta_{13}$ takes values in the 1σ range, $\sin^2\theta_{23}$ can be outside of its 1σ range, and if $\sin^2\theta_{13}$ is close to its maximum value (0.046) then $\sin^2\theta_{23}$ is necessarily non-maximal. For small $\sin^2\theta_{13}$ there is little deviation in $\sin^2\theta_{23}$. The blue plus signs in Fig. 6.3 show that there is little effect for small ($\epsilon \sim 0.03$) perturbations to the mass matrices.

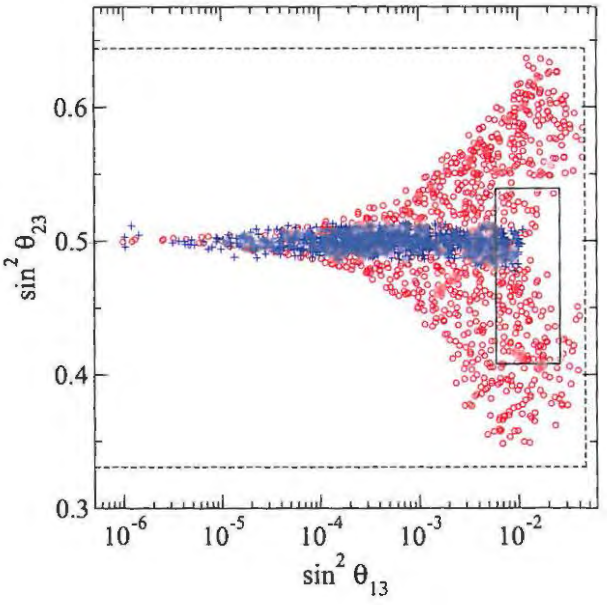

Figure 6.3: Scatter plot of $\sin^2\theta_{23}$ against $\sin^2\theta_{13}$ for the BM left-right model, normal hierarchy. Perturbations of order 0.03 were applied to both M_ν and M_ℓ (blue plus signs) and perturbations of order 0.3 were applied to M_ν only (red circles).

The phase change referred to above [Eq. (6.12)] has some effect on the value of $\langle m_{ee}\rangle$, as this quantity depends on the Majorana phases. As seen in Fig. 6.4, in the unperturbed case the points lie in the middle of the best-fit allowed range in $\langle m_{ee}\rangle - \sum m_\nu$ parameter space. This is in contrast to all other models studied so far,[6] where $\langle m_{ee}\rangle$ takes its maximum value in the unperturbed case. The sum of neutrino masses $\sum m_\nu$ is restricted to a certain range, regardless of perturbations, as the mass scale was fixed by $m_0 = 0.025$ eV. The effect of perturbations is to give a greater spread of $\langle m_{ee}\rangle$ values, with a minimum of 0.0034 eV, and a maximum of 0.031 eV. Note that there is not much difference between perturbing M_ν with $\epsilon \sim 0.3$ and perturbing both mass matrices with $\epsilon \sim 0.03$.

There is no mention of the effects of VEV alignment deviations in Ref. [261]. However, there is some discussion of the origin of the Cabibbo angle, which is attributed to higher order corrections. There is also a brief attempt (continued in Ref. [82])[7] in constructing a grand unified $SO(10) \times SU(3)$ version of the model – in this case right-handed neutrinos are included and the model effectively becomes "Type D" in

[6] An exception is the Babu & He model.

[7] See the BFM model in Section 6.2 below.

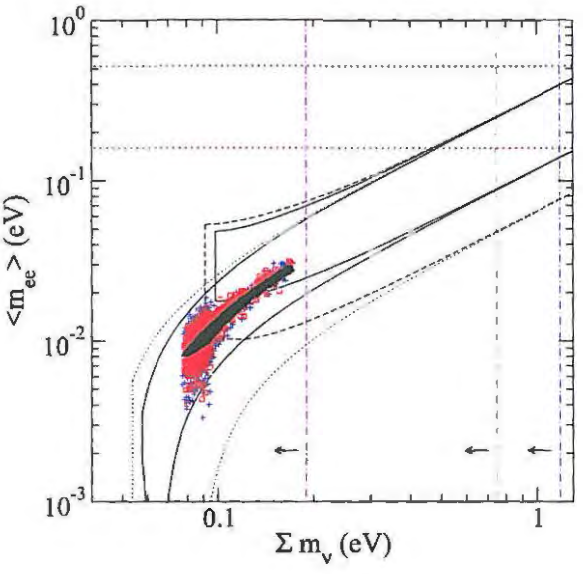

Figure 6.4: Scatter plot of $\langle m_{ee} \rangle$ against $\sum m_\nu$ for the BM left-right model, for the normal mass hierarchy. Blue plus signs represent points with perturbations in M_ν only ($\epsilon \sim 0.3$), with an unperturbed M_ℓ; red squares represent points with perturbations in both mass matrices ($\epsilon \sim 0.03$), and black triangles represent the unperturbed case.

the classification used here.

6.2 Type D models

In the final class of models studied, right-handed neutrinos are included, transforming as $\underline{3}$ under A_4. The other matter fields are also represented by an A_4 triplet $\underline{3}$, as in type C models. Most models of this type attempt to embed the A_4 discrete flavour symmetry into a larger GUT group like $SO(10)$ [80–82], with different variants of the seesaw mechanism employed in each model (see Table 6.3). This is in a sense a combination of the top-down and bottom-up approaches [29], since the GUT group is chosen *a priori*, but the mass matrices are constructed to give TBM. There are other models [79, 263] based on the recently proposed minimal renormalisable SUSY $SU(5)$ [268], which are not analysed here.

Chen et al. [75] were the first to discuss a model with these particle assignments, but their model does not predict TBM. Different cases of this model give specific forms for the neutrino mass matrix, which affect the mass parameters and complex phases.

Although different symbols have been used for the terms in the charged lepton mass matrix (see Table 6.3), the form of M_ℓ is essentially equivalent in all of these models. Thus the matrix M_ℓ in Eq. (6.2) and the deviated matrix M'_ℓ in Eq. (6.9) can be used in the analysis of these models. This means that the VEV alignment proportional to $(1,1,1)$ is deviated to $(1, 1+\epsilon_1^{ch}, 1+\epsilon_2^{ch})$, as before.

6.2.1 Morisi, Picariello, Torrente-Lujan (MPT) model

In a similar approach to the left-right model [261] in Section 6.1.2 above, an $SO(10)$ realisation [80] of the A_4 seesaw model can be constructed. The neutrino sector of the model is similar in structure to the Altarelli-Feruglio seesaw model discussed in Section 5.4, except that a different basis for A_4 is used.

The particle assignments of the model are given in Table 6.4: the fermionic matter fields are in the **16** representation of $SO(10)$, with the SM Higgs doublet as a **10**, four A_4 singlets (one $\mathbf{126}_s$ and three **45**s), and two A_4 triplets (a **45** and a $\mathbf{126}_t$). The "extra Abelian factors" Y and T_{3R} serve to separate the charged lepton and neutrino sectors [80].

It can be shown [80] that when the triplets $\mathbf{45}_C$ and $\mathbf{126}_t$ take VEVs in the directions

$$\langle \mathbf{45}_C \rangle = v_{\mathbf{45}_C}(1,1,1) \quad \text{and} \quad \langle \mathbf{126}_t \rangle = v_{\mathbf{126}_t}(1,0,0) \ , \tag{6.17}$$

Table 6.3: Summary of type D A_4 models.

Model	M_ℓ	M_ν	TBM?	Comments
Chen, Frigerio, Ma [75]	$\propto \begin{pmatrix} h_1 v_1 & h_2 v_2 & h_3 v_3 \\ h_3 v_3 & h_1 v_1 & h_2 v_2 \\ h_2 v_2 & h_3 v_3 & h_1 v_1 \end{pmatrix}$	$\propto \begin{pmatrix} d+a & b & c \\ b & d+\frac{b^2}{a} & -\frac{bc}{a} \\ a & -\frac{bc}{a} & d+\frac{c^2}{a} \end{pmatrix}$	No	"Hybrid seesaw model" Higgs doublets, triplets and singlets Different cases studied Focus on mass parameters
Morisi et al. (MPT) [80]	$\propto \begin{pmatrix} h_0 & A & B \\ B & h_0 & A \\ A & B & h_0 \end{pmatrix}$	$\propto \frac{m_{\rm D}^2}{a(b^2-a^2)} \begin{pmatrix} b^2-a^2 & 0 & 0 \\ 0 & -a^2 & b^2 \\ 0 & b^2 & -a^2 \end{pmatrix}$	Yes	$SO(10) \times A_4$ GUT model Type I seesaw Numerical fitting of mass parameters
Bazzocchi et al. (BMSS) [81]	$\propto \frac{m_3}{3} \begin{pmatrix} 1 & 1+\delta_1 & 1+\delta_2 \\ 1+\delta_2 & 1 & 1+\delta_1 \\ 1+\delta_1 & 1+\delta_2 & 1 \end{pmatrix}$	$M_{\rm L}, M_{\rm D}, M_{\rm R} \propto \begin{pmatrix} a & b & 0 \\ b & a\omega & 0 \\ 0 & 0 & a\omega^2 \end{pmatrix}$	Yes	A_4 embedded into $SU(3) \times U(1)$ $SO(10)$ GUT Type I & type II seesaw
Hirsch et al. (HMV) [262]	$\propto \begin{pmatrix} \alpha & \beta & \gamma \\ \gamma & \alpha & \beta \\ \beta & \gamma & \alpha \end{pmatrix}$	$\propto \begin{pmatrix} a^2 & 0 & 0 \\ 0 & a^2+b^2 & 2ab \\ 0 & 2ab & a^2+b^2 \end{pmatrix}$	Yes	Two alternative models: (i) $A_4 \times Z_2$, (ii) $A_4 \times Z_4$ Focus on $0\nu\beta\beta$ phenomenology
Bazzocchi et al. (BFM) [82]	$\propto \begin{pmatrix} A & B & C \\ C & A & B \\ B & C & A \end{pmatrix}$	$M_{\rm L}, M_{\rm D}, M_{\rm R} \propto \begin{pmatrix} a & 0 & b \\ 0 & c & 0 \\ b & 0 & a \end{pmatrix}$	Yes	$SO(10) \times A_4$ GUT model Type I & type II seesaw With non-renormalisable operators

Table 6.4: Matter and Higgs field representations in the MPT $SO(10) \times A_4$ model [80].

$SO(10)$	**16**	**10**	$\mathbf{45}_{T_{3R}}$	$\mathbf{45}_Y$	$\mathbf{45}_C$	$\mathbf{45}_D$	$\mathbf{126}_s$	$\mathbf{126}_t$
A_4	$\underline{3}$	$\underline{1}$	$\underline{1}$	$\underline{1}$	$\underline{3}$	$\underline{1}$	$\underline{1}$	$\underline{3}$

the charged lepton mass matrix takes a form analogous to Eq. (6.2), the Dirac mass matrix is proportional to the identity, and the Majorana mass matrix has the form

$$M_{\mathrm{R}} = \begin{pmatrix} a & 0 & 0 \\ 0 & a & b \\ 0 & b & a \end{pmatrix} . \tag{6.18}$$

The terms a and b are proportional to the VEVs of the A_4 singlet $\mathbf{126}_s$ and A_4 triplet $\mathbf{126}_t$. The light neutrino mass matrix comes from the type I seesaw mechanism, and is given by[8]

$$M_\nu = \frac{(h_0 v_u)^2}{a(b^2 - a^2)} \begin{pmatrix} b^2 - a^2 & 0 & 0 \\ 0 & -a^2 & b^2 \\ 0 & b^2 & -a^2 \end{pmatrix} , \tag{6.19}$$

where h_0 is a coupling constant and v_u is the VEV of the up component of the **10**. A scan of $a - b$ parameter space (not shown here) gives the same results as those shown in Fig. 5.22, which confirms the similarity with the Altarelli-Feruglio seesaw model.

The usual deviation of the VEV alignment gives the charged lepton mass matrix in Eq. (6.9), and the neutrino mass matrix

$$M'_\nu = \frac{(h_0 v_u)^2}{m} \begin{pmatrix} a^2 - b^2 & b(b\epsilon_2 - a\epsilon_1) & b(b\epsilon_1 - a\epsilon_2) \\ b(b\epsilon_2 - a\epsilon_1) & a^2 - b^2\epsilon_2^2 & b(b\epsilon_1\epsilon_2 - a) \\ b(b\epsilon_1 - a\epsilon_2) & b(b\epsilon_1\epsilon_2 - a) & a^2 - b^2\epsilon_1^2 \end{pmatrix} , \tag{6.20}$$

where $m = a^3 - ab^2(\epsilon_1^2 + \epsilon_2^2 + 1) + 2b^3\epsilon_1\epsilon_2$. Note that due to the charges Y and T_{3R}, there are no deviations in the Dirac mass matrix.

Both normal and inverted hierarchy can be realised in this model, and Fig. 6.5(a) shows a distinct difference in the response of mixing angle observables to perturbations in the different hierarchies. With the inverted hierarchy, for all values of $\sin^2\theta_{13}$, there is no deviation of $\sin^2\theta_{23}$ from its maximum value of 0.5, but with the normal hierarchy the deviations in $\sin^2\theta_{23}$ increase with increasing $\sin^2\theta_{13}$. In Fig. 6.5(b), the dependence

[8]This matrix is the equivalent of Eq. (5.53) in the neutrino mass basis.

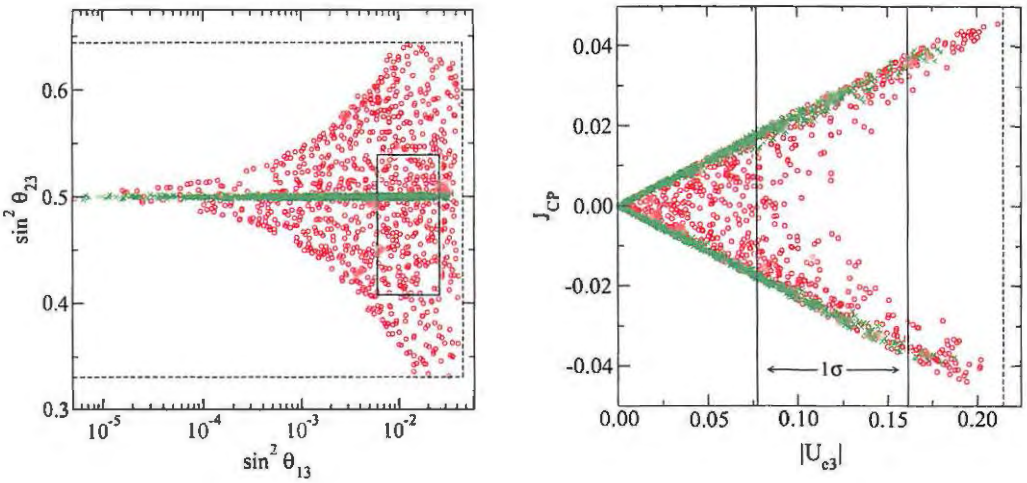

(a) (b)

Figure 6.5: Scatter plot of (a) $\sin^2\theta_{23}$ against $\sin^2\theta_{13}$ and (b) J_{CP} against $|U_{e3}|$ for the MPT $SO(10)$ model, with perturbations to M_ν only and both normal (red circles) and inverted (green crosses) hierarchies.

of J_{CP} on $|U_{e3}|$ differs between the hierarchies, with J_{CP} taking its maximum value in the inverted hierarchy but a spread of values in the normal hierarchy. For $|U_{e3}| \gtrsim 0.125$, J_{CP} also tends towards its maximum value in the normal hierarchy.

The scatter plot in Fig. 6.6 shows similarity with Fig. 5.27(a) – there is a separation in the value of $\langle m_{ee}\rangle$ between normal and inverted hierarchies, with neutrino masses in the hierarchical and quasi-degenerate regions, respectively. The allowed region in $\langle m_{ee}\rangle - \sum m_\nu$ parameter space is quite small in the case of normal hierarchy, and the solutions found with perturbations of order 0.03 do not have any effect (they are not displayed in Fig. 6.6). The value of $\sum m_\nu$ can get close to the CMB limit in the inverted hierarchy. Note that in the case of inverted hierarchy, the Fortran program did not converge to a solution when perturbations of order 0.03 were applied to both mass matrices – Fig. 6.6 simply shows the effect of perturbations to M_ν of order 0.3. The effect on the normal hierarchy is to increases the allowed range of $\langle m_{ee}\rangle$ ($0.0055 - 0.011$ eV), and there is little effect on the allowed range in the inverted hierarchy.

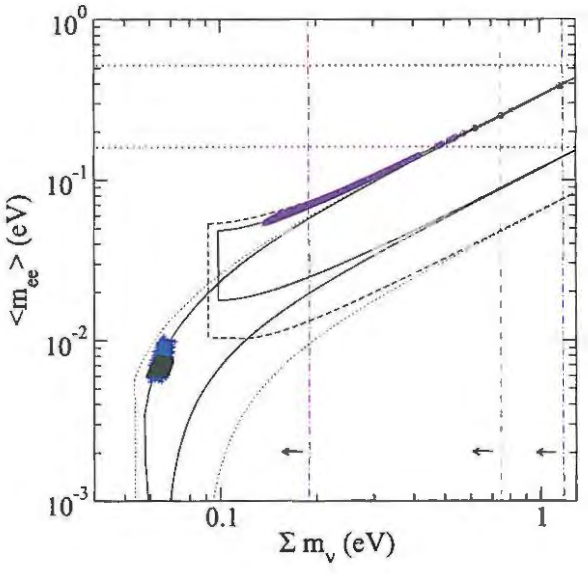

Figure 6.6: Scatter plot of $\langle m_{ee} \rangle$ against $\sum m_\nu$ for the MPT $SO(10)$ model. Perturbations were applied to the neutrino mass matrix only, with $\epsilon \sim 0.3$, for both normal (unperturbed given by black triangles, perturbed by blue plus signs) and inverted (unperturbed given by indigo circles, perturbed by green crosses) hierarchies.

6.2.2 Bazzocchi, Morisi et al. seesaw (BMSS) model

This model [81] is an extension of the left-right model [261] by the same authors (Section 6.1.2); the neutrino mass matrix takes a similar form, but the model also includes right-handed neutrinos, an $(SU(3) \times U(1))^F$ flavour symmetry and an $SO(10)$ GUT group. The idea is to take the ingredients of the left-right model, which address the charged lepton hierarchy and neutrino mixing, and combine them into a grand unified model under $SO(10)$.

Without outlining the details of the $(SU(3) \times U(1))^F$ symmetry in the charged lepton sector, note that M_ℓ takes the form in Eq. (6.11) (diagonalised by Eq. (6.12)), and when the VEV alignment of the Higgs triplets φ is deviated, M_ℓ becomes Eq. (6.9), as before. The particle assignments are similar to those in Table 6.4 above, and when the Higgs triplet φ' takes the alignment proportional to $(0, 0, 1)$, the neutrino mass matrices take the same form as Eq. (6.13), *viz.*

$$M_{\rm L} = \begin{pmatrix} a & b & 0 \\ b & \omega a & 0 \\ 0 & 0 & \omega^2 a \end{pmatrix} , \quad M_{\rm D} = \begin{pmatrix} c & d & 0 \\ d & \omega c & 0 \\ 0 & 0 & \omega^2 c \end{pmatrix} ,$$

$$\text{and} \quad M_{\rm R} = \begin{pmatrix} e & f & 0 \\ f & \omega e & 0 \\ 0 & 0 & \omega^2 e \end{pmatrix} . \tag{6.21}$$

The parameters a, b, c, d, e, f denote the products of different coupling constants with the VEV v' of the Higgs triplet φ'. Using both the type I and type II seesaw mechanisms, *viz.*[9]

$$M_\nu = M_{\rm L} + M_{\rm D} M_{\rm R}^{-1} M_{\rm D}^T , \tag{6.22}$$

the light neutrino mass matrix is

$$M_\nu = \frac{m_0}{m} \begin{pmatrix} M_{11} & M_{12} & M_{13} \\ \cdot & M_{22} & M_{23} \\ \cdot & \cdot & M_{33} \end{pmatrix} , \tag{6.23}$$

[9]Note that in Ref. [81] there is a plus sign in the seesaw formula, in contrast to Eq. (3.75).

where

$$M_{11} = e\left(ed^2 - 2cfd - af^2 + e\left(c^2 + ae\right)\omega\right) \tag{6.24}$$

$$M_{12} = e\left(-fc^2 + 2dec + be^2\right)\omega - ef\left(d^2 + bf\right) \tag{6.25}$$

$$M_{13} = 0 \tag{6.26}$$

$$M_{22} = e\omega\left(ed^2 - 2cfd - af^2 + e\left(c^2 + ae\right)\omega\right) \tag{6.27}$$

$$M_{23} = 0 \tag{6.28}$$

$$M_{33} = \left(c^2 + ae\right)\omega^2\left(e^2\omega - f^2\right) \ , \tag{6.29}$$

and $m = e(e^2\omega - f^2)$, with m_0 fixing the mass scale. An analysis of the $a-b-c-d-e-f$ parameter space shows a large allowed region. Since each of the mass matrices in Eq. (6.21) is diagonalised by the mixing matrix in Eq. (6.14), the light neutrino mass matrix M_ν also has this property, and Eq. (6.14) combines with Eq. (6.12) to give TBM.

By deviating the VEV alignment of $\langle\varphi'\rangle$ [Eq. (6.15)], the neutrino mass matrices become

$$M'_{\rm L} = \begin{pmatrix} a & b & b\epsilon_1 \\ b & \omega a & b\epsilon_2 \\ b\epsilon_1 & b\epsilon_2 & \omega^2 a \end{pmatrix} \ , \quad M'_{\rm D} = \begin{pmatrix} c & d & d\epsilon_1 \\ d & \omega c & d\epsilon_2 \\ d\epsilon_1 & d\epsilon_2 & \omega^2 c \end{pmatrix} \ ,$$

$$\text{and} \quad M'_{\rm R} = \begin{pmatrix} e & f & f\epsilon_1 \\ f & \omega e & f\epsilon_2 \\ f\epsilon_1 & f\epsilon_2 & \omega^2 e \end{pmatrix} \ , \tag{6.30}$$

and the resulting light neutrino mass matrix M'_ν is

$$M'_\nu = \frac{m_0}{m'} \begin{pmatrix} M'_{11} & M'_{12} & M'_{13} \\ \cdot & M'_{22} & M'_{23} \\ \cdot & \cdot & M'_{33} \end{pmatrix} \ , \tag{6.31}$$

where

$$M'_{11} = a\left(e^3\omega^3 - ef^2\left(\omega\left(\epsilon_1^2+\omega\right)+\epsilon_2^2\right)+2f^3\epsilon_1\epsilon_2\right)+c^2\left(e^2\omega^3-f^2\epsilon_2^2\right) + 2cdf\left(2f\epsilon_1\epsilon_2 - e\omega\left(\epsilon_1^2+\omega\right)\right)+d^2e\left(e\omega\left(\epsilon_1^2+\omega\right)-2f\epsilon_1\epsilon_2\right) \quad (6.32)$$

$$M'_{12} = e\omega^3\left(be^2+c^2(-f)+2cde\right)+\epsilon_1\omega\left(\epsilon_2(de-cf)^2-ef\epsilon_1\left(bf+d^2\right)\right) + f\epsilon_2\left(bf+d^2\right)\left(2f\epsilon_1-e\epsilon_2\right)-ef\omega^2\left(bf+d^2\right) \quad (6.33)$$

$$M'_{13} = e\epsilon_1\omega^3\left(be^2+c^2(-f)+2cde\right)+\omega^2\left(\epsilon_2(de-cf)^2-ef\epsilon_1\left(bf+d^2\right)\right) - ef\epsilon_1^3\omega\left(bf+d^2\right)+f\epsilon_1\epsilon_2\left(bf+d^2\right)\left(2f\epsilon_1-e\epsilon_2\right) \quad (6.34)$$

$$M'_{22} = \omega\left(e^2\omega^3\left(ae+c^2\right)-f^2\epsilon_1^2\omega\left(ae+c^2\right)+\epsilon_2(e\epsilon_2-2f\epsilon_1)\left(-af^2-2cdf+d^2e\right)\right) + \omega\left(e\omega^2\left(-af^2-2cdf+d^2e\right)\right) \quad (6.35)$$

$$M'_{23} = \omega^3\left(e\epsilon_2\left(be^2+c^2(-f)+2cde\right)+\epsilon_1(de-cf)^2\right)-ef\epsilon_1^2\epsilon_2\omega\left(bf+d^2\right) + f\epsilon_2^2\left(bf+d^2\right)\left(2f\epsilon_1-e\epsilon_2\right)-ef\epsilon_2\omega^2\left(bf+d^2\right) \quad (6.36)$$

$$M'_{33} = \omega^2\left(e^2\omega^3\left(ae+c^2\right)-f^2\omega^2\left(ae+c^2\right)+e\epsilon_1^2\omega\left(-af^2-2cdf+d^2e\right)\right) + \omega^2\left(\epsilon_2(e\epsilon_2-2f\epsilon_1)\left(-af^2-2cdf+d^2e\right)\right)\ , \quad (6.37)$$

and $m = e^3\omega^3 - ef^2\left(\omega\left(\epsilon_1^2+\omega\right)+\epsilon_2^2\right)+2f^3\epsilon_1\epsilon_2$. This matrix is used to analyse the effect of VEV alignment deviations.

The atmospheric mixing parameter $\sin^2\theta_{23}$ is more constrained with perturbations to both M_ν and M_ℓ of order 0.03 than it is for perturbations of order 0.3 to M_ν only, as seen in Fig. 6.7(a). The solar mixing angle θ_{12} is largely unconstrained in both cases, taking values throughout the 3σ range. In Fig. 6.7(b), the effect of perturbations on M_ν only is similar for both normal and inverted hierarchies, with $\sin^2\theta_{23}$ deviating from its maximal value (0.5) for large $\sin^2\theta_{13}$, but remaining close to 0.5 for values of $\sin^2\theta_{13}$ close to zero. There is little difference in the allowed values of J_{CP} between the hierarchies (not shown here).

As in the left-right model in Section 6.1.2 above, rephasing has the effect that the points lie in the middle of the best fit allowed range in $\langle m_{ee}\rangle - \sum m_\nu$ parameter space (Fig. 6.8). There is also some overlap of the allowed regions for normal and inverted hierarchies. Since each of the parameters in the neutrino mass matrix (a, b, c, d, e, f) were allowed to take values up to 2, there is a large allowed range in the $\sum m_\nu$ direction. The effect of perturbations is to increase the allowed range for $\langle m_{ee}\rangle$, with a minimum of 7.5×10^{-4} eV for the normal hierarchy and 0.025 eV for the inverted hierarchy. Once again, the Fortran program could not find solutions for perturbations

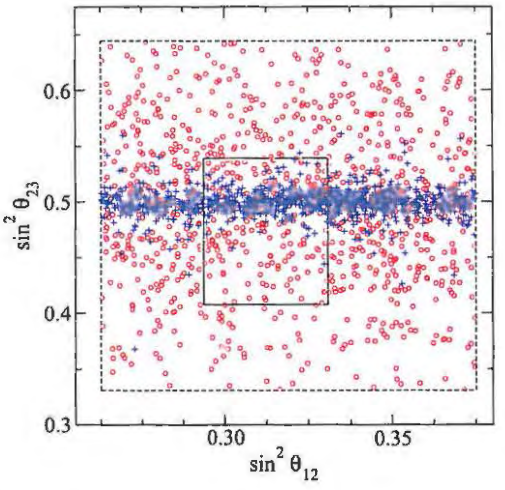

(a) $\sin^2\theta_{23}$ against $\sin^2\theta_{12}$, normal hierarchy, with perturbations to both M_ν and M_ℓ of order 0.03 (blue plus signs), and perturbations of order 0.3 to M_ν only (red circles).

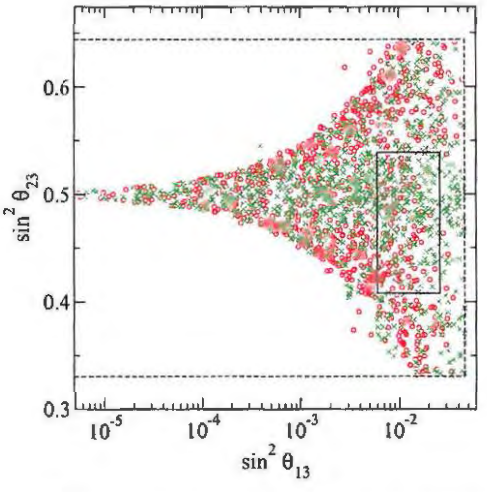

(b) $\sin^2\theta_{23}$ against $\sin^2\theta_{13}$, with perturbations to M_ν only and both normal (red circles) and inverted (green crosses) hierarchies.

Figure 6.7: Scatter plots of mixing angle observables for the BMSS $SO(10)$ model.

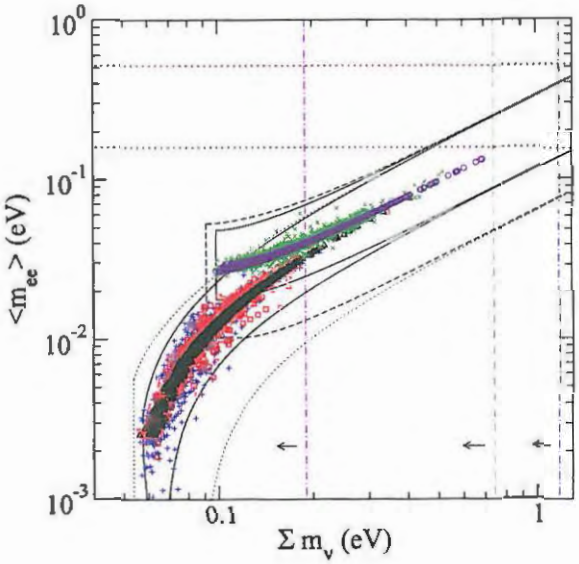

Figure 6.8: Scatter plot of $\langle m_{ee} \rangle$ against $\sum m_\nu$ for the BMSS $SO(10)$ model, with normal and inverted hierarchy. The unperturbed case (black triangles for normal and indigo circles for inverted) as well as the effect of perturbations of order $\epsilon \sim 0.3$ on M_ν (blue plus signs for normal and green crosses for inverted) are shown. Red squares represent points with perturbations ($\epsilon \sim 0.03$) in both mass matrices, for normal hierarchy.

of order 0.03 to both mass matrices in the inverted hierarchy case, but the effects of these perturbations are shown in the case of normal hierarchy.

6.2.3 Hirsch, Morisi, Valle (HMV) model

There are two similar models presented in Ref. [262]: the first is invariant under $A_4 \times Z_2$, contains four $SU(2) \times U(1)$ Higgs doublets, and is renormalisable; the second is invariant under $A_4 \times Z_4$, contains one Higgs doublet and additional gauge singlet scalars, and is non-renormalisable. In both models, the VEV alignments proportional to $(1,1,1)$ and $(0,0,1)$ in the charged lepton and neutrino sectors, respectively, break the A_4 symmetry and lead to TBM. The only difference is that the scalars are either doublets (model (i)) or singlets (model (ii)) under the gauge group $SU(2) \times U(1)$. In order to separate the charged leptons from the neutrinos, the discrete symmetries Z_2 and Z_4 are included in each model, respectively.

Here the Majorana mass matrix is proportional to the identity, and the Dirac mass

matrix is

$$M_{\rm D} = \begin{pmatrix} a & 0 & 0 \\ 0 & a & b \\ 0 & b & a \end{pmatrix} , \tag{6.38}$$

which is the exact opposite of the MPT model above [80]. The type I seesaw mechanism leads to the two parameter neutrino mass matrix

$$M_\nu = m_0 \begin{pmatrix} a^2 & 0 & 0 \\ 0 & a^2+b^2 & 2ab \\ 0 & 2ab & a^2+b^2 \end{pmatrix} , \tag{6.39}$$

which is fully determined by three physical parameters: the moduli of a and b and the relative phase between them. This model is in fact similar to the model presented in Section 5.4.5, and the allowed region in $a-b$ parameter space shown in Fig. 6.9 is similar to the region shown in Fig. 5.31.[10] Note that the inverted mass hierarchy cannot be realised in this model.

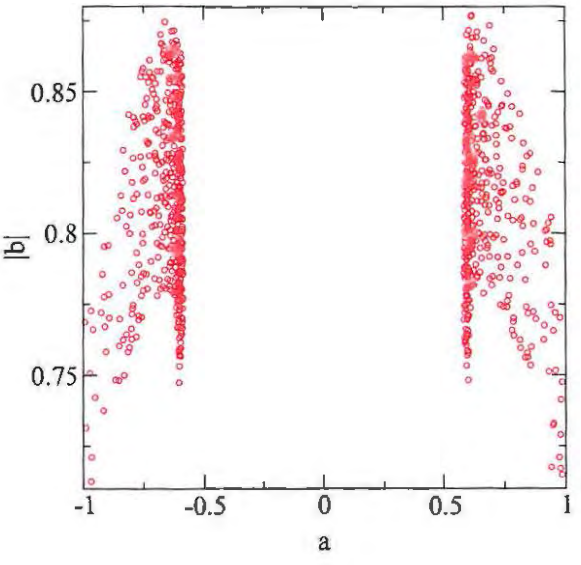

Figure 6.9: Scatter plot of the $a-b$ parameter space for the HMV model, normal hierarchy.

Deviating the VEV alignment in the neutrino sector to $\langle\varphi'\rangle = (v'\epsilon_1, v'\epsilon_2, v')$ leads

[10]The models are formulated in different bases for A_4, and the Chen & King model omits the factor of $\frac{1}{3}$ from the A_4 product rules.

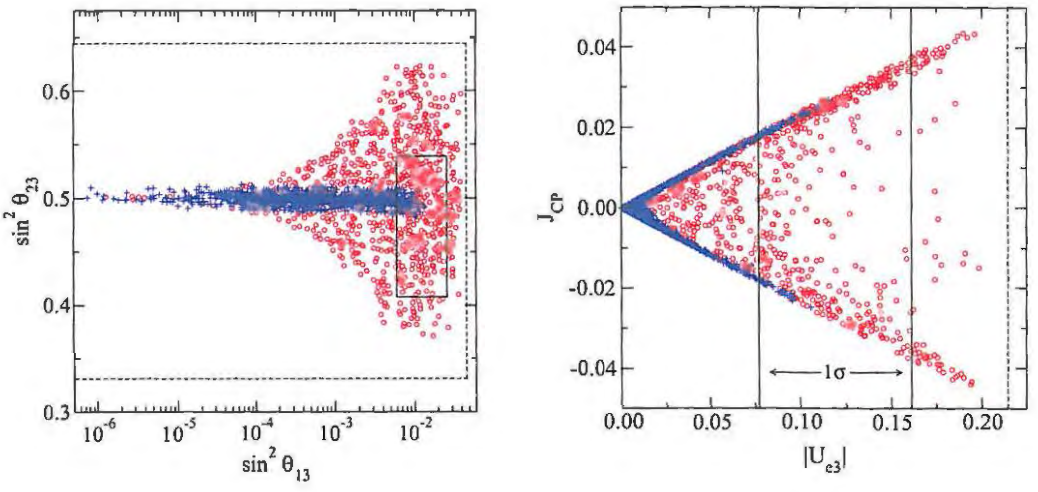

(a) (b)

Figure 6.10: Scatter plots of $\sin^2\theta_{23}$ against $\sin^2\theta_{13}$ (a) and J_{CP} against $|U_{e3}|$ (b) for the HMV model, normal hierarchy, with perturbations to both M_ν and M_ℓ of order 0.03 (blue plus signs), and perturbations of order 0.3 to M_ν only (red circles).

to the mass matrix

$$M'_\nu = m_0 \begin{pmatrix} a^2+b^2\epsilon_1^2+b^2\epsilon_2^2 & b^2\epsilon_2+2ab\epsilon_1 & b^2\epsilon_1+2ab\epsilon_2 \\ \cdot & a^2+b^2+b^2\epsilon_1^2 & b^2\epsilon_1\epsilon_2+2ab \\ \cdot & \cdot & a^2+b^2+b^2\epsilon_2^2 \end{pmatrix} , \qquad (6.40)$$

which can be combined with the deviated charged lepton mass matrix in Eq. (6.9) in order to analyse the deviations from TBM.

The scatter plot in Fig. 6.10(a) is similar to Fig. 6.3 – for the case of perturbations ($\epsilon \sim 0.3$) to M_ν only there is some correlation between non-maximal θ_{23} and large $\sin^2\theta_{13}$. With smaller perturbations ($\epsilon \sim 0.03$) to both mass matrices there is not much deviation from maximal θ_{23}, but $\sin^2\theta_{13}$ can take on a range of values. The plot of J_{CP} against $|U_{e3}|$ in Fig. 6.10(b) takes the same form as Fig. 6.1(c), i.e. if small perturbations are applied to both mass matrices, J_{CP} takes on specific values for each value of $|U_{e3}|$, but with larger perturbations to M_ν only, it can take on values throughout the allowed range.

Since the parameter m_0 was fixed to 0.025 eV, the allowed range of points in the $\langle m_{ee}\rangle - \sum m_\nu$ parameter space in Fig. 6.11 is in the hierarchical region for neutrino masses. VEV alignment deviations in M_ν ($\epsilon \sim 0.3$) allow for smaller values of $\langle m_{ee}\rangle$,

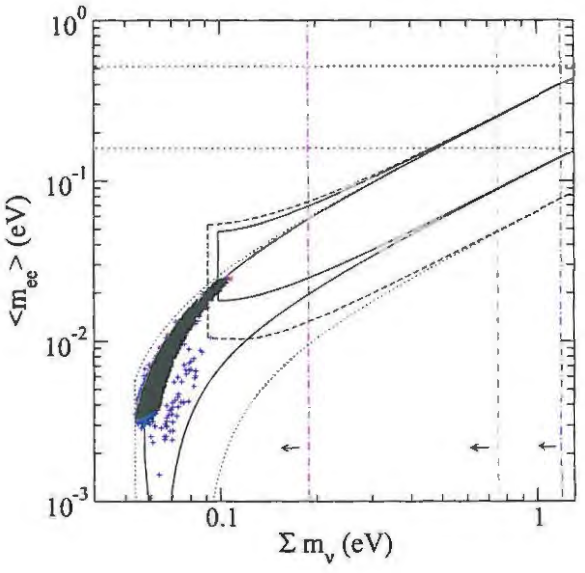

Figure 6.11: Scatter plot of $\langle m_{ee} \rangle$ against $\sum m_\nu$ for the HMV model, normal mass hierarchy, with perturbations applied to the lepton mass matrices. See the caption of Fig. 6.4 for an explanation of the symbols used.

with a minimum of 0.0015 eV in Fig. 6.11, but perturbations of order 0.03 in both mass matrices have little effect on the allowed range. The neutrino masses are well within the most stringent cosmological bound for $\sum m_\nu$.

6.2.4 Bazzocchi, Frigerio, Morisi (BFM) model

In Ref. [82] there is a systematic study of fermion masses and mixing in $SO(10)$ GUT models with A_4 family symmetry. Once again, the matter particles are in the **16** representation of $SO(10)$, and transform as $\underline{3}$ under A_4. There are additional Higgs singlets and an extra discrete symmetry that separates the charged lepton and neutrino sectors. It turns out [82] that TBM cannot be exactly realised with renormalisable models of this type, and non-renormalisable operators, proportional to powers of $M_{\rm GUT}/\Lambda$, where Λ is the cutoff scale,[11] must be introduced.

Without examining the charged lepton mass matrix in great detail,[12] note that when the Higgs triplet φ is aligned as $(1,1,1)$, M_ℓ takes the same form as Eqs. (6.2) and (6.11), is diagonalised by U_ω, and deviations can be studied as in Eq. (6.9).

[11] The cutoff scale can be either the Planck scale or the string scale.

[12] In Ref. [82] there is a detailed proposal of a solution to the family hierarchy problem.

This model has the Higgs fields ϕ and ξ, as well as the flavons σ and τ, all transforming as $\underline{1}$ under A_4. The flavons φ and φ' transform as $\underline{3}$ (see Table II in Ref. [82] for details). When the triplet φ' takes the alignment proportional to $(0,1,0)$, the neutrino mass matrices are

$$M_{\rm L} = \begin{pmatrix} a & 0 & b \\ 0 & a & 0 \\ b & 0 & a \end{pmatrix} c^2 \ , \quad M_{\rm R} = \begin{pmatrix} a & 0 & b \\ 0 & a & 0 \\ b & 0 & a \end{pmatrix} d^2 \ ,$$

$$\text{and} \quad M_{\rm D} = \begin{pmatrix} e+2acd & 0 & 2bcd \\ 0 & e+2acd & 0 \\ 2bcd & 0 & e+2acd \end{pmatrix} \ , \tag{6.41}$$

where

$$a = \frac{f_1 \tau}{\Lambda} \ , \quad b = \frac{f_{3s} \varphi'}{\Lambda} \ , \quad c^2 = \frac{(v_5^\xi)^2}{M_1} \ , \quad d^2 = \frac{(v_1^\xi)^2}{M_1} \ , \quad e = \frac{y_1 \sigma v_5^\phi}{\Lambda} \ , \tag{6.42}$$

and f_1, f_{3s} and y_1 are coupling constants. The terms v_5^ξ and v_5^ϕ are the VEVs of the singlets ξ and ϕ, respectively, and M_1 ensures the correct scale for light neutrino masses.

With the type I and type II seesaw mechanism in Eq. (3.75), the light neutrino mass matrix becomes

$$M_\nu = \begin{pmatrix} -3ac^2 - \frac{4ec}{d} - \frac{ae^2}{(a^2-b^2)d^2} & 0 & b\left(\frac{e^2}{(a^2-b^2)d^2} - 3c^2\right) \\ 0 & -\frac{(acd+e)(3acd+e)}{ad^2} & 0 \\ b\left(\frac{e^2}{(a^2-b^2)d^2} - 3c^2\right) & 0 & -3ac^2 - \frac{4ec}{d} - \frac{ae^2}{(a^2-b^2)d^2} \end{pmatrix} . \tag{6.43}$$

The matrices in Eqs. (6.41) and (6.43) are diagonalised by Eq. (5.28), which combines with the charged lepton mixing matrix (U_ω) to give TBM. Since there are a large number of parameters (a, b, c, d, e) in this model, one should expect a large allowed region in parameter space. This is confirmed in the scatter plots of the $a-b-c$ and $b-c-d$ parameter spaces shown in Figs. 6.12 and 6.13.

If one deviates the VEV alignment of φ' to

$$\langle \varphi' \rangle = (v'\epsilon_1, v', v'\epsilon_2) \ , \tag{6.44}$$

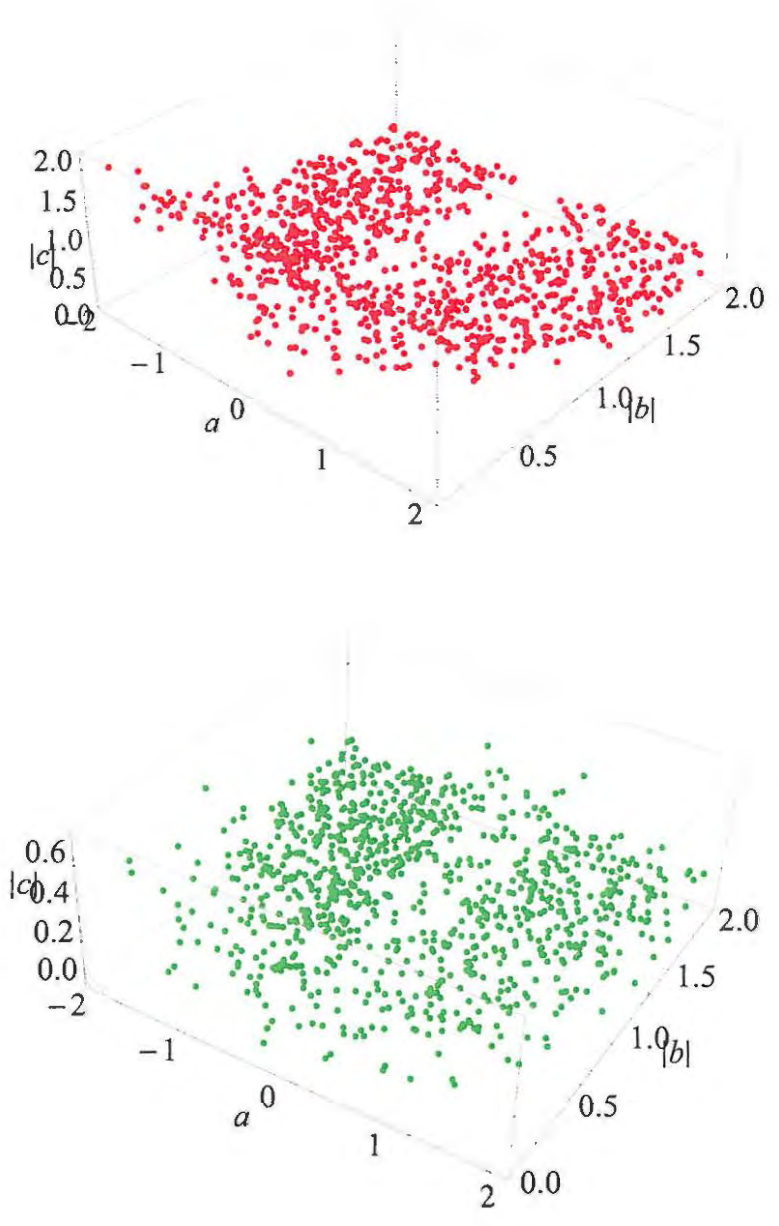

Figure 6.12: Scatter plots of the $a-b-c$ parameter space for the BFM seesaw model, for normal (red) and inverted (green) hierarchies.

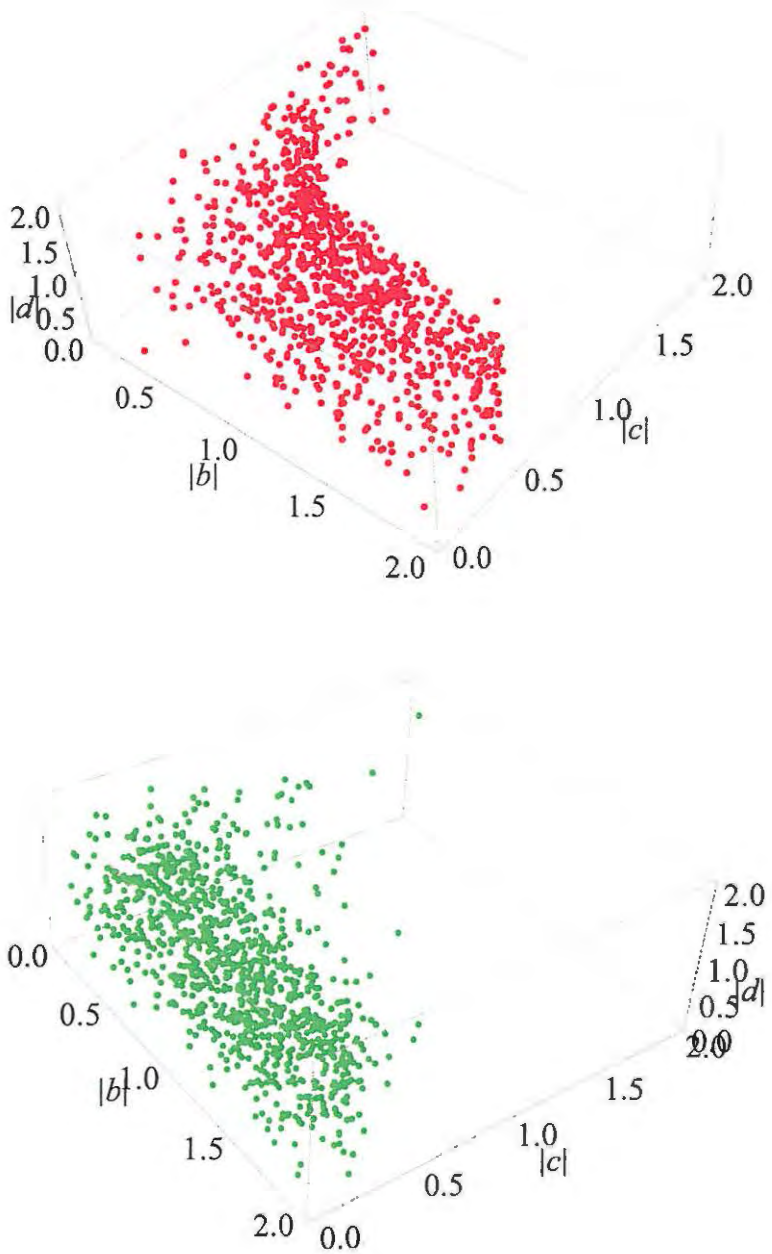

Figure 6.13: Scatter plots of the $b-c-d$ parameter space for the BFM seesaw model, for normal (red) and inverted (green) hierarchies.

the neutrino mass matrices become

$$M'_{\rm L} = \begin{pmatrix} a & b\epsilon_2 & b \\ b\epsilon_2 & a & b\epsilon_1 \\ b & b\epsilon_1 & a \end{pmatrix} c^2 \ , \quad M'_{\rm R} = \begin{pmatrix} a & b\epsilon_2 & b \\ b\epsilon_2 & a & b\epsilon_1 \\ b & b\epsilon_1 & a \end{pmatrix} d^2 \ ,$$

$$\text{and} \quad M'_{\rm D} = \begin{pmatrix} e+2acd & 2b\epsilon_2 cd & 2bcd \\ 2b\epsilon_2 cd & e+2acd & 2b\epsilon_1 cd \\ 2bcd & 2b\epsilon_1 cd & e+2acd \end{pmatrix} \ , \tag{6.45}$$

and the light neutrino mass matrix is

$$M'_\nu = \frac{m_0}{m'} \begin{pmatrix} M'_{11} & M'_{12} & M'_{13} \\ \cdot & M'_{22} & M'_{23} \\ \cdot & \cdot & M'_{33} \end{pmatrix} \ , \tag{6.46}$$

where

$$\begin{aligned} M'_{11} &= -3a^4c^2d^2 - 4a^3cde + a^2\left(3b^2c^2d^2\left(\epsilon_1^2+\epsilon_2^2+1\right) - e^2\right) \\ &\quad + 2ab^2cd\left(2e\left(\epsilon_1^2+\epsilon_2^2+1\right) - 3bcd\epsilon_1\epsilon_2\right) + b^2e\epsilon_1(e\epsilon_1 - 8bcd\epsilon_2) \end{aligned} \tag{6.47}$$

$$\begin{aligned} M'_{12} &= b\left(a\epsilon_2\left(e^2 - 3a^2c^2d^2\right) + 3ab^2c^2d^2\epsilon_2\left(\epsilon_1^2+\epsilon_2^2+1\right)\right) \\ &\quad - b\left(6b^3c^2d^2\epsilon_1\epsilon_2^2 - be^2\epsilon_1\right) \end{aligned} \tag{6.48}$$

$$M'_{13} = b\left(-3a^3c^2d^2 + a\left(3b^2c^2d^2\left(\epsilon_1^2+\epsilon_2^2+1\right) + e^2\right) - b\epsilon_1\epsilon_2\left(6b^2c^2d^2 + e^2\right)\right) \tag{6.49}$$

$$\begin{aligned} M'_{22} &= -3a^4c^2d^2 - 4a^3cde + a^2\left(3b^2c^2d^2\left(\epsilon_1^2+\epsilon_2^2+1\right) - e^2\right) \\ &\quad + 2ab^2cd\left(2e\left(\epsilon_1^2+\epsilon_2^2+1\right) - 3bcd\epsilon_1\epsilon_2\right) + b^2e(e - 8bcd\epsilon_1\epsilon_2) \end{aligned} \tag{6.50}$$

$$\begin{aligned} M'_{23} &= b\left(-3a^3c^2d^2\epsilon_1 + a\epsilon_1\left(3b^2c^2d^2\left(\epsilon_1^2+\epsilon_2^2+1\right) + e^2\right)\right) \\ &\quad - b^2\left(\epsilon_2\left(6b^2c^2d^2\epsilon_1^2 + e^2\right)\right) \end{aligned} \tag{6.51}$$

$$M'_{33} = M'_{11} \ , \tag{6.52}$$

with $m' = d^2\left(a^3 - ab^2\left(\epsilon_1^2+\epsilon_2^2+1\right) + 2b^3\epsilon_1\epsilon_2\right)$. The term m_0 is included to fix the mass scale.

The value of $\sin^2\theta_{23}$ is more constrained around the TBM value for the inverted hierarchy; for normal hierarchy the deviation increases for increasing $\sin^2\theta_{13}$ [Fig. 6.14(a)]. The scatter plot in Fig. 6.15(a) shows that with small perturbations ($\epsilon \sim 0.03$) applied to both mass matrices, there is little deviation from maximal $\sin^2\theta_{23}$, and $\sin^2\theta_{13} \leq$

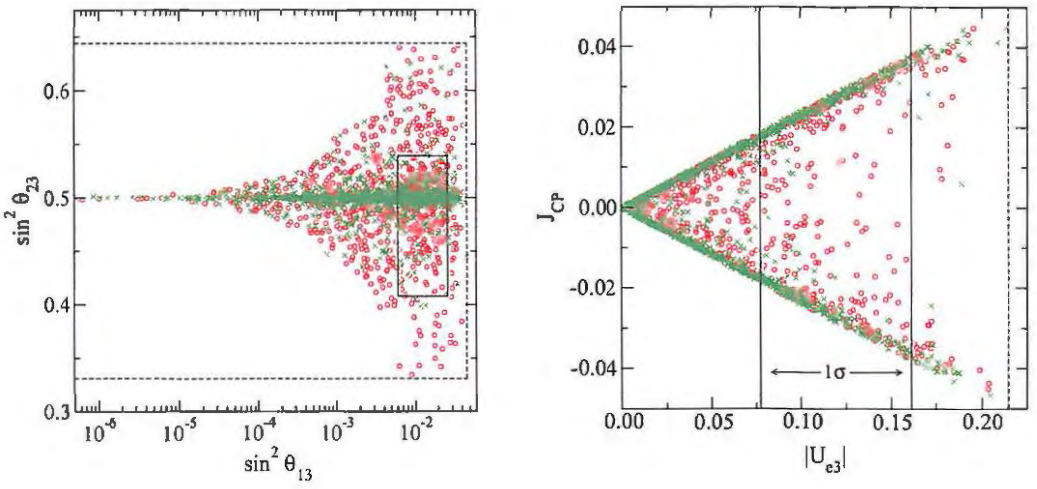

(a) (b)

Figure 6.14: Scatter plots of $\sin^2\theta_{23}$ vs $\sin^2\theta_{13}$ (a) and J_{CP} against $|U_{e3}|$ (b) for the BFM seesaw model, with perturbations of order 0.3 to M_ν only, for normal (red circles) and inverted (green crosses) hierarchies.

0.012. In Fig. 6.14(b), J_{CP} is closer to its maximal value in the case of inverted hierarchy, but can take on a range of values in the normal hierarchy. The effect of small perturbations is seen in Fig. 6.15(b), where J_{CP} takes on a spread of values for small $|U_{e3}|$, and as $|U_{e3}|$ increases, J_{CP} tends to be greater (but not maximal).

This model has five parameters (a, b, c, d, e) in the neutrino mass matrix, and the absolute value of each parameter was allowed to vary up to 2. The parameter m_0 was set to 0.025 eV and 0.05 eV for normal and inverted hierarchies, respectively. For this choice of values, the allowed region for $\langle m_{ee}\rangle$ and $\sum m_\nu$ covers a large region of parameter space (see Fig. 6.16), and $\sum m_\nu$ exceeds the CMB limit. In the unperturbed case, $\langle m_{ee}\rangle$ takes its maximum value, and the perturbations of order 0.3 applied to M_ν allow for smaller values of $\langle m_{ee}\rangle$, with a minimum of 0.0030 eV in the normal hierarchy and 0.020 eV in the inverted hierarchy. The application of perturbations of order 0.03 to both mass matrices has little effect in the normal hierarchy case. Note that in the inverted hierarchy case the Fortran program did not converge to solutions if perturbations were applied to M_ℓ and M_ν simultaneously.

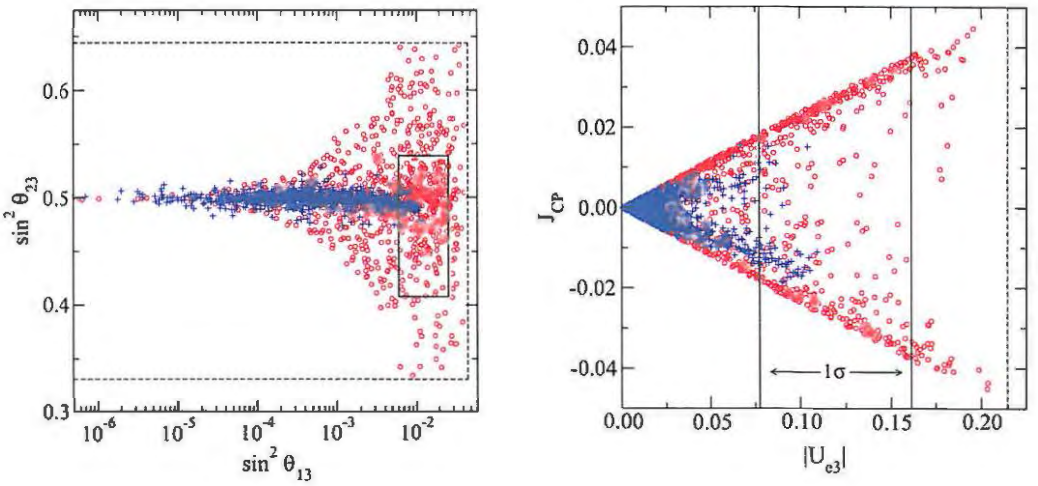

(a) (b)

Figure 6.15: Scatter plots of (a) $\sin^2\theta_{23}$ against $\sin^2\theta_{13}$ and (b) J_{CP} against $|U_{e3}|$ for the BFM seesaw model, normal hierarchy, with perturbations of order 0.03 to both M_ν and M_ℓ (blue plus signs) and perturbations of order 0.3 to M_ν only (red circles).

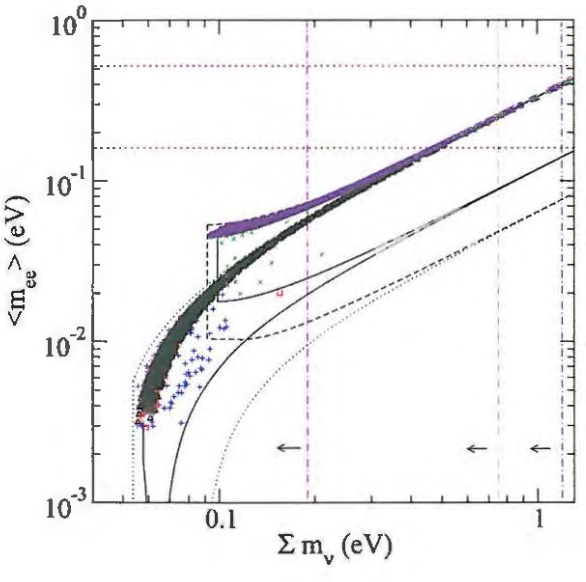

Figure 6.16: Scatter plot of $\langle m_{ee}\rangle$ against $\sum m_\nu$ for the BFM seesaw model, for normal and inverted mass hierarchies, with perturbations applied to the lepton mass matrices. See the caption of Fig. 6.8 for an explanation of the symbols used.

Table 6.5: Particle assignments in the Frampton-Matsuzaki model [85].

Particle	A_4	Z_2
ℓ_L	$\underline{3}$	$+1$
τ^c, μ^c, e^c	$\underline{1}$, $\underline{1}'$, $\underline{1}''$	-1
$N_R^{(i)}$	$\underline{1}$, $\underline{1}'$, $\underline{1}''$	-1
h_3	$\underline{3}$	$+1$
h_3'	$\underline{3}$	-1

6.3 Other models

Models of type A, B, C and D have been discussed so far, with an in-depth analysis of the deviations from TBM in each case. Table 5.1 on page 53 also lists models of type E, F, G and H, with different A_4 particle assignments. Only those models [85, 87, 88] that claim to reproduce the TBM pattern will be considered below.

6.3.1 Frampton and Matsuzaki

Frampton and Matsuzaki [85] present a minimal renormalisable A_4 model of lepton mixing, with only one A_4 triplet of Higgs doublets coupling to neutrinos. This model claims more predictivity regarding neutrino masses, and a minimal number of free parameters in the Higgs sector. Although the model is constructed to give TBM in the neutrino sector, this is in fact not the case, as the VEV alignment proportional to $(1, -2, 1)$ gives the wrong mass eigenvalues for neutrinos.

Note that in Ref. [85], the mixing matrices are defined differently, i.e., the mixing matrix is defined by

$$\begin{pmatrix} \nu_1 \\ \nu_2 \\ \nu_3 \end{pmatrix} = U_{\text{PMNS}} \begin{pmatrix} \nu_\tau \\ \nu_\mu \\ \nu_e \end{pmatrix} , \tag{6.53}$$

and the TBM matrix is defined by

$$U'_{\text{TBM}} = \begin{pmatrix} -\frac{1}{\sqrt{6}} & -\frac{1}{\sqrt{6}} & \frac{2}{\sqrt{6}} \\ \frac{1}{\sqrt{3}} & \frac{1}{\sqrt{3}} & \frac{1}{\sqrt{3}} \\ \frac{1}{\sqrt{2}} & -\frac{1}{\sqrt{2}} & 0 \end{pmatrix} , \tag{6.54}$$

which is in effect "rotated" by 90 degrees from the TBM matrix in Eq. (4.9).

With the particle assignments in table 6.5,[13] the right-handed neutrino mass matrix is[14]

$$M_{\rm N} = \begin{pmatrix} M_1 & 0 & 0 \\ 0 & 0 & M_{23} \\ 0 & M_{23} & 0 \end{pmatrix} , \tag{6.55}$$

and if the Higgs scalar h_3 takes the VEV

$$\langle h_3 \rangle = (v_1, v_2, v_3) , \tag{6.56}$$

the Dirac mass matrix becomes

$$M_{\rm D} = \begin{pmatrix} y_1 v_1 & y_2 v_3 & y_3 v_2 \\ y_1 v_3 & y_2 v_2 & y_3 v_1 \\ y_1 v_2 & y_2 v_1 & y_3 v_3 \end{pmatrix} . \tag{6.57}$$

Using the type I seesaw mechanism, the light neutrino mass matrix is

$$M_\nu = \begin{pmatrix} a v_1^2 + 2b v_2 v_3 & a v_1 v_3 + b\left(v_2^2 + v_1 v_3\right) & a v_1 v_2 + b\left(v_3^2 + v_1 v_2\right) \\ \cdot & a v_3^2 + 2b v_1 v_2 & a v_2 v_3 + b\left(v_1^2 + v_2 v_3\right) \\ \cdot & \cdot & a v_2^2 + 2b v_1 v_3 \end{pmatrix} , \tag{6.58}$$

with $a = y_1^2/M_1$ and $b = y_2 y_3 / M_{23}$.

In order to produce the TBM matrix in Eq. (6.54), one must choose the correct alignment for h_3. In Ref. [85], two different alignments are studied. The first is

$$\langle h_3 \rangle = (v, v, v) , \tag{6.59}$$

which gives the eigenstates $m_1 = m_3 = 0$ and $m_2 = 3(a + 2b)v^2$, and the wrong mixing matrix. These eigenvalues are clearly not compatible with the observed neutrino mass hierarchy. The second alignment studied in Ref. [85] is

$$\langle h_3 \rangle = (v, -2v, v) , \tag{6.60}$$

which gives the eigenstates $m_1 = 3(2a+b)v^2$, $m_2 = 0$ and $m_3 = -9bv^2$. Once again, this is not compatible with TBM: although the mixing matrix is correct, the eigenvalue corresponding to the maximally mixed eigenvector ($\propto (1,1,1)^T$) is zero. However

[13] The Higgs doublet scalar h_3' is used to give the charged lepton masses.

[14] This model is constructed in the flavour basis.

Ref. [85] claims that the mass spectrum is $m_3 \gg m_1 = m_2$, which is incorrect.

There is a third VEV alignment

$$\langle h_3 \rangle = (v, 0, -v) \ , \tag{6.61}$$

which when substituted into Eq. (6.58) gives TBM, but again the eigenvalue with trimaximal mixing is zero. This means that the model presented in Ref. [85] cannot simultaneously produce TBM and the correct hierarchy of neutrino masses.

6.3.2 Lin and Altarelli-Meloni

In the models in category H [87,88] of Table 5.1, all three charged leptons transform as $\underline{1}$ under A_4, which is different to the type A and type B models studied above, where each charged lepton is assigned to a different A_4 singlet representation ($\underline{1}$, $\underline{1}'$ and $\underline{1}''$). The neutrino sector is unchanged (at leading order), with the same structure as the original Altarelli-Feruglio model studied in Section 5.3, but the charged lepton sector is different. The VEV alignment of the original model [Eq. (5.18)] is now modified to

$$\langle \varphi \rangle = (0, v, 0) \ , \tag{6.62}$$

instead of $\langle \varphi \rangle = (v, 0, 0)$. The difference between these alignments is as follows: since $(1,0,0)^n = (1,0,0)$, all positive powers are aligned in the same direction, whereas for $(0,1,0)$, it follows that $(0,1,0)^2 = (0,0,1)$ and $(0,1,0)^3 = (1,0,0)$. The three different directions are used to give the observed hiearachy of charged lepton masses, so that [87,88]

$$M_\ell = \begin{pmatrix} \varphi^3/\Lambda^3 & 0 & 0 \\ 0 & \varphi^2/\Lambda^2 & 0 \\ 0 & 0 & \varphi/\Lambda \end{pmatrix} v_d \ , \tag{6.63}$$

where v_d is the VEV of the SM Higgs doublet h_d. An additional Z_3 symmetry is necessary to force the different charged leptons to couple with different powers of φ.

One can study [88] the effect of next to the leading order (NLO) corrections to M_ℓ, and the corresponding deviations from TBM. (This model was not analysed in detail here; further investigation is required.)

Chapter 7

Conclusion

There is now conclusive evidence of the existence of neutrino oscillations. This means that neutrinos are massive and that the mass eigenstates mix, which implies some sort of physics beyond the SM. There exist a plethora of models that attempt to explain the origin of neutrino mass, with the seesaw mechanism as the most widely accepted theory. However, the heavy, sterile, right-handed neutrinos postulated in the seesaw mechanism have not been observed, and the Dirac or Majorana nature of neutrinos is still an open question.

The TBM hypothesis presented by Harrision et al. [27] is a good approximation to the neutrino oscillation data, but recent global analyses [25, 104] have provided evidence of $\theta_{13} > 0$, which is not compatible with exact TBM. One can therefore regard TBM as a zeroth order approximation to lepton mixing, as the allowed deviations can only be small (10-15%), and this has lead to extensive research into models of family symmetries.

The majority of these models employ a bottom-up approach, in a simple attempt to link the three lepton families and their observed mixing patterns. However, models with discrete unbroken family symmetries are problematic, as the $SU(2)_L$ symmetry of the SM is violated. The immediate implication is that the proposed family symmetry must be broken, and therefore several Higgs scalars with non-zero VEVs must be introduced. Type A and type B models are an example of this bottom-up approach.

In order to link neutrino masses and mixings with the bigger picture of quarks and fundamental forces, one can also employ a top-down approach. The models classed as type D fit into this category, where the A_4 family symmetry is combined with a GUT group, with implications for the properties of other fermions. The bottom-up and top-down approaches complement each other, and the ultimate theory of flavour may indeed result from a combination of these two techniques.

After the analysis of fifteen different A_4 models in this work, there are various conclusions that can be drawn. The ultimate aim is to find a model that can successfully reproduce the TBM pattern at leading order, and that fits in with the global data from oscillation and $0\nu\beta\beta$ experiments and cosmology. However, the current limits [25] on the neutrino oscillation data do not necessarily rule out any of these models; future precision measurements are required to distinguish the models.

If the maximum number of VEV alignment deviations are applied, most of the A_4 models deviate from TBM in a random fashion, and it is difficult to draw any conclusions. Some notable exceptions include: (i) the Morisi model, in which $\sin^2\theta_{13}$ lies below 0.005, and $\sin^2\theta_{23}$ shows some dependence on $\sin^2\theta_{13}$; (ii) all type C and type D models, in which $\sin^2\theta_{23}$ is further from maximal for larger values of $\sin^2\theta_{13}$ (the Ma supersymmetric model is different, as $\sin^2\theta_{23}$ stays close to maximal for all values of $\sin^2\theta_{13}$).

If $\sin^2\theta_{23}$ deviates considerably from maximal, and one assumes that $\sin^2\theta_{13}$ will be measured accurately within the present 1σ range from Ref. [25], then the Morisi $(Z_2)^3$ model can be ruled out. The Ma TBM model (equivalent to the A-F model with three singlets) gives a random spread of points in the deviated case, and cannot be ruled out by the present data. In the MPT model, with inverted hierarchy, there is no deviation from maximal atmospheric mixing ($\sin^2\theta_{23} = 0.5$). However, the value of $\sin^2\theta_{23}$ does deviate from maximal in the normal hierarchy case of this model. The inverted hierarchy also shows maximal CP violation.

The Altarelli-Feruglio model includes three different cases, with one, two or three Higgs singlets, and these respond differently to deviations from TBM. The results show that the one Higgs singlet case has a low value of $\sin^2\theta_{13}$, and is effectively ruled out by the 1σ range from Ref. [25]; the two singlet case shows more deviation from maximal $\sin^2\theta_{23}$ and maximal CP violation than the three singlet case. In the Altarelli-Feruglio seesaw model, the inverted hierarchy case shows a low value of $\sin^2\theta_{13}$, below the 1σ range. A comparison of this model with and without seesaw, for one Higgs singlet, shows that a measurement of $\sin^2\theta_{13}$ within the 1σ range would favour the seesaw version.

In the Chen & King and MPT models, CP violation is close to maximal if U_{e3} lies within the 1σ range, so that an accurate measurement of $\sin^2\theta_{13}$ and δ could potentially rule out these models. In the Ma supersymmetric type C model, $\sin^2\theta_{23}$ is close to maximal, but larger deviations in M_ℓ could change this. In fact, the results obtained for type C and type D models could be improved upon by applying larger perturbations ($\epsilon \sim 0.3$) to both mass matrices, not just M_ν. However, this is difficult to achieve,

considering the fine tuning required in the parameters of M_ℓ in these models.

Of the model categories listed, only models of types A, B, C, D and H have been constructed to give TBM. The analysis herein concentrates on types A, B, C and D models, but one could also look at models of type H, and it may be interesting to construct models of types E, F and G that can also reproduce TBM.

The scatter plots of $\langle m_{ee} \rangle - \sum m_\nu$ parameter space were different in each model, and this is an indication of the importance of $0\nu\beta\beta$ decay and cosmology in neutrino mass models. A positive signal for $0\nu\beta\beta$ decay would provide a test for the models presented in this work, and in some cases would allow one to distinguish the favoured neutrino mass hierarchy. In addition to this, further accurate measurements of $\sum m_\nu$ would clarify the absolute mass scale of neutrinos, ruling out certain models.

The mass scale was fixed in the present analysis: the coefficient m_0 was chosen to be 0.025 eV and 0.05 eV in the normal and inverted hierarchy case, respectively. However, this choice is rather prescriptive, and one could also investigate each model with different values of m_0. This would allow the study of each model in different portions of parameter space, with both hierarchical and degenerate neutrino masses. With the chosen mass scale, the MPT and BFM models showed the highest values of $\sum m_\nu$, and are both ruled out by the Cosmic Microwave Background (CMB) data.

The deviations induced by altering the VEV alignment had the effect of reducing the allowed value of $\langle m_{ee} \rangle$, and this can be attributed to additional complex phases, which cause cancellations in the calculation of $\langle m_{ee} \rangle$ (see Appendix B). The exceptions to this are the two models with rephased fields: the BM left-right model and the BM seesaw model. In this case the scatter plots show that in the unperturbed case $\langle m_{ee} \rangle$ takes a value close to the centre of its allowed range, and the effect of perturbations can cause an increase or a decrease in $\langle m_{ee} \rangle$. In the Babu & He seesaw model, normal hierarchy, the effect of perturbations can also increase the value of $\langle m_{ee} \rangle$, but the allowed range is very small.

Some of the seesaw models showed a large splitting between the value of $\langle m_{ee} \rangle$ for the normal and inverted hierarchies, which means that a measurement of $0\nu\beta\beta$ could determine the allowed hierarchy in these models. The Babu & He model, the A-F seesaw model (one singlet) and the MPT $SO(10)$ model all showed this characteristic. The A-F model with one singlet gives a very low value (0.0042 eV) of $\langle m_{ee} \rangle$ for the normal mass hierarchy, too low to be probed by the next generation of $0\nu\beta\beta$ decay experiments. Other models which give similarly small values of $\langle m_{ee} \rangle$ for normal hierarchy are the Babu & He model, the BM left-right model, the MPT model and the HMV model.

The Altarelli-Feruglio model with one Higgs singlet showed some evidence of fine tuning between the parameters a and d, which come from the VEVs of the Higgs singlet ξ and Higgs triplet φ', respectively. There are three other models with essentially the same form in the neutrino sector: the Morisi model, the Ma supersymmetric type C model, and the BM left-right model. The neutrino mass matrix is determined by two parameters in each case; if both of the parameters are real then they must take specific values to reproduce the correct mass-squared differences, and if one parameter is complex the allowed region is not that much greater.

Other models with a restricted parameter space include the Zee model, the Babu & He model, the Ma supersymmetric seesaw model, the A-F seesaw model, the Chen & King model and the HMV model. Although it is not true in every case, an overall conclusion of this analysis is that models with less parameters have more predictive power, and the plots of mixing angle observables can provide useful relationships or show the dependence of one mixing angle on another. This can be seen in tbe A-F model with and without seesaw (one singlet), the Morisi model, the Ma supersymmetric type C model, the BM left-right model, the MPT model and the HMV model.

In the BMSS and BFM models, the large number of parameters means that the parameter space is less restricted. However, one can still make some predictions from the mixing angle scatter plots, but in this analysis the large ($\epsilon \sim 0.3$) perturbations were only applied to M_ν. In these models there is overlap in the value of $\langle m_{ee} \rangle$ between the two hierarchies, in contrast to the other seesaw models, and the greater number of parameters allows a larger value for $\sum m_\nu$, with the same value chosen for m_0.

The type C and type D models are attractive in that one can accommodate all the leptons in one representation. However, M_ℓ is very sensitive to deviations, and the program used in this analysis did not converge to solutions with perturbations of order $\epsilon \sim 0.3$ applied to M_ℓ.

The A_4 models analysed herein provide an attractive explanation for the neutrino mixing pattern, which is approximated by TBM. However, this requires several additional parameters and an enlarged Higgs sector. The models depend on the VEV alignment of these Higgs scalars, and the model predictions are affected to some degree by deviations in this alignment. The present analysis can be extended to include the effects of radiative corrections and the renormalisation group evolution of neutrino masses [250]. One can also study the exact origin of the VEV alignment deviations in more detail, by examining the Higgs potential in each case. The approach used in this work can be applied to models with other symmetry groups, allowing a comparison of the predictions of those models with the A_4 models analysed here.

A complete understanding of the physics of flavour will ultimately require a combined effort between theory and experiment. Future precision measurements of the neutrino oscillation and neutrino mass parameters will help to reduce the number of models that are allowed, and may lead to more economical and natural theories.

Appendices

Appendix A

A_4 Tetrahedral Symmetry

The following is an outline of the A_4 symmetry group [34,74,228,269], upon which the models in this analysis are based .

A.1 Introduction to A_4

A_4 is the alternating group of order 4, and is also the group of all even permutations of four objects, isomorphic to the group of rotational symmetries of the regular tetrahedron. It is a finite, non-Abelian subgroup of SO(3) [270] and SU(3). A_4 has 12 elements, which can be divided into 4 conjugacy classes with membership 1, 3, 4 and 4. The dimensionality theorem implies that there are 4 irreducible representations with dimension d_j such that $\sum_j d_j^2 = 12$. The only solution is $d_1 = d_2 = d_3 = 1$ and $d_4 = 3$, and the representations are labeled as $\underline{1}$, $\underline{1}'$, $\underline{1}''$ and $\underline{3}$, which means that there are three one-dimensional representations and one three-dimensional representation. The character table of A_4 is shown in Table A.1, with $\omega \equiv e^{i2\pi/3}$ the cube root of unity.[1]

Table A.1: Character table of A_4, where n represents the number of elements in each conjugacy class.

Class	n	χ^1	$\chi^{1'}$	$\chi^{1''}$	χ^3
C_1	1	1	1	1	3
C_2	4	1	ω	ω^2	0
C_3	4	1	ω^2	ω	0
C_4	3	1	1	1	-1

[1]Note that $\omega = e^{i2\pi/3} = -1/2 + \sqrt{3}/2$ satisfies $\omega^2 = \omega^*$ and $1 + \omega + \omega^2 = 0$.

A.2 Bases for A_4

There are two bases for A_4 commonly used in lepton family symmetry models: the Ma-Rajasekaran basis and the Altarelli-Feruglio basis.

A.2.1 Ma-Rajasekaran basis

A_4 can be generated by two basic permutations S and T, given by $S = (4321)$ and $T = (2314)$, where the generic permutation $(1,2,3,4) \to (n_1, n_2, n_3, n_4)$ is denoted by $(n_1 n_2 n_3 n_4)$. It follows that

$$S^2 = T^3 = (ST)^3 = 1\,, \tag{A.1}$$

which defines a "presentation" of the group. The one-dimensional unitary representations are generated by

$$\begin{aligned} &1 \quad S = 1 \quad T = 1 \\ &1' \quad S = 1 \quad T = e^{i2\pi/3} \equiv \omega \\ &1'' \quad S = 1 \quad T = e^{i4\pi/3} \equiv \omega^2\,, \end{aligned} \tag{A.2}$$

and the three-dimensional unitary representation (in this basis) is built up from the generators

$$S = \begin{pmatrix} 1 & 0 & 0 \\ 0 & -1 & 0 \\ 0 & 0 & -1 \end{pmatrix}\,, \quad T = \begin{pmatrix} 0 & 1 & 0 \\ 0 & 0 & 1 \\ 1 & 0 & 0 \end{pmatrix}\,. \tag{A.3}$$

The 3×3 matrices of the natural three-dimensional representation $\underline{3}$ are:

$$
\begin{aligned}
C_1 &: \begin{pmatrix} 1 & 0 & 0 \\ 0 & 1 & 0 \\ 0 & 0 & 1 \end{pmatrix}, \\
C_2 &: \begin{pmatrix} 0 & 0 & 1 \\ 1 & 0 & 0 \\ 0 & 1 & 0 \end{pmatrix}, \begin{pmatrix} 0 & 0 & 1 \\ -1 & 0 & 0 \\ 0 & -1 & 0 \end{pmatrix}, \begin{pmatrix} 0 & 0 & -1 \\ 1 & 0 & 0 \\ 0 & -1 & 0 \end{pmatrix}, \begin{pmatrix} 0 & 0 & -1 \\ -1 & 0 & 0 \\ 0 & 1 & 0 \end{pmatrix}, \\
C_3 &: \begin{pmatrix} 0 & 1 & 0 \\ 0 & 0 & 1 \\ 1 & 0 & 0 \end{pmatrix}, \begin{pmatrix} 0 & 1 & 0 \\ 0 & 0 & -1 \\ -1 & 0 & 0 \end{pmatrix}, \begin{pmatrix} 0 & -1 & 0 \\ 0 & 0 & 1 \\ -1 & 0 & 0 \end{pmatrix}, \begin{pmatrix} 0 & -1 & 0 \\ 0 & 0 & -1 \\ 1 & 0 & 0 \end{pmatrix}, \\
C_4 &: \begin{pmatrix} 1 & 0 & 0 \\ 0 & -1 & 0 \\ 0 & 0 & -1 \end{pmatrix}, \begin{pmatrix} -1 & 0 & 0 \\ 0 & 1 & 0 \\ 0 & 0 & -1 \end{pmatrix}, \begin{pmatrix} -1 & 0 & 0 \\ 0 & -1 & 0 \\ 0 & 0 & 1 \end{pmatrix}, \qquad \text{(A.4)}
\end{aligned}
$$

where each matrix is a product of the generators S and T in Eq. (A.3). It is evident that the characters of the $\underline{3}$ representation (the last column of table A.1) are simply the traces of the matrices in each class.

The multiplication rules are given by

$$\underline{1} \times \underline{1} = \underline{1}\,, \qquad \text{(A.5)}$$

$$\underline{1}' \times \underline{1}'' = \underline{1}\,, \qquad \text{(A.6)}$$

$$\underline{1}'' \times \underline{1}' = \underline{1}\,, \qquad \text{(A.7)}$$

$$\underline{1}' \times \underline{1}' = \underline{1}''\,, \qquad \text{(A.8)}$$

$$\underline{1}'' \times \underline{1}'' = \underline{1}'\,, \qquad \text{(A.9)}$$

$$\underline{3} \times \underline{3} = \underline{1} + \underline{1}' + 1'' + \underline{3}_{as} + \underline{3}_{s}\,, \qquad \text{(A.10)}$$

where $\underline{3}_{as}$ and $\underline{3}_{s}$ are "asymmetric" and "symmetric" combinations respectively. If $\underline{3}_a \sim (a_1, a_2, a_3)$ and $\underline{3}_b \sim (b_1, b_2, b_3)$ are two triplets transforming by the matrices in

Eq. (A.4), then the three singlets and two triplets in the product in Eq. (A.10) are

$$\underline{1} = a_1 b_1 + a_2 b_2 + a_3 b_3 \ , \tag{A.11}$$

$$\underline{1}' = a_1 b_1 + \omega^2 a_2 b_2 + \omega a_3 b_3 \ , \tag{A.12}$$

$$\underline{1}'' = a_1 b_1 + \omega a_2 b_2 + \omega^2 a_3 b_3 \ , \tag{A.13}$$

$$\underline{3}_1 \sim (a_2 b_3, a_3 b_1, a_1 b_2) \ , \tag{A.14}$$

$$\underline{3}_2 \sim (a_3 b_2, a_1 b_3, a_2 b_1) \ . \tag{A.15}$$

A.2.2 Altarelli-Feruglio basis

In the Ma-Rajasekaran basis, the generator S in Eq. (A.3) is diagonal. However, one can also represent A_4 in a basis where T is diagonal, obtained through the unitary transformation:

$$T' = V^\dagger T V = \begin{pmatrix} 1 & 0 & 0 \\ 0 & \omega & 0 \\ 0 & 0 & \omega^2 \end{pmatrix} \ , \tag{A.16}$$

$$S' = V^\dagger S V = \frac{1}{3} \begin{pmatrix} -1 & 2 & 2 \\ 2 & -1 & 2 \\ 2 & 2 & -1 \end{pmatrix} \ , \tag{A.17}$$

where

$$V = \frac{1}{\sqrt{3}} \begin{pmatrix} 1 & 1 & 1 \\ 1 & \omega & \omega^2 \\ 1 & \omega^2 & \omega \end{pmatrix} \ . \tag{A.18}$$

Note that the matrix V is the so-called "magic matrix", which appears in A_4 models as the unitary matrix that diagonalises the charged lepton mass matrix. In the S', T' basis, the multiplication rules are identical to those in Eqs. (A.5) – (A.10), but the product of two triplets gives the composition of the following irreducible representations:

$$\underline{1} = a_1 b_1 + a_2 b_3 + a_3 b_2 \ , \tag{A.19}$$

$$\underline{1}' = a_3 b_3 + a_1 b_2 + a_2 b_1 \ , \tag{A.20}$$

$$\underline{1}'' = a_2 b_2 + a_1 b_3 + a_3 b_1 \ , \tag{A.21}$$

$$\underline{3}_s \sim \frac{1}{3} (2a_1 b_1 - a_2 b_3 - a_3 b_2 \ , 2a_3 b_3 - a_1 b_2 - a_2 b_1 \ , 2a_2 b_2 - a_1 b_3 - a_3 b_1) \ , \tag{A.22}$$

$$\underline{3}_{as} \sim \frac{1}{3} (a_2 b_3 - a_3 b_2, a_1 b_2 - a_2 b_1, a_1 b_3 - a_3 b_1) \ . \tag{A.23}$$

Appendix B

Model Building and Analysis

This Appendix describes in detail the model building procedure for the case of dimension-5 operators, and covers various other details used in the analysis in Chapters 5 and 5.

B.1 Neutrino mass matrix from dimension-5 operators

The deviated neutrino mass matrix in the Zee model [74] was given in Eq. (5.31) in section 5.3. Using the A_4 multiplication rules in Section A.2.1, this matrix can be constructed with dimension-5 operators, as shown explicitly below.

The Higgs scalars transform under A_4 as $\xi \sim \underline{1}$ and $\varphi' \sim \underline{3}$, and the lepton doublets $\ell = (\ell_e, \ell_\mu, \ell_\tau)$ transform as $\ell \sim \underline{3}$. There are three dimension-5 operators allowed: $(\xi\ell)^2$, $(\xi\ell)(\varphi'\ell)$ and $(\varphi'\ell)^2$. In what follows, a and b denote the terms that come from the VEVs of ξ and φ', respectively.

The first operator is

$$(\xi\ell)^2 = (\xi\ell)(\xi\ell) = \xi^2(\ell_e\ell_e + \ell_\mu\ell_\mu + \ell_\tau\ell_\tau) \ , \tag{B.1}$$

which contributes a term proportional to the identity matrix multiplied by $\langle\xi\rangle^2$ (which is a^2). The second operator is

$$(\xi\ell)(\varphi'\ell) = \xi(\ell_e\varphi'_2\ell_\tau + \ell_\mu\varphi'_3\ell_e + \ell_\tau\varphi'_1\ell_\mu) + \xi(\ell_e\varphi'_3\ell_\mu + \ell_\mu\varphi'_1\ell_\tau + \ell_\tau\varphi'_2\ell_e) \ . \tag{B.2}$$

If the VEV alignment is proportional to $(0,1,0)$, this results in terms in the $(1,3)$ and $(3,1)$ positions, denoted by β in Eq. (5.29), but if this VEV alignment is deviated [Eq. (5.30)], there are additional off-diagonal terms. Thus the operator $(\xi\ell)(\varphi'\ell)$

contributes the following terms to the mass matrix:

$$\begin{pmatrix} 0 & ab\epsilon_2 & ab \\ ab\epsilon_2 & 0 & ab\epsilon_1 \\ ab & ab\epsilon_1 & 0 \end{pmatrix} . \tag{B.3}$$

The operator $(\varphi'\ell)^2$ is more complicated, since it is formed by $(\underline{3} \times \underline{3}) \times (\underline{3} \times \underline{3})$, which contains $\underline{1} \times \underline{1}$, $\underline{1}' \times \underline{1}''$, $\underline{1}'' \times \underline{1}'$, $\underline{3} \times \underline{3}$, $\underline{3} \times \underline{3}$ and $\underline{3} \times \underline{3}$. Each of these operators contributes to the mass matrix as follows:

$$\underline{1} \times \underline{1}: \quad (\varphi'_1\ell_e + \varphi'_2\ell_\mu + \varphi'_3\ell_\tau)^2 \tag{B.4}$$

gives

$$\begin{pmatrix} b^2\epsilon_1^2 & b^2\epsilon_1 & b^2\epsilon_1\epsilon_2 \\ b^2\epsilon_1 & b^2 & b^2\epsilon_2 \\ b^2\epsilon_1\epsilon_2 & b^2\epsilon_2 & b^2c_2^2 \end{pmatrix} ; \tag{B.5}$$

$$\underline{1}' \times \underline{1}'': \quad (\varphi'_1\ell_e + \omega\varphi'_2\ell_\mu + \omega^2\varphi'_3\ell_\tau)(\varphi'_1\ell_e + \omega^2\varphi'_2\ell_\mu + \omega\varphi'_3\ell_\tau) \tag{B.6}$$

gives

$$\begin{pmatrix} b^2\epsilon_1^2 & \omega^2b^2\epsilon_1 & \omega b^2\epsilon_1\epsilon_2 \\ \omega b^2\epsilon_1 & b^2 & \omega^2b^2\epsilon_2 \\ \omega^2b^2\epsilon_1\epsilon_2 & \omega b^2\epsilon_2 & b^2c_2^2 \end{pmatrix} , \tag{B.7}$$

and

$$\underline{1}'' \times \underline{1}': \quad (\varphi'_1\ell_e + \omega^2\varphi'_2\ell_\mu + \omega\varphi'_3\ell_\tau)(\varphi'_1\ell_e + \omega\varphi'_2\ell_\mu + \omega^2\varphi'_3\ell_\tau) \tag{B.8}$$

gives

$$\begin{pmatrix} b^2\epsilon_1^2 & \omega b^2\epsilon_1 & \omega^2b^2\epsilon_1\epsilon_2 \\ \omega^2b^2\epsilon_1 & b^2 & \omega b^2\epsilon_2 \\ \omega b^2\epsilon_1\epsilon_2 & \omega^2b^2\epsilon_2 & b^2\epsilon_2^2 \end{pmatrix} . \tag{B.9}$$

There are four ways of forming $\underline{3} \times \underline{3}$:

$$\underline{3}_1 \times \underline{3}_2: \quad (\varphi'_2\ell_\tau, \varphi'_3\ell_e, \varphi'_1\ell_\mu).(\varphi'_3\ell_\mu, \varphi'_1\ell_\tau, \varphi'_2\ell_e) = \varphi'_2\ell_\tau\varphi'_3\ell_\mu + \varphi'_3\ell_e\varphi'_1\ell_\tau + \varphi'_1\ell_\mu\varphi'_2\ell_e \tag{B.10}$$

gives

$$\begin{pmatrix} 0 & 0 & b^2\epsilon_1\epsilon_2 \\ b^2\epsilon_1 & 0 & 0 \\ 0 & b^2\epsilon_2 & 0 \end{pmatrix} , \tag{B.11}$$

$$\underline{3}_2 \times \underline{3}_1: \quad (\varphi'_3\ell_\mu, \varphi'_1\ell_\tau, \varphi'_2\ell_e).(\varphi'_2\ell_\tau, \varphi'_3\ell_e, \varphi'_1\ell_\mu) = \varphi'_3\ell_\mu\varphi'_2\ell_\tau + \varphi'_1\ell_\tau\varphi'_3\ell_e + \varphi'_2\ell_e\varphi'_1\ell_\mu \tag{B.12}$$

gives

$$\begin{pmatrix} 0 & b^2\epsilon_1 & 0 \\ 0 & 0 & b^2\epsilon_2 \\ b^2\epsilon_1\epsilon_2 & 0 & 0 \end{pmatrix} , \tag{B.13}$$

$$\underline{3}_1 \times \underline{3}_1: \quad (\varphi'_2\ell_\tau, \varphi'_3\ell_e, \varphi'_1\ell_\mu).(\varphi'_2\ell_\tau, \varphi'_3\ell_e, \varphi'_1\ell_\mu) = (\varphi'_2\ell_\tau)^2 + (\varphi'_3\ell_e)^2 + (\varphi'_1\ell_\mu)^2 \tag{B.14}$$

gives

$$\begin{pmatrix} b^2\epsilon_2^2 & 0 & 0 \\ 0 & b^2\epsilon_1^2 & 0 \\ 0 & 0 & b^2 \end{pmatrix} , \tag{B.15}$$

and

$$\underline{3}_2 \times \underline{3}_2: \quad (\varphi'_3\ell_\mu, \varphi'_1\ell_\tau, \varphi'_2\ell_e).(\varphi'_3\ell_\mu, \varphi'_1\ell_\tau, \varphi'_2\ell_e) = (\varphi'_3\ell_\mu)^2 + (\varphi'_1\ell_\tau)^2 + (\varphi'_2\ell_e)^2 \tag{B.16}$$

gives

$$\begin{pmatrix} b^2 & 0 & 0 \\ 0 & b^2\epsilon_2^2 & 0 \\ 0 & 0 & b^2\epsilon_1^2 \end{pmatrix} . \tag{B.17}$$

The terms in Eqs. (B.1), (B.2), (B.5), (B.7), (B.9), (B.11), (B.13),(B.15) and (B.17) can be combined[1] to form the mass matrix in Eq. (5.31), *viz.*

$$M'_\nu = \begin{pmatrix} a^2 + b^2\left(1 + 3\epsilon_1^2 + \epsilon_2^2\right) & ab\epsilon_2 + b^2\epsilon_1 & ab + b^2\epsilon_1\epsilon_2 \\ \cdot & a^2 + b^2\left(3 + \epsilon_1^2 + \epsilon_2^2\right) & ab\epsilon_1 + b^2\epsilon_2 \\ \cdot & \cdot & a^2 + b^2\left(1 + \epsilon_1^2 + 3\epsilon_2^2\right) \end{pmatrix} . \tag{B.18}$$

Here, the coupling constants in front of the operators in Eqs. (B.14) and (B.16) are set to be equal, which is not the general case [74].

B.2 Calculation of observables

This section provides explicit expressions for the mixing angle, CP violation and mass dependent observables, in terms of the eigenvectors ($U_{\alpha k}$) and eigenvalues (m_k) of the diagonalised mass matrices. The standard parameterisation of the PMNS matrix

[1]Note that $1 + \omega + \omega^2 = 0$, so that the antisymmetric terms in Eqs. (B.5), (B.7) and (B.9) cancel each other out.

(without Majorana phases) is

$$U_{\text{PMNS}} = \begin{pmatrix} c_{12}c_{13} & s_{12}c_{13} & s_{13}e^{-i\delta} \\ -s_{12}c_{23} - c_{12}s_{23}s_{13}e^{i\delta} & c_{12}c_{23} - s_{12}s_{23}s_{13}e^{i\delta} & s_{23}c_{13} \\ s_{12}s_{23} - c_{12}c_{23}s_{13}e^{i\delta} & -c_{12}s_{23} - s_{12}c_{23}s_{13}e^{i\delta} & c_{23}c_{13} \end{pmatrix}, \tag{B.19}$$

with $c_{ij} \equiv \cos\theta_{ij}$, $s_{ij} \equiv \sin\theta_{ij}$ and δ the CP violating Dirac phase. Rewriting this matrix as

$$U_{\text{PMNS}} = \begin{pmatrix} U_{e1} & U_{e2} & U_{e3} \\ U_{\mu 1} & U_{\mu 2} & U_{\mu 3} \\ U_{\tau 1} & U_{\tau 2} & U_{\tau 3} \end{pmatrix}, \tag{B.20}$$

it follows that the mixing angle observables are given by

$$\begin{aligned} \sin^2\theta_{12} &= \frac{|U_{e2}|^2}{1-|U_{e3}|^2}\ , \\ \sin^2\theta_{13} &= |U_{e3}|^2\ , \\ \sin^2\theta_{23} &= \frac{|U_{\mu 3}|^2}{1-|U_{e3}|^2}\ . \end{aligned} \tag{B.21}$$

The Jarlskog invariant

$$J_{CP} = \Im\mathrm{m}[U_{\mu 3}U_{e2}U^*_{\mu 2}U^*_{e3}] \tag{B.22}$$

was defined in Section 2.3, and this can be explicitly calculated from U_{PMNS}.

The mass dependent observables are the neutrinoless double beta decay amplitude

$$\langle m_{ee}\rangle = \left|\sum_{i=1}^{3} U_{ei}^2\, m_i\right|\ , \tag{B.23}$$

and the sum of absolute neutrino masses

$$\sum m_\nu = |m_1| + |m_2| + |m_3| \tag{B.24}$$

respectively, where m_i is a complex mass eigenvalue. In the standard parameterisation [Eq. (2.25)], $\langle m_{ee}\rangle$ becomes

$$\begin{aligned} \langle m_{ee}\rangle &= \left|c_{12}^2c_{13}^2 m_1 + e^{2i\lambda_2}s_{12}^2c_{13}^2 m_2 + e^{2i(\lambda_3-\delta)}s_{13}^2 m_3\right| \\ &= \left||U_{e1}|^2 m_1 + e^{i\alpha_2}|U_{e2}|^2 m_2 + e^{i\alpha_3}|U_{e3}|^2 m_3\right|\ , \end{aligned} \tag{B.25}$$

with the definitions $\alpha_2 \equiv 2\lambda_2$ and $\alpha_3 \equiv 2(\lambda_3 - \delta)$. Using the mass-squared differences

$$\begin{aligned} \Delta m^2_{21} &= m^2_2 - m^2_1 \,, \\ \Delta m^2_{31} &= m^2_3 - m^2_1 \,, \end{aligned} \tag{B.26}$$

one can define the mass of each neutrino in terms of the lightest neutrino mass and the observed mass-squared differences. For the normal hierarchy, m_1 is the lightest mass, and

$$\begin{aligned} m_2 &= \sqrt{m^2_1 + \Delta m^2_{21}} \,, \\ m_3 &= \sqrt{m^2_1 + \Delta m^2_{31}} \,, \end{aligned} \tag{B.27}$$

whereas for the inverted hierarchy, m_3 is the lightest mass, and

$$\begin{aligned} m_1 &= \sqrt{m^2_3 + \Delta m^2_{31}} \,, \\ m_2 &= \sqrt{m^2_3 + \Delta m^2_{21} + \Delta m^2_{31}} \,. \end{aligned} \tag{B.28}$$

With these definitions, $\langle m_{ee} \rangle$ and $\sum m_\nu$ can be expressed as

$$\begin{aligned} \langle m_{ee} \rangle &= c^2_{12} c^2_{13} m_1 + e^{i\alpha_2} s^2_{12} c^2_{13} \sqrt{m^2_1 + \Delta m^2_{21}} + e^{i\alpha_3} s^2_{13} \sqrt{m^2_1 + \Delta m^2_{31}} \,, \\ \sum m_\nu &= |m_1| + \sqrt{m^2_1 + \Delta m^2_{21}} + \sqrt{m^2_1 + \Delta m^2_{31}} \end{aligned} \tag{B.29}$$

for the normal hierarchy, and as

$$\begin{aligned} \langle m_{ee} \rangle &= e^{i\alpha_3} s^2_{13} m_3 + c^2_{12} c^2_{13} \sqrt{m^2_3 + \Delta m^2_{31}} + e^{i\alpha_2} s^2_{12} c^2_{13} \sqrt{m^2_3 + \Delta m^2_{21} + \Delta m^2_{31}} \,, \\ \sum m_\nu &= |m_3| + \sqrt{m^2_3 + \Delta m^2_{31}} + \sqrt{m^2_3 + \Delta m^2_{21} + \Delta m^2_{31}} \end{aligned} \tag{B.30}$$

for the inverted hierarchy. Eqs. (B.29) and (B.30) were used to plots the limits in the $\langle m_{ee} \rangle - \sum m_\nu$ parameter space in Fig. 2.4 and in the subsequent model analysis, with the phases in the range $0 \leq \alpha_i \leq 2\pi$, and the neutrino oscillation parameters taking the best-fit and 3σ values in Table 2.1.

B.3 Normal or inverted hierarchy?

It is possible to determine [243], from an expression for the mass eigenvalues, whether a specific model allows for the normal or inverted mass hierarchy, or both. In the original Altarelli-Feruglio model (Section 5.3), the neutrino mass matrix takes the form

$$M_\nu = \begin{pmatrix} a+\frac{2d}{3} & -\frac{d}{3} & -\frac{d}{3} \\ -\frac{d}{3} & \frac{2d}{3} & a-\frac{d}{3} \\ -\frac{d}{3} & a-\frac{d}{3} & \frac{2d}{3} \end{pmatrix} , \tag{B.31}$$

with eigenvalues $a+d$, a and $-a+d$. Hence, the mass squared differences are

$$\begin{aligned} \Delta m^2_{21} &= (-d^2 - 2ad) , \\ \Delta m^2_{31} &= -4ab . \end{aligned} \tag{B.32}$$

Since it is known [24] that $\Delta m^2_{21} > 0$, it follows that $-2ad > d^2$, which implies that $-2ad > 0$. This means that a and d have opposite signs, and from Eq. (B.32), Δm^2_{31} must be positive. In other words, the inverted mass hierarchy is impossible in this model.

This procedure was applied to all of the models analysed in this work, to ascertain which of the neutrino mass hierarchies was allowed in each case.

B.4 Rephasing of complex parameters

The Majorana mass terms in Eq. (3.41) couple left- and right-handed neutrino fields, and the complex symmetric Majorana mass matrix in Eq. (3.56) couples three generations of such neutrino fields. Although a general complex symmetric matrix has 12 parameters, breaking the A_4 symmetry with the required VEV alignment results in lepton matrices with less parameters. In order to reduce the number of parameters even further, it is possible to rephase these fields and absorb some of the complex phases. This can be illustrated with a simple example from the Altarelli-Feruglio model (Section 5.3.2), with one Higgs singlet.

In this model [32], the deviated neutrino mass matrix is given by Eq. (5.25), which

results in the mass term

$$\begin{pmatrix} \nu_e^c & \nu_\mu^c & \nu_\tau^c \end{pmatrix} \begin{pmatrix} a+\frac{2d}{3} & -\frac{1}{3}d(\epsilon_2+1) & -\frac{1}{3}d(\epsilon_1+1) \\ -\frac{1}{3}d(\epsilon_2+1) & \frac{2}{3}d(\epsilon_1+1) & a-\frac{d}{3} \\ -\frac{1}{3}d(\epsilon_1+1) & a-\frac{d}{3} & \frac{2}{3}d(\epsilon_2+1) \end{pmatrix} \begin{pmatrix} \nu_e \\ \nu_\mu \\ \nu_\tau \end{pmatrix} , \tag{B.33}$$

where a, d, ϵ_1 and ϵ_2 are complex parameters, as are the left- and right-handed neutrino fields ν_α and ν_α^c. Expanding Eq. (B.33) gives the individual mass terms,

$$\begin{aligned} &a\nu_e^c\nu_e + d\nu_e^c\nu_e - d\nu_e^c\nu_\mu - d\epsilon_2\nu_e^c\nu_\mu - d\nu_e^c\nu_\tau - d\epsilon_1\nu_e^c\nu_\tau - d\nu_\mu^c\nu_e - d\epsilon_2\nu_\mu^c\nu_e + d\nu_\mu^c\nu_\mu \\ &+ d\epsilon_1\nu_\mu^c\nu_\mu + a\nu_\mu^c\nu_\tau - d\nu_\mu^c\nu_\tau - d\nu_\tau^c\nu_e - d\epsilon_1\nu_\tau^c\nu_e + a\nu_\tau^c\nu_\mu - d\nu_\tau^c\nu_\mu + d\nu_\tau^c\nu_\tau + d\epsilon_2\nu_\tau^c\nu_\tau , \end{aligned} \tag{B.34}$$

where the coefficients $-\frac{1}{3}$ and $\frac{2}{3}$ have been omitted. In order to eliminate the complex phase of a, denoted by ϕ_a, the products $\nu_e^c\nu_e$ can be given the additional phase $-\phi_a$. However, Eq. (B.34) also contains the terms $a\nu_\mu^c\nu_\tau$ and $a\nu_\tau^c\nu_\mu$, so that the products $\nu_\mu^c\nu_\tau$ and $\nu_\tau^c\nu_\mu$ must also be assigned the additional phase $-\phi_a$. This means that each individual ν_α and ν_α^c field has the additional phase $-\phi_a/2$, and there are effectively only four different types of terms in Eq. (B.34), given by

$$|a|e^{i\phi_a}\nu , \tag{B.35}$$

$$|d|e^{i\phi_d}\nu , \tag{B.36}$$

$$|d|e^{i\phi_d}|\epsilon_1|e^{i\phi_{\epsilon_1}}\nu , \tag{B.37}$$

$$|d|e^{i\phi_d}|\epsilon_2|e^{i\phi_{\epsilon_2}}\nu , \tag{B.38}$$

where ν denotes the product $\nu_\alpha^c\nu_\alpha$, and ν has the phase $-\phi_a$. The phase of a is absorbed by the rephased product ν, but since the term $|d|e^{i\phi_d}\nu$ appears in Eq. (B.36), the phase of d cannot be eliminated. However, one can add $-\phi_{\epsilon_1}$ to the phase of d, so that the terms in Eqs. (B.37) and (B.38) become

$$|d|e^{i(\phi_d-\phi_{\epsilon_1})}|\epsilon_1|e^{i\phi_{\epsilon_1}}\nu = |d|e^{i\phi_d}|\epsilon_1|\nu , \tag{B.39}$$

$$|d|e^{i(\phi_d-\phi_{\epsilon_1})}|\epsilon_2|e^{i\phi_{\epsilon_2}}\nu = |d|e^{i\phi_d}|\epsilon_2|e^{i(\phi_{\epsilon_2}-\phi_{\epsilon_1})}\nu , \tag{B.40}$$

and the phase of ϵ_1 is also eliminated. However, from Eq. (B.40), it is evident that the phase of ϵ_2 cannot be eliminated. Alternatively, if the phase of ϵ_2 was eliminated, the phase of ϵ_1 would remain; the phases of ϵ_1 and ϵ_2 cannot both be eliminated.

In this model, the parameters a and ϵ_1 can be taken as real, with d and ϵ_2 complex. The technique outlined above was applied to the charged lepton and neutrino mass terms throughout this work, with as many of the complex phases eliminated as possible.

Appendix C

Details of Numerical Analysis

C.1 Fortran code

C.1.1 Algorithm

This is an outline of the Fortran program used to analyse the deviations from TBM in different A_4 models:

1. Input the desired number of points, the hierarchy (normal or inverted), and the allowed data range (3σ or 1σ)[1]
2. Generate an array of random numbers, initialising the random number generator with the system clock
3. Use the array of random numbers to create the charged lepton and neutrino mass matrices, with the form of the matrix dictated by the A_4 flavour symmetry and the specific particle assignments of the model
4. Combine these matrices into the hermitian matrices $M_\ell M_\ell^\dagger$ and $M_\nu M_\nu^\dagger$.
5. Diagonalize both matrices using ZGEEV
6. Sort the eigenvalues in ascending order, and keep the corresponding eigenvectors in the same order
7. For the neutrino sector, determine the mass hierarchy, and if inverted, shift the eigenvectors so that they correspond to the correct sorted mass eigenvalues

[1] Although the program allows the user to choose between the 3σ and 1σ ranges, only the 3σ range was used in this analysis.

8. Combine eigenvectors from the charged lepton and neutrino sectors into the U_{PMNS} mixing matrix

9. Calculate values for mixing angles, mass-squared differences, CP violation, double beta decay amplitude and sum of neutrino masses

10. Check whether the calculated mixing angles and mass-squared differences lie within the allowed ranges in Table 2.1: if they do then write the values of all of the observables (step 9) to file

11. Repeat steps 2 - 9 until the desired number of points are found[2]

C.1.2 Testing

In order to make sure that the Fortran program returned the correct results, tests were performed using the Mathematica package Mixing Parameter Tools (MPT) 1.0 [271]. By inputting the same mass matrix into both programs, one can check that the calculated values of the mixing angles and mass-squared differences match up, as well as the amplitude for $0\nu\beta\beta$ and the sum of absolute neutrino masses. The program was also tested with different mass matrices that yield both hierarchical and degenerate neutrino masses.

C.2 Efficiency of numerical diagonalisation

In this analysis the 3σ range was used as an input to the diagonalisation program, as the program was very slow in finding points within the 1σ range. The mass squared differences and charged lepton masses play the major role here: without these constraints the program would easily find points that satisfy the 1σ limits of the three mixing angles. The two mass squared differences have different orders of magnitude, and therefore require very specific eigenvalues to give the correct values for both, as well as for the mixing angles.

Another consideration is the choice of diagonalisation package, which in this case was the ZGEEV subroutine from LAPACK. This routine is designed for general complex matrices, however, since the program diagonalised two hermitian matrics, i.e. $M_\nu M_\nu^\dagger$ and $M_\ell M_\ell^\dagger$, it may have been more expedient to use ZHEEV, which only accepts hermitian matrices.

[2]In this analysis 1000 points were recorded in each case.

Although the LAPACK routines are numerically accurate, they are designed mainly for large matrices. In this work the matrices are all 3×3, and thus computational power is wasted. Ref. [272] discusses the accuracy and speed of different methods of diagonalising 3×3 matrices, comparing different algorithms used in this process. It turns out that Jacobi's method is the most accurate but also the slowest, and the conclusion is that the LAPACK routines are suitable for most applications. However, the author of Ref. [272] provides a simpler implementation of `ZHEEV` entitled `ZHEEVQ3`, which is specifically designed for 3×3 matrices. Thus the Fortran program developed for this work could be refined to incorporate these packages, which would hopeully improve processing speed.

There is also a lesser known method for diagonalising complex symmetric matrices: the Takagi method [20,273]. Here the $N \times N$ matrix is split into its real and imaginary parts, so that the problem is reduced to the diagonalisation of a $2N \times 2N$ real symmetric matrix. This method was not attempted in this thesis, but could indeed provide greater speed and accuracy in diagonalising the complex symmetric neutrino mass matrices.

C.3 Model parameters

Each of the models analysed in this work had different numbers of real and complex parameters, as discussed in Section B.4. Furthermore, in each numerical run the parameters took different values. These details are presented in Tables C.1 and C.2. All parameters were taken to be complex, except those that were real after rephasing, indicated in the last column of each table.

The Yukawa coupling constants y_e, y_μ and y_τ were taken to be real, and were set to specific values in the model analyses. In type A and type B models, they were randomly varied over the ranges

$$0.45 \leq y_e \leq 0.55 \,, \tag{C.1}$$

$$95 \leq y_\mu \leq 115 \,, \tag{C.2}$$

$$1600 \leq y_\mu \leq 1950 \,, \tag{C.3}$$

and M_ℓ was multiplied by the factor 10^6 eV or $10^6/\sqrt{3}$ eV to set the mass scale, depending on the basis used for A_4.

Table C.1: Details of the real and complex parameters used in the type A and type B A_4 model analysis in Chapter 5, for normal (NH) and inverted (IH) hierarchies.

Model	Mass matrix parameters NH	Mass matrix parameters IH	Deviation parameters ($\epsilon \leq 0.3$)	Real parameters
Ma TBM	$\lvert a\rvert \leq 1$ $\lvert b\rvert \leq 1$ $\lvert d\rvert \leq 2$	$\lvert a\rvert \leq 0.5$ $\lvert b\rvert \leq 1$ $\lvert d\rvert \leq 1$	ϵ_1, ϵ_2, ϵ_3 ϵ_1^{ch}, ϵ_2^{ch}	a, ϵ_1, ϵ_2
A-F 1 Higgs	$\lvert a\rvert \leq 1$ $\lvert d\rvert \leq 2$	n/a n/a	ϵ_1, ϵ_2 ϵ_1^{ch}, ϵ_2^{ch}	a, ϵ_1, ϵ_1^{ch}
A-F 2 Higgs	$\lvert c\rvert \leq 2$ $\lvert d\rvert \leq 2$	$\lvert c\rvert \leq 1$ $\lvert d\rvert \leq 1$	ϵ_1, ϵ_2, ϵ_3 ϵ_1^{ch}, ϵ_2^{ch}	c, ϵ_1, ϵ_1^{ch}
A-F 3 Higgs	$\lvert a\rvert \leq 1$ $\lvert c\rvert \leq 1$ $\lvert d\rvert \leq 2$	$\lvert a\rvert \leq 0.5$ $\lvert c\rvert \leq 1$ $\lvert d\rvert \leq 1.5$	ϵ_1, ϵ_2, ϵ_3 ϵ_1^{ch}, ϵ_2^{ch}	a, ϵ_1, ϵ_1^{ch}
Zee	$\lvert a\rvert \leq 2$ $\lvert b\rvert \leq 1$	$a \leq 1$ $\lvert b\rvert \leq 1$	ϵ_1, ϵ_2 ϵ_1^{ch}, ϵ_2^{ch}	a
Morisi	$\lvert a\rvert \leq 2$ $\lvert b\rvert \leq 0.5$	n/a n/a	ϵ_1, ϵ_2 ϵ_1^{ch}, ϵ_2^{ch}	a, ϵ_1, ϵ_1^{ch}, ϵ_2^{ch}
Babu & He	$\lvert a\rvert \leq 1$ $\lvert b\rvert \leq 2$ $\lvert c\rvert \leq 2$	$\lvert a\rvert \leq 3$ $\lvert b\rvert \leq 5$ $\lvert c\rvert \leq 5$	ϵ_1, ϵ_2 ϵ_1^{ch}, ϵ_2^{ch}	a, ϵ_1
Ma SUSY Seesaw	$\lvert a\rvert \leq 2$ $\lvert b\rvert \leq 2$ $\lvert c\rvert \leq 2$	$\lvert a\rvert \leq 1$ $\lvert b\rvert \leq 4$ $\lvert c\rvert \leq 4$	ϵ_1, ϵ_2 ϵ_1^{ch}, ϵ_2^{ch}	a
A-F Seesaw 1 Higgs	$\lvert a\rvert \leq 4$ $\lvert d\rvert \leq 4$	$\lvert a\rvert \leq 2$ $\lvert d\rvert \leq 1.5$	ϵ_1, ϵ_2 ϵ_1^{ch}, ϵ_2^{ch}	a, ϵ_1
A-F Seesaw 3 Higgs	$\lvert a\rvert \leq 4$ $\lvert b\rvert \leq 2.5$ $\lvert d\rvert \leq 4$	$\lvert a\rvert \leq 2.5$ $\lvert b\rvert \leq 1.5$ $\lvert d\rvert \leq 2.5$	ϵ_1, ϵ_2, ϵ_3 ϵ_1^{ch}, ϵ_2^{ch}	a, ϵ_1, ϵ_3
Yin	$\lvert a\rvert \leq 1$ $\lvert b\rvert \leq 1.5$ $\lvert c\rvert \leq 2$	– – –	ϵ_1, ϵ_2 ϵ_1^{ch}, ϵ_2^{ch}	a, ϵ_1
Chen & King	$\lvert a\rvert \leq 1.5$ $\lvert b\rvert \leq 1$	– –	ϵ_1, ϵ_2 ϵ_1^{ch}, ϵ_2^{ch}	a, ϵ_1

Table C.2: Details of the real and complex parameters used in the type C and type D A_4 model analysis in Chapter 6, for normal (NH) and inverted (IH) hierarchies.

Model	Mass matrix parameters NH	Mass matrix parameters IH	Deviation parameters ($\epsilon \leq 0.3$) or ($\epsilon \leq 0.03$)	Real parameters
Ma SUSY	$\|a\| \leq 2$ $\|b\| \leq 1$	– $\|b\| \leq 1$	ϵ_1, ϵ_2 ϵ_1^{ch}, ϵ_2^{ch}	a, ϵ_1, ϵ_1^{ch}
BM Left-Right	$\|a\| \leq 2$ $\|b\| \leq 1.5$	– –	ϵ_1, ϵ_2 ϵ_1^{ch}, ϵ_2^{ch}	a, ϵ_1, ϵ_1^{ch}
MPT	$\|a\| \leq 3$ $\|b\| \leq 4$	$\|a\| \leq 1$ $\|b\| \leq 1$	ϵ_1, ϵ_2 ϵ_1^{ch}, ϵ_2^{ch}	a, ϵ_1, ϵ_1^{ch}
BM Seesaw	$\|a\|, \|b\|, \|c\| \leq 2$ $\|d\|, \|e\|, \|f\| \leq 2$	$\|a\|, \|b\|, \|c\| \leq 2$ $\|d\|, \|e\|, \|f\| \leq 2$	ϵ_1, ϵ_2 ϵ_1^{ch}, ϵ_2^{ch}	a, ϵ_1, ϵ_1^{ch}
HMV	$\|a\| \leq 1$ $\|b\| \leq 1$	– –	ϵ_1, ϵ_2 ϵ_1^{ch}, ϵ_2^{ch}	a, ϵ_1, ϵ_1^{ch}
BFM	$\|a\|, \|b\|, \|c\| \leq 2$ $\|d\|, \|e\| \leq 2$	$\|a\|, \|b\|, \|c\| \leq 2$ $\|d\|, \|e\| \leq 2$	ϵ_1, ϵ_2 ϵ_1^{ch}, ϵ_2^{ch}	a, ϵ_1, ϵ_1^{ch}

References

[1] B. Pontecorvo, Sov. Phys. JETP **6**, 429 (1957).

[2] B. Pontecorvo, Sov. Phys. JETP **7**, 172 (1958).

[3] B. Pontecorvo, Sov. Phys. JETP **26**, 984 (1968).

[4] Super-Kamiokande, Y. Fukuda *et al.*, Phys. Rev. Lett. **82**, 2644 (1999), hep-ex/9812014.

[5] Super-Kamiokande, Y. Fukuda *et al.*, Phys. Rev. Lett. **81**, 1562 (1998), hep-ex/9807003.

[6] Super-Kamiokande, Y. Fukuda *et al.*, Phys. Lett. **B436**, 33 (1998), hep-ex/9805006.

[7] SNO, Q. R. Ahmad *et al.*, Phys. Rev. Lett. **87**, 071301 (2001), nucl-ex/0106015.

[8] SNO, Q. R. Ahmad *et al.*, Phys. Rev. Lett. **89**, 011301 (2002), nucl-ex/0204008.

[9] SNO, Q. R. Ahmad *et al.*, Phys. Rev. Lett. **89**, 011302 (2002), nucl-ex/0204009.

[10] S. M. Bilenky, C. Giunti, and W. Grimus, Prog. Part. Nucl. Phys. **43**, 1 (1999), hep-ph/9812360.

[11] W. Haxton and B. Holstein, Am. J. Phys **68**, 15 (2000).

[12] W. Haxton and B. Holstein, Am. J. Phys **72**, 18 (2004).

[13] M. C. Gonzalez-Garcia and Y. Nir, Rev. Mod. Phys. **75**, 345 (2003), hep-ph/0202058.

[14] W. M. Alberico and S. M. Bilenky, Phys. Part. Nucl. **35**, 297 (2004), hep-ph/0306239.

[15] Z.-z. Xing, Int. J. Mod. Phys. **A19**, 1 (2004), hep-ph/0307359.

[16] M. C. Gonzalez-Garcia and M. Maltoni, Phys. Rept. **460**, 1 (2008), 0704.1800.

[17] Particle Data Group, C. Amsler *et al.*, Phys. Lett. **B667**, 1 (2008).

[18] U. Dore and D. Orestano, Rept. Prog. Phys. **71**, 106201 (2008), 0811.1194.

[19] C. Giunti and M. Laveder, (2003), hep-ph/0310238.

[20] C. Giunti and C. Kim, *Fundamentals of Neutrino Physics and Astrophysics* (Oxford University Press, 2007).

[21] G. Altarelli and D. Meloni, Nucl. Phys. **B809**, 158 (2009), 0809.1041.

[22] H. Nunokawa, S. J. Parke, and J. W. F. Valle, Prog. Part. Nucl. Phys. **60**, 338 (2008), 0710.0554.

[23] G. L. Fogli, E. Lisi, A. Marrone, and A. Palazzo, Prog. Part. Nucl. Phys. **57**, 742 (2006), hep-ph/0506083.

[24] G. L. Fogli *et al.*, Phys. Rev. D **75**, 053001 (2007), hep-ph/0608060.

[25] G. L. Fogli *et al.*, Phys. Rev. D **78**, 033010 (2008), 0805.2517.

[26] T. Schwetz, M. Tortola, and J. W. F. Valle, New J. Phys. **10**, 113011 (2008), 0808.2016.

[27] P. F. Harrison, D. H. Perkins, and W. G. Scott, Phys. Lett. **B530**, 167 (2002), hep-ph/0202074.

[28] S. F. King, Neutrino Mass Models: a road map, in *Neutrino '08, New Zealand*, 2008, 0810.0492.

[29] R. N. Mohapatra and A. Y. Smirnov, Ann. Rev. Nucl. Part. Sci. **56**, 569 (2006), hep-ph/0603118.

[30] C. Giunti and M. Laveder, Neutrino unbound, `http://www.nu.to.infn.it/`, 2010.

[31] E. Ma, Phys. Rev. D **70**, 031901 (2004), hep-ph/0404199.

[32] G. Altarelli and F. Feruglio, Nucl. Phys. **B720**, 64 (2005), hep-ph/0504165.

[33] G. Altarelli and F. Feruglio, Nucl. Phys. **B741**, 215 (2006), hep-ph/0512103.

[34] E. Ma and G. Rajasekaran, Phys. Rev. D **64**, 113012 (2001), hep-ph/0106291.

[35] S. Morisi, Nuovo Cim. **123B**, 886 (2008), 0807.4013.

[36] P. F. Harrison and W. G. Scott, Phys. Lett. **B557**, 76 (2003), hep-ph/0302025.

[37] R. N. Mohapatra, S. Nasri, and H.-B. Yu, Phys. Lett. **B639**, 318 (2006), hep-ph/0605020.

[38] M. Mitra and S. Choubey, Phys. Rev. D **78**, 115014 (2008), 0806.3254.

[39] M. Tanimoto and T. Yanagida, Phys. Lett. **B633**, 567 (2006), hep-ph/0511336.

[40] W. Grimus, L. Lavoura, and P. O. Ludl, J. Phys. **G36**, 115007 (2009), 0906.2689.

[41] G. Altarelli, F. Feruglio, and L. Merlo, JHEP **05**, 020 (2009), 0903.1940.

[42] F. Bazzocchi, L. Merlo, and S. Morisi, Nucl. Phys. **B816**, 204 (2009), 0901.2086.

[43] H. Ishimori, Y. Shimizu, and M. Tanimoto, Prog. Theor. Phys. **121**, 769 (2009), 0812.5031.

[44] C. Hagedorn, M. Lindner, and R. N. Mohapatra, JHEP **06**, 042 (2006), hep-ph/0602244.

[45] H. Zhang, Phys. Lett. **B655**, 132 (2007), hep-ph/0612214.

[46] E. Ma, Phys. Lett. **B632**, 352 (2006), hep-ph/0508231.

[47] F. Feruglio, C. Hagedorn, Y. Lin, and L. Merlo, Nucl. Phys. **B775**, 120 (2007), hep-ph/0702194.

[48] D. A. Eby, P. H. Frampton, and S. Matsuzaki, Phys. Lett. **B671**, 386 (2009), 0810.4899.

[49] D. A. Eby, P. H. Frampton, and S. Matsuzaki, Phys. Rev. D **80**, 053007 (2009), 0907.3425.

[50] P. H. Frampton, T. W. Kephart, and S. Matsuzaki, Phys. Rev. D **78**, 073004 (2008), 0807.4713.

[51] P. H. Frampton, Int. J. Mod. Phys. **A24**, 3359 (2009), 0903.5228.

[52] I. de Medeiros Varzielas, AIP Conf. Proc. **903**, 397 (2007), hep-ph/0610351.

[53] E. Ma, Mod. Phys. Lett. **A21**, 1917 (2006), hep-ph/0607056.

[54] E. Ma, Phys. Lett. **B660**, 505 (2008), 0709.0507.

[55] C. Luhn, S. Nasri, and P. Ramond, J. Math. Phys. **48**, 073501 (2007), hep-th/0701188.

[56] E. Ma, Phys. Lett. **B649**, 287 (2007), hep-ph/0612022.

[57] E. Ma, Europhys. Lett. **79**, 61001 (2007), hep-ph/0701016.

[58] C. Hagedorn, M. A. Schmidt, and A. Y. Smirnov, Phys. Rev. D **79**, 036002 (2009), 0811.2955.

[59] I. de Medeiros Varzielas and G. G. Ross, Nucl. Phys. **B733**, 31 (2006), hep-ph/0507176.

[60] T. Appelquist, Y. Bai, and M. Piai, Phys. Rev. D **74**, 076001 (2006), hep-ph/0607174.

[61] S. Antusch, S. F. King, and M. Malinsky, JHEP **06**, 068 (2008), 0708.1282.

[62] S. F. King and M. Malinsky, JHEP **11**, 071 (2006), hep-ph/0608021.

[63] S. F. King, JHEP **08**, 105 (2005), hep-ph/0506297.

[64] A. B. Balantekin, (2009), 0910.1814.

[65] C. S. Lam, Phys. Rev. D **78**, 073015 (2008), 0809.1185.

[66] G. Altarelli, Theoretical Models of Neutrino Mixing: Recent Developments, in *Talk at the 13th International Workshop on Neutrino Telescopes, Venice, March 10-13*, 2009, 0905.2350.

[67] G. Altarelli, Status of Neutrino Masses and Mixing in 2009, in *Talk given at the Rencontres de Physique de la Vallee d'Aoste, La Thuile, Aosta Valley (Italy). March 1-7*, 2009, 0905.3265.

[68] E. Ma, Mod. Phys. Lett. **A17**, 2361 (2002), hep-ph/0211393.

[69] E. Ma, Pramana **67**, 803 (2006), hep-ph/0606039.

[70] K. S. Babu, E. Ma, and J. W. F. Valle, Phys. Lett. **B552**, 207 (2003), hep-ph/0206292.

[71] E. Ma, Phys. Rev. D **73**, 057304 (2006), hep-ph/0511133.

[72] K. S. Babu and X.-G. He, (2005), hep-ph/0507217.

[73] X.-G. He, Y.-Y. Keum, and R. R. Volkas, JHEP **04**, 039 (2006), hep-ph/0601001.

[74] A. Zee, Phys. Lett. **B630**, 58 (2005), hep-ph/0508278.

[75] S.-L. Chen, M. Frigerio, and E. Ma, Nucl. Phys. **B724**, 423 (2005), hep-ph/0504181.

[76] E. Ma, Mod. Phys. Lett. **A20**, 2601 (2005), hep-ph/0508099.

[77] E. Ma, Mod. Phys. Lett. **A21**, 2931 (2006), hep-ph/0607190.

[78] E. Ma, Mod. Phys. Lett. **A22**, 101 (2007), hep-ph/0610342.

[79] P. Ciafaloni, M. Picariello, E. Torrente-Lujan, and A. Urbano, Phys. Rev. D **79**, 116010 (2009), 0901.2236.

[80] S. Morisi, M. Picariello, and E. Torrente-Lujan, Phys. Rev. D **75**, 075015 (2007), hep-ph/0702034.

[81] F. Bazzocchi, S. Morisi, M. Picariello, and E. Torrente-Lujan, J. Phys. G **36**, 015002 (2009), 0802.1693.

[82] F. Bazzocchi, M. Frigerio, and S. Morisi, Phys. Rev. D **78**, 116018 (2008), 0809.3573.

[83] M. Hirsch, A. S. Joshipura, S. Kaneko, and J. W. F. Valle, Phys. Rev. Lett. **99**, 151802 (2007), hep-ph/0703046.

[84] L. Lavoura and H. Kuhbock, Mod. Phys. Lett. **A22**, 181 (2007), hep-ph/0610050.

[85] P. H. Frampton and S. Matsuzaki, (2008), 0806.4592.

[86] S. Morisi, Phys. Rev. D **79**, 033008 (2009), 0901.1080.

[87] Y. Lin, Nucl. Phys. **B813**, 91 (2009), 0804.2867.

[88] G. Altarelli and D. Meloni, J. Phys. G **36**, 085005 (2009), 0905.0620.

[89] S. M. Bilenky and B. Pontecorvo, Phys. Rept. **41**, 225 (1978).

[90] C. Giunti, AIP Conf. Proc. **1026**, 3 (2008), 0801.0653.

[91] W. Grimus and P. Stockinger, Phys. Rev. D **54**, 3414 (1996), hep-ph/9603430.

[92] W. Grimus, S. Mohanty, and P. Stockinger, (1999), hep-ph/9904340.

[93] C. Giunti, JHEP **11**, 017 (2002), hep-ph/0205014.

[94] H. J. Lipkin, Phys. Lett. **B642**, 366 (2006).

[95] H. J. Lipkin, Phys. Lett. **B348**, 604 (1995).

[96] H. J. Lipkin, Phys. Lett. **B579**, 355 (2003).

[97] B. Kayser, Phys. Rev. D **24**, 110 (1981).

[98] J. Rich, Phys. Rev. D **48**, 4318 (1993).

[99] K. Kiers, S. Nussinov, and N. Weiss, Phys. Rev. D **53**, 537 (1996), hep-ph/9506271.

[100] Z. Maki, M. Nakagawa, and S. Sakata, Prog. Theor. Phys. **28**, 870 (1962).

[101] C. Jarlskog, Z. Phys. **C29**, 491 (1985).

[102] C. Jarlskog, Phys. Rev. Lett. **55**, 1039 (1985).

[103] A. de Gouvea, Neutrino physics, in *TASI lectures on neutrino physics, Boulder, Colorado, 6 June - 2 July*, 2004, hep-ph/0411274.

[104] G. L. Fogli, E. Lisi, A. Marrone, A. Palazzo, and A. M. Rotunno, Phys. Rev. Lett. **101**, 141801 (2008), 0806.2649.

[105] R. Davis, Jr., D. S. Harmer, and K. C. Hoffman, Phys. Rev. Lett. **20**, 1205 (1968).

[106] B. T. Cleveland *et al.*, Astrophys. J. **496**, 505 (1998).

[107] J. N. Bahcall, M. H. Pinsonneault, and S. Basu, Astrophys. J. **555**, 990 (2001), astro-ph/0010346.

[108] KAMIOKANDE-II, K. S. Hirata *et al.*, Phys. Rev. Lett. **63**, 16 (1989).

[109] KAMIOKANDE-II, K. S. Hirata *et al.*, Phys. Rev. Lett. **65**, 1301 (1990).

[110] KAMIOKANDE-II, K. S. Hirata *et al.*, Phys. Rev. Lett. **65**, 1297 (1990).

[111] Kamiokande, Y. Fukuda *et al.*, Phys. Rev. Lett. **77**, 1683 (1996).

[112] Super-Kamiokande, Y. Fukuda *et al.*, Phys. Rev. Lett. **81**, 1158 (1998), hep-ex/9805021.

[113] Super-Kamiokande, Y. Fukuda *et al.*, Phys. Rev. Lett. **82**, 1810 (1999), hep-ex/9812009.

[114] Super-Kamiokande, Y. Fukuda *et al.*, Phys. Rev. Lett. **82**, 2430 (1999), hep-ex/9812011.

[115] Super-Kamiokande, S. Fukuda *et al.*, Phys. Rev. Lett. **86**, 5651 (2001), hep-ex/0103032.

[116] Super-Kamiokande, S. Fukuda *et al.*, Phys. Rev. Lett. **86**, 5656 (2001), hep-ex/0103033.

[117] Super-Kamiokande, S. Fukuda *et al.*, Phys. Lett. **B539**, 179 (2002), hep-ex/0205075.

[118] Super-Kamkiokande, J. Hosaka *et al.*, Phys. Rev. D **D73**, 112001 (2006), hep-ex/0508053.

[119] GALLEX, P. Anselmann *et al.*, Phys. Lett. **B285**, 390 (1992).

[120] GALLEX, P. Anselmann *et al.*, Phys. Lett. **B314**, 445 (1993).

[121] GALLEX, P. Anselmann *et al.*, Phys. Lett. **B327**, 377 (1994).

[122] GALLEX, P. Anselmann *et al.*, Phys. Lett. **B357**, 237 (1995).

[123] GALLEX, W. Hampel *et al.*, Phys. Lett. **B447**, 127 (1999).

[124] SAGE, J. N. Abdurashitov *et al.*, Phys. Rev. Lett. **83**, 4686 (1999), astro-ph/9907131.

[125] SAGE, J. N. Abdurashitov *et al.*, Phys. Rev. **C60**, 055801 (1999), astro-ph/9907113.

[126] SAGE, J. N. Abdurashitov *et al.*, J. Exp. Theor. Phys. **95**, 181 (2002), astro-ph/0204245.

[127] L. Wolfenstein, Phys. Rev. D **17**, 2369 (1978).

[128] GNO, M. Altmann *et al.*, Phys. Lett. **B490**, 16 (2000), hep-ex/0006034.

[129] GNO, M. Altmann *et al.*, Phys. Lett. **B616**, 174 (2005), hep-ex/0504037.

[130] SNO, B. Aharmim *et al.*, Phys. Rev. C **75**, 045502 (2007), nucl-ex/0610020.

[131] SNO, S. N. Ahmed *et al.*, Phys. Rev. Lett. **92**, 181301 (2004), nucl-ex/0309004.

[132] SNO, B. Aharmim *et al.*, Phys. Rev. C **72**, 055502 (2005), nucl-ex/0502021.

[133] SNO, B. Aharmim *et al.*, Phys. Rev. Lett. **101**, 111301 (2008), 0806.0989.

[134] KamLAND, K. Eguchi *et al.*, Phys. Rev. Lett. **90**, 021802 (2003), hep-ex/0212021.

[135] KamLAND, T. Araki *et al.*, Phys. Rev. Lett. **94**, 081801 (2005), hep-ex/0406035.

[136] KamLAND, S. Abe *et al.*, Phys. Rev. Lett. **100**, 221803 (2008), 0801.4589.

[137] Borexino, C. Arpesella *et al.*, Phys. Lett. **B658**, 101 (2008), 0708.2251.

[138] Borexino, C. Arpesella *et al.*, Phys. Rev. Lett. **101**, 091302 (2008), 0805.3843.

[139] T. J. Haines *et al.*, Phys. Rev. Lett. **57**, 1986 (1986).

[140] D. Casper *et al.*, Phys. Rev. Lett. **66**, 2561 (1991).

[141] R. Becker-Szendy *et al.*, Phys. Rev. D **46**, 3720 (1992).

[142] Kamiokande-II, K. S. Hirata *et al.*, Phys. Lett. **B205**, 416 (1988).

[143] Kamiokande, Y. Fukuda *et al.*, Phys. Lett. **B335**, 237 (1994).

[144] K2K, M. H. Ahn *et al.*, Phys. Rev. D **74**, 072003 (2006), hep-ex/0606032.

[145] MINOS, P. Adamson *et al.*, Phys. Rev. Lett. **101**, 221804 (2008), 0807.2424.

[146] MINOS, P. Adamson *et al.*, Phys. Rev. Lett. **101**, 131802 (2008), 0806.2237.

[147] MINOS, P. Adamson *et al.*, Phys. Rev. D **77**, 072002 (2008), 0711.0769.

[148] OPERA, M. Guler *et al.*, CERN-SPSC-2000-028.

[149] ICARUS, F. Arneodo *et al.*, (2001), hep-ex/0103008.

[150] T2K, Y. Itow *et al.*, The JHF-Kamioka neutrino project, in *3rd Workshop on Neutrino Oscillations and Their Origin (NOON 2001), Kashiwa, Japan, 5-8 Dec*, 2001, hep-ex/0106019.

[151] CHOOZ, M. Apollonio *et al.*, Phys. Lett. **B420**, 397 (1998), hep-ex/9711002.

[152] CHOOZ, M. Apollonio *et al.*, Phys. Lett. **B466**, 415 (1999), hep-ex/9907037.

[153] CHOOZ, M. Apollonio *et al.*, Eur. Phys. J. **C27**, 331 (2003), hep-ex/0301017.

[154] M. Maltoni and T. Schwetz, (2008), 0812.3161.

[155] A. B. Balantekin and D. Yilmaz, J. Phys. **G35**, 075007 (2008), 0804.3345.

[156] F. Ardellier *et al.*, (2004), hep-ex/0405032.

[157] S. Berridge *et al.*, (2004), hep-ex/0410081.

[158] NOνA, D. Ayres *et al.*, (2002), hep-ex/0210005.

[159] NOνA, D. S. Ayres *et al.*, (2004), hep-ex/0503053.

[160] Daya-Bay, X. Guo *et al.*, (2007), hep-ex/0701029.

[161] LSND, C. Athanassopoulos *et al.*, Phys. Rev. Lett. **77**, 3082 (1996), nucl-ex/9605003.

[162] LSND, C. Athanassopoulos *et al.*, Phys. Rev. Lett. **81**, 1774 (1998), nucl-ex/9709006.

[163] KARMEN, B. Armbruster *et al.*, Phys. Rev. D **65**, 112001 (2002), hep-ex/0203021.

[164] S. M. Bilenky, C. Giunti, and W. Grimus, Eur. Phys. J. **C1**, 247 (1998), hep-ph/9607372.

[165] V. D. Barger, S. Pakvasa, T. J. Weiler, and K. Whisnant, Phys. Rev. D **58**, 093016 (1998), hep-ph/9806328.

[166] M. Maltoni, T. Schwetz, and J. W. F. Valle, Phys. Lett. **B518**, 252 (2001), hep-ph/0107150.

[167] MiniBooNE, A. A. Aguilar-Arevalo *et al.*, Phys. Rev. Lett. **103**, 061802 (2009), 0903.2465.

[168] MiniBooNE, A. A. Aguilar-Arevalo *et al.*, Phys. Rev. Lett. **98**, 231801 (2007), 0704.1500.

[169] MiniBooNE, A. A. Aguilar-Arevalo *et al.*, Phys. Rev. D **78**, 012007 (2008), 0805.1764.

[170] S. N. Gninenko, (2009), 0902.3802.

[171] M. Maltoni and T. Schwetz, Phys. Rev. D **76**, 093005 (2007), 0705.0107.

[172] T. Schwetz, JHEP **02**, 011 (2008), 0710.2985.

[173] G. Karagiorgi, Z. Djurcic, J. M. Conrad, M. H. Shaevitz, and M. Sorel, Phys. Rev. D **80**, 073001 (2009), 0906.1997.

[174] C. Kraus *et al.*, Eur. Phys. J. **C40**, 447 (2005), hep-ex/0412056.

[175] V. M. Lobashev *et al.*, Phys. Lett. **B460**, 227 (1999).

[176] G. L. Fogli *et al.*, Phys. Rev. D **70**, 113003 (2004), hep-ph/0408045.

[177] C. Weinheimer, Nucl. Phys. Proc. Suppl. **168**, 5 (2007).

[178] H. V. Klapdor-Kleingrothaus *et al.*, Eur. Phys. J. **A12**, 147 (2001), hep-ph/0103062.

[179] H. V. Klapdor-Kleingrothaus, I. V. Krivosheina, A. Dietz, and O. Chkvorets, Phys. Lett. B **586**, 198 (2004), hep-ph/0404088.

[180] H. V. Klapdor-Kleingrothaus and I. V. Krivosheina, Mod. Phys. Lett. A **21**, 1547 (2006).

[181] IGEX, C. E. Aalseth *et al.*, Phys. Rev. C **59**, 2108 (1999).

[182] IGEX, C. E. Aalseth *et al.*, Phys. Rev. D **65**, 092007 (2002), hep-ex/0202026.

[183] CUORICINO, C. Arnaboldi *et al.*, Phys. Rev. C **78**, 035502 (2008), 0802.3439.

[184] C. E. Aalseth *et al.*, Mod. Phys. Lett. **A17**, 1475 (2002), hep-ex/0202018.

[185] S. R. Elliott and J. Engel, J. Phys. **G30**, R183 (2004), hep-ph/0405078.

[186] CUORE, C. Arnaboldi *et al.*, Nucl. Instrum. Meth. **A518**, 775 (2004), hep-ex/0212053.

[187] E. Fiorini, Phys. Rept. **307**, 309 (1998).

[188] GERDA, S. Schonert *et al.*, Nucl. Phys. Proc. Suppl. **145**, 242 (2005).

[189] NEMO, I. Nasteva, AIP Conf. Proc. **1078**, 332 (2009), 0810.0637.

[190] NEMO-3, R. L. Flack, J. Phys. Conf. Ser. **136**, 022032 (2008), 0810.5497.

[191] Z. Daraktchieva, Nucl. Phys. **A827**, 495c (2009), 0901.2720.

[192] Majorana, C. E. Aalseth *et al.*, Phys. Atom. Nucl. **67**, 2002 (2004), hep-ex/0405008.

[193] Majorana, F. T. Avignone, III, J. Phys. Conf. Ser. **120**, 052059 (2008), 0711.4808.

[194] WMAP, J. Dunkley *et al.*, Astrophys. J. Suppl. **180**, 306 (2009), 0803.0586.

[195] WMAP, E. Komatsu *et al.*, Astrophys. J. Suppl. **180**, 330 (2009), 0803.0547.

[196] SDSS, M. Tegmark *et al.*, Phys. Rev. D **74**, 123507 (2006), astro-ph/0608632.

[197] C. L. Reichardt *et al.*, Astrophys. J. **694**, 1200 (2009), 0801.1491.

[198] C. Dickinson *et al.*, Mon. Not. Roy. Astron. Soc. **353**, 732 (2004), astro-ph/0402498.

[199] A. C. S. Readhead *et al.*, Astrophys. J. **609**, 498 (2004), astro-ph/0402359.

[200] C. J. MacTavish *et al.*, Astrophys. J. **647**, 799 (2006), astro-ph/0507503.

[201] HST, W. L. Freedman *et al.*, Astrophys. J. **553**, 47 (2001), astro-ph/0012376.

[202] SNLS, P. Astier *et al.*, Astron. Astrophys. **447**, 31 (2006), astro-ph/0510447.

[203] SDSS, D. J. Eisenstein *et al.*, Astrophys. J. **633**, 560 (2005), astro-ph/0501171.

[204] SDSS, P. McDonald *et al.*, Astrophys. J. Suppl. **163**, 80 (2006), astro-ph/0405013.

[205] SDSS, P. McDonald *et al.*, Astrophys. J. **635**, 761 (2005), astro-ph/0407377.

[206] R. Slansky, Phys. Rept. **79**, 1 (1981).

[207] W. Greiner, *Relativistic Quantum Mechanics* (Springer-Verlag Berlin Heidelberg, 1990).

[208] E. Majorana, Nuovo Cim. **14**, 171 (1937).

[209] R. R. Volkas, Prog. Part. Nucl. Phys. **48**, 161 (2002), hep-ph/0111326.

[210] P. H. Frampton, S. L. Glashow, and T. Yanagida, Phys. Lett. **B548**, 119 (2002), hep-ph/0208157.

[211] W. Grimus and L. Lavoura, Phys. Lett. **B671**, 456 (2009), 0810.4516.

[212] W. Grimus and L. Lavoura, JHEP **09**, 106 (2008), 0809.0226.

[213] W. Grimus and L. Lavoura, JHEP **04**, 013 (2009), 0811.4766.

[214] S. F. King, Rept. Prog. Phys. **67**, 107 (2004), hep-ph/0310204.

[215] W. Grimus, PoS **P2GC**, 001 (2006), hep-ph/0612311.

[216] P. Minkowski, Phys. Lett. B **67**, 421 (1977).

[217] S. L. Glashow, NATO Adv. Study Inst. Ser. B Phys. **59**, 687 (1980).

[218] M. Gell-Mann, P. Ramond, and R. Slansky, *Supergravity* (North Holland, 1980).

[219] R. N. Mohapatra and G. Senjanovic, Phys. Rev. Lett. **44**, 912 (1980).

[220] T. Yanagida, Horizontal gauge symmetry and masses of neutrinos, in *Proc. of the Workshop on Unified Theories*, Tsukuba, Japan, 13-14 Feb, 1979.

[221] M. C. Gonzalez-Garcia, Nucl. Phys. **A827**, 5c (2009), 0901.2505.

[222] J. Schechter and J. W. F. Valle, Phys. Rev. D **22**, 2227 (1980).

[223] R. Foot, H. Lew, X. G. He, and G. C. Joshi, Z. Phys. **C44**, 441 (1989).

[224] L. Wolfenstein, Phys. Rev. D **18**, 958 (1978).

[225] C. I. Low and R. R. Volkas, Phys. Rev. D **68**, 033007 (2003), hep-ph/0305243.

[226] S. F. King, (2009), 0909.2969.

[227] M.-C. Chen and S. F. King, JHEP **06**, 072 (2009), 0903.0125.

[228] G. Altarelli, Lectures on Models of Neutrino Masses and Mixings, in *Two lectures given at the Summer Institute Fuji-Yoshida, Japan, 3-10 August*, 2007, 0711.0161.

[229] F. Wilczek and A. Zee, Phys. Rev. Lett. **42**, 421 (1979).

[230] A. Y. Smirnov, Neutrino-2008: Where are we? Where are we going?, in *Neutrino '08, New Zealand*, 2008, 0810.2668.

[231] C. H. Albright and M.-C. Chen, Phys. Rev. D **74**, 113006 (2006), hep-ph/0608137.

[232] C. H. Albright, (2009), 0905.0146.

[233] P. F. Harrison and W. G. Scott, Phys. Lett. **B547**, 219 (2002), hep-ph/0210197.

[234] W. Grimus, S. Kaneko, L. Lavoura, H. Sawanaka, and M. Tanimoto, JHEP **01**, 110 (2006), hep-ph/0510326.

[235] S. L. Glashow, (2007), 0710.3719.

[236] P. F. Harrison and W. G. Scott, Phys. Lett. **B535**, 163 (2002), hep-ph/0203209.

[237] W. Ledermann, *Introduction to group characters* (Cambridge University Press, 1977), .

[238] S. Sternberg, *Group Theory and Physics* (Cambridge University Press, 1995).

[239] C. I. Low, Phys. Rev. D **71**, 073007 (2005), hep-ph/0501251.

[240] P. H. Frampton and S. Matsuzaki, (2009), 0902.1140.

[241] M.-C. Chen and K. T. Mahanthappa, Phys. Lett. **B681**, 444 (2009), 0904.1721.

[242] B. Adhikary, B. Brahmachari, A. Ghosal, E. Ma, and M. K. Parida, Phys. Lett. **B638**, 345 (2006), hep-ph/0603059.

[243] B. Brahmachari, S. Choubey, and M. Mitra, Phys. Rev. D **77**, 073008 (2008), 0801.3554.

[244] M. Hirsch, A. Villanova del Moral, J. W. F. Valle, and E. Ma, Phys. Rev. D **72**, 091301 (2005), hep-ph/0507148.

[245] M. Hirsch, S. Morisi, and J. W. F. Valle, Phys. Rev. D **79**, 016001 (2009), 0810.0121.

[246] M. Honda and M. Tanimoto, Prog. Theor. Phys. **119**, 583 (2008), 0801.0181.

[247] C. H. Albright and W. Rodejohann, Phys. Lett. **B665**, 378 (2008), 0804.4581.

[248] W. Rodejohann, Nucl. Phys. Proc. Suppl. **188**, 336 (2009), 0901.0248.

[249] G. L. Fogli, E. Lisi, A. Marrone, A. Palazzo, and A. M. Rotunno, (2009), 0905.3549.

[250] S. Goswami, S. T. Petcov, S. Ray, and W. Rodejohann, Phys. Rev. D **80**, 053013 (2009), 0907.2869.

[251] G. Altarelli, F. Feruglio, and C. Hagedorn, JHEP **03**, 052 (2008), 0802.0090.

[252] G. Altarelli, F. Feruglio, and Y. Lin, Nucl. Phys. **B775**, 31 (2007), hep-ph/0610165.

[253] E. Ma, Phys. Rev. D **72**, 037301 (2005), hep-ph/0505209.

[254] F. Bazzocchi, S. Kaneko, and S. Morisi, JHEP **03**, 063 (2008), 0707.3032.

[255] F. Feruglio, C. Hagedorn, Y. Lin, and L. Merlo, Nucl. Phys. **B809**, 218 (2009), 0807.3160.

[256] E. Ma, Mod. Phys. Lett. **A17**, 627 (2002), hep-ph/0203238.

[257] M. Hirsch, J. C. Romao, S. Skadhauge, J. W. F. Valle, and A. Villanova del Moral, Phys. Rev. D **69**, 093006 (2004), hep-ph/0312265.

[258] F. Yin, Phys. Rev. D **75**, 073010 (2007), 0704.3827.

[259] B. Adhikary and A. Ghosal, Phys. Rev. D **78**, 073007 (2008), 0803.3582.

[260] C. Csaki, C. Delaunay, C. Grojean, and Y. Grossman, JHEP **10**, 055 (2008), 0806.0356.

[261] F. Bazzocchi, S. Morisi, and M. Picariello, Phys. Lett. **B659**, 628 (2008), 0710.2928.

[262] M. Hirsch, S. Morisi, and J. W. F. Valle, Phys. Rev. D **78**, 093007 (2008), 0804.1521.

[263] P. Ciafaloni, M. Picariello, A. Urbano, and E. Torrente-Lujan, Phys. Rev. **D81**, 016004 (2010), 0909.2553.

[264] S. F. King and M. Malinsky, Phys. Lett. **B645**, 351 (2007), hep-ph/0610250.

[265] A. Dighe, S. Goswami, and W. Rodejohann, Phys. Rev. D **75**, 073023 (2007), hep-ph/0612328.

[266] M. Lindner, A. Merle, and W. Rodejohann, Phys. Rev. D **73**, 053005 (2006), hep-ph/0512143.

[267] W. Grimus and L. Lavoura, JHEP **01**, 018 (2006), hep-ph/0509239.

[268] P. Fileviez Perez, Phys. Rev. D **76**, 071701 (2007), 0705.3589.

[269] S. S. C. Law, *Neutrino Models and Leptogenesis*, PhD thesis, University of Melbourne, 2009, 0901.1232.

[270] J. Berger and Y. Grossman, JHEP **02**, 071 (2010), 0910.4392.

[271] S. Antusch, J. Kersten, M. Lindner, M. Ratz, and M. Schmidt, REAP / MPT, `http://users.physik.tu-muenchen.de/rge/index.html`, 2005.

[272] J. Kopp, Int. J. Mod. Phys. **C19**, 523 (2008), physics/0610206.

[273] T. Hahn, (2006), physics/0607103.